ANISOTROPIC MEDIA AND THE DETERMINATION OF SUBSURFACE VELOCITY BY THE USE OF SURFACE SEISMIC REFLECTION DATA

by

Donald Alan Vossler

Dissertation submitted to the Graduate Faculty of the
Virginia Polytechnic Institute and State University
in partial fulfillment of the requirements for the degree of

DOCTOR OF PHILOSOPHY

in

Geophysics

APPROVED:

J. K. Costain, Chairman

E. S. Robinson

G. C. Grender

G. A. Bollinger

C. B. Ling

December, 1971

Blacksburg, Virginia

ACKNOWLEDGMENTS

First of all, I wish to thank my wife, Marilyn, for her never failing encouragement without which this work would have been impossible. I wish to thank my advisor, John Costain, for the many hours of helpful discussion that clarified many of the subjects discussed herein. Special thanks are due to Mrs. Marie Gee for her generous assistence in the preparation of the final typed manuscript. Finally, I wish to thank the remainder of my advisory committee for their reading and commenting on the dissertation.

Anisotropic Media and the Determination of Subsurface Velocity by the Use of Surface Seismic Reflection Data

1. Introduction

The term anisotropy as it will be used herein refers to physical properties that are dependent on the direction along which measurements are taken. This is to be contrasted with isotropy for which media properties are independent of direction. The particular anisotropic property in which we are interested is the velocity at which sound waves propagate within that part of the earth subject to exploration by reflection seismic techniques.

Perhaps one of the most generalized examples of anisotropy in the earth sciences is the concept of an undisturbed sedimentary sequence. Such a sedimentary sequence is characterized by layers of large areal extent deposited one on top of the other. All variation within the section is regarded as occurring in a direction normal to the layering. Therefore, since the section does possess a unique direction, it may be regarded as being anisotropic in its large scale properties.

Experimental evidence presented in the literature implies that almost all rocks are anisotropic to some extent. Velocity anisotropy, with which we are concerned, may occur in two principal ways. The material under consideration may be truly anisotropic in its elastic properties. This form of anisotropy arises in a variety of ways, such as vertical compression due to gravity, crystal structure, micro-orientation of grains, and horizontal or oblique compression due to tectonic forces. A second kind of macroscopic anisotropy results from an alternating series of isotropic layers overlying each other and with the thicknesses of the individual units small compared to

the wavelengths traversing the section.

Any indirect study of geological structure should take anisotropy into account if possible. If the possibility of anisotropy is not taken into account, it is quite possible to make incorrect interpretations of field data and arrive at invalid conclusions concerning the underlying geological structure. In the particular case of seismic exploration, failure to consider anisotropy could result in significant errors in the determination of the thicknesses of the underlying lithologic units. Consequently, the study of anisotropy is of immediate practical significance in exploration seismology.

2. Previous Work

Field measurements of subsurface velocity anisotropy (hereafter referred to as anisotropy) have been reported in the literature since the early 1950's for both reflection and refraction experiments. The occurrence of anisotropy in surface rocks has been reported by a number of investigators. McCollum and Snell (1932) reported an anisotropy factor of 1.4 (ratio of the velocity parallel to the velocity normal to the bedding) for the Lorraine shale in Canada. The Arbuckle limestone in Oklahoma was found to possess an anisotropy factor of 1.3 by Weatherby, et. al. (1934). White and Sengbush (1953) reported anisotropy factors at Dallas, Texas of 1.17 for the Austin chalk and 1.33 for the Eagle Ford shale.

Cholet and Richard (1954) noted that many geophysicists who attempted to evaluate anisotropy in the field provided very little information concerning the methods used to record and interpret data. They pointed out that the determination of anisotropy is difficult and, if it is to be reliable, it must be measured under controlled conditions. If this is not done, apparent velocity changes may in part be assigned to anisotropy while actually being caused by other factors such as topography, dip, velocity increase with depth, or layer heterogeneity. They described measurements from the Berriane district in the northern Sahara where stratification may be considered as strictly horizontal and velocity varies very little as a function of depth and is primarily dependent upon lithology.

Variations of lithology at Berriane are discussed as a function

of depth. The measured geological cross section is:

0-80 m: Hard limestones and soft chalky limestones alternating.

80-310 m: Slightly sandy clays with some thin anhydrite and limestone beds.

310-1225 m: Clay and sand complex, sometimes marly, with several anhydrite or limestone intercalations. Sand content falls to a very low value below 800 m.

1225-1250 m: Top of Jurassic, clays, marls, limestones.

Seismic data were recorded by placing geophones at varying depths within the well. A series of shots was detonated at successively greater distances from the well starting at 100 meters and continuing to a maximum distance of 1600 meters. The study compared actual arrival times at various well geophones with computed times utilizing different values of anisotropy. The theory of elliptical anisotropy was used for all computations. The anisotropy values that minimized the differences between actual and computed arrival times were assumed to be the correct values.

Cholet and Richard concluded that an average anisotropy factor for the entire sedimentary section was 1.09 (ratio of velocity parallel to bedding to velocity normal to bedding). This value applied over a depth range of 1250 meters. A concluding recommendation was made that additional studies needed to be performed, especially concerning the effects of lithology on anisotropy.

Hagedoorn (1955) demonstrated the existence of an anisotropic

velocity layer by comparing the results from a number of seismic velocity well logging surveys and adjacent refraction sections. Results were presented for studies performed at three locations about 10 kilometers apart. At the first location, velocity determinations were made in two wells, only 1200 meters apart, one of which was situated at the intersection of two refraction lines. At the second location, only one well, situated at the intersection of two refraction lines, was shot. The third case concerns a well situated at a distance of 1250 meters from a single refraction line and this case was included because a good velocity log was obtained in the well.

The technique used in the detection of anisotropy utilized the comparison of velocity well-logging surveys and adjacent refraction sections. Traveltime curves were plotted and in all three cases one layer was found to possess different horizontal and vertical velocity components. The lithology of the section was not discussed. The thickness of the anisotropic layer was 700 meters. The vertical velocity was determined to be 2550m/sec and the horizontal velocity was 2750 m/sec.

Studies of velocity anisotropy up to 1955 have been summarized by Uhrig and Van Melle (1955). A review of surface measurements are included as well as studies of the type performed by Cholet and Richard (1954). Uhrig and Van Melle reported that velocity anisotropy has been widely observed. The anisotropy factor for relatively homogeneous samples of surface outcrops from Canada, Oklahoma, and Texas was reported as varying between 1.17 and 1.40, and at depths

of 7000 to 8000 feet in clastic and carbonate sediments, it varies between 1.10 and 1.19. The available data suggest that velocity anisotropy is common enough to be a factor of importance in seismic computations. Since the amount of information on anisotropy is limited, Uhrig and Van Melle suggest that measurements of velocity anisotropy be made when vertical velocity surveys are conducted.

Postma (1955) discussed the effects of wave propagation in a stratified medium and showed that a periodic structure consisting of alternating plane, parallel, isotropic, and homogeneous elastic layers can be replaced by a homogeneous, transversely isotropic material as far as the large-scale elastic behavior of the medium is concerned. The five elastic moduli of the equivalent transversely isotropic medium are expressed in terms of the elastic properties and the ratio of the thicknesses of the individual isotropic layers. The condition that the Lame constants in the isotropic layers be positive is imposed, and a number of inequalities are derived which show the limits of the values the five elastic constants of the anisotropic medium can assume. The wave equation is derived from the stress-strain relations and the equation of motion. It is shown that there are in general three characteristic velocities, all functions of the direction of propagation. A graphical procedure is given for the derivation of these characteristic velocities from the five elastic moduli and the average density of the medium. A few numerical examples are presented in which the graphical procedure is applied. Examples are given of cases which are likely to be encountered in

nature, as well as of cases which emphasize the peculiarities which may occur for a physically possible, but less likely, choice of properties of the constituent isotropic layers. Postma utilized three main examples. In the first two cases, the isotropic layers are alternately limestone and sandstone. The difference between the two cases lies in the ratio of the thickness of the limestone layer to the thickness of the sandstone layer. For case 1, the ratio is 1:3, and for case 2, the ratio is 3:1. The third case is more extreme since the first layer is limestone and the second is water. The ratio of layer thicknesses of limestone and water is 1:0.01. This third case is included as a demonstration of the peculiarities which may occur in extreme cases. One such peculiarity is that shear waves do not propagate in the vertical direction. Finally, a few remarks are made on the possible applications of this theory to actual field problems.

Kleyn (1956) discussed the analytical solution of refraction problems in anisotropic media and presented an analysis of the anisotropic behavior of the sedimentary section near Betun, South Sumatra. The refraction theory developed is based on the assumptions that the velocity stratification is horizontal and that the successive strata are uniaxial anisotropic media with elliptical anisotropy. Theory is developed for the refraction angle and for the traveltime equations governing refraction. The sedimentary section in the Betun No. 1 well consists for the most part of Tertiary shales and sandy shales. The top of the igneous pre-Tertiary lies at 2075 meters below sea-level. The time-depth curve from the well velocity survey shows that,

on the whole, the vertical velocity increases steadily with depth. This smooth increase of the vertical velocity is interrupted by a low-velocity brown coal bed approximately 120 meters thick at 650 meters below sea-level, and a high velocity limestone, approximately 65 meters thick at 1800 meters below sea-level. The vertical velocities of the brown coal and of the limestone are 1530 and 5000 m/sec respectively. The refraction theory derived is applied to the anisotropic behavior of the sedimentary section in the vicinity of the well. Results from a refraction profile, a well velocity survey, and a radial well survey are used in the analysis. The results from a refraction profile across the Betun No. 1 well indicate that the anisotropy factor is unity or very close to unity immediately below the ground surface and that it probably increases to a maximum value of 1.13 or possible 1.15 at a depth of about 1300 meters below sea-level. The traveltime curve from the radial well survey, by including the information obtained from the refraction profile across the well, can be matched closely by assigning an overall value of 1.04 for the anisotropy factor in the section below 1500 meters below sea-level. Table 2-1 shows the results obtained for the analysis. The importance of this table is that it shows the details of the variation of anisotropy with depth. Unfortunately, there was not the corresponding amount of detail about the lithology in the well. One of the alternate analyses used a constant anisotropy factor of 1.06 for the entire sedimentary section. This value is precisely the result of averaging the interval anisotropy values.

Jolly (1956) investigated some of the fundamental properties of

Table 2-1. Betun Refraction Study

Depth Interval Meters	Vertical Velocity m/sec	Horizontal Velocity m/sec	Anisotropy Factor
0-100	1695	1695	1.00
100-200	1795	1795	1.00
200-300	1895	1895	1.00
300-400	1995	1995	1.00
400-500	2095	2221	1.06
500-630	2207	2339	1.06
630-750*	1530	1622	1.06
750-800	2184	2315	1.06
800-900	2257	2392	1.06
900-1000	2355	2595	1.10
1000-1100	2453	2703	1.10
1100-1200	2551	2811	1.10
1200-1300	2649	2995	1.13
1300-1400	2747	3107	1.13
1400-1500	2845	3220	1.13
1500-1600	2933	3050	1.04
1600-1700	3031	3152	1.04
1700-1750	3105	3229	1.04
1750-1815**	5000	5000	1.00
1815-1900	3234	3363	1.04
1900-2000	3325	3458	1.04
2000-2075	3410	3346	1.04

* Brown Coal
** Limestone

shear waves and explored the possibilities of using horizontally polarized (SH) shear waves for reflection prospecting. A special source was devised to produce a shearing motion which was detectable as far as 400 feet vertically and 1000 feet horizontally. Direct, refracted, and reflected SH and SV shear waves were identified on a series of surface and sub-surface recordings in a thick, uniform, and near surface shale section. A strong, highly dispersive surface wave, which satisfied the theoretical criteria of Love waves, was also observed.

Anomalous features of Jolly's data which did not conform to the predictions of simple isotropic theory were readily explained by considering the stratified section under observation to be transversely isotropic in the manner discussed by Postma (1955). It was found that the horizontal SH velocity exceeded the vertical SV velocity by 100 percent in the weathered surface layer, while the corresponding compressional wave velocities differed by only 12 percent. Studies of direct and refracted SH, SV, and P waves demonstrated conclusively that the stratified shale section under consideration was highly anisotropic to shear waves while being only slightly so to P waves. Anisotropy of the SH wave was manifested by the fact that the horizontal velocity was twice the vertical velocity, and that of SV waves was revealed by abnormally high velocities for near-vertical ray paths and by the presence of what are apparently two branches of the SV wave. All unusual features of the data could easily be explained by considering the elastic symmetry to be that of a transversely

isotropic solid. Theoretical predictions, such as the equivalence of vertical SH and horizontal SV velocity, the equality of vertical and horizontal SV velocity, the ellipsoidal shape of SH wave surfaces, and the complex nature of SV wave surfaces, were all confirmed experimentally.

The continuous velocity log (CVL) was applied to anisotropy measurements in the Northern Sahara by Dunoyer de Segonzac and Laherrere (1959). Measurements of anisotropy were made in two wells 300 kilometers apart in the Northern Sahara in order to improve the interpretation of seismic refraction surveys. These measurements were based on the shortening of experimental oblique traveltimes with respect to theoretical traveltimes computed by disregarding anisotropy. Because of the need for a precise knowledge of the velocity distribution, it was felt that a continuous velocity log was indispensible.

The results for the two wells were in agreement, and showed that anisotropy is essentially a function of lithology. The following values for the anisotropy factor, k, were obtained:

Sandstone, sands	k = 1.00
Salt	k = 1.00 to 1.05
Limestone	k = 1.08 to 1.12
Anhydrite	k = 1.15 to 1.20

The theoretical background for Dunoyer de Segonzac and Laherrere's work assumed an elliptical anisotropy such that the

wave surfaces in a homogeneous formation are ellipsoids of revolution with a vertical axis. A wave surface, as used herein, is defined as the loci of points which are undergoing the same phase of motion in a one-to-one correspondence at a given instant of time. Using this theory as a base, the consequences pertaining to seismic refraction are: Depths computed without anisotropy were too small by 8 to 9 percent, i. e., about 300 meters for this study. The error on offset distances to the point of critical refraction reached 70 percent. Depth computations carried out by assigning anisotropy factors according to the type of lithology gave very satisfactory results. Highly anisotropic formations with high interval velocities, such as anhydrite, played an important part in the propagation of refracted waves and in interpretation. Some consequences pertaining to seismic relections are: an analysis of field data yields velocities closer to horizontal velocities than to vertical velocities; depth and migration computations are significantly influenced by high velocity, highly anisotropic formations such as anhydrite.

Richards (1960) discussed velocity anisotropy in the context of wide angle reflections and their application to finding limestone structures in the foothills of western Canada. He developed and used the theory of elliptical anisotropy defined

by the traveltime equation:

$$T^2 = X^2/V_x^2 + Z^2/V_z^2 \qquad (2\text{-}1)$$

where T is the traveltime between two points whose cartesian coordinates are 0,0 and X,Z. V_x and V_z are the average velocities in the horizontal and vertical directions respectively. Earlier workers did not start with equation 2-1 in their theoretical development, but started with an ellipsoidally anisotropic version of Snell's law. The anisotropy factor, k, is defined as

$$k = V_x/V_z \qquad (2\text{-}2)$$

and is experimentally determined in two ways. The first is the well-geophone technique used by Cholet and Richard (1954) and discussed earlier. The second approach makes use of the reflection traveltimes to a reflector near the horizon under consideration and at increasing distances from a well or point where the depth and velocity (V_z) are both known. The anisotropy factor follows from an analysis of a T^2-X^2 plot and the application of the above traveltime equation which yields the V_x. Near Nevis, in the Province of Alberta, Canada, k = 1.12 in an area where the Mississippian has been eroded away and the reflections appear to occur in a high velocity Devonian limestone at a depth of 4800 feet. A value of k = 1.10 was reported for measurements along

the strike in a foothills section where the lithology is predominantly (70%) Cretaceous shale. In two other areas where the depth and vertical velocities to the Mississippian limestone were also known, the k values were 1.08 and 1.06, the shale content being about 60% in both cases. The conclusion was drawn that in a general application of elliptical anisotropy of the foothills area, a value of k of about 1.08 should be introduced.

An analysis of surface wave dispersion in transversely isotropic media has been made by Anderson (1961). He reports that this kind of anisotropy is "exhibited by hexagonal crystals, sediments, planar igneous bodies, ice sheets, and rolled metal sheets where the unique axis is perpendicular to the direction of surface wave propagation and the other axes are distributed randomly in the plane of the layers". Period equations have been derived for Rayleigh, Stoneley, and Love waves, and comparisons are made, in certain cases, with ray theoretical and plane stress solutions. Anisotropy can have a pronounced effect on both the range of existence and the shape of the dispersion curves and can lead to an apparent discrepancy be- Love and Rayleigh wave data. Attention has been focused on a single solid layer (a free plate)

and a solid layer in contact with a fluid halfspace. The single layer solutions are generalized to n-layer media by the use of Haskell (1953) matrices.

Rayleigh wave dispersion in plates for three materials exhibiting transverse isotropy was calculated. These materials were beryl, ice, and a laminated solid. Beryl was chosen in order to extend Stoneley's results to a free plate. Ice was chosen as an example of a solid which exhibits a rather strong anisotropy and because lake ice commonly forms with a vertical c-axis (unique axis) orientation. The other axes are randomly oriented, but since they are all equivalent the result is a large plate having the properties of a single crystal. A finely laminated solid is transversely isotropic with the unique axis normal to the laminations. However, the effective elastic constants of a laminated solid must obey certain ordering rules which restricts the extent anisotropy may be approximated by layering. The elastic constants for Postma's (1955) Case 1 were used for the dispersion study of the laminated solid.

Anderson (1962) analyzed Love wave dispersion in heterogeneously anisotropic media for a medium composed of transversely isotropic layers. The exact boundary value problem is solved for a simple layer and extended to multilayered media by a generalization of Haskell's (1953) technique. By a suitable redefinition of parameters, it is possible to put the anisotropic problem into isotropic form so that existing programs, tables and graphs can be used to determine the structure of layered anisotropic media. It can be shown that the Love

wave period equation expresses the condition of constructive interference between multiply reflected SH waves with directionally dependent velocities. Several numerical examples were computed to illustrate the range of validity of the laminated solid approximation developed by Postma (1955) and as an independent test of the theory developed within the paper. In the first example, phase velocities were computed for Love-type motion of a laminated, 10 layer plate and for the equivalent homogeneous anisotropic plate. The parameters are taken from Postma's (1955) Case 1. The difference in period for the two approaches is about 2.5 percent at a wavelength corresponding to about 10 times the thickness of the largest individual layer. The difference becomes more pronounced for shorter wavelengths and would become smaller if the laminations were made smaller.

In the second example, a three layer half-space was constructed corresponding to a layer of Postma Solid 1 over a layer of Postma Solid 2 over an isotropic half-space. Dispersion was computed for each surface layer split into 20 laminations and then into 40 laminations, and also for the equivalent anisotropic layers. As the number of laminations increases, the dispersion converges to the anisotropic case. While Anderson did not explicitly discuss layer thickness vs. wavelength for this second example, from his figure 4 it may be seen that the minimum departure from the anisotropic case occurs for a ratio of wavelength to lamina thickness of approximately 50.1. The maximum error for the 20 lamination case is about 3 percent. It is

about half of that for the 40 lamination case. If we assume that the same 50:1 ratio of wavelength to lamina thickness yields correspondingly good results in the case of reflection seismology, then for a typical wavelength on the order of 250 feet, lamina thickness would be approximately 5 feet. This is a quite reasonable scale for lamina variation.

Helbig (1966) proposed a graphical method of interpretation for refraction data where there is an anisotropic overburden. He used the model of transverse isotropy since any more complex form of anisotropy quickly becomes intractable. The analytical solution of the problem of anisotropy would involve the solution of a number of equations implicitly containing several parameters. The method of successive approximation is regarded as being rather cumbersome, hence the proposal of a graphical method.

Vander Stoep (1966) studied velocity anisotropy in two wells located in New Mexico and Texas. Postma's (1955) work showing theoretically that an ellipsoidal wavefront is not to be expected in layered, transversely isotropic media is quoted as justification for redefinition of the anisotropy factor. The anisotropy factor is redefined as "the ratio of the horizontal axis to the vertical axis of the ellipsoid that fits the wavefront in a limited zone about the vertical which is of interest in reflection seismology". Two wells were analyzed for anisotropy, one located in Lea County, New Mexico, and the other 50 miles northeast of Houston, Texas. The first well was approximately 2400 feet deep and the second 12,000 feet deep.

In this latter example, data obtained outside of the zone of good ellipsoidal fit corroborates Postma's theory for transversely isotropic media. The technique used was essentially that of the well-geophone method together with the analysis of a sonic log.

The results of the anisotropy analysis of the well in Texas yielded the following anisotropy factors vs. depth:

k = 1.00,	0 to 5000 feet
k = 1.10,	5000 to 7000 feet
k = 1.025,	7000 to 12000 feet

The entire geologic section measured by this survey is predominantly a sand-shale sequence of Miocene and Eocene age. The top of the Wilcox (Eocene) formation occurs at a depth of 6846 feet. No additional lithological detail is available for this well. The theory of elliptical anisotropy was utilized in the analysis. This theory was shown to be inadequate for offset distances beyond about 6000 feet and was believed to substantiate Postma's theory of transversely isotropic media. The anisotropy factor for the entire 12,000 foot section was reported as being 1.03, a figure which is obtained by an arithmetic average of the anisotropy over the whole section.

Hodgkinson (1970) developed a procedure for determining the anisotropy of sedimentary layers by comparing actual values of normal moveout, as measured in a seismic field survey, with theoretical values of normal moveout, as computed for a layered model. The model is derived from a sonic log taken in a bore-hole which penetrates the sedimentary layers under consideration, and which measures the vertical

velocity in each layer. The anisotropy of individual model layers is varied until a fit is achieved between the field values of normal moveout and those computed from the model. The values of anisotropy required to achieve such a fit are considered to be those existing in the sedimentary layers.

The procedure comprises three phases:

(1) Development of layered model from a sonic log, and the subsequent computations of theoretical traveltimes for oblique ray-paths through the model.

(2) Analysis of field seismograms to determine the empirical values of normal moveout, and correction of these values for the effects of ground elevation and shot-hole depth and for variation in the thickness of near-surface low-velocity layers.

(3) Comparison of theoretical and empirical values of normal moveout, and the introduction of anisotropy to achieve agreement between these two sets of values.

The method is an extension of that developed by Dunoyer de Segonzac and Laherrere (1959), who measured oblique traveltimes from a surface source to a receiver at depth in a bore-hole. The theory of elliptical anisotropy used in the method is the same as that developed by Kleyn (1956) and Dunoyer de Segonzac and Laherrere (1959).

Theoretical considerations are discussed and analyzed, and the specific problems encountered in each of the three phases are considered in detail. The field parameters necessary for a successful application of the technique are developed from an analysis of the

problems encountered in its development. Based on the velocities and anisotropy factors expected to be encountered in the Western Canadian Basin, a theoretical model is constructed to demonstrate the effects on normal moveout of the introduction of anisotropy into the sedimentary section.

Laboratory measurements on rocks from Western Canada have yielded the following anisotropy factors:

Paskapoo sandstone	$k = 1.03$
Belly River sandstone	$k = 1.06$
Mississippian limestone	$k = 1.09$

A summary of the anisotropy factors reported in the preceding discussion is contained in Table 2-2. Where the information is available, rock type and/or the location where the data were obtained is included.

Table 2-2. Summary of Reported Anisotropy Factors

Year	Investigators	k	Rock Type	Location
1932	McCollum and Snell	1.4	Lorraine shale	Canada
1933	Weatherby, et. al.	1.3	Arbuckle limestone	Oklahoma
1953	White and Sengbush	1.17	Austin chalk	Dallas, Texas
		1.33	Eagle Ford shale	Dallas, Texas
1954	Cholet and Richard	1.09	Ls., clay, sand	Berraine District, Northern Sahara
1956	Kleyn	1.00-1.13	Shales, sandy shales	Betun, South Sumatra (See Table 2-1)
1956	Jolly	1.12	Shale	Oklahoma
1959	Dunoyer de Segonzac and Laherrere	1.00	Sandstone, sands	Northern Sahara
		1.00-1.05	Salt	Northern Sahara
		1.08-1.12	Limestone	Northern Sahara
		1.15-1.20	Anhydrite	Northern Sahara
1960	Richards	1.12	Devonian limestone	Nevis, Alberta, Canada
1966	Vander Stoep	1.03	Sand-shale sequence	near Houston, Texas
1970	Hodgkinson	1.03	Paskapoo sandstone	Western Canada
		1.06	Belly Run sandstone	Western Canada
		1.09	Mississippian limestone	Western Canada

3. Purpose of Study

The purpose of this study is to evaluate the feasibility of determining the subsurface velocity in anisotropic media using surface seismic reflection techniques. The elastic theory for transversely isotropic media will be used in the analysis of anisotropic media for two principal reasons: first, transverse isotropy appears to be an acceptable model for some geologic applications; and second, the use of more complex forms of elastic anisotropy becomes computationally intractable because of the number of elastic coefficients that must be determined.

Mathematical techniques will be developed for the analysis of subsurface velocity in transversely isotropic media using surface seismic reflection data of the type obtained in petroleum exploration. A number of synthetic earth models will be analyzed both for velocity and to determine the limits of resolution of the anisotropic analysis technique. These models will be uniformly anisotropic for the most part. In addition, the effects of a buried anisotropic interval in an otherwise isotropic section will be studied. A qualitative study of some of the effects of dipping interfaces will be made. A quantitative investigation of the problem of dipping interfaces is a major study in itself and separate from the problem of velocity anisotropy.

A limitation will be placed on the synthetic data used in that it will include only primary reflections. Multiple reflections will not be considered. This restriction will not affect the validity of the results of this study.

4. Wave Propagation in Anisotropic Media

4.1 Introduction

In the general theory of anisotropic media there are 21 elastic constants relating stress and strain. Against this background, isotropy becomes a highly degenerate case, and the study of waves in isotropic media throws little light on the mathematical structure of the theory of waves in anisotropic media. In the following treatment, the general case of anisotropy will be reviewed as well as the isotropic case, and selected forms of anisotropy of interest to reflection seismic exploration will be derived.

This chapter is, in general, a distillation of various works on the theory of wave propagation in anisotropic material together with expansions of these ideas. Section 4.3 is largely taken from Bennett (1968), Love (1944), and Frederick and Chang (1965). The isotropic case is presented in section 4.4 for purposes of comparison. Section 4.5 is largely a unified development of material found in a variety of papers in the seismic literature. The theory of elliptical anisotropy is of historical significance since the majority of previously published field studies of velocity anisotropy have relied on this theory for the analysis of data. The development of the theory for transverse isotropy in section 4.6 comes in part from Bennett (1968). Section 4.7 is a discussion of the theory presented by Postma (1955) relating the elastic coefficients in this special form of transverse isotropy.

4.2 Notation

$X_x,\ldots$	Stress components (stress in x-direction across x-face)
$X_y,\ldots$	Stress components (stress in x-direction across y-face)
	Stress components having the same face as direction are compressional or tensile stresses, all others are shear stresses.
$e_{xx},\ldots,e_{xy},\ldots$	Strain components
c_{rs}	Elastic constants or stiffness coefficients (r,s = 1,2,...,6)
x,y,z	Coordinate axes
W	Strain energy function
ρ	Density
$\lambda_{11},\ldots$	Christoffel moduli
l,m,n	Direction cosines of the velocity vector $\vec{V}$ or the wave normal vector
$\vec{V}$	Velocity vector
V	Phase velocity
$\Diamond$	Unit vector indicating the direction normal to the wave front with direction cosines (l,m,n). This vector is parallel to $\vec{V}$ and therefore indicates the direction of wave propagation.
k	Wave number ω/V

$\vec{A}$	Generalized time independent vector at the wave front with components (A_x, A_y, A_z).
u,v,w	Displacements parallel to coordinate axes at (x,y,z)

4.3 The General Case of Anisotropy

4.3.1 Fundamental Equations

One of the fundamental concepts used in the theory of elasticity of solid bodies is that of the generalized Hooke's Law. This law states that at any point of a body each of the nine components of stress (p_{ij}) at that point is a linear function of the nine components of strain (e_{kl}) at the same point. In tensor notation (Bennett, 1968; Frederick and Chang, 1965), this may be expressed as:

$$p_{ij} = c_{ijkl}e_{kl} \tag{4.3-1}$$

where the elastic constants c_{ijkl} total 81. By assuming the body to be in equilibrium, the stress and strain tensors become symmetrical, i.e., $p_{ij} = p_{ji}$ and $e_{ij} = e_{ji}$. This results in the following relationship among the elastic constants:

$$c_{ijkl} = c_{jikl} = c_{ijlk} = c_{jilk} \tag{4.3-2}$$

This assumption reduces the number of elastic constants to 36 and results in only six independent components of stress and strain.

In what is to follow, the notation of Love (1944) will be used to facilitate comparison with the literature. In this notation, the six components of stress may be expressed in terms of the six components of strain as follows:

$$\begin{aligned}
X_x &= c_{11}e_{xx} + c_{12}e_{yy} + c_{13}e_{zz} + c_{14}e_{yz} + c_{15}e_{zx} + c_{16}e_{xy} \\
Y_y &= c_{21}e_{xx} + c_{22}e_{yy} + c_{23}e_{zz} + c_{24}e_{yz} + c_{25}e_{zx} + c_{26}e_{xy} \\
Z_z &= c_{31}e_{xx} + c_{32}e_{yy} + c_{33}e_{zz} + c_{34}e_{yz} + c_{35}e_{zx} + c_{36}e_{xy} \\
Y_z &= c_{41}e_{xx} + c_{42}e_{yy} + c_{43}e_{zz} + c_{44}e_{yz} + c_{45}e_{zx} + c_{46}e_{xy}
\end{aligned} \tag{4.3-3}$$

$$Z_x = c_{51}e_{xx} + c_{52}e_{yy} + c_{53}e_{zz} + c_{54}e_{yz} + c_{55}e_{zx} + c_{56}e_{xy}$$

$$X_y = c_{61}e_{xx} + c_{62}e_{yy} + c_{63}e_{zz} + c_{64}e_{yz} + c_{65}e_{zx} + c_{66}e_{xy}$$

As indicated above, there are only six equations since $X_y = Y_x$, $X_z = Z_x$, and $Y_z = Z_y$. These equations may also be written in terms of particle displacements if we note the relations defining the strain components:

$$\begin{aligned} e_{xx} &= \partial u/\partial x, \quad e_{yy} = \partial v/\partial y, \quad e_{zz} = \partial w/\partial z, \\ e_{yz} &= \partial v/\partial z + \partial w/\partial y, \quad e_{zx} = \partial w/\partial x + \partial u/\partial z, \\ e_{xy} &= \partial u/\partial y + \partial v/\partial x \end{aligned} \tag{4.3-4}$$

If we assume that when a perfectly elastic material is stressed, the change of state takes place either adiabatically or isothermally, Love has shown that a strain energy function, W, exists (Frederick and Chang, 1965). The strain energy function represents the potential energy per unit volume stored up in the body by the strain and is related to stress and strain by the following equations:

$$X_x = \partial W/\partial e_{xx}, \ldots, \quad Y_z = \partial W/\partial e_{yz}, \ldots. \tag{4.3-5}$$

The existence of a strain energy function implies that the increment of energy gained or lost in going from one state of stress to a second state of stress is identical regardless of the stress cycle chosen (Bennett, 1968). If we apply these properties of the strain energy function, it follows that:

$$\partial X_x/\partial e_{yz} = \partial^2 W/\partial e_{yz}\partial e_{xx} = \partial^2 W/\partial e_{xx}\partial e_{yz} = \partial Y_z/\partial e_{xx} \tag{4.3-6}$$

therefore, the relations

$$c_{rs} = c_{sr}; \quad r,s = 1,\ldots,6 \tag{4.3-7}$$

hold for the coefficients of equations 4.3-3. The number of elastic coefficients is thereby reduced from 36 to 21. The general form for the strain energy function (Love, 1944; Frederick and Chang, 1965) is then:

$$\begin{aligned} W = {} & \tfrac{1}{2}c_{11}e^2_{xx} + c_{12}e_{xx}e_{yy} + c_{13}e_{xx}e_{zz} + c_{14}e_{xx}e_{yz} \\ & + c_{15}e_{xx}e_{zx} + c_{16}e_{xx}e_{xy} \\ & + \tfrac{1}{2}c_{22}e^2_{yy} + c_{23}e_{yy}e_{zz} + c_{24}e_{yy}e_{yz} + c_{25}e_{yy}e_{zx} \\ & + c_{26}e_{yy}e_{xy} \\ & + \tfrac{1}{2}c_{33}e^2_{zz} + c_{34}e_{zz}e_{yz} + c_{35}e_{zz}e_{zx} + c_{36}e_{zz}e_{xy} \\ & + \tfrac{1}{2}c_{44}e^2_{yz} + c_{45}e_{yz}e_{zx} + c_{46}e_{yz}e_{xy} \\ & + \tfrac{1}{2}c_{55}e^2_{zx} + c_{56}e_{zx}e_{xy} \\ & + \tfrac{1}{2}c_{66}e^2_{xy} \end{aligned} \qquad (4.3\text{-}8)$$

Equations of Small Motion

The equations of small motion may be derived by considering a volume element dxdydz and equating the force on this unit due to its acceleration and the force due to the stress upon it. The equations do not consider the forces due to gravity which are of the second order. Parallel to the x,y,z coordinate axes these equations become:

$$\begin{aligned} \rho\,\partial^2 u/\partial t^2 &= \partial X_x/\partial x + \partial X_y/\partial y + \partial X_z/\partial z \\ \rho\,\partial^2 v/\partial t^2 &= \partial Y_x/\partial x + \partial Y_y/\partial y + \partial Y_z/\partial z \\ \rho\,\partial^2 w/\partial t^2 &= \partial Z_x/\partial x + \partial Z_y/\partial y + \partial Z_z/\partial z \end{aligned} \qquad (4.3\text{-}9)$$

4.3.2 Propagation of Plane Waves

The wave surface normal, $\hat{\nu}$, points in the direction of wave prop-

agation and is defined as

$$\hat{\nu} = (l,m,n) \tag{4.3-10}$$

where l,m,n are direction cosines with respect to the x,v,z axes. The phase velocities, V_i, corresponding to the three types of body waves which may be propagated in any general anisotropic medium may be determined as follows. The displacements u,v,w for plane waves propagated in the direction $\hat{\nu}$ are given by

$$(u,v,w) = (A_x,A_y,A_z)\exp[-ik(lx+my+nz-Vt)]. \tag{4.3-11}$$

Substituting these values into the equations of small motion (4.3-9) and using equations 4.3-3 and 4.3-4 yields

$$\begin{aligned}
(\lambda_{11} - \rho V^2)A_x + \lambda_{12} A_y + \lambda_{13} A_z &= 0 \\
\lambda_{12} A_x + (\lambda_{22} - \rho V^2)A_y + \lambda_{23} A_z &= 0 \\
\lambda_{13} A_x + \lambda_{23} A_y + (\lambda_{33} - \rho V^2)A_z &= 0
\end{aligned} \tag{4.3-12}$$

where,

$$\begin{aligned}
\lambda_{11} &= l^2c_{11} + m^2c_{66} + n^2c_{55} + 2mnc_{56} + 2nlc_{15} + 2mlc_{16} \\
\lambda_{22} &= l^2c_{66} + m^2c_{22} + n^2c_{44} + 2mnc_{24} + 2nlc_{46} + 2mlc_{26} \\
\lambda_{33} &= l^2c_{55} + m^2c_{44} + n^2c_{33} + 2mnc_{34} + 2nlc_{35} + 2mlc_{45} \\
\lambda_{12} &= l^2c_{16} + m^2c_{26} + n^2c_{45} + mn(c_{46} + c_{25}) \\
&\quad + ln(c_{14} + c_{56}) + lm(c_{12} + c_{66}) \\
\lambda_{13} &= l^2c_{15} + m^2c_{46} + n^2c_{35} + mn(c_{45} + c_{36}) \\
&\quad + ln(c_{13} + c_{55}) + lm(c_{14} + c_{56}) \\
\lambda_{23} &= l^2c_{56} + m^2c_{24} + n^2c_{34} + mn(c_{44} + c_{23}) \\
&\quad + ln(c_{36} + c_{45}) + lm(c_{25} + c_{46})
\end{aligned} \tag{4.3-13}$$

In order that equation 4.3-12 have a non-zero solution for A_x,A_y,

A_z the determinant of these equations must equal zero. If the determinant does equal zero, a solution exists. Therefore,

$$\begin{vmatrix} \lambda_{11} - \rho V^2 & \lambda_{12} & \lambda_{13} \\ \lambda_{12} & \lambda_{22} - \rho V^2 & \lambda_{23} \\ \lambda_{13} & \lambda_{23} & \lambda_{33} - \rho V^2 \end{vmatrix} = 0 \qquad (4.3\text{-}14)$$

Since this is a cubic equation in ρV^2, there are, in general, three possible velocities of propagation for plane waves whose normal is given by $\hat{\nu}$.

4.4 The Isotropic Case

4.4.1 Fundamental Equations

Love (1944) has shown that to leave the stress-strain relations and the strain energy function unchanged after a rotation of the coordinate axes, then we require the following condition on the coefficients relating stress and strain:

$$c_{ij} = 0 \text{ for } i \neq j \text{ and } i \text{ or } j = 4,5,6$$

$$c_{11} = c_{22} = c_{33} = \lambda + 2\mu$$

$$c_{12} = c_{13} = c_{23} = \lambda$$

$$c_{44} = c_{55} = c_{66} = \mu$$

Thus, two elastic constants suffice to describe an isotropic medium. Therefore, equations 4.3-3 may be rewritten as

$$\begin{aligned} X_x &= (\lambda + 2\mu)e_{xx} + \lambda e_{yy} + \lambda e_{zz} \\ Y_y &= \lambda e_{xx} + (\lambda + 2\mu)e_{yy} + \lambda e_{zz} \\ Z_z &= \lambda e_{xx} + \lambda e_{yy} + (\lambda + 2\mu)e_{zz} \\ Y_z &= \mu e_{yz} \\ Z_x &= \mu e_{zx} \\ X_y &= \mu e_{xy} \end{aligned} \tag{4.4-1}$$

4.4.2 Propagation of Plane Waves

In the isotropic case, equation 4.3-14 has the solution

$$\rho V^2 = \lambda + 2\mu,\ \mu,\ \mu \tag{4.4-2}$$

Therefore, in the isotropic case we have two rather than three phase velocities.

4.4.3 Snell's Law for Isotropic Media

Snell's law describes refraction at an interface between two media. If elastic energy is incident on the interface in medium 1 at an angle θ_1, as measured from the vertical, the angle θ_2, at which the energy is refracted away from the interface in medium 2 is given by:

$$\sin \theta_1/V_1 = \sin \theta_2/V_2 = p = \text{(constant)} \qquad (4.4\text{-}3)$$

where p is the ray parameter or ray constant. This is the usual manner in which Snell's law is stated.

Snell's law may also be derived by using Fermat's principle of minimum time. It can be shown that minimization of the integral (Goldstein, 1950):

$$\delta \int f(x,z,\dot{x})dz = 0 \qquad (4.4\text{-}4)$$

is accomplished whenever the Euler-Lagrange equation is satisfied:

$$\partial f/\partial x - \frac{d}{dz}(\partial f/\partial \dot{x}) = 0 \qquad (4.4\text{-}5)$$

where $\dot{x} = dx/dz$.

In our case, we wish to minimize to the traveltime given by the integral:

$$T = \int ds/V = \int \frac{\sqrt{1 + \dot{x}^2}dz}{V}, \quad ds^2 = dx^2 + dz^2 \qquad (4.4\text{-}6)$$

In the present case, f may be replaced by

$$f = \sqrt{1 + \dot{x}^2}/V. \qquad (4.4\text{-}7)$$

Measuring angles from the vertical, we have $\dot{x} = \tan \theta$, and

$$f = \sqrt{1 + \tan^2\theta}/V. \qquad (4.4\text{-}8)$$

In the isotropic case, V is not a function of position or orientation.

Therefore, substituting f into the Euler-Lagrange equation and solving, we have:

$$\partial f/\partial x = 0$$

$$\frac{d}{dz}\left(\frac{\partial f}{\partial \dot{x}}\right) = \frac{d}{dz}\left(\frac{\dot{x}}{V\sqrt{1 + \dot{x}^2}}\right) = 0 \qquad (4.4\text{-}9)$$

$$\therefore \frac{\dot{x}}{V\sqrt{1 + \dot{x}^2}} = \text{constant} = p$$

However, substituting $\dot{x} = \tan\theta$, we obtain:

$$p = \tan\theta/V\sqrt{1 + \tan^2\theta} = \sin\theta/V \qquad (4.4\text{-}10)$$

This is identical to the result given in equation 4.4-3.

4.5 Elliptical Anisotropy

We may define elliptical velocity anisotropy by the following traveltime equation:

$$T^2 = x^2/V_x^2 + z^2/V_z^2 \qquad \text{(Richards, 1960)} \qquad (4.5\text{-}1)$$

where T is the traveltime between points (0,0) and (x,z). V_x and V_z are the velocities in the horizontal and vertical directions respectively. This traveltime equation defines a certain mathematical form for the variation of the velocity with direction. If we change to a polar coordinate system with angles measured from the vertical (z-axis), then it is possible to define the velocity for any arbitrary direction of propagation. Let $x = r \sin\theta$ and $z = r \cos\theta$, then

$$T^2 = r^2(\sin^2\theta/V_x^2 + \cos^2\theta/V_z^2). \qquad (4.5\text{-}2)$$

Dividing by T^2 and rearranging, we have

$$V_\theta^2 = V_x^2V_z^2/(V_x^2\cos^2\theta + V_z^2\sin^2\theta) \quad (= r^2/T^2). \qquad (4.5\text{-}3)$$

If we substitute for V_z in terms of V_x, i.e., $V_z = V_x/k$, then

$$V_\theta^2 = V_x^2/(k^2\cos^2\theta + \sin^2\theta). \qquad (4.5\text{-}4)$$

4.5.1 Snell's Law for Elliptical Anisotropy

The mathematical form of the ray parameter again may be determined very simply by the use of Fermat's principle of minimum time. The procedure is identical to that discussed in section 4.4. The only difference is that we are now using the elliptical velocity function defined by equation 4.5-4. Again, the ray parameter is given by:

$$p = \text{(constant)} = \partial f/\partial\dot{x} = \partial f/\partial\tan\theta. \qquad (4.5\text{-}5)$$

Therefore, using 4.5-4 and 4.5-5, we have:

$$p = \sin\theta/[V_x(k^2\cos^2\theta + \sin^2\theta)^{\frac{1}{2}}] \qquad (4.5\text{-}6)$$

This is the resultant form of Snell's law for elliptical anisotropy.

4.5.2 The Application of Elliptical Anisotropy

The velocity funcition defined by 4.5-4 has been used extensively in seismic exploration studies of velocity anisotropy (See chapter 2). The value of k appropriate to each interval within a stratigraphic section is usually determined by some variation of the basic well-geophone technique. Geophones are placed at various depths within a well and shots are detonated at successsively greater distances from the well. Usually, a sonic log of velocity within the well is available. Then, it is primarily a matter of adjusting k values until there is good agreement between predicted and recorded arrival times. This technique allows for the determination of anisotropy over the entire extent of the well.

4.5.3 The Limitations of Elliptical Anisotropy

Both practical and theoretical limitations apply to the use of elliptical velocity anisotropy. With this theory alone, it is impossible to determine if anisotropy is present within a stratigraphic section by the use of surface data alone. Well control is required for such an analysis, the reason being that if only surface data are used, then "x" (See equation 4.5-1) is the only distance parameter that is known. Hence an analysis, such as the T^2-X^2 method (Dobrin, 1960), cannot discriminate between the isotropic and elliptically anisotropic cases.

The definition of elliptical anisotropy given in equation 4.5-1 is a very natural extension of the traveltime relation for an isotropic medium. However, no combination of elastic constants describing the propagation of compressional wave motion that is physically realistic and that will also yield a velocity function of the form given in 4.5-4 exists. When one derives the elastic conditions necessary for compressional waves to propagate at one velocity parallel to the bedding and at another velocity normal to the bedding, the end result is the theory governing wave propagation in transversely isotropic media. For small offset distances, elliptical anisotropy may be accurate enough to describe a velocity function; however, modern techniques of common-depth-point shooting lead to large offset distances and elliptical velocity functions may not adequately describe the velocity anisotropy present (Vander Stoep, 1966).

4.6 Transverse Isotropy

The theory of transverse isotropy describes media having only a single direction in which the velocity of propagation is unique. For the purposes of this study, this unique direction is the vertical (z) direction.

4.6.1 Fundamental Equations

Love (1944) has shown that if we require every direction of wave propagation normal to the z-axis (unique axis) to be equivalent, then this requires that the stress-strain relations be unchanged and also that the strain energy function be unchanged. These conditions impose the following restrictions on the elastic coefficients as defined in 4.3-3:

$$c_{ij} = 0 \text{ for } i \neq j \text{ and } i \text{ or } j = 4,5,6$$

$$c_{22} = c_{11}, \quad c_{23} = c_{13}, \quad c_{55} = c_{44},$$

$$c_{66} = \tfrac{1}{2}(c_{11} - c_{12})$$

The stress-strain equations in 4.3-3 then reduce to

$$X_x = c_{11}e_{xx} + c_{12}e_{yy} + c_{13}e_{zz}$$

$$Y_y = c_{12}e_{xx} + c_{11}e_{yy} + c_{13}e_{zz}$$

$$Z_z = c_{13}e_{xx} + c_{13}e_{yy} + c_{33}e_{zz}$$

$$Y_z = c_{44}e_{yz}$$

$$Z_x = c_{44}e_{zx}$$

$$X_y = c_{66}e_{xy}$$

The number of elastic coefficients is thereby reduced from 21 to 5.

4.6.2 Propagation of Plane Waves

The phase velocities, V_i, corresponding to the three types of body waves which may be propagated can be determined as follows: The displacements u,v,w for plane waves propagated in the direction $\hat{\nu}$ = (l,m,n), as noted earlier, are given by equation 4.3-11. For the case of transversely isotropic media, all planes normal to the x-y plane are equivalent due to symmetry about the z-axis. Therefore, if the direction of propagation is chosen to be in the x-z plane, nothing has been lost with regard to the generality of the results, and it is possible to simplify the algebra (Bennett, 1968). Setting m = 0, the resulting form for the particle displacements in the x-z plane is:

$$(u,v,w) = (A_x,A_y,A_z)\exp[-ik(lx + ny - Vt)] \qquad (4.6\text{-}2)$$

The stress-strain equations (4.6-1) are then written in terms of the particle displacements

$$X_x = c_{11}\partial u/\partial x + c_{12}\partial v/\partial y + c_{13}\partial w/\partial z$$

$$Y_y = c_{12}\partial u/\partial x + c_{11}\partial v/\partial y + c_{13}\partial w/\partial z$$

$$Z_z = c_{13}\partial u/\partial x + c_{13}\partial v/\partial y + c_{33}\partial w/\partial z$$

$$Y_z = c_{44}(\partial v/\partial z + \partial w/\partial y)$$

$$Z_x = c_{44}(\partial w/\partial x + \partial u/\partial z)$$

$$X_y = c_{66}(\partial u/\partial y + \partial v/\partial x)$$

and these results put into the equations of small motion given by 4.3-9 (Bennett, 1968).

$$\rho\,\partial^2 u/\partial t^2 = c_{11}\partial^2 u/\partial x^2 + c_{66}\partial^2 u/\partial y^2 + c_{44}\partial^2 u/\partial z^2 + (c_{12} + c_{66})\partial^2 v/\partial x\partial y + (c_{13} + c_{44})\partial^2 w/\partial x\partial z$$

$$\rho\partial^2 v/\partial t^2 = c_{66}\partial^2 v/\partial x^2 + c_{11}\partial^2 v/\partial y^2 + c_{44}\partial^2 v/\partial z^2$$
$$+ (c_{12} + c_{66})\partial^2 u/\partial x\partial y + (c_{13} + c_{44})\partial^2 w/\partial y\partial z \qquad (4.6\text{-}4)$$
$$\rho\partial^2 w/\partial t^2 = c_{44}\partial^2 w/\partial x^2 + c_{44}\partial^2 w/\partial y^2 + c_{33}\partial^2 w/\partial z^2$$
$$+ (c_{13} + c_{44})\partial^2 u/\partial z\partial x + (c_{13} + c_{44})\partial^2 v/\partial y\partial z$$

The next step is to substitute for the particle displacements in terms of the plane wave solution. Since the plane wave is propagating in the x-z plane (m = 0), then all partials with respect to y are zero. Equations 4.6-4 then reduce to:

$$(l^2 c_{11} + n^2 c_{44} - \rho V^2)A_x + ln(c_{13} + c_{44})A_z = 0$$
$$(l^2 c_{66} + n^2 c_{44} - \rho V^2)A_y = 0 \qquad (4.6\text{-}5)$$
$$ln(c_{13} + c_{44})A_x + (l^2 c_{44} + n^2 c_{33} - \rho V^2)A_z = 0$$

The second of these equations is independent of A_x,A_z and can be solved immediately ($A_y \neq 0$) to give one of the three phase velocities. This velocity will be designated as V_3.

$$V_3^2 = l^2(c_{66}/\rho) + n^2(c_{44}/\rho) \qquad (4.6\text{-}6)$$

If the determinant of the remaining two equations is set equal to zero, solutions may be obtained for the other phase velocities.

$$\begin{vmatrix} l^2 c_{11} + n^2 c_{44} - \rho V^2 & ln(c_{13} + c_{44}) \\ ln(c_{13} + c_{44}) & l^2 c_{44} + n^2 c_{33} - \rho V^2 \end{vmatrix} = 0 \qquad (4.6\text{-}7)$$

Therefore,

$$V_{1,2}^2 = l^2\frac{c_{11}+c_{44}}{2\rho} + n^2\frac{c_{33}+c_{44}}{\rho} \pm \left[\left(l^2\frac{c_{11}-c_{44}}{2\rho} - n^2\frac{c_{33}-c_{44}}{2\rho}\right)^2 + l^2n^2\left(\frac{c_{13}+c_{44}}{\rho}\right)^2\right]^{\frac{1}{2}} \qquad (4.6\text{-}8)$$

In what is to follow, these wave types will be referred to as if

they were pure compressional and pure shear. In fact, they are quasi-compressional and quasi-shear since the particle motion is in general not exactly parallel or perpendicular to the direction of propagation (Bennett, 1968).

Bennett (1968) has shown that $V_{2,3}$ correspond to shear waves (SV, SH) and V_1 to a compressional (P) wave. If angles between the direction of propagation and the vertical are measured, the direction cosines l and n may be replaced by sin θ and cos θ respectively. Therefore,

$$V_{1,2}^2 = \sin^2\theta \underline{c}_{11}\frac{+c}{\rho}_{44} + \cos^2\theta \underline{c}_{33}\frac{+c}{\rho}_{44} \pm \left[\left(\sin^2\theta \underline{c}_{11}\frac{-c}{\rho}_{44} - \cos^2\theta \underline{c}_{33}\frac{-c}{\rho}_{44}\right)^2 + \sin^2\theta\cos^2\theta\left(\underline{c}_{13}\frac{+c}{\rho}_{44}\right)^2\right]^{\frac{1}{2}} \tag{4.6-9}$$

$$V_3^2 = \sin^2\theta \underline{c}_{\rho}^{66} + \cos^2\theta \underline{c}_{\rho}^{44}$$

The velocities parallel ($\theta = 0°$) and normal ($\theta = 90°$) to the z-axis are:

$$\begin{aligned} V_{1z}^2 &= c_{33}/\rho & V_{1x}^2 &= c_{11}/\rho \\ V_{2z}^2 &= c_{44}/\rho & V_{2x}^2 &= c_{44}/\rho \\ V_{3z}^2 &= c_{44}/\rho & V_{3x}^2 &= c_{66}/\rho \end{aligned} \tag{4.6-10}$$

4.6.3 Snell's Law for Transversely Isotropic Media

Fermat's minimum time principle will now be applied to determine the form that Snell's law takes for transverse isotropy. The procedure is identical to that discussed in section 4.4.3. Briefly, we wish to minimize the traveltime

$$T = \int ds/V = \int \sqrt{1 + \dot{x}^2}\, dz = \int f dz \qquad (4.4\text{-}6)$$

where as in 4.4.3 the minimization is accomplished by f satisfying the Euler-Lagrange equation (4.4-5). In the present case, the ray parameters corresponding to V_1, V_2, and V_3 are derived as follows: We may, for convenience, rewrite equations 4.6-6 and 4.6-8

$$V_{1,2}^2 = A\sin^2\theta + B\cos^2\theta \pm [(C\sin^2\theta - D\cos^2\theta)^2 + E\sin^2\theta\cos^2\theta]^{\frac{1}{2}}$$
$$V_3^2 = AA\sin^2\theta + BB\cos^2\theta \qquad (4.6\text{-}11)$$

where,

$$A = \frac{c_{11} \pm c_{44}}{2\rho}, \quad B = \frac{c_{33} \pm c_{44}}{2\rho}, \quad C = \frac{c_{11} - c_{44}}{2\rho}, \quad D = \frac{c_{33} - c_{44}}{2\rho},$$

$$E = \left(\frac{c_{13} \pm c_{44}}{\rho}\right), \quad AA = c_{66}/\rho, \quad BB = c_{44}/\rho$$

Then, our f-functions become (4.4-8):

$$f_{1,2} = \frac{\sqrt{1 + \tan^2\theta}}{V_{1,2}} = \frac{1 + \tan^2\theta}{[A\tan^2\theta + B \pm \{(C\tan^2\theta - D)^2 + E\tan^2\theta\}^{\frac{1}{2}}]^{\frac{1}{2}}}$$
$$f_3 = \frac{1 + \tan^2\theta}{[AA\tan^2\theta + BB]^{\frac{1}{2}}} \qquad (4.6\text{-}12)$$

However, since f is a function of tan θ alone, the ray parameters are again given by (4.4-9):

$$p_i = (\text{constant}) = \partial f_i/\partial\tan\theta; \quad i = 1,2,3 \qquad (4.6\text{-}13)$$

Therefore,

$$p_{1,2} = \frac{2\sin\theta}{V_{1,2}} - \frac{1}{V_{1,2}^3}\left\{A\sin^2\theta \pm \frac{C\sin\theta(C\sin^2\theta - D\cos^2\theta) + \frac{1}{2}E\sin\theta\cos^2\theta}{[(C\sin^2\theta - D\cos^2\theta)^2 + E\sin^2\theta\cos^2\theta]^{\frac{1}{2}}}\right.$$
$$p_3 = \frac{\tan\theta[AA(\tan^2\theta - 1) + 2BB]}{(AA\tan^2\theta + BB)^{3/2}} \qquad (4.6\text{-}14)$$

This is the resultant form of Snell's law for the three (P,SV,SH) wave components in a transversely isotropic medium. One important implica-

tion of equations 4.6-14 is that in a layered medium, if all components initially propagate away from the source at the same initial angle to the vertical, θ, then each component will follow a separate path through the medium. In the isotropic case, all body waves would follow the identical path through the medium since $p_1 = p_2 = p_3$.

4.7 Pseudo-Transverse Isotropy

Pseudo-transverse isotropy arises with a periodic variation in the elastic properties of an isotropic medium. The scale of the variations must be small compared to the wavelengths traversing the medium. In the limit as the ratio of wavelength to layer thickness becomes infinitely large, the traveltimes for events propagating in a pseudo-transversely isotropic medium become identical with those in a medium which is transversely isotropic at every point. This form of transverse isotropy has two important aspects. First, a simple mechanism is provided for producing anisotropic wave propagation in geologically realistic media. Second, the theory, as developed, allows the computation of the five elastic coefficients corresponding to a given degree of anisotropy (anisotropy factor).

The majority of the material that follows has been taken from Postma (1955) and his terminology will be used throughout. If we assume the geological situation envisioned by Postma, we have a stratified medium consisting of a large number of alternating plane, parallel layers of two homogeneous, isotropic materials for which the elastic behavior is given by Lame's constants λ_1,μ_1 and λ_2,μ_2 respectively. The layer thickness for the first material is d_1; for the second it is d_2. Take the z-axis perpendicular and the x and y axes parallel to the layers, and consider an elementary rectangular parallelopiped with faces parallel to the coordinate planes. Let the height of the parallelopiped be $n(d_1+d_2)$, where n is an integer (See Figure 4.7-1).

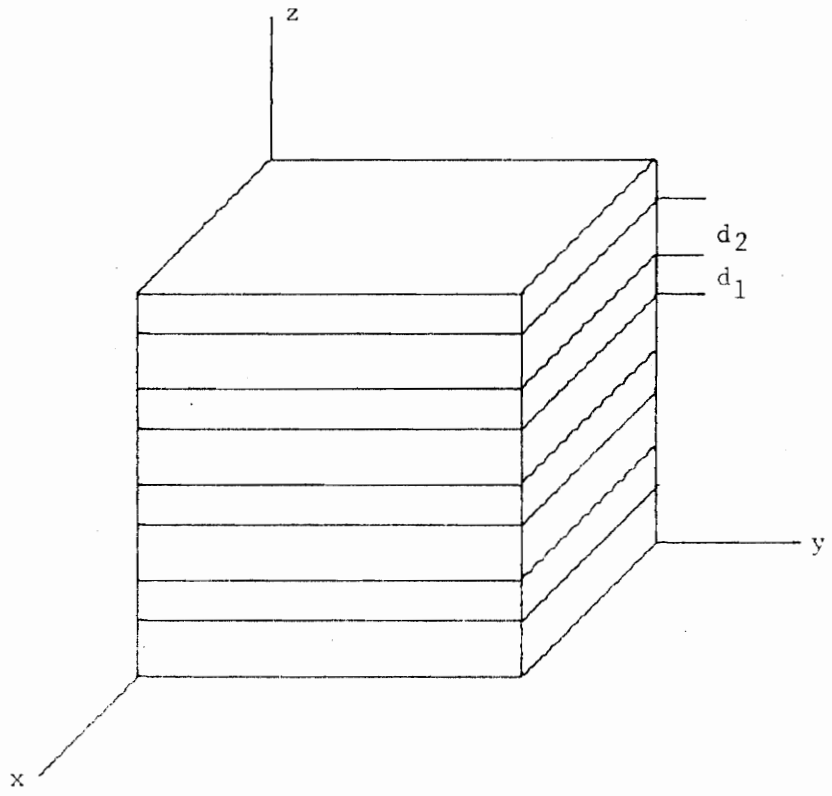

Figure 4.7-1. Elementary Volume of Stratified Medium (Postma, 1955)

Suppose that on the faces perpendicular to the z-axis a normal stress Z_z is exerted and that there are no tangential components Y_z X_z. On the faces perpendicular to the x-axis we also have only normal stresses, i.e., a normal stress X_{x1} on the layers d_1 and a normal stress X_{x2} on the layers d_2. Similiarly, we have on the faces perpendicular to the y-axis normal stresses Y_{y1} and Y_{y2}. The normal stresses $X_{x1}, X_{x2}, Y_{y1}, Y_{y2}$ are such that $e_{xx1} = e_{xx2} = e_{xx}$ and $e_{yy1} = e_{yy2} = e_{yy}$, where e_{xx1} is the linear dilatation of a line element in the direction of the x-axis in the layers d_1, etc. This restriction is necessary to insure the continuity of the displacement as a function of the radius vector. The linear dilatation of a linear element parallel to the z-axis in the d_1 layers is e_{zz1}; in the d_2 layers it is e_{zz2}. In general $e_{zz1} \neq e_{zz2}$.

In the first isotropic medium, Hooke's law gives:

$$\begin{aligned} X_{x1} &= (\lambda_1 + 2\mu_1)e_{xx} + \lambda_1 e_{yy} + \lambda_1 e_{zz1} \\ Y_{y1} &= \lambda_1 e_{xx} + (\lambda_1 + 2\mu_1)e_{yy} + \lambda_1 e_{zz1} \\ Z_z &= \lambda_1 e_{xx} + \lambda_1 e_{yy} + (\lambda_1 + 2\mu_1)e_{zz1}. \end{aligned} \tag{4.7-1}$$

The equations for the second isotropic layer are obtained by replacing the index 1 by the index 2. The average stress on a face perpendicular to the x-axis becomes

$$X_x = \frac{d_1 X_{x1} + d_2 X_{x2}}{d_1 + d_2}, \tag{4.7-2}$$

and on a face perpendicular to the y-axis,

$$Y_y = \frac{d_1 Y_{y1} + d_2 Y_{y2}}{d_1 + d_2}, \tag{4.7-3}$$

while the stress on the face perpendicular to the z-axis is Z_z.

From the above equations, we find:

$$\begin{aligned}
(d_1 + d_2)X_x &= e_{xx}[d_1(\lambda_1 + 2\mu_1) + d_2(\lambda_2 + 2\mu_2)] \\
&\quad + e_{yy}(\lambda_1 d_1 + \lambda_2 d_2) + e_{zz1}\lambda_1 d_1 + e_{zz2}\lambda_2 d_2 \\
(d_1 + d_2)Y_y &= e_{yy}[d_1(\lambda_1 + 2\mu_1) + d_2(\lambda_2 + 2\mu_2)] \\
&\quad + e_{xx}(\lambda_1 d_1 + \lambda_2 d_2) + e_{zz1}\lambda_1 d_1 + e_{zz2}\lambda_2 d_2 \\
(d_1 + d_2)Z_z &= e_{xx}(\lambda_1 d_1 + \lambda_2 d_2) + e_{yy}(\lambda_1 d_1 + \lambda_2 d_2) \\
&\quad + e_{zz1}d_1(\lambda_1 + 2\mu_1) + e_{zz2}d_2(\lambda_2 + 2\mu_2).
\end{aligned} \tag{4.7-4}$$

We define e_{zz} by

$$(d_1 + d_2)e_{zz} = d_1 e_{zz1} + d_2 e_{zz2}, \tag{4.7-5}$$

where e_{zz} is the overall dilatation of a linear element parallel to the z-axis, which contains an equal number of sections through the layers d_1 and d_2. Solving the above equations for e_{zz1} and e_{zz2}:

$$\begin{aligned}
e_{zz1} &= \frac{(d_1 + d_2)(\lambda_2 + 2\mu_2) - (\lambda_1 - \lambda_2)(e_{xx} + e_{yy})d_2}{d_1(\lambda_2 + 2\mu_2) + d_2(\lambda_1 + 2\mu_1)} \\
e_{zz2} &= \frac{(d_1 + d_2)(\lambda_1 + 2\mu_1) + (\lambda_1 - \lambda_2)(e_{xx} + e_{yy})d_1}{d_1(\lambda_2 + 2\mu_2) + d_2(\lambda_1 + 2\mu_1)}.
\end{aligned} \tag{4.7-6}$$

Substituting these results into the stress-strain equations,

$$\begin{aligned}
X_x &= \frac{e_{xx}}{D}\Big[(d_1+d_2)^2(\lambda_1+2\mu_1)(\lambda_2+2\mu_2)+d_1 d_2\{[(\lambda_1+2\mu_1)-(\lambda_2+2\mu_2)]^2 \\
&\quad - (\lambda_1-\lambda_2)^2\}\Big] \\
&\quad + \frac{e_{yy}}{D}\{\lambda_1\lambda_2(d_1+d_2)^2 + 2(\lambda_1 d_1+\lambda_2 d_2)(\mu_2 d_1+\mu_1 d_2)\} \\
&\quad + \frac{e_{zz}}{D}\{(d_1+d_2)[\lambda_1 d_1(\lambda_2+2\mu_2) + \lambda_2 d_2(\lambda_1+2\mu_1)]\} \\
Y_y &= \frac{e_{xx}}{D}\{\lambda_1\lambda_2(d_1+d_2)^2 + 2(\lambda_1 d_1+\lambda_2 d_2)(\mu_2 d_1+\mu_1 d_2)\}
\end{aligned} \tag{4.7-7}$$

$$+ \frac{e_{yy}}{D}\{(d_1+d_2)^2(\lambda_1+2\mu_1)(\lambda_2+2\mu_2)+d_1d_2\{[(\lambda_1+2\mu_1)-(\lambda_2+2\mu_2)]^2$$

$$- (\lambda_1-\lambda_2)^2\}\}$$

$$+ \frac{e_{zz}}{D}\{(d_1+d_2)[\lambda_1d_1(\lambda_2+2\mu_2) + \lambda_2d_2(\lambda_1+2\mu_1)]\}$$

$$Z_z = \frac{(e_{xx}+e_{yy})}{D}\{(d_1+d_2)[\lambda_1d_1(\lambda_2+2\mu_2) + \lambda_2d_2(\lambda_1+2\mu_1)]\}$$

$$+ \frac{e_{zz}}{D}\{(d_1+d_2)^2(\lambda_1+2\mu_1)(\lambda_2+2\mu_2)\}$$

where D is written for $(d_1+d_2)[d_1(\lambda_2+2\mu_2) + d_2(\lambda_1+2\mu_1)]$.

Proceeding in the same way by applying to the faces perpendicular to the z-axis a tangential stress Y_z, we have:

$$(d_1 + d_2)e_{yz} = d_1e_{yz1} + d_2e_{yz2}$$
$$Y_z = \mu_1e_{yz1}, \quad Y_z = \mu_2e_{yz2} \qquad (4.7\text{-}8)$$

Therefore,

$$(d_1 + d_2)e_{yz} = [d_1/\mu_1 + d_2/\mu_2]Y_z \qquad (4.7\text{-}9)$$

$$\text{or } Y_z = \frac{(d_1 + d_2)\mu_1\mu_2e_{yz}}{d_1\mu_2 + d_2\mu_1}$$

Similarly, we find:

$$(d_1 + d_2)e_{zx} = [d_1/\mu_1 + d_2/\mu_2]X_z \qquad (4.7\text{-}10)$$

$$\text{and } X_z = \frac{(d_1 + d_2)\mu_1\mu_2e_{zx}}{d_1\mu_2 + d_2\mu_1}.$$

Finally applying a tangential force to the faces perpendicular to the y-axis of the d_1 layers and to the corresponding faces of the d_2 layers and realizing that e_{xy1} must be equal to e_{xy2} in order to insure the continuity of the displacement, we find that $X_{y1} = \mu_1e_{xy}$; $X_{y2} = \mu_2e_{xy}$, so that when X_y is the average tangential stress on the parall-

opiped,

$$(d_1 + d_2)X_y = d_1X_{y1} + d_2X_{y2} = (\mu_1 d_1 + \mu_2 d_2)e_{xy}$$
$$\text{or } X_y = \frac{\mu_1 d_1 + \mu_2 d_2}{d_1 + d_2} e_{xy}. \qquad (4.7\text{-}11)$$

Comparing these results with those for the stress-strain matrix coefficients (equation 4.6-1), we see that, when viewed on a proper scale, the layered medium may be considered as transversely isotropic. The resulting elastic coefficients are:

$$c_{11} = \frac{1}{D}\{(d_1+d_2)^2(\lambda_1+2\mu_1)(\lambda_2+2\mu_2) + 4d_1d_2(\mu_1 - \mu_2)[(\lambda_1+\mu_1) - (\lambda_2+\mu_2)]\}$$

$$c_{12} = \frac{1}{D}\{(d_1+d_2)^2\lambda_1\lambda_2 + 2(\lambda_1 d_1+\lambda_2 d_2)(\mu_2 d_1+\mu_1 d_2)\}$$

$$c_{13} = \frac{1}{D}\{(d_1+d_2)[\lambda_1 d_1(\lambda_2+2\mu_2) + \lambda_2 d_2(\lambda_1+2\mu_1)]\} \qquad (4.7\text{-}12)$$

$$c_{33} = \frac{1}{D}\{(d_1+d_2)^2(\lambda_1+2\mu_1)(\lambda_2+2\mu_2)\}$$

$$c_{44} = \frac{(d_1+d_2)\mu_1\mu_2}{d_1\mu_2+d_2\mu_1}$$

$$c_{66} = \frac{\mu_1 d_1+\mu_2 d_2}{d_1+d_2}$$

Among c_{11}, c_{12}, and c_{66} there exists the relation $c_{66} = \frac{1}{2}(c_{11} - c_{12})$ as becomes apparent by substitution. It must be noted that these coefficients are dependent upon the combined properties of the layers and not only upon their individual properties. Consequently, this theory is applicable only at wavelengths sufficiently long that a single wavelength samples many layers simultaneously and hence "sees" a composite medium and not the individual layers.

Once we know the form of these elastic coefficients in terms of the properties of the individual layers and their relative thicknesses d_1 and d_2, the proper elastic coefficients may then be specified for a transversely isotropic medium of any degree of anisotropy. The anisotropy factor was defined earlier (Chapter 2) as the ratio of the velocity (compressional) parallel to the layers to the velocity normal to the layers, i.e.,

$$A = \sqrt{c_{11}/\rho} \; / \; \sqrt{c_{33}/\rho} = \sqrt{c_{11}/c_{33}} \tag{4.7-13}$$

However, from equations 4.7-12, we may write:

$$A^2 = \frac{c_{11}}{c_{33}} = 1 + \frac{4d_1d_2(\mu_1-\mu_2)[(\lambda_1+2\mu_1) - (\lambda_2+2\mu_2)]}{(d_1+d_2)^2(\lambda_1+2\mu_1)(\lambda_2+2\mu_2)}. \tag{4.7-14}$$

When it is assumed that the layer properties are fixed, then the anisotropy is solely dependent on the relative sizes of d_1 and d_2. The procedure adopted herein for purposes of calculating synthetic models is to set $d_1 = 1$, and then to solve 4.7-14 for the value of d_2 necessary to yield the desired value of A.

There is a limiting value of A (4.7-14) beyond which either d_1 or d_2 becomes complex. If we require that d_1 and d_2 are always real and positive, then an upper limit exists for A for a given set of elastic constant pairs λ_1,μ_1 and λ_2,μ_2. This may be demonstrated by rewriting 4.7-14 in terms of Poisson's ratio as follows:

$$\begin{aligned} A^2 &= 1 + \frac{4d_1d_2}{(d_1+d_2)^2}\left(\frac{\mu_1-\mu_2}{\lambda_2+2\mu_2} + \frac{\mu_2-\mu_1}{\lambda_1+2\mu_1}\right) \\ &= 1 + \frac{4d_1d_2}{(d_1+d_2)^2}\left(\frac{\mu_1/\mu_2-1}{\lambda_2/\mu_2+2} + \frac{\mu_2/\mu_1-1}{\lambda_1/\mu_1+2}\right) \end{aligned} \tag{4.7-15}$$

We may now introduce the identity

$$\lambda/\mu + 2 = 2(1 - \sigma)/(1 - 2\sigma) \tag{4.7-16}$$

where σ is Poisson's ratio.

Therefore,

$$A^2 = 1 + \frac{2d_1d_2}{(d_1+d_2)^2}\left[\frac{(\mu_1/\mu_2-1)(1-2\sigma_2)}{1-\sigma_2} + \frac{(\mu_2/\mu_1-1)(1-2\sigma_1)}{1-\sigma_1}\right] \tag{4.7-17}$$

If, for the sake of computational ease, we let $\sigma_1 = \sigma_2 = \sigma$, then immediately we may write:

$$A^2 = 1 + \frac{2d_1d_2}{(d_1+d_2)^2}\cdot\frac{1 - 2\sigma}{1 - \sigma}\cdot\frac{(\mu_1 - \mu_2)}{\mu_1\mu_2} \tag{4.7-18}$$

Equations 4.7-17 and 4.7-18 have maximum values for $d_1 = d_2$ which may be shown by differentiating and setting $dA^2 = 0$. If $d_1 = d_2$, then

$$A_{max}^2 = 1 + \frac{1}{2}\cdot\frac{1 - 2\sigma}{1 - \sigma}\cdot\frac{(\mu_1 - \mu_2)^2}{\mu_1\mu_2} \tag{4.7-19}$$

Therefore, the maximum anisotropy is directly dependent on the difference between the shear moduli μ_1 and μ_2. It is also obvious that for both equations 4.7-17 and 4.7-18 that media properties again behave isotropically in the case that $\mu_1 = \mu_2$.

The proper scale for the application of this theory to be valid is such in general that the wavelength of the elastic waves propagating through the medium is conventionally of the order of five to ten times as long as the individual lithologic unit thicknesses. Furthermore, once we have specified the velocities of the individual isotropic layers, all that remains is to specify a value for an anisotropy factor, A, and then all of the relations among the individual velocities of the equivalent transversely isotropic section are determined. We may go one step further and scale the elastic coefficients either up or down.

Now, we have the capability of generating transversely isotropic elastic coefficients for any velocity range that is desired, the implication being that for any given level of anisotropy we need only specify a single velocity component of the system to uniquely determine all other corresponding velocities.

4.8 Summary

The theory necessary for analyzing wave propagation in anisotropic media has been developed for the general case and for several specific forms of anisotropy. The isotropic case was presented for purposes of comparison with the various anisotropic cases, refraction at an interface is no longer the simple situation that exists for the isotropic case since each wave component may propagate along a separate path through a layered medium. For the particular case of transversely isotropic media, techniques have been developed that allow for the computation of the five elastic coefficients corresponding to a given degree of anisotropy. This development will later make practical the analysis of seismic reflection data for anisotropy without the shortcomings associated with the theory of elliptical anisotropy.

5. Seismic Reflection Data

5.1 Introduction

The seismic reflection data used in this study are entirely synthetic which makes it possible to exercise complete control over the data. This control provides a basis for judgment of the efficiency of the data analysis techniques. In addition, in the early stages of development of new analytical methods, it is desirable to be able to work with noise-free data. This situation rarely, if ever, arises with field data. Coherent noise arising from ghosts, multiples, diffraction, etc. was never added to the synthetic data. The analysis of such noise constitutes a separate problem and this omission in no way invalidates the analysis techniques developed in later chapters.

A variety of synthetic earth models is studied. Each model is characterized by a particular form of variation of seismic velocity with depth. The principal reason for using such a variety of models is to demonstrate that the data analysis methods are independent of any particular model.

5.2 Ray-Path Computation

In reflection seismology, the quantity of direct interest is the two-way reflection traveltime between shot and geophone. The mathematical method used herein to obtain this traveltime consists of a numerical integration along the ray from the shotpoint to the reflection-point, and then from the reflection-point to the geophone. The equation for the total traveltime is

$$T = \int_c ds/V \qquad (5.2\text{-}1)$$

where T is the traveltime and c represents the path (ray) along which Snell's law holds. V is the velocity function and ds is an element of arc length defined as:

$$ds^2 = dx^2 + dz^2 \qquad (5.2\text{-}2)$$

where the geometry is the same as that discussed in chapter 4. A digital computer program was written to perform the numerical integration indicated of equation 5.2-1 and is discussed in the Appendix (See subroutine DREFL in Appendix).

5.3 Velocity Functions

The velocity finctions to be discussed all describe the velocity associated with the elastic coefficient c_{11}. All other velocities will depend on the degree of anisotropy present. This choice of c_{11} allows for the ready comparison of models that differ only in the amount of anisotropy.

The particular velocity models chosen illustrate a reasonable diverse range of possibilities. The five basic models to be used are a uniform halfspace, a section with velocity increasing linearly with depth, a discrete stepwise increase of velocity with depth, an isotropic stepwise increase of velocity containing a buried anisotropic interval, and a linear increase of velocity with continuously changing dip as a function of depth. The velocity functions for each model are displayed in figures referenced in the discussions of individual models. Each figure contains both interval and rms (root-mean-square) velocities. The interval velocity cirve represents the actual medium velocity variation vs. depth. The rms velocity curve represents the "average" velocity associated with a reflection arriving from a particular depth at a specific two-way reflection time. A more complete discussion of the relationship between rms and interval velocity is given in chapter 6. The interval velocity plotted for the P velocity component is the horizontal velocity component.

5.3.1 Single Anisotropic Layer

This model is a homogeneous half-space. Because it is uncomplica-

ted, the effects of normal moveout (isotropic or anisotropic) may be studied without complications due to variations of velocity. Normal moveout is defined, as usual, as the difference in two-way reflection time for a geophone located some distance away from the shotpoint as compared with the two-way traveltime for a normal incidence reflection. The velocity function used is simply:

$$V = 8000 \text{ ft/sec} \qquad (5.3\text{-}1)$$

In order to obtain reflections within such a medium, this velocity must be considered as an average velocity. Small perturbations of the actual velocity about this average give rise to the reflections.

5.3.2 Linear Increase of Velocity with Depth

This velocity function has often been used to represent the variation of velocity with depth of burial in sedimentary basins. The velocity function used is (See Figure 5.3-1):

$$V = 8000 + z \text{ ft/sec} \qquad (5.3\text{-}2)$$

5.3.3 Stepwise Increase of Velocity with Depth

This velocity model has been used extensively in synthetic modelling for many years. The particular form of step increase used here is to start with a surface velocity of 8000 ft/sec and every 100 ft in depth to increase the velocity by an additional 100 ft/sec. This velocity function is shown in Figure 5.3-2.

5.3.4 Buried Anisotropic Interval

This model was generated primarily to test the sensitivity of an-

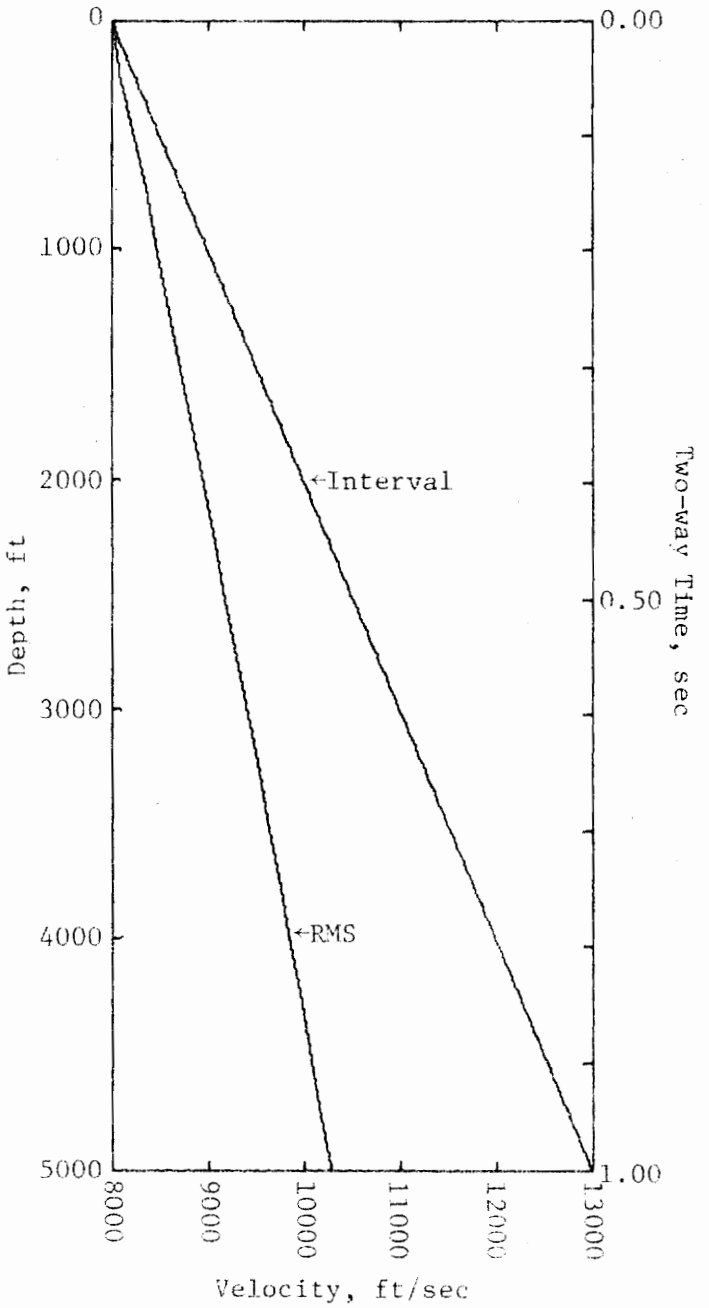

Figure 5.3-1a. Linear Increase of Velocity
Interval and RMS Velocities
P Component

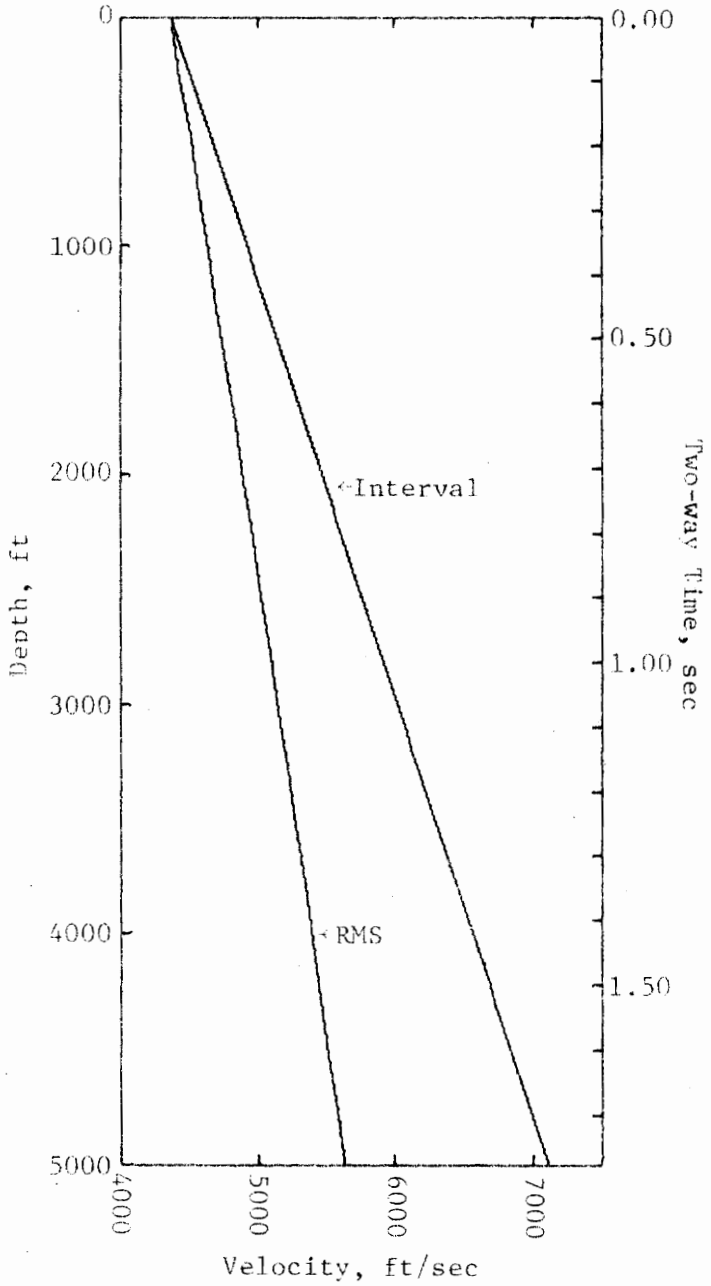

Figure 5.3-1b. Linear Increase of Velocity
Interval and RMS Velocities
SV Component

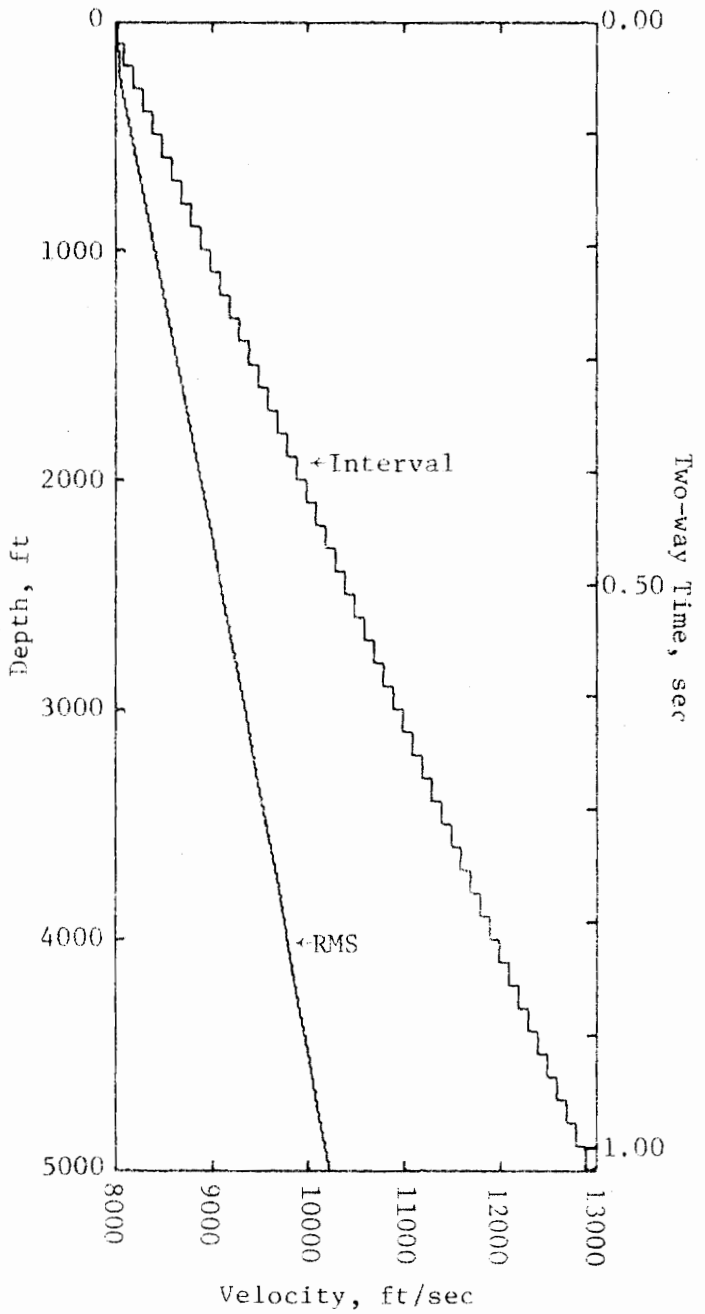

Figure 5.3-2a. Stepwise Increase of Velocity Interval and RMS Velocities
P Component

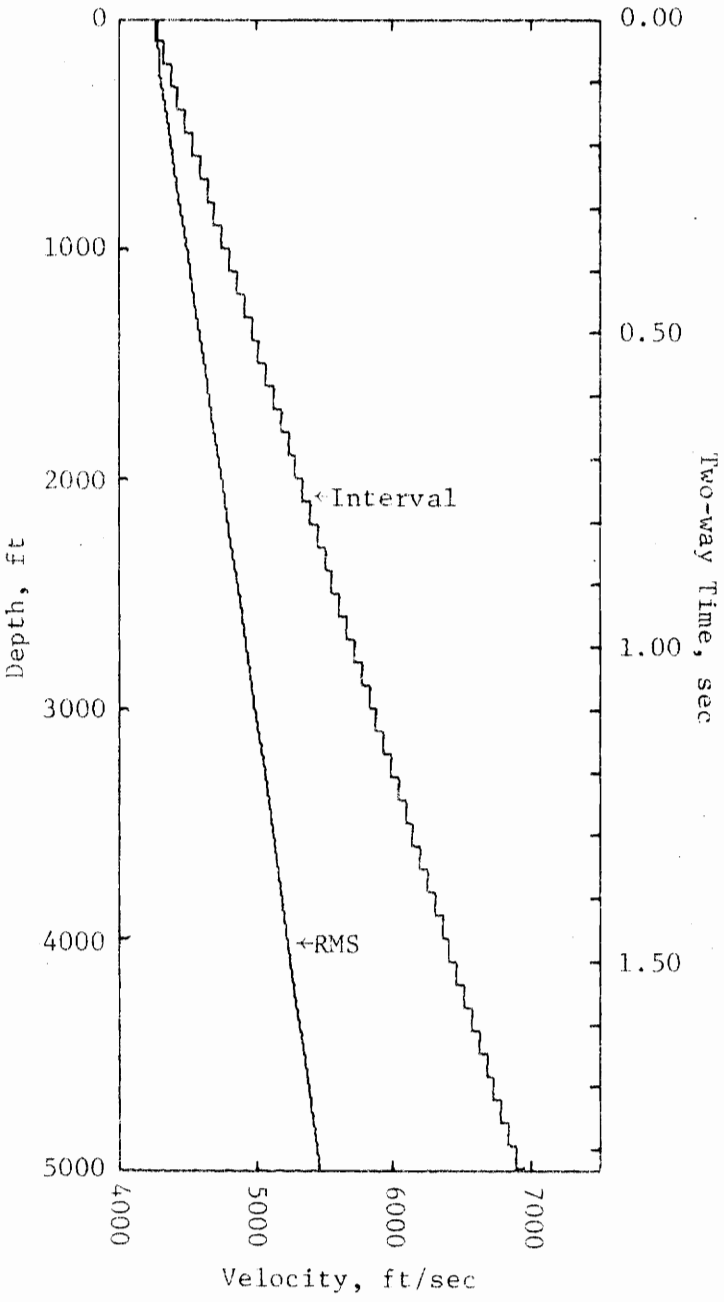

Figure 5.3-2b. Stepwise Increase of Velocity Interval and RMS Velocities
SV Component

alysis methods to changes in the degree of anisotropy. The model is isotropic from the surface to a depth of 3000 ft and is again isotropic for depths greater than 4000 ft. The interval from 3000 to 4000 ft is transversely isotropic with an anisotropy factor of 1.10. The velocity function used is shown in Figure 5.3-3 and is identical to that described in 5.3.3.

5.3.5 Continuously Changing Dip

Two models are employed to demonstrate some of the difficulties encountered in the analysis of data where the strata are dipping and where the amount of dip continuously changes (See Figure 5.3-4). Geologically these models might simulate a deltaic or offshore sedimentary section. In an even more general context, these models are important because dipping strata are frequently encountered in exploration. Because the theory used in the analysis of field data generally assumes flat lying strata, these models will be useful in pointing out the limitations imposed by geologically reasonable departures from that assumption. The continuous increase of dip with depth is also useful in the determination of the maximum amount of dip that may be present without significantly degrading the subsequent analysis of the seismic data.

The first model will be referred to as the polar velocity model and it has the following velocity function:

$$V = 8000 + kR\theta \text{ ft/sec} \qquad (5.3\text{-}3)$$

where θ is the angle of dip in radians, R is the radial distance from

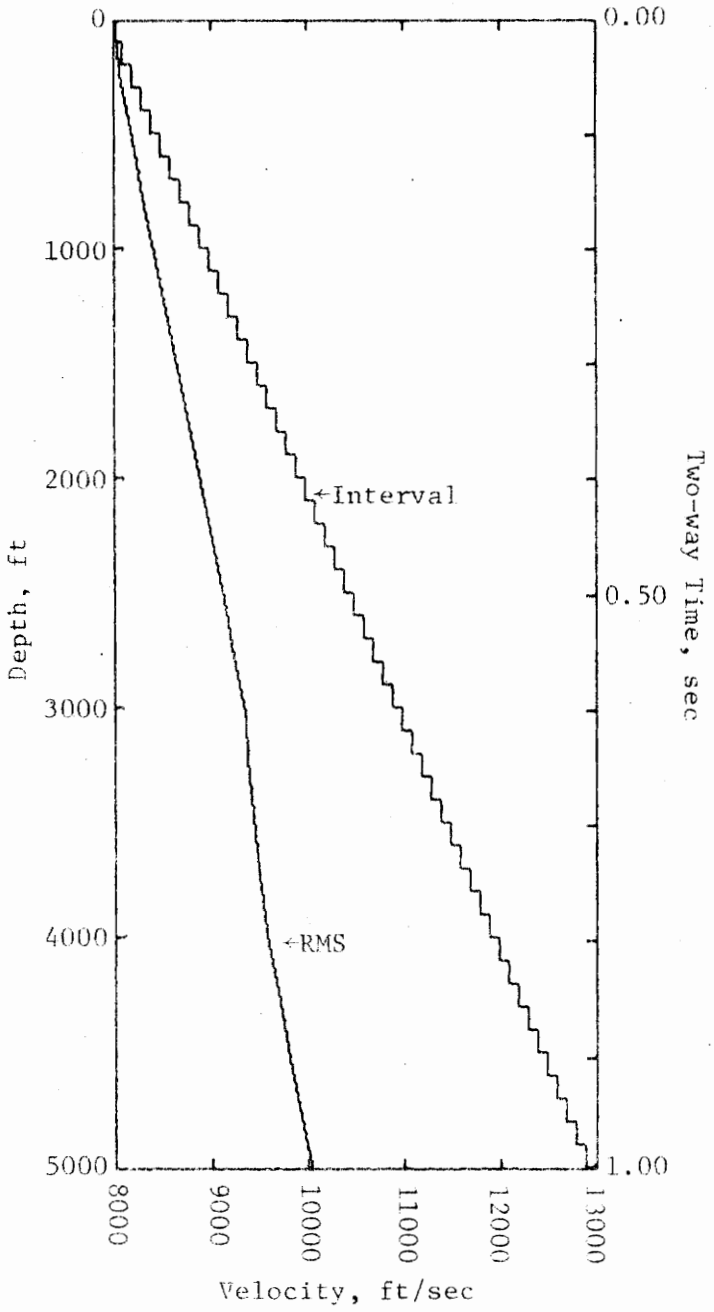

Figure 5.3-3a. Buried Anisotropic Section
Interval and RMS Velocities
P Component

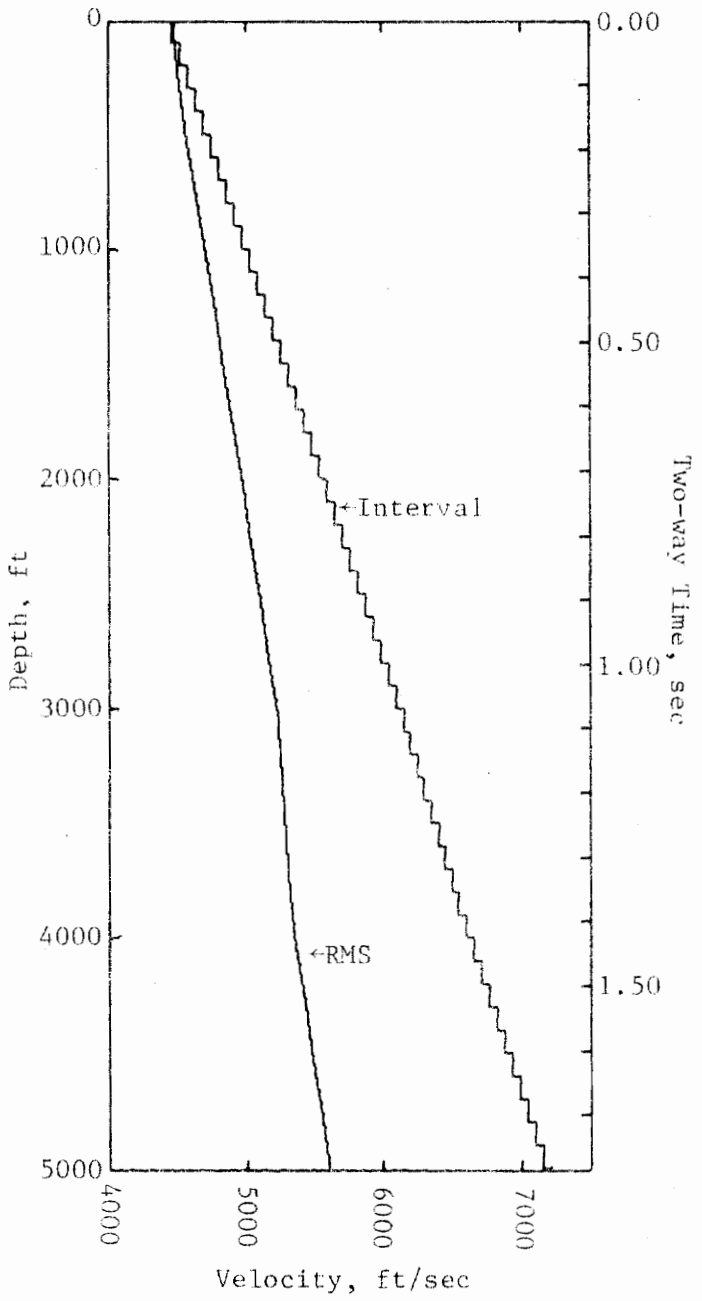

Figure 5.3-3b. Buried Anisotropic Section
Interval and RMS Velocities
SV Component

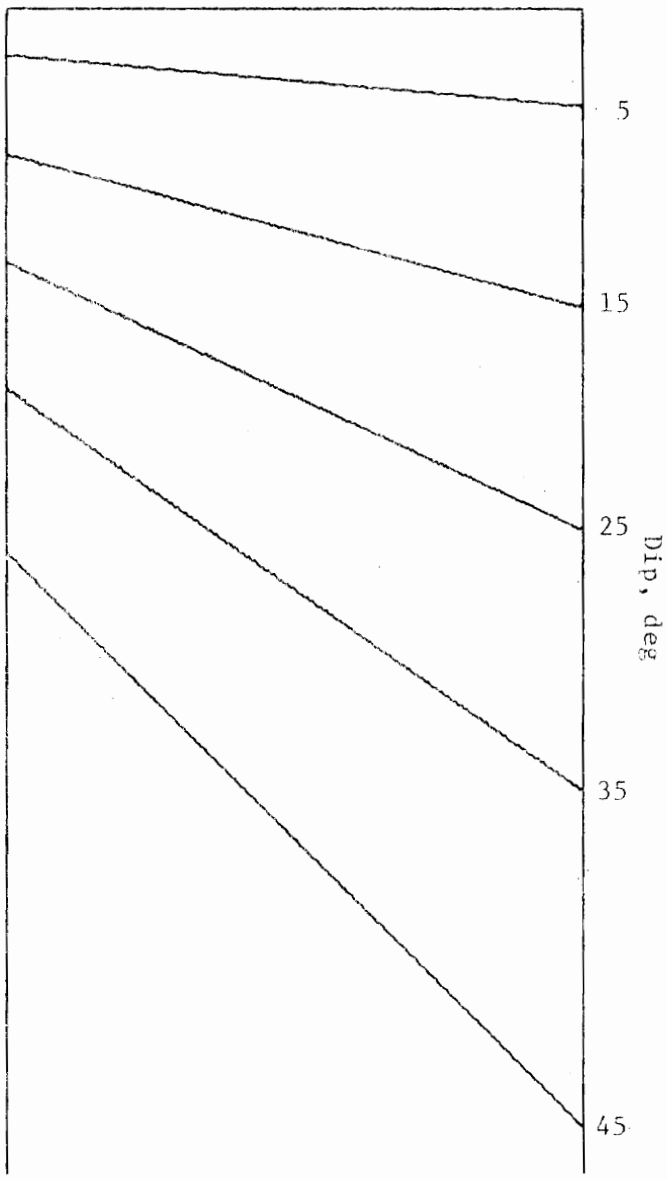

Figure 5.3-4. Continuous Dip Models
Layering Geometry

a center of curvature, and k is a constant with fixed values for various ranges of θ. These values are: $k = 0$ for $\theta < 5°$, $k = 0.1$ for $5° < \theta < 15°$, $k = 0.2$ for $15° < \theta < 25°$, $k = 0.3$ for $25° < \theta < 35°$, and $k = 0.4$ for $35° < \theta < 45°$.

The second model will be known as the constant velocity dipping layer model. The layer geometry is identical to that of the polar velocity model and is also shown by Figure 5.3-4. The velocity function for the constant velocity dipping layer model is: $V = 8000$ ft/sec for $\theta < 5°$, $V = 9000$ ft/sec for $5° < \theta < 15°$, $V = 10000$ ft/sec for $15° < \theta < 25°$, $V = 11000$ ft/sec for $25° < \theta < 35°$, and $V = 12000$ ft/sec for $35° < \theta < 45°$. The initial shotpoint used with both models is for $R = 5000$ ft. The geophones would be located at still greater values of R. The velocity functions for these models are shown graphically in Figures 5.3-5 and 5.3-6.

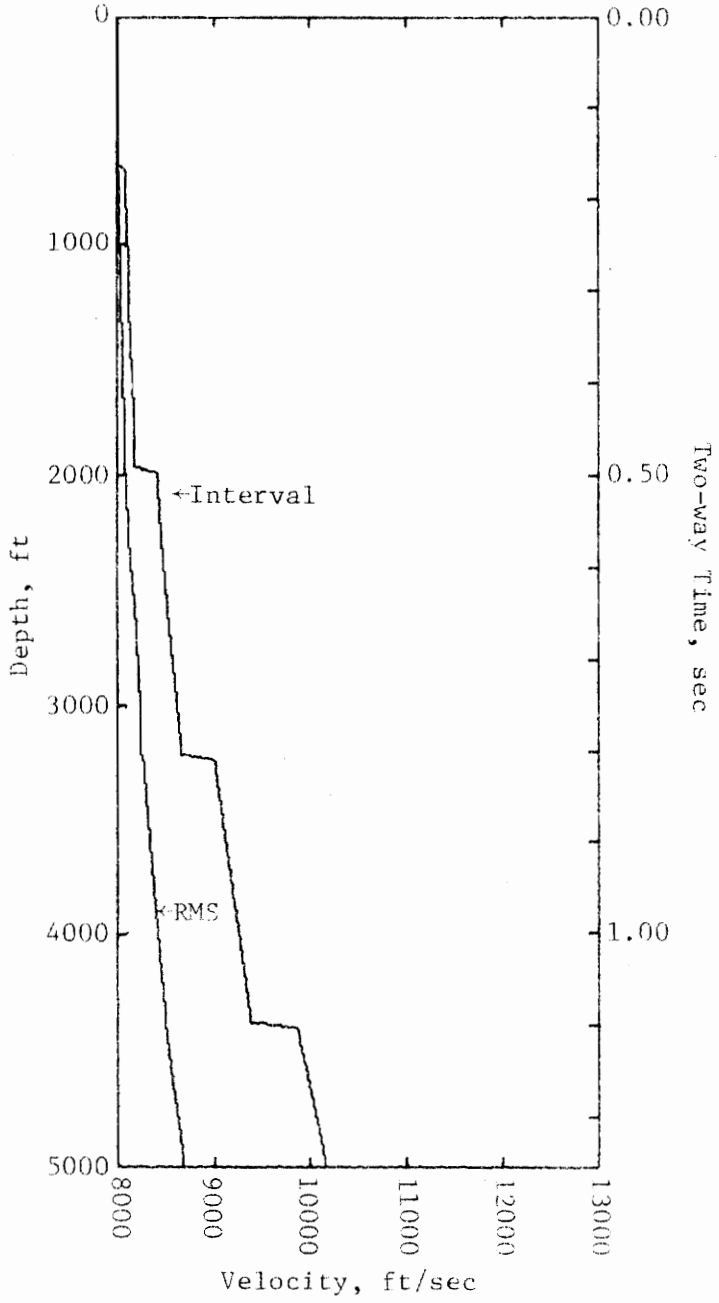

Figure 5.3-5a. Continuously Varying Dip
Polar Velocity Model
Interval and RMS Velocities
P Component

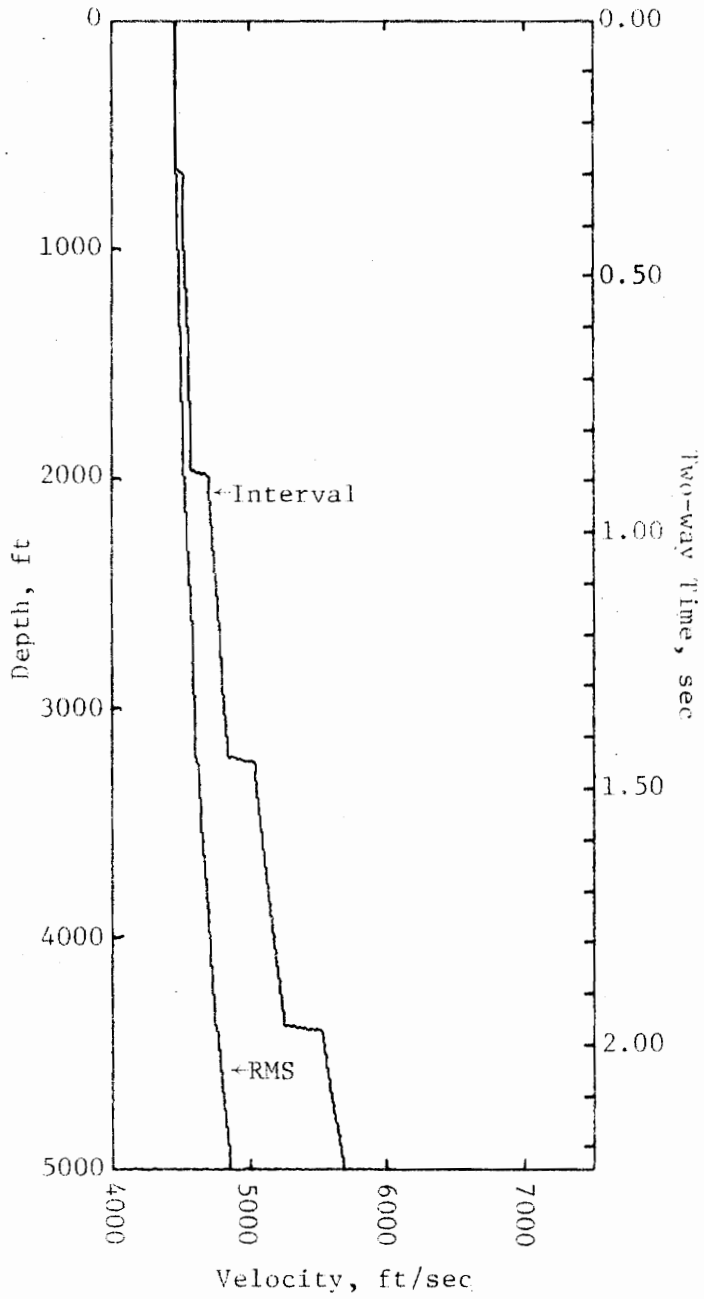

Figure 5.3-5b. Continuously Varying Dip
Polar Velocity Model
Interval and RMS Velocities
SV Component

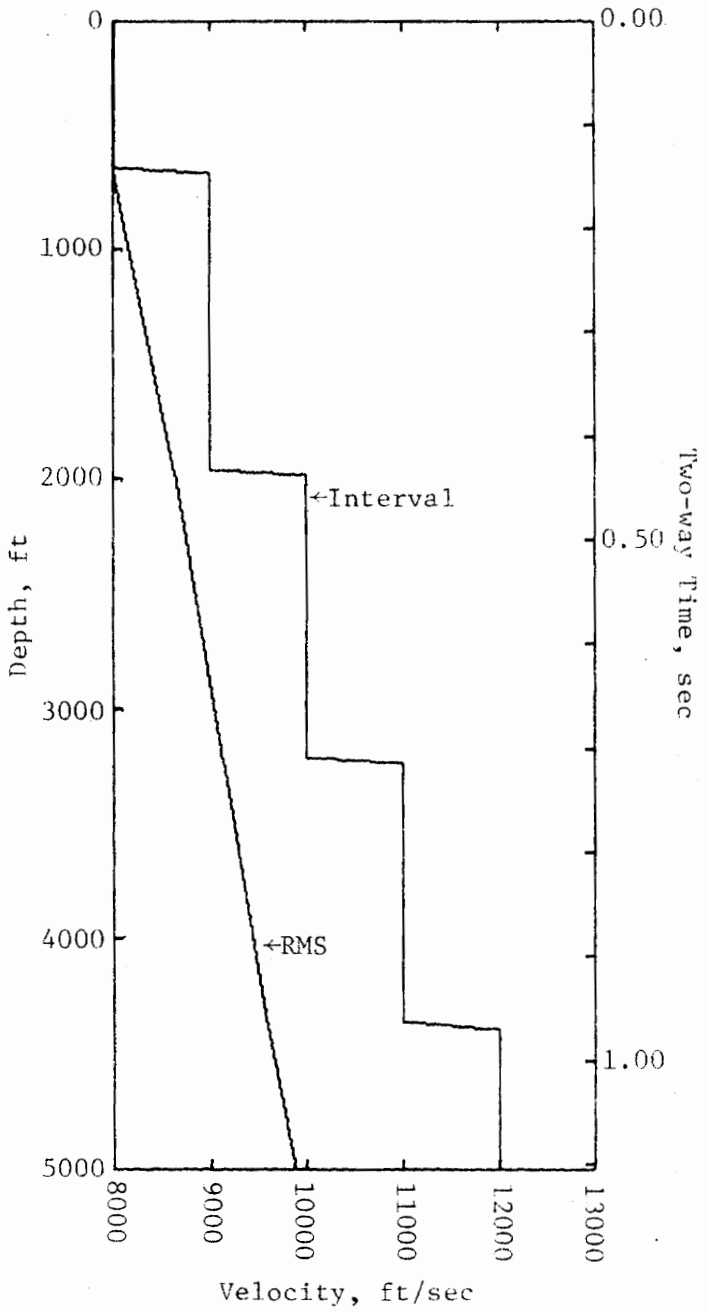

Figure 5.3-6a. Continuously Varying Dip
Constant Velocity Dipping Layers
Interval and RMS Velocities
P Component

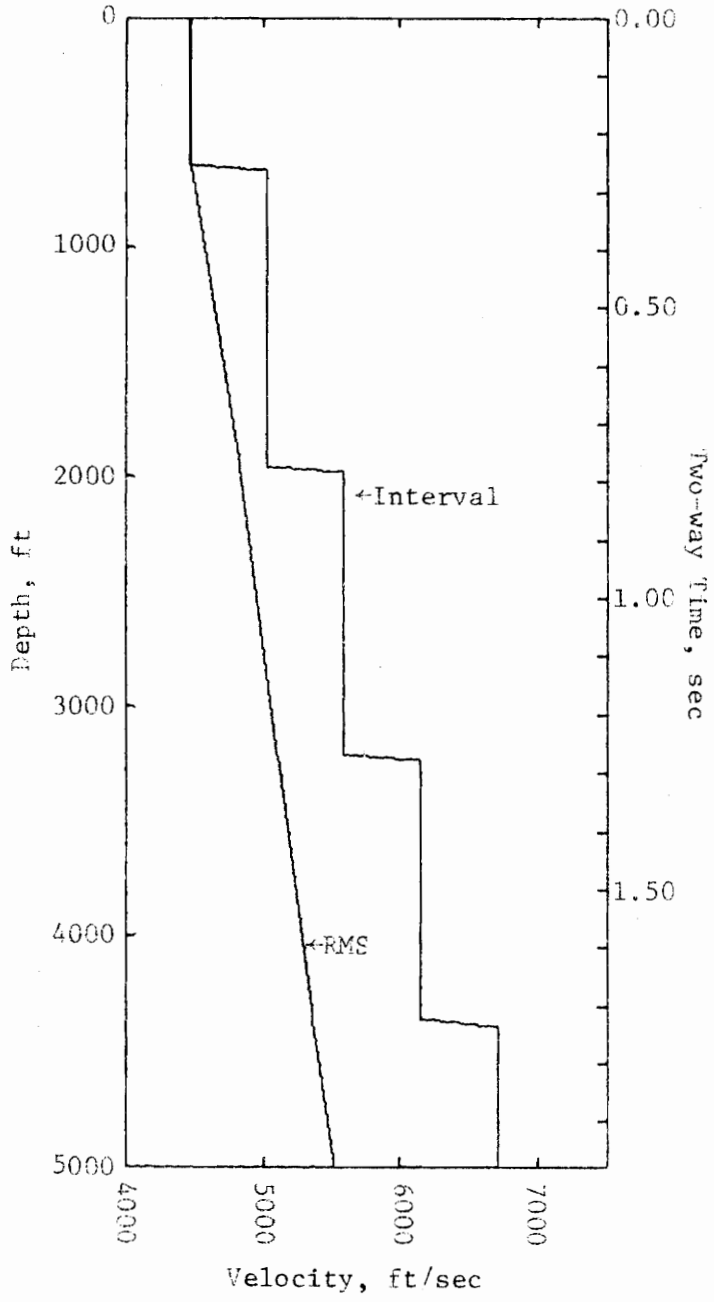

Figure 5.3-6b. Continuously Varying Dip
Constant Velocity Dipping Layers
Interval and RMS Velocities
SV Component

5.4 Synthetic Seismograms

The arrival times for reflections are computed by the techniques described in section 5.2. At this stage in the generation of the synthetic data there exists only a set of arrival times corresponding to a given shot-geophone distance and reflector geometry and, as such, these data do not constitute a seismogram. Corresponding to each reflector there is associated a reflection coefficient. In the synthetic seismograms used in this work a series of random numbers has been used to simulate the reflection coefficients associated with the reflectors. This choice of random numbers is appropriate since actual reflection coefficients determined experimentally from field data using continuous velocity well logs have been found to be approximately randomly distributed (Agard and Grau, 1961; Warnaca and Ferree, 1967). A seismogram is then created by convolving a seismic wavelet (See Figure 5.4-1) with the reflection coefficients (See Figure 5.4-2) which are spaced at times corresponding to the two-way traveltimes to the reflectors. If a sufficient number of closely spaced reflections are used, the resultant seismogram will be continuous rather than consisting of discrete events, and such a seismogram looks and processes much like field data. Finally, random noise may be added to the synthetic seismograms to further simulate conditions associated with field data. Figure 5.4-3 is an example of one set of noise-free synthetic seismograms used in this work.

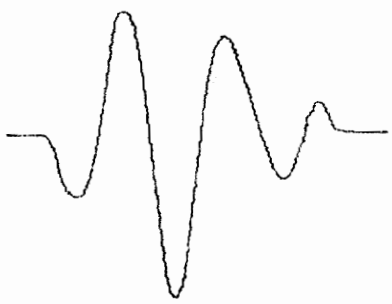

Figure 5.4-1. Seismic Wavelet

Figure 5.4-2. Reflection Coefficients

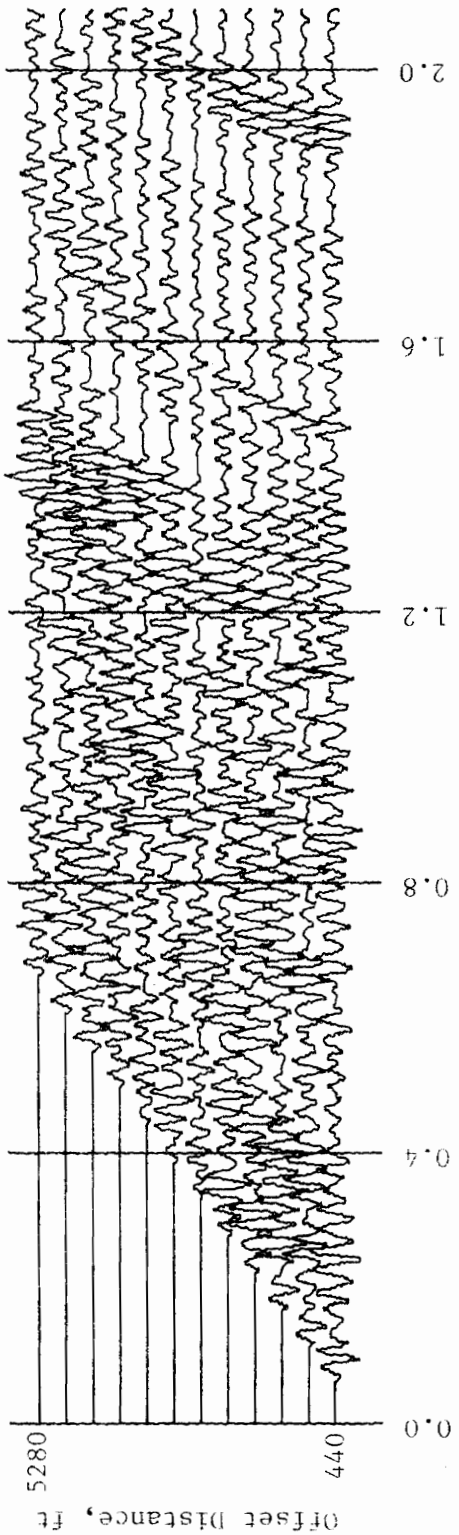

Figure 5.4-3. 12-Fold Reflection Seismograms

5.5 Common-Depth-Point Geometry

Common-depth-point geometry places shotpoints and geophones in such an arrangement that the reflections for each shotpoint-geophone combination occur at a common reflecting point. Thus, when stacking traces, each trace in the stack will ideally contain the same reflector information. Figure 5.5-1 depicts the reflection geometry for three shot-geophone distances so arranged that all reflections occur at the same point, the Common-Depth-Point, in space. This is an example of common-depth-point (CDP) geometry for the case where the reflector is parallel to the surface. Twelve sets of CDP traces (12-fold) were generated for each of the models described in section 5.3. Each of the shotpoint-geophone distances is a multiple of 440 feet starting with 440 feet.

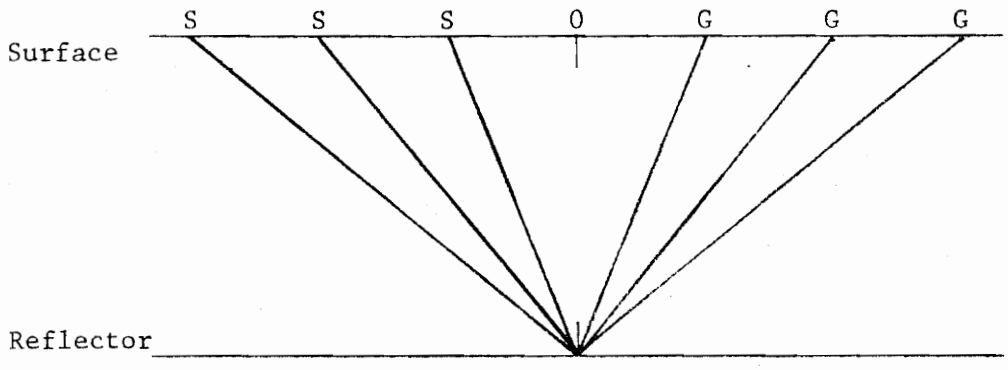

Figure 5.5-1. CDP Geometry

5.6 Summary

The seismic modelling process discussed in section 5.2 may be used to obtain synthetic reflection data for arbitrarily complex models. For example, this process is capable of modelling lenses, faults, wedges, transgressive-regressive sequences, and any other type of lithologic variation. Both isotropic and anisotropic (transversely isotropic) lithology may be modelled. Reflection data have been generated for a variety of simple models that are often used in seismic modelling work. Each model possesses a different form of variation of velocity with depth. Every set of 12-fold data so created possesses a maximum shotpoint-geophone distance of 5280 feet.

6. Velocity Scan of Isotropic Data

6.1 Introduction

The problem of interpreting seismic reflection profile records consists of analyzing arrival times of reflections arriving at various shot-geophone distances to determine the velocity distribution of the transmitting medium and the depths to the subsurface horizons. Consider a single horizontal reflector at a depth Z with a constant velocity medium above (See Figure 6.1-1). The equation for the reflection times as a function of shot-geophone distance is simply

$$T^2 = X^2/V^2 + 4Z^2/V^2 \qquad (6.1\text{-}1)$$

This equation for the reflection time is a hyperbola. If, as is the usual case, the velocity, V, is a function of depth, the ray paths will be curved and the simple relation given by equation 6.1-1 for the reflection times will not hold. However, if the geophones are near the shot the reflected ray paths will be nearly vertical, and the ray paths may be approximated by straight lines. From equation 6.1-1 we see that for a given increment of distance away from the shot the reflection time will increase by a corresponding increment in time. For reflections from successively deeper reflectors, the increment in reflection time will be less for the same increment in distance. The progressive increase of reflection time with distance for a reflection from a given reflector is referred to as moveout. If the reflector is horizontal, the increase in time is referred to as normal moveout.

One widely used method of analyzing such a profile of reflection seismograms is the so-called "T^2-X^2" method. The hyperbolic equation

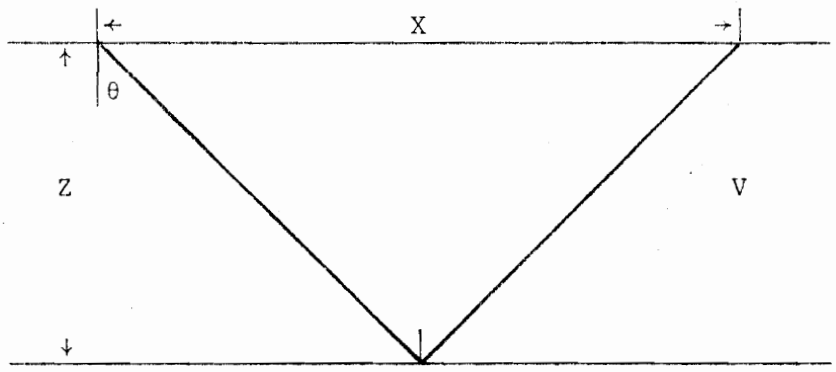

Figure 6.1-1. Reflection Geometry

(Equation 6.1-1) may also be treated mathematically as the equation of a straight line with T^2 and X^2 the dependent and independent variables respectively. The slope of this line is then the inverse square of the average velocity associated with the reflector. The analysis procedure entails the picking of reflection times for each geophone and the plot of the square of these times versus the square of the shot-geophone distances. The slope of this line then yields the square of the velocity which in turn may be used in the interpretation of geologic structure. The principal disadvantage to this analysis method is that there must be strong reflections present on the seismograms. If there is not a good contrast between a reflection and the remainder of the seismogram, then it is not possible to pick accurately the corresponding arrival times across a profile of records and the method breaks down.

The determination of seismic velocities from surface measurements was studied by Dix (1955). Dix's analysis is important because the background for many of the techniques currently used in the digital analysis of subsurface velocity are discussed here. The initial discussion involves a single plane, non-dipping reflector. The traveltime equation

$$T_x^2 = T_o^2 + X^2/V^2 \qquad (6.1\text{-}2)$$

is usually referred to as the hyperbolic traveltime equation because of its mathematical form. T_x is the reflection time to horizontal distance X, V is the layer velocity, and T_o is the reflection time for zero offset. Equation 6.1-2 is the same as equation 6.1-1 with the two-way zero offset time, $2Z/V$, being replaced by T_o. The two layer

case is also analyzed by Dix and the results are then generalized to the n-layer case. There are two important results of this generalization. The first is the form of the velocity to be used in equation 6.1-2 for the n^{th} layer:

$$\bar{V}_n^2 \sum_1^n \Delta T_i = \sum_1^n V_i^2 \Delta T_i \qquad (6.1\text{-}3)$$

where V_i is the velocity in the n^{th} layer and ΔT_i is the two-way reflection time within the n^{th} layer. $\bar{V}_n$ is the root-mean-square (rms) velocity associated with the n^{th} layer. The second result uses equation 6.1-3 to recover interval velocities:

$$V_n^2 = (\bar{V}_n^2 \sum_1^n \Delta T_i - \bar{V}_{n-1}^2 \sum_1^{n-1} \Delta T_i)/\Delta T_n. \qquad (6.1\text{-}4)$$

Equations 6.1-2, 6.1-3, and 6.1-4 have been extensively applied in the digital analysis of subsurface velocity.

Recently, new techniques have been developed for the determination of subsurface velocity. As with the T^2-X^2 method, these newer techniques depend upon the analysis of normal moveout to yield velocities associated with different reflecting horizons. These techniques are statistical in nature, and they involve computer correlation rather than the visual determination of reflection arrivals.

Taner and Koehler (1969) introduced a great advance in the area of digital computer derivation and applications of velocity functions. Multifold ground coverage by seismic techniques such as the common-depth-point (CDP) method provides a multiplicity of wave travel path

information which allows direct determination of root-mean-square velocities associated with such paths. Underlying the method is the well-established principle of employing a correlation-like technique on an assemblage of seismic traces which contain redundant information so that an improved estimate of some desired quantity may be made. Hyperbolic (See equation 6.1-2) searches for correlation among appropriately gathered arrays of traces form the basis upon which velocities are estimated. Measured correlation coefficients are presented as a velocity spectral display. Interpretation of the information can give velocities with meaningful accuracy for primary as well as multiple events. In addition, the velocity data can help to correctly identify events. Taner and Koehler discuss the fundamental principles for calculating velocity spectral displays and examples are presented to illustrate the depth and detail of geological information which may be obtained from the interpretation of such displays.

Proper identification of primary reflections in a background of noise and multiple reflections was a major problem when all seismic work was single coverage and is still a problem in the CDP multifold coverage method. Many analog and digital techniques have been developed to reduce this undesirable interference and these techniques have been utilized with varying degrees of success.

The objective of improved signal-to-noise ratio and attenuation of multiples utilizing the CDP method can be accomplished only by applying the proper time corrections to the seismic data, so that the primary

reflection signals will be moved in-phase and stacked properly. It is first necessary to determine corrections for all primary reflections on all the traces (with different shotpoint-geophone distances) which will be stacked into a single trace.

Taner and Koehler discuss the velocity spectral display as a powerful tool for identifying both primary reflections and the velocities to be used for correction of traces prior to stacking in the CDP method. Information relevant to lithology has also been interpreted from these displays.

In the past, time corrections have been estimated from previously measured nearby well velocities utilizing simple straight-ray or curved ray methods, and resulting misalignments were corrected by applying residual normal moveout corrections. This procedure is somewhat unsatisfactory because it is time consuming and, since the data are handled more than once, it is costly. It becomes more unsatisfactory when there are no well data available. In any case, the time corrections are generally calculated from the simple case of horizontally layered media and the effects of dipping beds are not considered.

A schematic diagram of the velocity scan process is shown in Figure 6.1-2. After the alignment of the input data with respect to a given hyperbolic delay pattern, a digital filter is computed for each trace that would selectively pass events common to all traces. Then, these are stacked together to give the best estimate of the input signal. Computation of power spectra for a given set of traces is done on

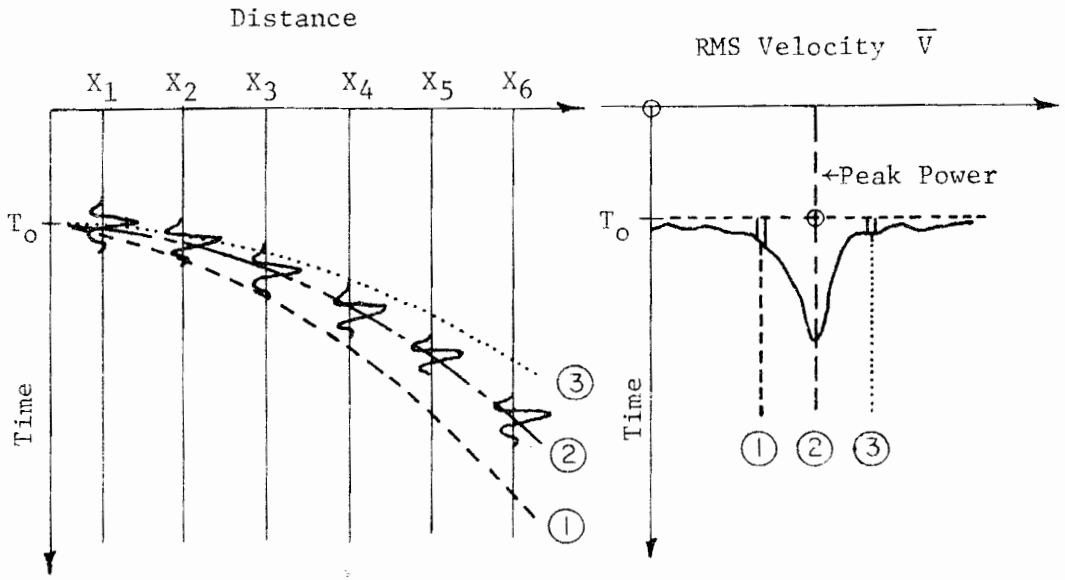

Figure 6.1-2. Velocity Scan Process

a grid pattern. First, a reference time, T_o (equation 6.1-2), is chosen. The time is kept constant and $\overline{V}_n$ (rms velocity) is then varied at regular intervals between a minimum and maximum $\overline{V}$ for a given area. Each set of T_o and $\overline{V}_n$ will give a particular hyperbolic pattern. Each trace is displaced an amount corresponding to the X distance, passed through the correlation filter, and output power is displayed with respect to its corresponding T_o and $\overline{V}_n$ values as shown in Figure 6.1-2. Peaks on the spectrum thus indicate the arrival of reflected energy at this particular T_o time with a velocity indicated by the corresponding $\overline{V}_n$ coordinate.

Velocity spectra have several principal uses. They help to determine the velocity function required for optimum stacking. They may be used to check the final seismic section against any procedural, interpretational, or computational error. Velocity spectra aid in determining the effect of multiple interference. Because they encompass all reflections, it is, in many cases, possible to determine the timing, order, apparent velocity, and relative power of multiples.

6.2 Isotropic Scan

6.2.1 Mathematical Description of Normal Moveout

Since, in general, the depth to various reflectors is not known, it will be convenient to rewrite equation 6.1-2 in terms of the rms velocity, $\overline{V}$, associated with a given reflector (See equation 6.1-3). Therefore, equation 6.1-2 may be written as

$$T_x^2 = T_o^2 + X^2/\overline{V}^2 \qquad (6.2\text{-}1)$$

where T_x is the two-way reflection time measured at a horizontal distance X from the shotpoint. The difference between T_x and T_o is the normal moveout for the horizontal offset X. The meaning of this equation is that, for a given value of T_o, there will be an associated value of $\overline{V}$. This is precisely the characteristic used in the T^2-X^2 analysis. This relationship between T_o and $\overline{V}$ is also the basis for the analysis technique to be discussed in the next section.

6.2.2 Determination of Normal Moveout

As discussed earlier, correlation techniques form the basis in this work for relating T_o and $\overline{V}$ (See equation 6.2-1). The correlation measure chosen is the semblance coefficient (Taner and Koehler, 1969). This is a normalized correlation coefficient varying in magnitude between 0 and 1. The semblance coefficient is sensitive to variations in amplitude between traces as well as within traces. The mathematical definition of the semblance coefficient is given by:

$$S_c = \frac{\sum_{j=1}^{N} \left[\sum_{i=1}^{M} f_{i,j(i)} \right]^2}{M \sum_{j=1}^{N} \sum_{i=1}^{M} f_{i,j(i)}^2} \qquad (6.2\text{-}2)$$

where M is the number of traces, N equals the number of samples from each trace, which is also referred to as the 'gate length' or 'window width', i is the trace number, and $f_{i,j(i)}$ is the amplitude of the j^{th} sample in the i^{th} trace.

The analysis proceeds as follows: First, a value of T_o is chosen. Then, while T_o is kept constant, $\overline{V}$ is varied at regular intervals between minimum and maximum values. The intervals that are used in the variation of T_o and $\overline{V}$ are normally referred to as 'scan intervals'. Semblance coefficient calculations are performed for each moveout curve thus defined. Figure 6.1-2 depicts three possible hyperbolic trajectories which are scanned. The second scan was chosen such that it was the correct one for the signal displayed. The plot of the semblance values allows the correct choice of rms velocity to be made. That is, the maximum semblance indicates that a particular choice of $\overline{V}$ best fits the observed moveout at the time specified by T_o. Therefore, by observing the variation of semblance values throughout a range of T_o and $\overline{V}$ values, it is possible to define the variation of rms velocity over the entire length of a set of records which determines the normal moveout associated with this data.

The method does have one limitation. For a given spread length, there is a limit to the depth for which it is possible to adequately

resolve velocity structure. For $T_o >> X/\overline{V}$, it is difficult to resolve velocities since there is very little moveout.

6.2.3 Demonstration of the Method

The analysis of normal moveout for rms velocity as discussed above will be referred to as a "velocity analysis." The results of a velocity analysis are usually in the form of a matrix of semblance coefficients. Variation along one side of the matrix represents variation in velocity. The direction normal to this represents variation in two-way normal incidence reflection time. Therefore, if the semblance matrix is contoured, the result is a map where the highs represent the best choice of velocity vs. two-way time. The value of such a contour map for which the semblance values range between 0 and 1 is that the contour values are directly indicative of the amount of confidence that can be placed in the results of the analysis. The above statements may best be illustrated by the use of a simple model. For this model, it will be assumed that velocity remains constant with depth of burial in the manner discussed in section 5.3.1. The seismic traces for this model are shown in Figure 6.2-1. Figure 6.2-2 is the velocity analysis performed on the data. It will be noted that the peaks in the analysis are all centered at 8000 ft/sec. For velocities either higher or lower than 8000 ft/sec, the semblance values rapidly decrease in magnitude. The magnitudes of the semblance peaks are not uniform throughout the analysis because the extent that moveout and hence velocity may be determined depends to large extent on the contrast existing between suc-

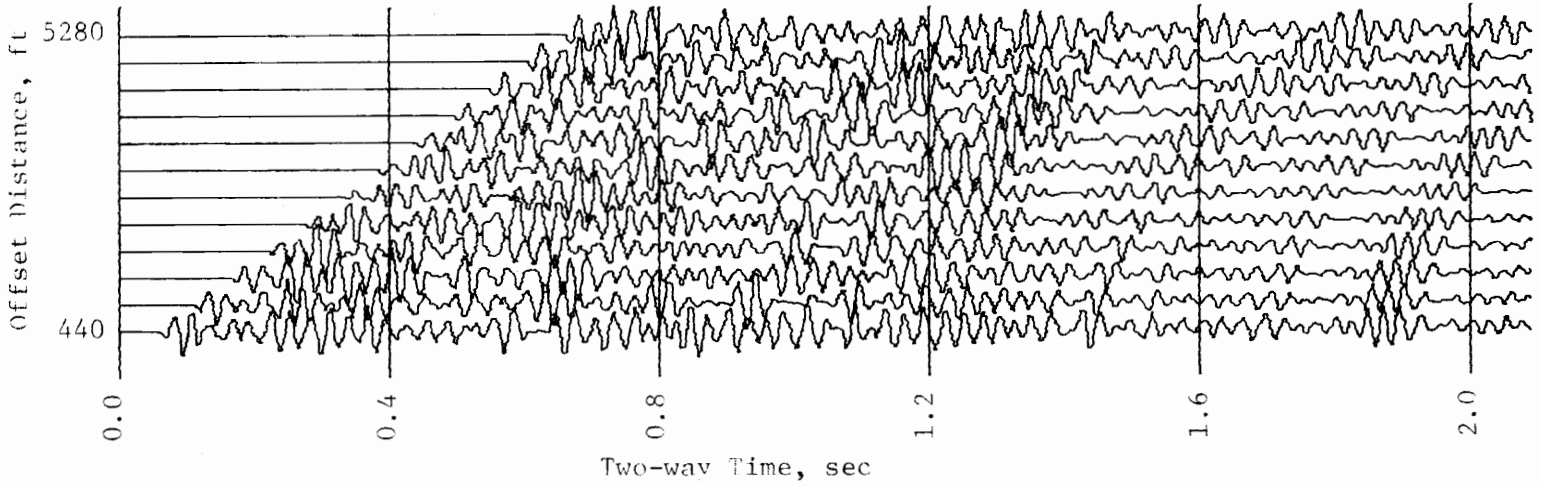

Figure 6.2-1. 12-Fold Reflection Seismograms

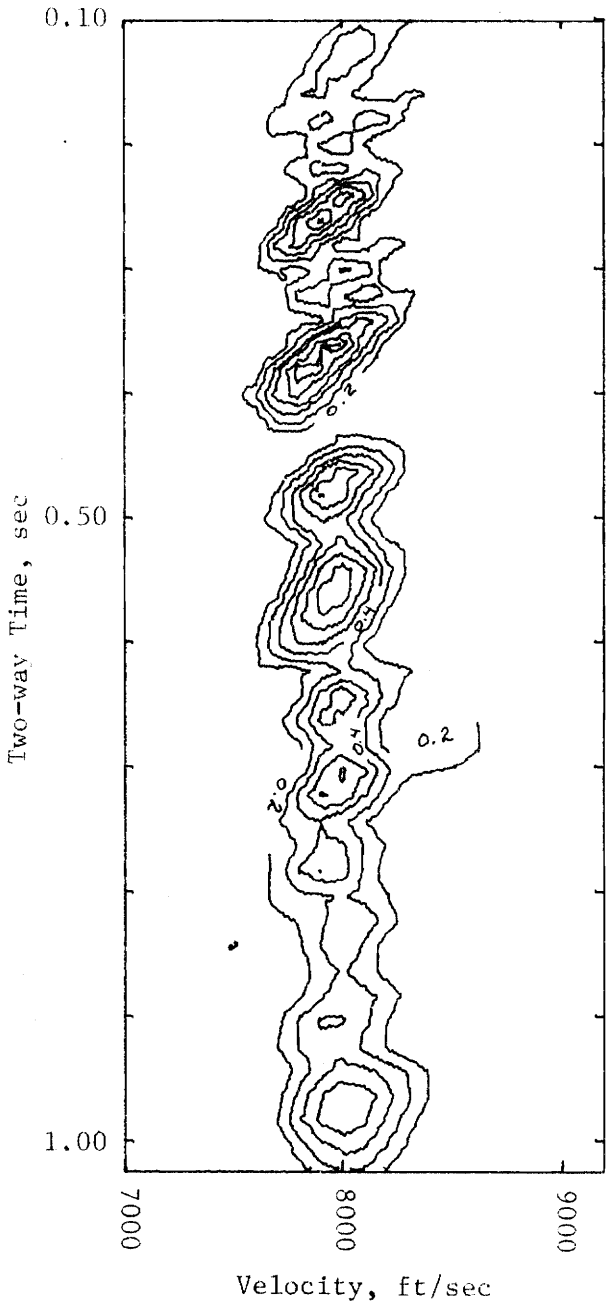

Figure 6.2-2. Velocity Analysis of P Component
Scan Increments = 20 ms and 100 ft/sec,
Window Width = 50 ms

cessive reflection coefficients. A reflection seismogram is a superposition of many reflections so that when a good contrast between reflection coefficients exists a particular reflection may stand out above the general background. This is just the characteristic that made the T^2-X^2 method workable. However, the difference here is that using a correlation technique, such as semblance, the reflection coefficient contrast need not be as great as for the T^2-X^2 method. In addition, the use of correlation methods allows for the efficient automation of the rms velocity determination.

In Figure 6.2-2 and in all other velocity analyses in this and later chapters, the lowest (outermost) contour level will always correspond to a semblance value of 0.2. The value 0.2 was chosen for the start of contouring because tests have shown that spurious semblance values up to about 0.2 may occasionally arise due to fortuitous lineups of non-related events on the seismic traces during scanning. A contour interval of 0.1 is used for all velocity analyses. The caption for each velocity analysis contains all pertinent information relating to the analysis. The first information listed indicates whether the analysis is over the seismic P or over the SV wave component. The entry identified as "scan increments" gives the steps by which two-way reflection time and rms velocity are varied in the analysis. For example, in Figure 6.2-2 for an initial two-way time of 0.1 sec, each successive time differs from the preceding time by 20 ms. Similarly, each rms velocity after the initial value differs from the preceding value

by 100 ft/sec. The "window width" identifies the amount of data taken from each trace that is to be correlated. In Figure 6.2-2, the window width is 50 ms. This indicates that, for every semblance calculation, 50 ms of data were used from every trace. The velocity analyses in the next chapter have two additional headings in the caption. The first, labelled "data anisotropy", gives the actual anisotropy factor for the data being analyzed. The second entry is "anisotropy scan level" which is the anisotropy factor utilized in that particular velocity analysis. Figure 6.2-3 is an enlargement of a portion of Figure 6.2-2. In this figure the contours are labelled to illustrate more clearly the manner in which the semblance magnitudes vary. The significance of the contour plot is that the ridge and peaks identified by the semblance maxima define the velocity function for the medium being analyzed.

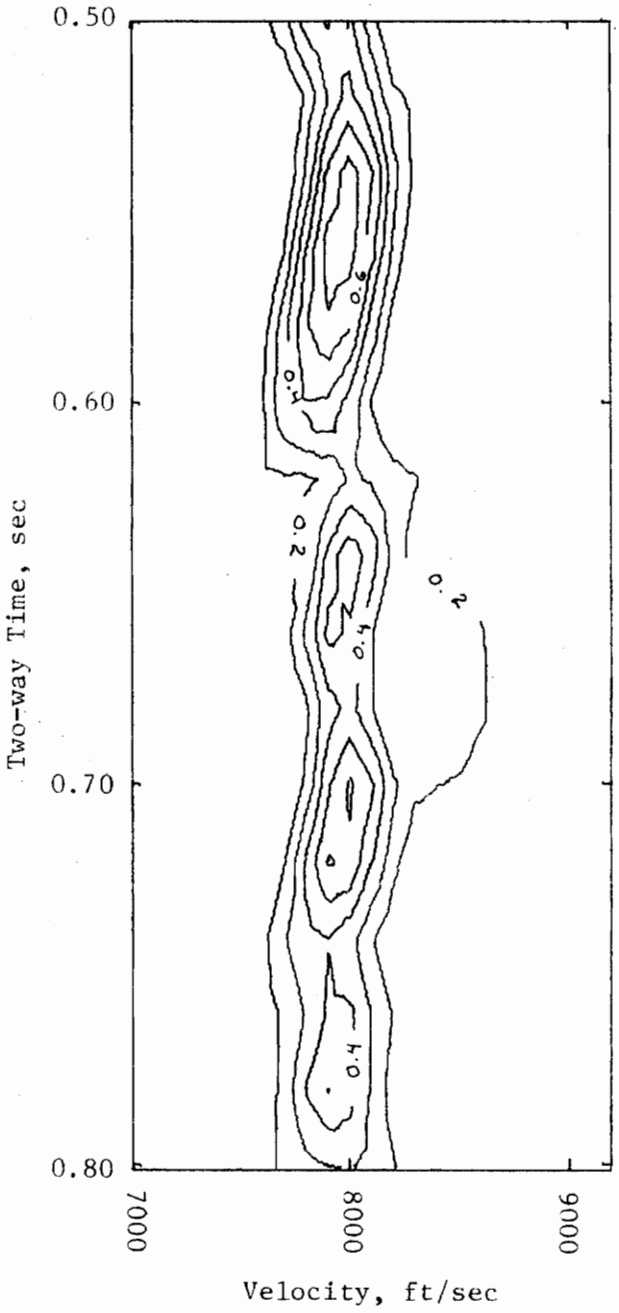

Figure 6.2-3. Velocity Analysis of P Component
Scan Increments = 20 ms and 100 ft/sec,
Window Width = 50 ms

7. Velocity Scans of Anisotropic Data

7.1 Introduction

Normal moveout was shown to be the key to analysis of seismic reflection data for the isotropic case (See chapter 6). The same is true when the transmitting medium is anisotropic. Moveout analysis becomes more difficult in the case of velocity anisotropy because of the functional dependence of the propagation velocity on the direction of propagation with respect to the axis of symmetry (See section 4.6). The form that the moveout equations assume depends upon the kind of anisotropy present. The models used here are transversely isotropic. Theoretically, transverse isotropy is a better description of anisotropic media than is the theory of elliptical anisotropy which has been extensively used (See sections 4.5.2 and 4.5.3). This was first shown theoretically by Postma (1955) and field confirmation was obtained by Jolly (1956) and Vander Stoep (1966).

The practicality of using shear waves in seismic exploration has been demonstrated by Cherry (1968) and Erickson, et. al. (1968). The results of these studies indicate that it is possible to obtain the same depth of penetration as with compressional waves. Horizontal vibrators were used as the source of energy in these experiments. The conclusions reached by these experimentors were that shear waves could be used for exploration in much the same way that compressional waves are used.

7.2 Mathematical Description of Normal Moveout

Searches for semblance, as discussed in section 6.2.2, utilizing CDP data forms the basis upon which rms velocities are estimated for the case of transversely isotropic media. However, in this case the trajectories scanned are not hyperbolic, but depend on the more complex velocity relationships existing in a transversely isotropic medium (See section 4.6).

In a transversely isotropic medium, as has been shown earlier, velocity is a function of the direction of propagation with respect to the axis of symmetry. As in section 4.6, the axis of symmetry will be chosen to coincide with the vertical or z-axis. The three directionally dependent velocities, corresponding to P, SV, and SH are given by equations 4.6-6 and 4.6-8. The velocities, both parallel and normal to the z-axis, are given by equation 4.6-10. Since in practice we do not work with perfectly homogeneous and uniform materials, we will want to rewrite equations 4.6-10 in terms of quantities that are physically measureable by us. Therefore,

$$@\ \theta = 0^\circ$$

$$V_1 \rightarrow V_{1z},\quad V_2 \rightarrow V_{2z},\quad V_3 \rightarrow V_{3z}$$

$$@\ \theta = 90^\circ$$

$$V_1 \rightarrow V_{1x},\quad V_2 \rightarrow V_{2x},\quad V_3 \rightarrow V_{3x}$$

but from equations 4.6-10 we know that $V_{2x} = V_{2z} = V_{3z}$. In particular, V_{1x} is the horizontal component of the compressional velocity, V_{1z} is the vertical component of the compressional velocity, and V_{2x} is the

horizontal component of the shear velocity (SV). Next, the velocity relations given by equations 4.6-6 and 4.6-8 will be rewritten in terms of the velocities defined by equations 7.2-1.

$$V_{1,2}^2 = \sin^2\theta V_{1x}^2 + V_{2x}^2 + \cos^2\theta V_{1z}^2 + V_{2x}^2 \pm \left(\left(\sin^2\theta V_{1x}^2 - V_{2x}^2 - \cos^2\theta V_{1z}^2 - V_{2x}^2 \right)^2 + \sin^2\theta\cos^2\theta (V_{13}^2 + V_{2x}^2)^2 \right)^{\frac{1}{2}} \qquad (7.2\text{-}2)$$

$$V_3^2 = \sin^2\theta V_{3x}^2 + \cos^2\theta V_{3z}^2$$

The next step will be to make use of these velocity relations to write traveltime equations for the medium. Let:

$$T_{1,2}^2 = D^2/V_{1,2}^2$$
$$T_3^2 = D^2/V_3^2 \qquad (7.2\text{-}3)$$

where D is the total length of the reflection path. D has the same methematical form as in the isotropic case, i.e., $D = \sqrt{X^2 + 4Z^2}$, where X is the shotpoint-geophone distance and Z is the reflecion depth. First, the traveltime equations will be written in terms of X and Z. Then, Z will be replaced in terms of the more conventional zero-offset two-way reflection time. Also sin θ and cos θ may be expressed in terms of X and Z (See Figure 6.1-1) where

$$\sin\theta = X/\sqrt{X^2 + 4Z^2}, \quad \cos\theta = 2Z/\sqrt{X^2 + 4Z^2}. \qquad (7.2\text{-}4)$$

Substituting into equation 7.2-2, we obtain:

$$V_{1,2}^2 = \frac{X^2}{X^2+4Z^2} \cdot V_{1x}^2 + V_{2x}^2 + \frac{4Z^2}{X^2+4Z^2} \cdot V_{1z}^2 + V_{2x}^2 \pm \left(\left(\frac{X^2}{X^2+4Z^2} \cdot V_{1x}^2 - V_{2x}^2 - \frac{4Z^2}{X^2+4Z^2} \cdot V_{1z}^2 - V_{2x}^2 \right)^2 + \frac{4X^2Z^2}{(X^2+4Z^2)^2} \cdot (V_{13}^2 + V_{2x}^2)^2 \right)^{\frac{1}{2}} \qquad (7.2\text{-}5)$$

$$V_3^2 = \frac{X^2}{X^2+4Z^2} \cdot V_{3x} + \frac{4Z^2}{X^2+4Z^2} \cdot V_{3z} .$$

Then, the traveltime equations become

$$T_1^2 = (X^2 + 4Z^2)/V_1^2, \quad T_2^2 = (X^2 + 4Z^2)/V_2^2, \quad T_3^2 = (X^2 + 4Z^2)/V_3^2. \tag{7.2-6}$$

If we set X = 0, we have:

$$T_{10}^2 = 4Z^2/V_{1z}^2, \quad T_{20}^2 = 4Z^2/V_{2x}^2, \quad T_{30}^2 = 4Z^2/V_{3z}^2 \tag{7.2-7}$$

where T_{10}, T_{20}, and T_{30} are the two-way zero offset reflection times for P, SV, and SH respectively. Next, similar to the procedure adopted in the isotropic case, substitution for Z in terms of the appropriate two-way zero offset time will be made:

$$4Z^2 = T_{10}^2V_{1z}^2 = T_{20}^2V_{2x}^2 = T_{30}^2V_{3z}^2. \tag{7.2-8}$$

Therefore, upon substitution into equations 7.2-5, we have:

$$T_1^2 = \frac{2(X^2+T_{10}^2V_{1z}^2)^2}{X^2(V_{1x}^2+V_{2x}^2) + T_{10}^2V_{1z}^2(V_{1z}^2+V_{2x}^2) + A}$$

$$T_2^2 = \frac{2(X^2+T_{20}^2V_{2x}^2)^2}{X^2(V_{1x}^2+V_{2x}^2) + T_{20}^2V_{2x}^2(V_{1z}^2+V_{2x}^2) - B}$$

$$T_3^2 = \frac{(X^2 + T_{30}^2V_{3z}^2)^2}{X^2V_{3x}^2 + T_{30}^2V_{3z}^2} \tag{7.2-9}$$

$$A = \{[X^2(V_{1x}^2-V_{2x}^2)-T_{10}^2V_{1z}^2(V_{1z}^2-V_{2x}^2)]^2+4X^2T_{10}^2V_{1z}^2(V_{13}^2+V_{2x}^2)^2\}^{\frac{1}{2}}$$

$$B = \{[X^2(V_{1x}^2-V_{2x}^2)-T_{20}^2V_{2x}^2(V_{1z}^2-V_{2x}^2)]^2+4X^2T_{20}^2V_{2x}^2(V_{13}^2+V_{2x}^2)^2\}^{\frac{1}{2}}$$

These are the traveltime equations used to calculate normal moveout in the velocity analysis of a transversely isotropic medium.

Inspection of the first two of equations 7.2-9 reveals that, for a single velocity scan, that not one, but four velocities must be specified simultaneously. Only a single velocity need be specified for the isotropic case. However, this is not as formidable a problem as might

appear at first sight. The procedure adopted is to use V_{1x} as a reference velocity and to vary it between some minimum and maximum values by predetermined steps. Also, the degree of anisotropy is specified and a value of Poisson's ratio assumed. The procedure adopted herein is to use a value of Poisson's ratio of 0.283 for the models being studied. This is the value used by Postma (1955) for his Case I. This is a reasonable value and falls approximately in the midrange of values listed by Birch (1966) for sedimentary rocks. The majority of sedimentary rocks listed fell within the range 0.25 to 0.35. Poisson's ratio for limestones and sandstones had ranges of 0.25 to 0.34 and 0.17 to 0.29 respectively. The majority of tabulated values for these rocks were in the range 0.27 to 0.31. The assumption of a single value for Poisson's ratio throughout an entire section is not necessarily as restrictive as it might first appear. The seismic energy propagating through a section at any instant is affected by the properties of the medium averaged over a distance of one wavelength. Therefore, existing variations within the medium tend, in effect, to be smoothed. One further indication that this assumption of a constant value of Poisson's ratio is not necessarily injurious is the ratio of the shear to the compressional velocity. For a Poisson's ratio of 0.30, the ratio of the shear to the compressional velocity is 0.535. This velocity ratio is 0.580 and 0.480 for Poisson's ratios of 0.25 and 0.35 respectively. This corresponds to a variation in this ratio of about 10 percent in either direction from 0.30. Once a value of Poisson's ratio is

assumed, it is then possible to use the theory relating elactic coefficients in a transversely isotropic medium developed in section 4.7 to calculate the values of V_{1z}, V_{2x}, and V_{13} corresponding to V_{1x} and the level of anisotropy specified. At this point, the velocity analysis of transversely isotropic media becomes almost as straightforward as for the isotropic case. Finally, as expected, for an isotropic medium, equations 7.2-9 reduce to the hyperbolic equation (Equation 6.1-1). We proceed next to the application of anisotropic velocity scanning methods to the idealized models described in chapter 5 in order to evaluate the possibilities of such analytical techniques in exploration seismology.

7.3 Stepwise Increase of Velocity with Depth

This model is a horizontal layered structure with the surface layer having a horizontal compressional velocity of 8000 ft/sec. This first layer is 125 ft. thick. All other layers are 100 ft. thick and the horizontal compressional velocity component increases by 100 ft/sec in each successively deeper layer. All other velocity components are determined by the ratios existing among the elastic coefficients and the value of the horizontal compressional component. The ratios among the elastic coefficients depend, of course, on the degree of anisotropy (See section 4.7). The horizontal compressional component was chosen as a reference for ease of comparison with the results of isotropic scan velocity analysis (See chapter 6). This velocity function was used to generate three sets of synthetic reflection data having anisotropy factors of 1.02, 1.043, and 1.08 respectively.

7.3.1 Effects of Variation of Model Parameters on Velocity Analysis

Spread Dimensions

All reflection data for this model were created using a Common-Depth-Point reflection geometry. The maximum shotpoint-geophone distance used was 5280 feet. Some 4-fold and 6-fold data were also generated with the same overall shotpoint-geophone distance for purposes of comparison with the 12-fold data. The shotpoint-geophone spacings for the 4-fold data are multiples of 1320 feet and 880 feet for the 6-fold data. Greater distances are not feasible with this model because critical angles are exceeded for the shallower reflections. A critical angle as used herein refers to the angle that

the seismic ray path makes with the vertical at some interface when the angle becomes large enough that no seismic energy is transmitted any deeper than that interface.

Fold Multiplicity

The fold multiplicity employed for velocity analysis has important consequences with regard to the resolving power of the analysis. A velocity analysis is essentially a correlation analysis used to determine the values of normal moveout best satisfying the data. When a small number of traces is used, it is possible for an accidental lineup of information (i.e., peaks and troughs) to produce a correlation peak. As the number of traces increases, it becomes less and less likely that significant correlations will occur away from their correct position.

An example of the importance of fold multiplicity may be shown by using the data described above under the heading 'Spread Dimensions'. The 12-fold data for each of the three levels of anisotropy are shown in Figures 7.3-1, 7.3-2, and 7.3-3. The 4-fold data are obtained by using only every third trace and the 6-fold data by using only every other trace. Figure 7.3-4 shows the results for velocity scans of 4, 6, and 12-fold data respectively for the data shown in Figure 7.3-2. These analyses are for the compressional (P) velocity component. In all three analyses the minimum contour level is 0.2 (See section 6.2.3) and the contour interval is 0.1. The 4-fold analysis is noisy and it is difficult to determine where the best correlations exist. The situation is much improved in the 6-fold analysis. Although there is

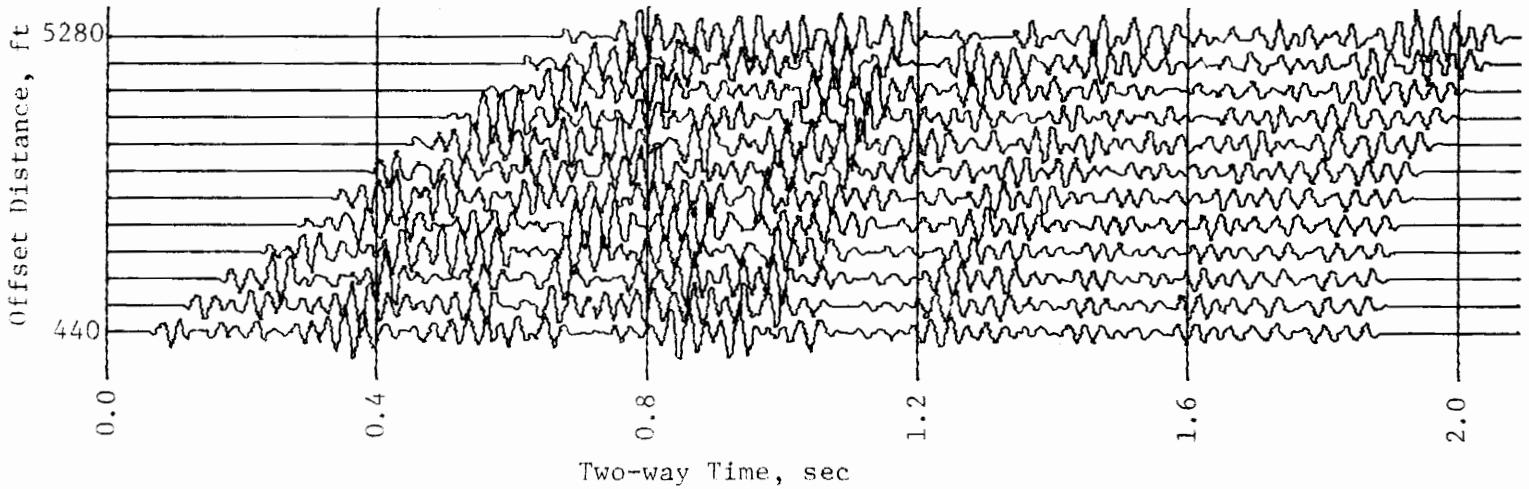

Figure 7.3-1. Stepwise Velocity Increase
12-Fold Reflection Seismograms
Data Anisotropy = 1.043

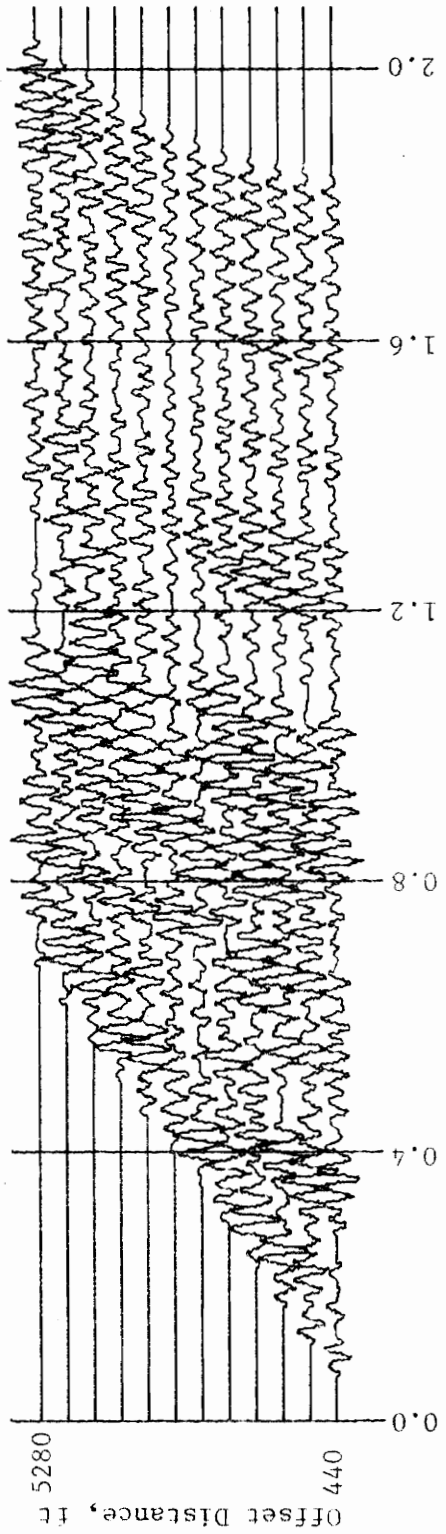

Figure 7.3-2. Stepwise Velocity Increase
12-Fold Reflection Seismograms
Data Anisotropy = 1.02

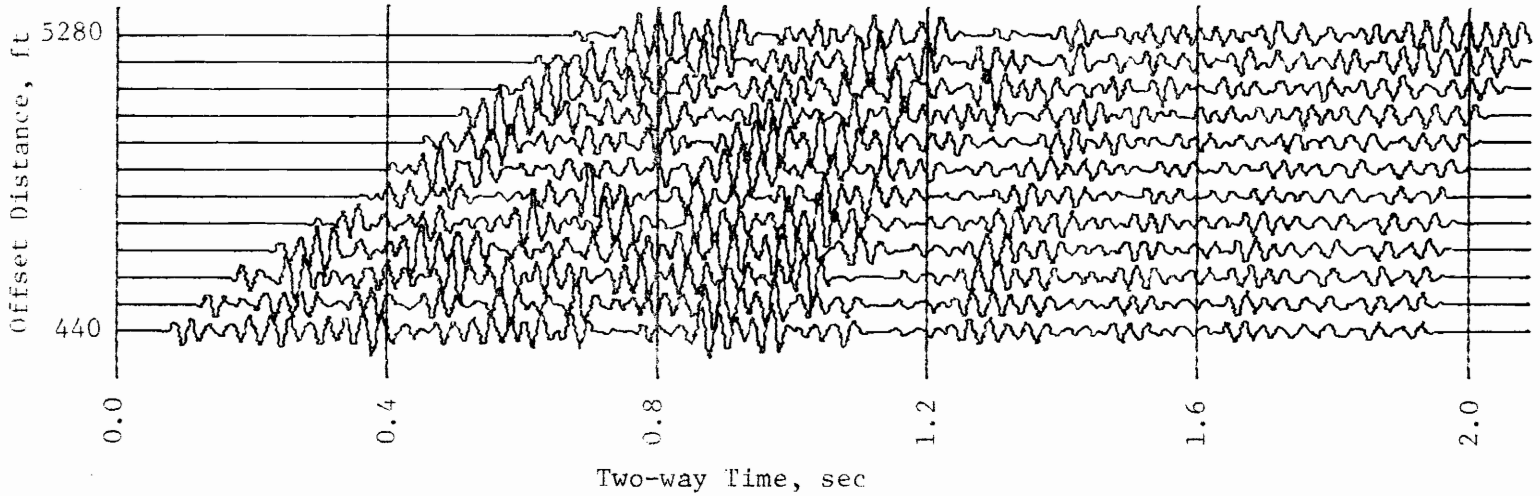

Figure 7.3-3. Stepwise Velocity Increase
12-Fold Reflection Seismograms
Data Anisotropy = 1.08

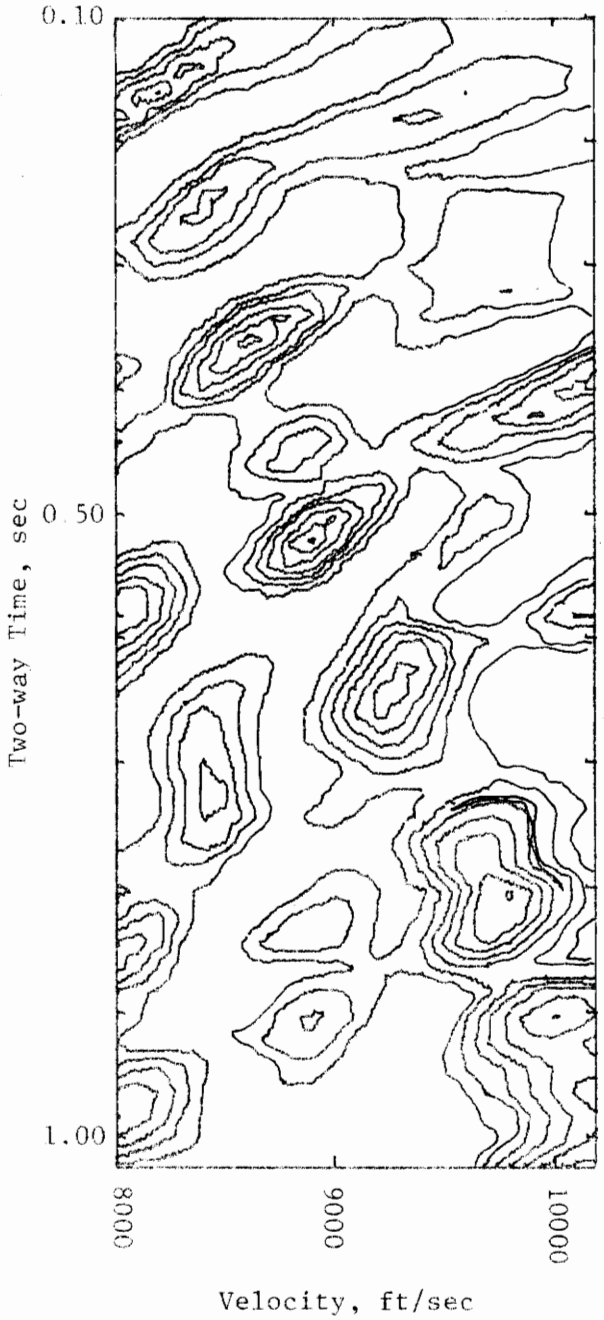

Figure 7.3-4a. Velocity Analysis of P Component Data Anisotropy = 1.043, Window Width = 50 ms, Scan Increments = 20 ms and 100 ft/sec, Anisotropy Scan Level = 1.043, Initial Contour = 0.2, 4-Fold Multiplicity

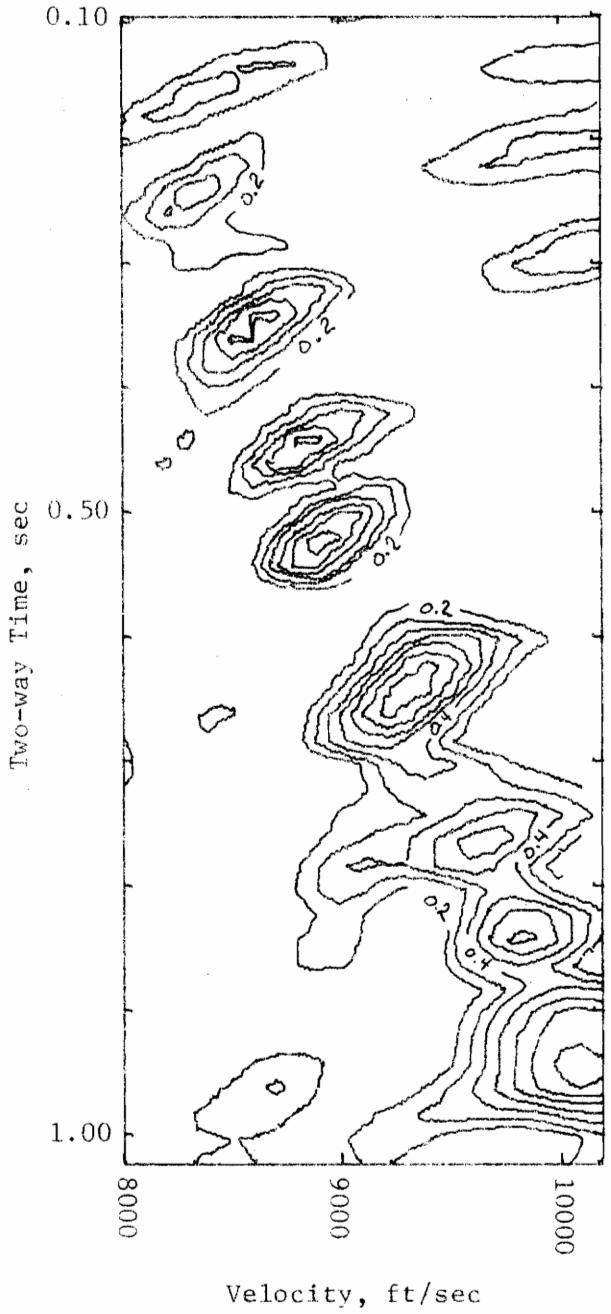

Figure 7.3-4b. Velocity Analysis of P Component Data Anisotropy = 1.043, Window Width = 50 ms, Scan Increments = 20 ms and 100 ft/sec, Anisotropy Scan Level = 1.043, 6-Fold Multiplicity

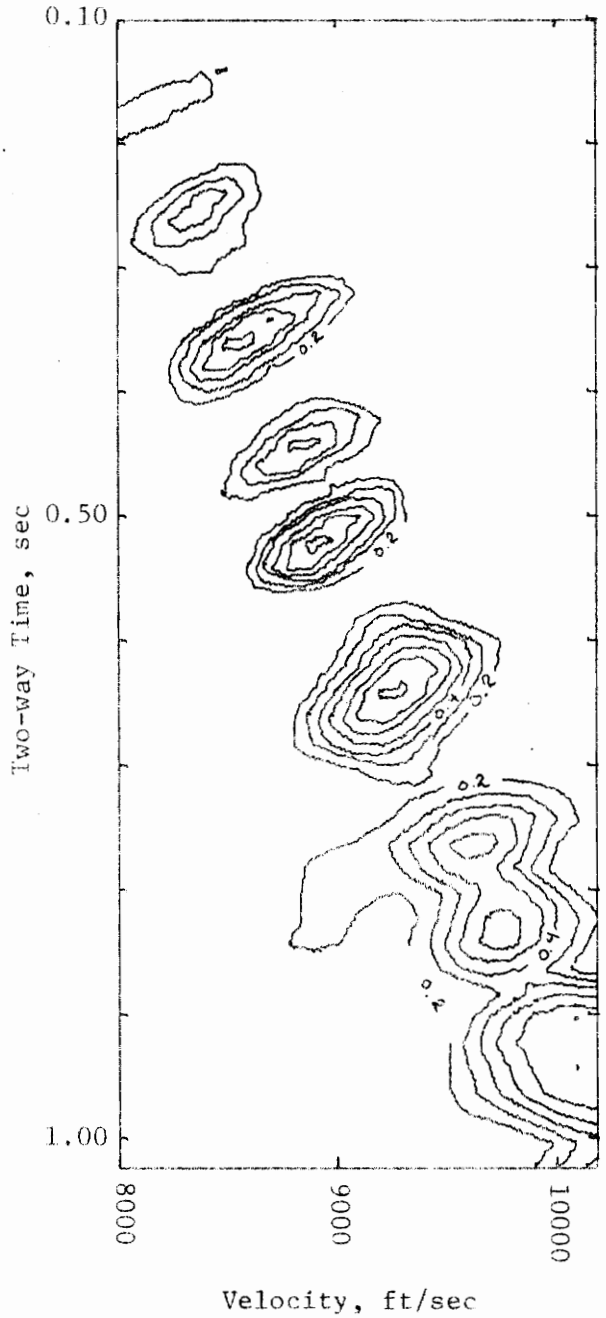

Figure 7.3-4c. Velocity Analysis of P Component
Data Anisotropy = 1.043, Window Width = 50 ms,
Scan Increments = 20 ms and 100 ft/sec,
Anisotropy Scan Level = 1.043,
12-Fold Multiplicity

still considerable noise present, it does not greatly degrade the analysis. For the 12-fold analysis there is no longer a problem with background noise and the peaks are well defined. It should be clear from these examples that, aside from other factors, a sufficient number of traces must be used just to eliminate unwarranted correlations due to fortuitous lineups of peaks and troughs on the traces. For this reason, all data subsequently analyzed for anisotropy are 12-fold.

Critical Angles

Severe problems may exist when velocity analyses are performed upon seismic traces where the reflections are not present on all traces because critical angles are exceeded. The problem normally exists for the early parts of the seismic record and is the most severe for the outer traces because of the larger offsets involved. Therefore, because velocity analysis is a correlation process, the results can be expected to be severely degraded when reflections are present in some (near) traces and are absent from others (far traces). This accounts for the lower magnitude of the correlation peaks prior to 0.3 sec two-way time in Figure 7.3-4c. Table 7.3-1 shows the first depth from which a reflection is received for each trace. Reflections are not received from shallower depths because critical angles are exceeded.

Variations in Reflection Coefficients

As discussed in section 6.2.3, a reflection seismogram is a superposition of many reflections. Where a good contrast between reflection coefficients exists, a particular reflection may stand out above the general background. The peaks depicted by a con-

Table 7.3.-1. Depth of First Reflection

Data Anisotropy = 1.02

Trace No..	1	2	3	4	5	6	7	8	9	10	11	12
P:	100	100	100	150	250	375	550	750	950	1175	1475	1850
SV:	100	100	100	150	275	450	650	850	1050	1275	1575	1875

Data Anisotropy = 1.043

P:	100	100	100	150	250	350	475	675	875	1075	1375	1675
SV:	100	100	100	175	350	475	675	875	1075	1350	1650	1900

Data Anisotropy = 1.08

P:	100	100	100	150	175	350	450	575	775	975	1250	1475
SV:	100	100	150	250	375	375	575	950	1175	1400	1675	1950

toured velocity analysis represents parts of the seismic data that are characterized by good contrast between adjacent reflection coefficients. For parts of the seismic record where the difference between nearby reflection coefficients is small, the correlation process tends to lose resolution because of the loss of contrast that occurs when the nearly equal amplitude wavelets are summed in the superposition process used in generating a seismic trace.

In order to facilitate the comparison of velocity analyses scanned assuming different levels of anisotropy, the entire range of times and velocities contained within each set of data will not be displayed, but only sections containing good contrasts between reflection coefficients will be used. We will thus compare only how major peaks (corresponding to good reflections) on the velocity analyses change with anisotropy scan level. This will provide the information necessary to judge the resolving power of the analytic technique for determining various levels of anisotropy.

Resolution of Anisotropy

The step velocity function described above was used to generate three sets of seismic traces (See Figures 7.3-1, 7.3-2, and 7.3-3). Each set of traces is 12-fold. The shotpoint-geophone distances are described above. The three sets of data are all anisotropic with anistropy factors of 1.02, 1.043, and 1.08 respectively. All sets of data contain both P and SV arrivals. Velocity analyses were performed over both P and SV to test the anisotropy resolving capability of

each component. One characteristic of the SV velocity analyses to be noted is that the velocity range is slightly different for each individual anisotropy scan value. The horizontal P velocity component was used as a reference and therefore, the same P velocity range has a slightly different corresponding SV velocity range for each anisotropy factor scanned.

Quantitative comparisons of velocity scans for differing degrees of anisotropy may be made by integrating the volume under the surface defined by the matrix of semblence values. The analysis which most closely matches the actual degree of anisotropy in the data will yield the largest semblance maxima and, therefore, the greatest volume upon integration of the semblance matrix. To facilitate comparison among analyses, the integrated volumes are normalized on the basis of the largest value being set equal to 100 with all other values then scaled accordingly.

The first set of data analyzed has an anisotropy factor of 1.043. The velocity scans utilized anisotropy factors from 1.02 to 1.06 in steps of 1.01. Velocity analyses for P and SV are given in Figures 7.3-5 and 7.3-6 respectively. The results of the analyses are shown in Table 7.3-2 for both P and SV. The results of the P analyses are inconclusive as there is not a single sharp maxima. The SV results, on the other hand, are characterized by a sharp maximum. The location of this peak value at an anisotropy scan value of 1.04 and the sharp decrease on either side of 1.04 are directly indicative of the resolving power of the analysis. The value at 1.05 is almost as large as

the 1.04 value since the actual anisotropy factor is 1.043. A qualitative interpretation of these figures supports the quantitative results in Table 7.3-2. The correct anisotropy factor for these data can be determined within an uncertainty of ± 0.005. For this model, the horizontal and vertical P velocity components are 8000 ft/sec and 7670 ft/sec respectively at the surface. A determination of anisotropy to within ± 0.005 implies that, for this model, the measured velocity difference for the P components would fall within the range 330 ± 40 ft/sec.

It is readily apparent from Figures 7.3-5 and 7.3-6 that the entire range of data available is not depicted. The analyses for P and SV were limited to two-way reflection times for which there was good contrast between nearby reflection coefficients as discussed above. The two-way reflection time ranges chosen for P and SV were 0.6 - 0.9 sec and 1.2 - 1.5 sec respectively.

Since the results of analysis of the SV data with anisotropy factor 1.043 were satisfactory, it was decided to extend these results by analysis of data having half the anisotropy and double the anisotropy. It was reasoned that if the anisotropy could be resolved successfully over this broad range, that the resolution of the analysis method would be amply demonstrated. Therefore, two sets of seismic data having anisotropy factors of 1.02 and 1.08 were generated. All three sets of data were created in the same manner with the same reflection coefficients being used in all cases.

The analysis of the data with anisotropy level 1.02 is the most

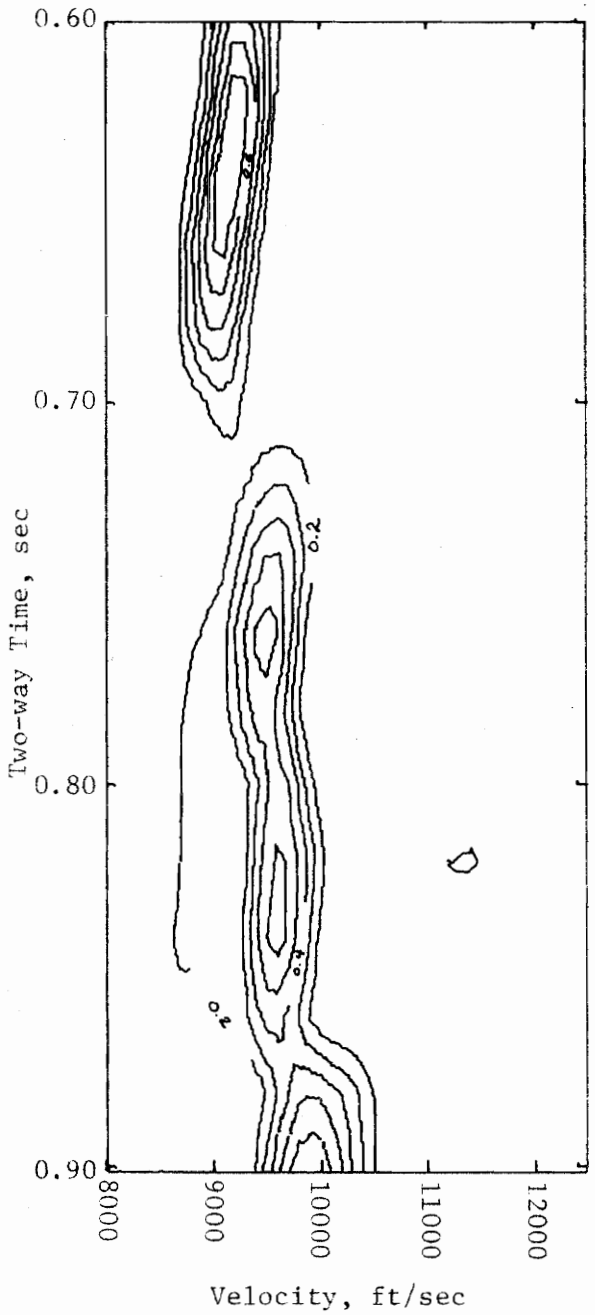

Figure 7.3-5a. Velocity Analysis of P Component Data Anisotropy = 1.043, Window Width = 50 ms, Scan Increments = 20 ms and 100 ft/sec, Anisotropy Scan Level = 1.02

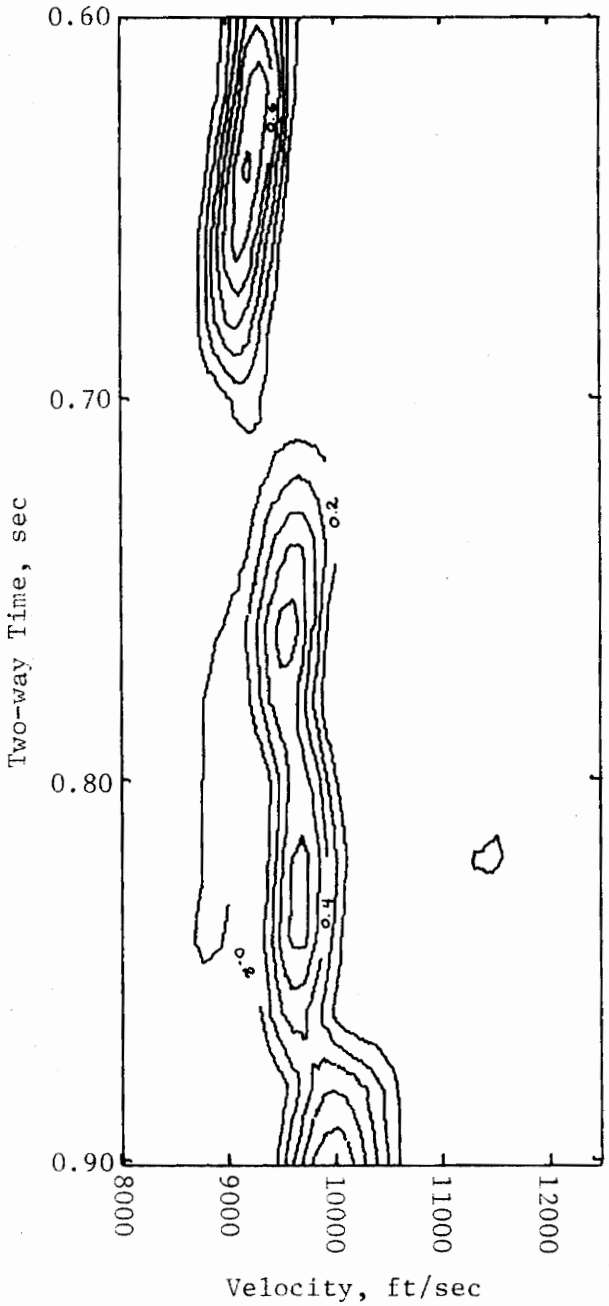

Figure 7.3-5b. Velocity Analysis of P Component Data Anisotropy = 1.043, Window Width = 50 ms, Scan Increments = 20 ms and 100 ft/sec, Anisotropy Scan Level = 1.03

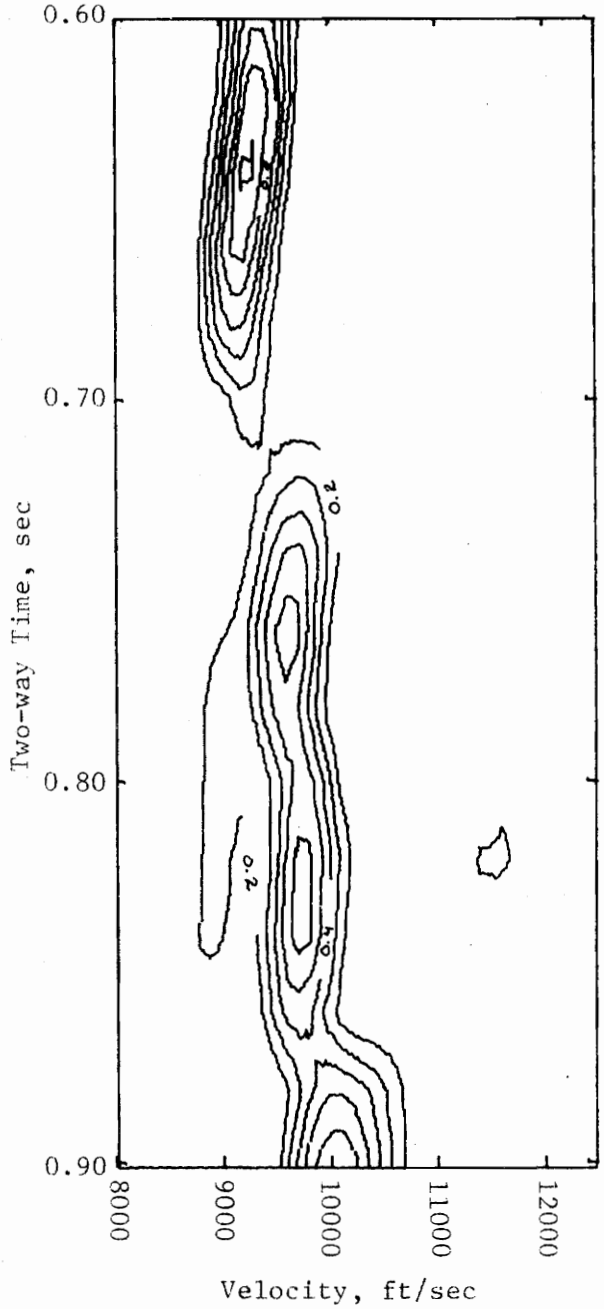

Figure 7.3-5c. Velocity Analysis of P Component Data Anisotropy = 1.043, Window Width = 50 ms, Scan Increments = 20 ms and 100 ft/sec, Anisotropy Scan Level = 1.04

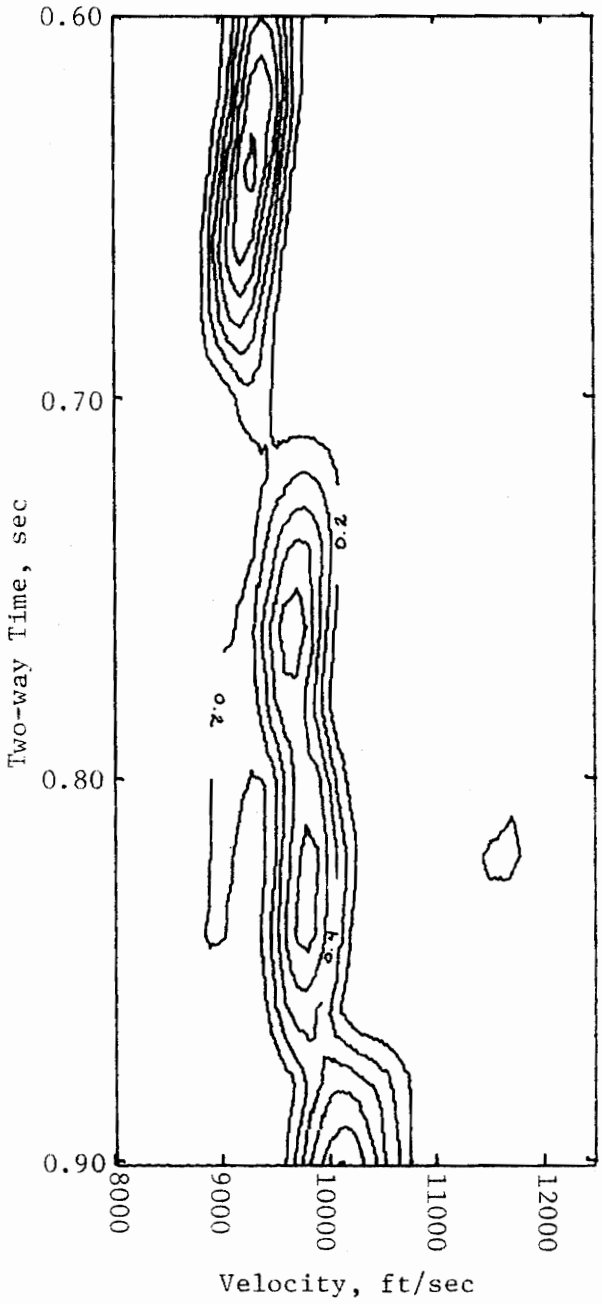

Figure 7.3-5d. Velocity Analysis of P Component Data Anisotropy = 1.043, Window Width = 50 ms, Scan Increments = 20 ms and 100 ft/sec, Anisotropy Scan Level = 1.05

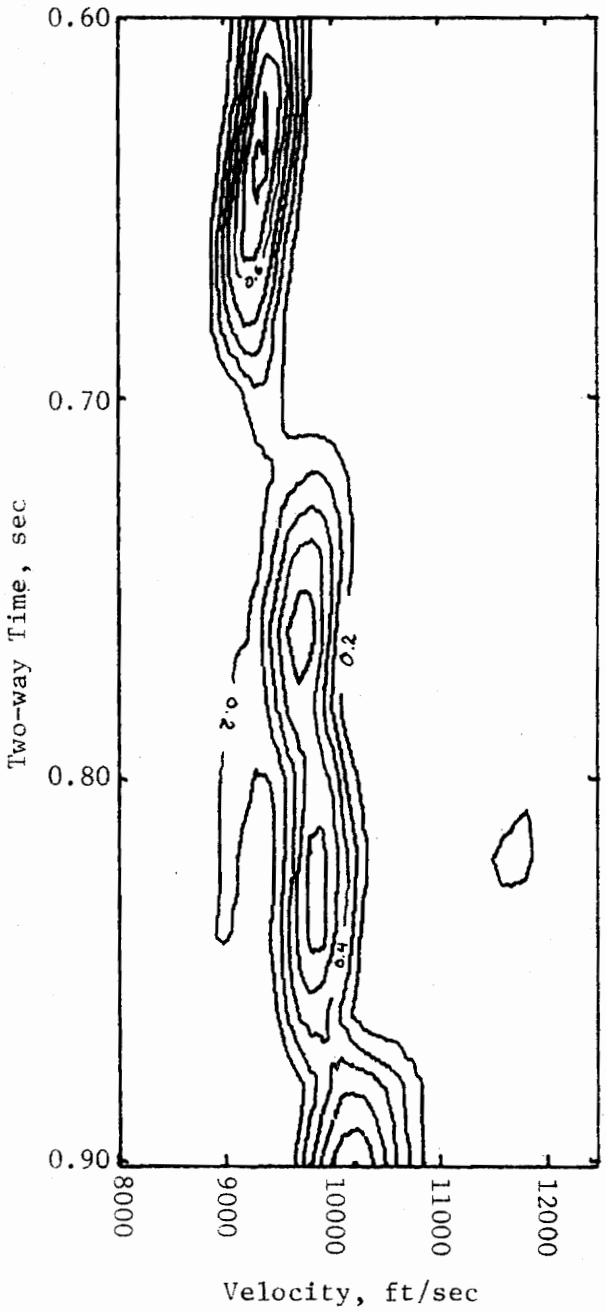

Figure 7.3-5e. Velocity Analysis of P Component Data Anisotropy = 1.043, Window Width = 50 ms, Scan Increments = 20 ms and 100 ft/sec, Anisotropy Scan Level = 1.06

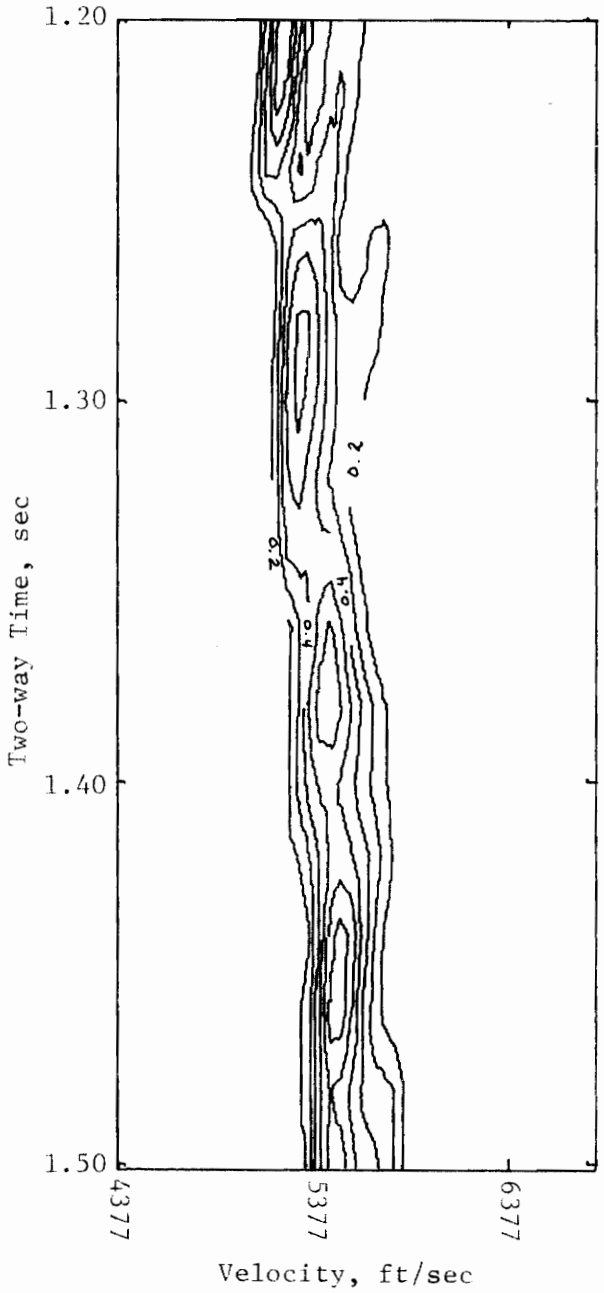

Figure 7.3-6a. Velocity Analysis of SV Component Data Anisotropy = 1.043, Window Width = 50 ms, Scan Increments = 20 ms and 54 ft/sec, Anisotropy Scan Level = 1.02

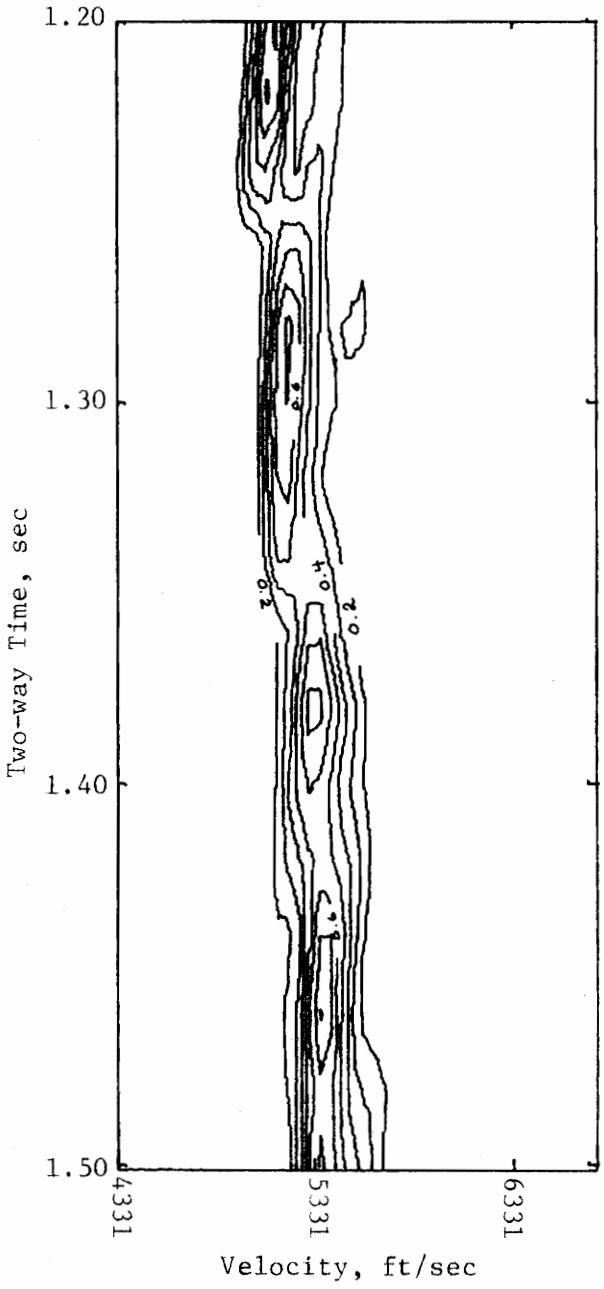

Figure 7.3-6b. Velocity Analysis of SV Component Data Anisotropy = 1.043, Window Width = 50 ms, Scan Increments = 20 ms and 54 ft/sec, Anisotropy Scan Level = 1.03

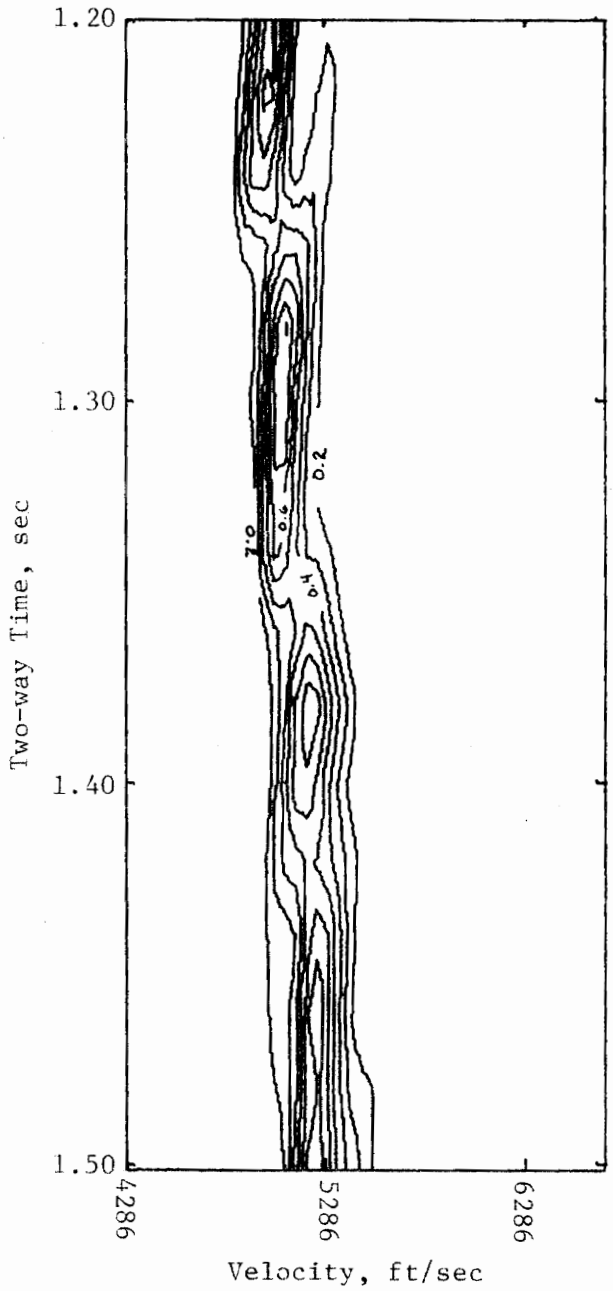

Figure 7.3-6c. Velocity Analysis of SV Component Data Anisotropy = 1.043, Window Width = 50 ms, Scan Increments = 20 ms and 53 ft/sec, Anisotropy Scan Level = 1.04

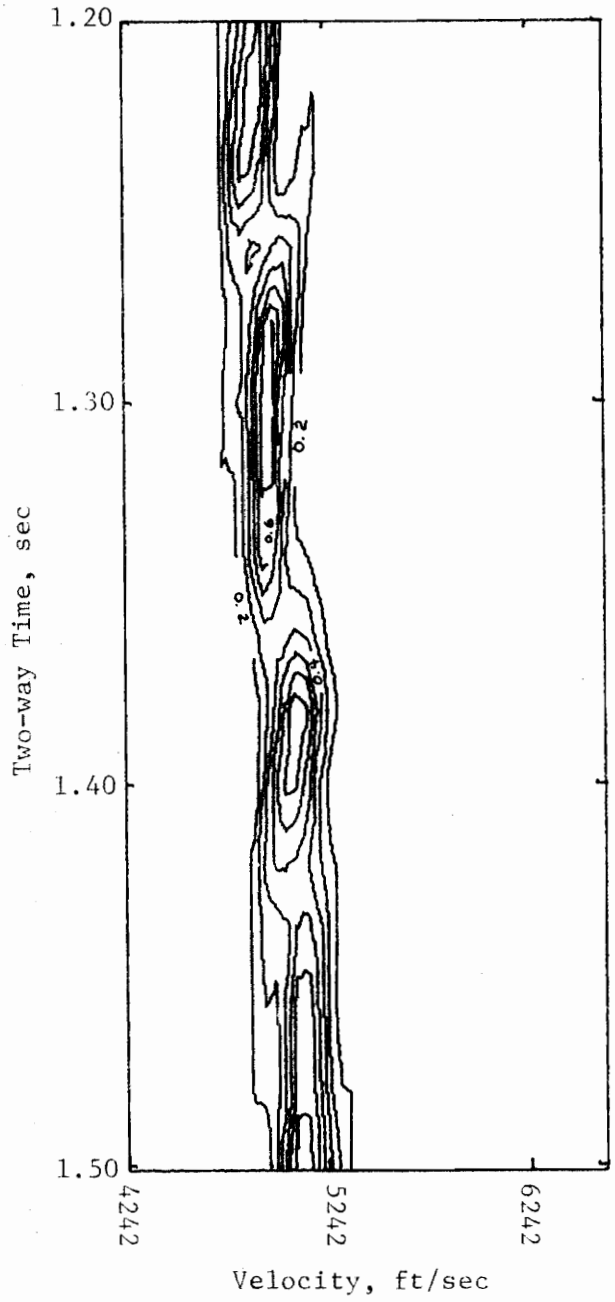

Figure 7.3-6d. Velocity Analysis of SV Component Data Anisotropy = 1.043, Window Width = 50 ms, Scan Increments = 20 ms and 53 ft/sec, Anisotropy Scan Level = 1.05

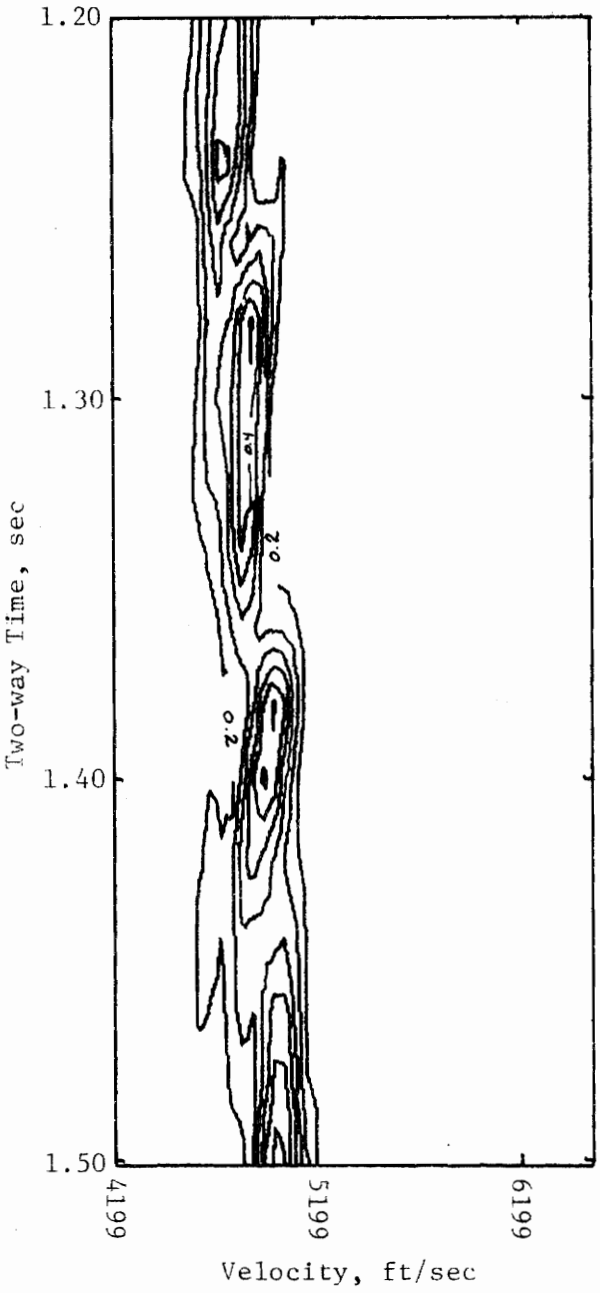

Figure 7.3-6e. Velocity Analysis of SV Component
Data Anisotropy = 1.043, Window Width = 50 ms,
Scan Increments = 20 ms and 52 ft/sec,
Anisotropy Scan Level = 1.06

Table 7.3-2. Integrated Velocity Analysis Results

Velocity Analysis Parameters: See Figures 7.3-5 and 7.3-6.

Integration Range: Semblance Values > 0.4

Data Anisotropy = 1.043

Assumed Anisotropy Scan Value	Normalized Results of Integration	
	P	SV
1.02	87.5	98.3
1.03	91.5	98.5
1.04	94.5	100.0
1.05	91.3	95.2
1.06	100.0	73.6

difficult test of resolving power since the amount of anisotropy is small. The velocity analyses for P are shown in Figure 7.3-7 for anisotropy scan levels from 1.00 to 1.04. The velocity analyses for SV over the same scan level range are shown in Figure 7.3-8. Table 7.3-3 contains the normalized results of integration of the velocity analyses depicted in Figures 7.3-7 and 7.3-8. This table shows quite clearly that the P analyses again are not useful for resolution of the anisotropy. The SV portion of this table demonstrates that even for such a small amount of anisotropy that it can be resolved to within $\pm$0.01. This is equivalent to resolving the difference between the horizontal and vertical velocity component (P) at the surface to within about $\pm$80 ft/sec where the actual velocities are 8000 and 7850 ft/sec respectively. As was expected, the resolving power of the method is not as great for this set of data as for the data set with anisotropy 1.043.

The resolving power of the method was found to be the greatest when the data set with an anisotropy factor of 1.08 was analyzed. Again, the velocity analyses over P were inconclusive as is shown in Table 7.3-4 and Figure 7.3-9. The anisotropy scan levels used ranged from 1.06 to 1.10 for both P and SV. The SV analyses are shown in Figure 7.3-10. The results (SV) in Table 7.3-4 show that there is no ambiguity in choosing the correct anisotropy level.

The analysis of these three sets of data is indicative of the general resolution capabilities of the analysis method. The P component velocity analyses of these data are insensitive to the degree of anisotropy. The SV component velocity analyses are quite sensitive to

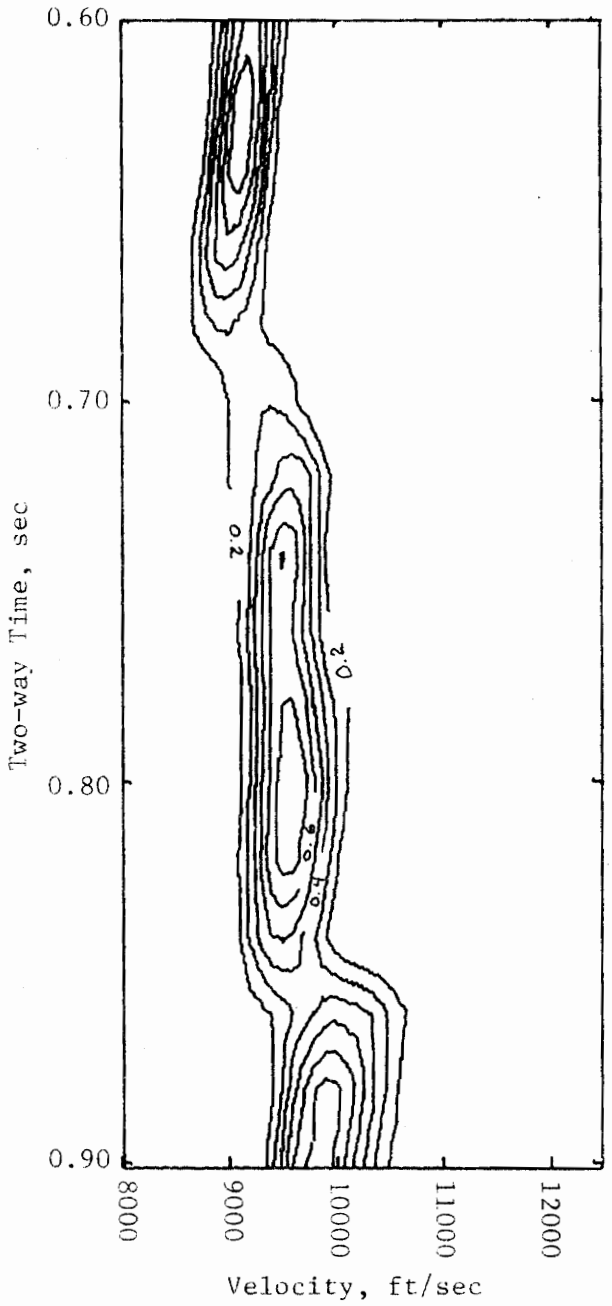

Figure 7.3-7a. Velocity Analysis of P Component
Data Anisotropy = 1.02, Window Width = 50 ms,
Scan Increments = 20 ms and 100 ft/sec,
Anisotropy Scan Level = 1.00

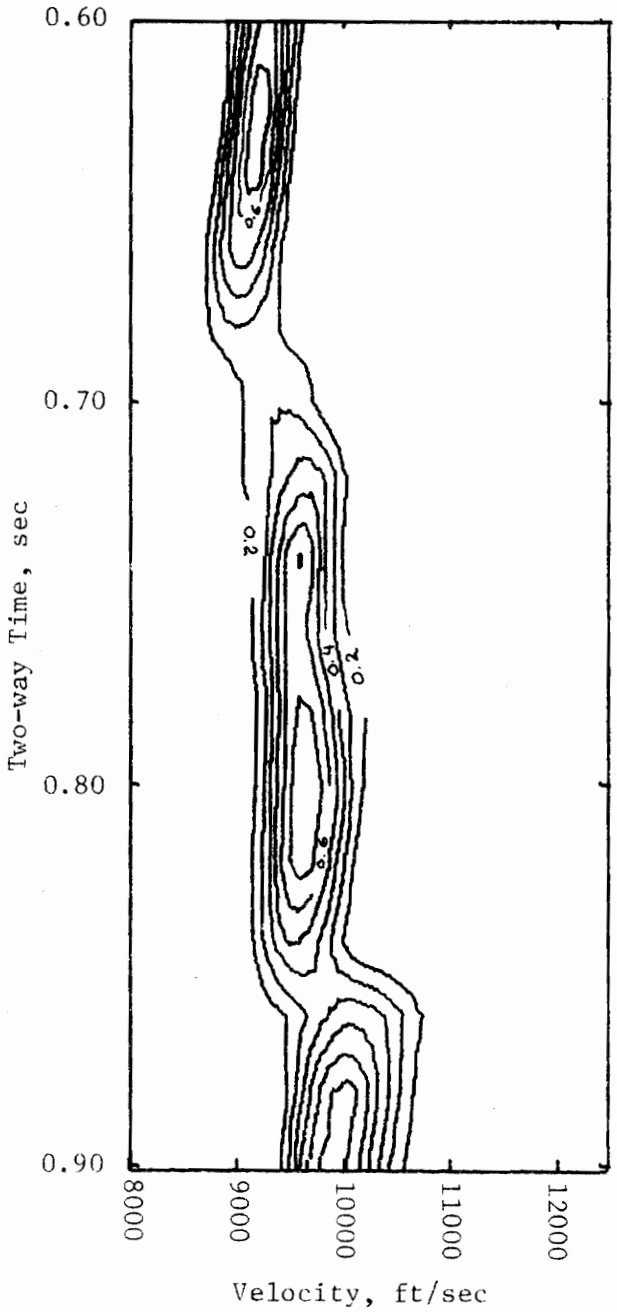

Figure 7.3-7b. Velocity Analysis of P Component Data Anisotropy = 1.02, Window Width = 50 ms, Scan Increments = 20 ms and 100 ft/sec, Anisotropy Scan Level = 1.01

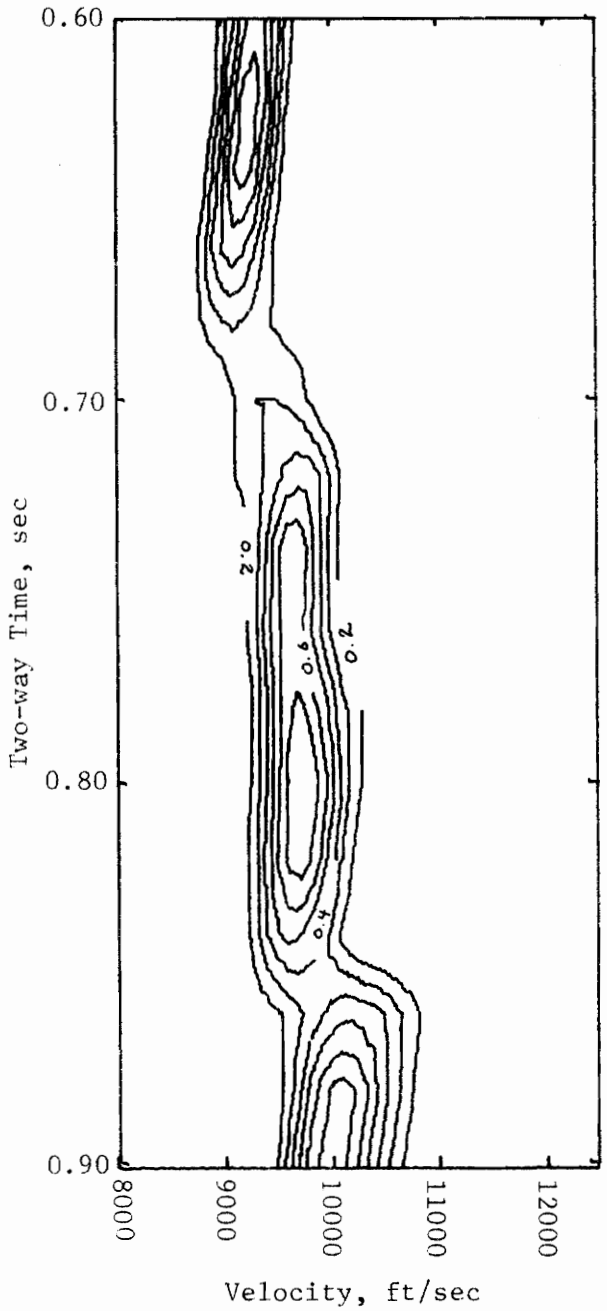

Figure 7.3-7c. Velocity Analysis of P Component
Data Anisotropy = 1.02, Window Width = 50 ms,
Scan Increments = 20 ms and 100 ft/sec,
Anisotropy Scan Level = 1.02

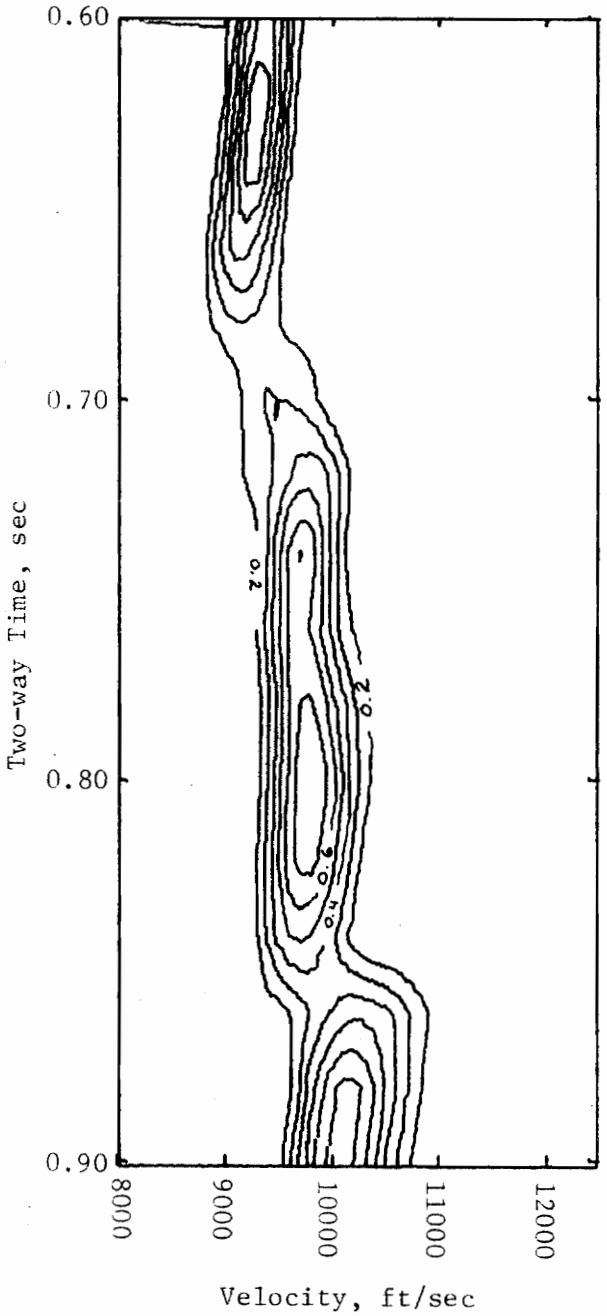

Figure 7.3-7d. Velocity Analysis of P Component
Data Anisotropy = 1.02, Window Width = 50 ms,
Scan Increments = 20 ms and 100 ft/sec,
Anisotropy Scan Level = 1.03

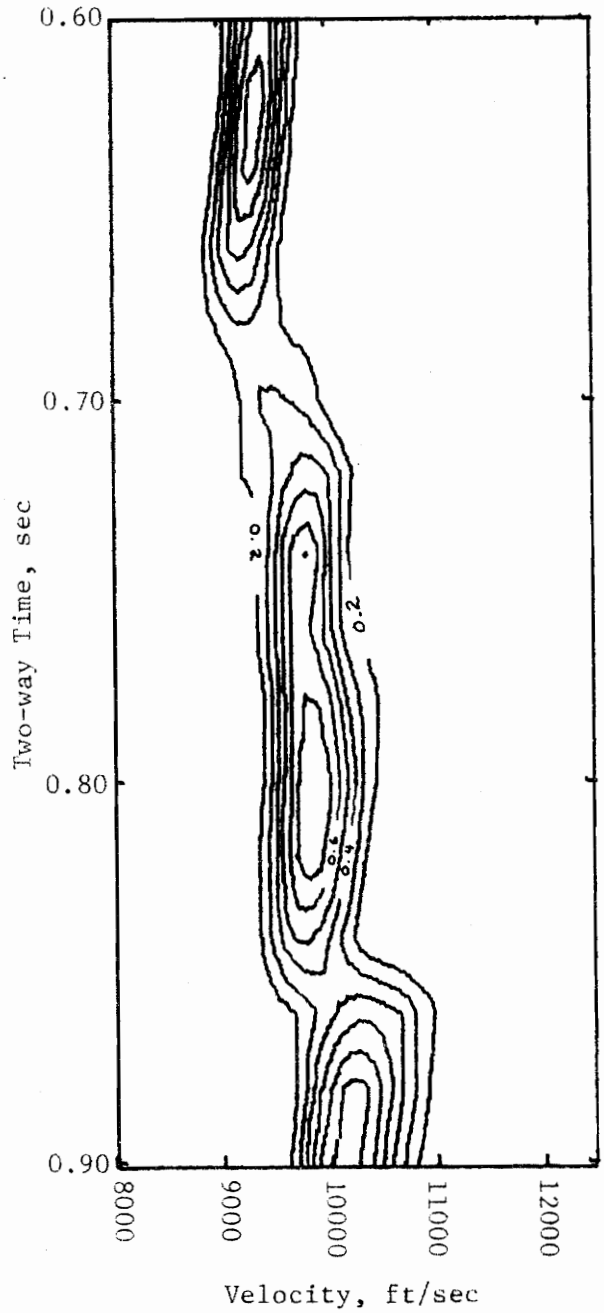

Figure 7.3-7e. Velocity Analysis of P Component Data Anisotropy = 1.02, Window Width = 50 ms, Scan Increments = 20 ms and 100 ft/sec, Anisotropy Scan Level = 1.04

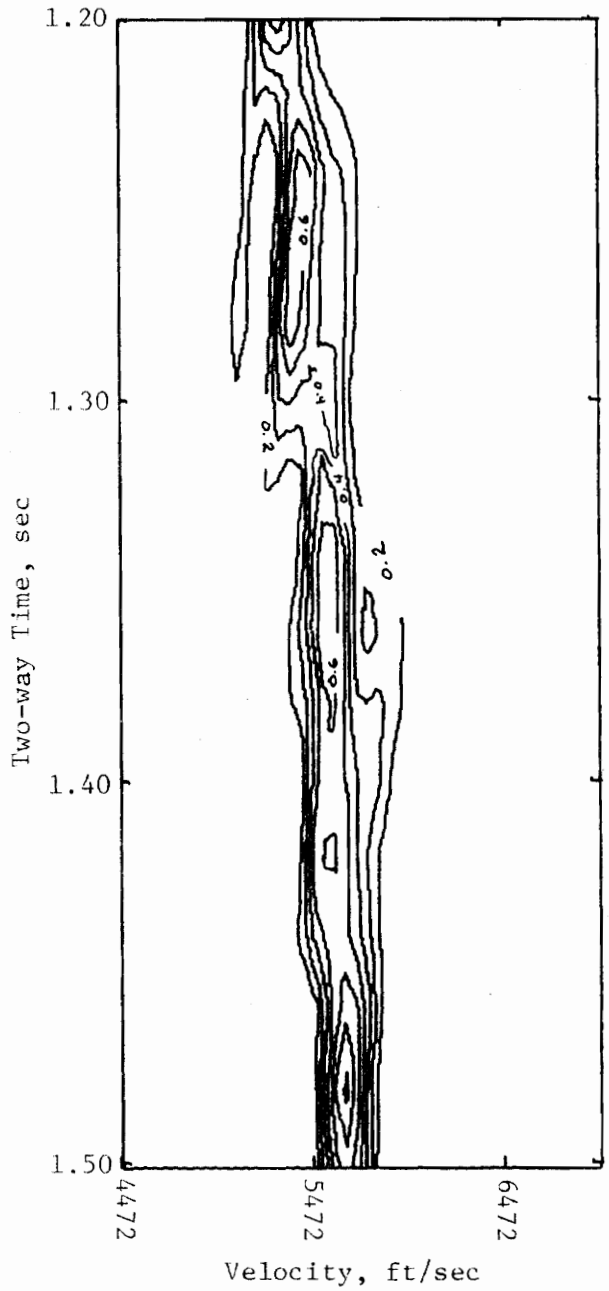

Figure 7.3-8a. Velocity Analysis of SV Component
Data Anisotropy = 1.02, Window Width = 50 ms,
Scan Increments = 20 ms and 55 ft/sec,
Anisotropy Scan Level = 1.00

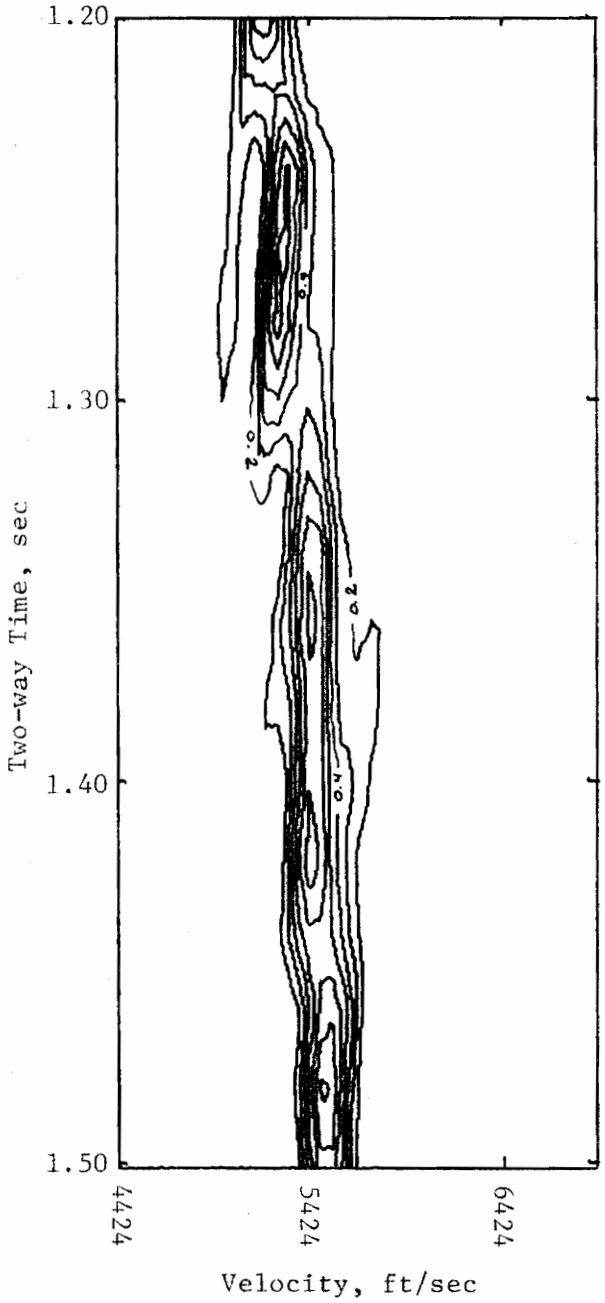

Figure 7.3-8b. Velocity Analysis of SV Component
Data Anisotropy = 1.02, Window Width = 50 ms,
Scan Increments = 20 ms and 55 ft/sec,
Anisotropy Scan Level = 1.01

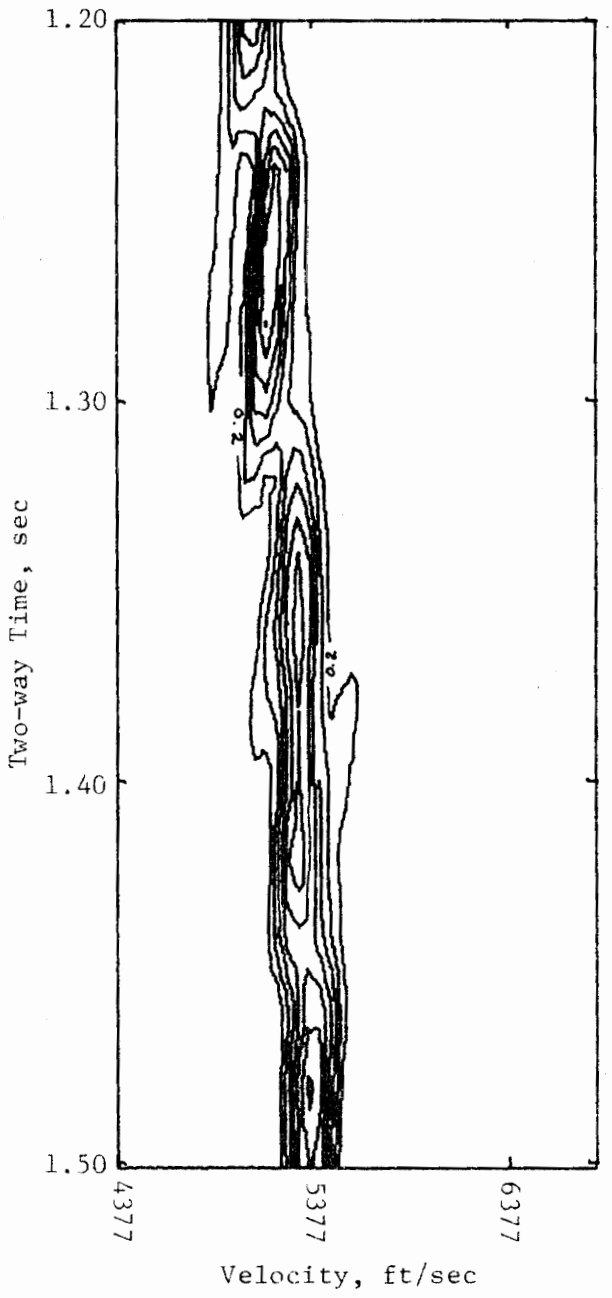

Figure 7.3-8c. Velocity Analysis of SV Component Data Anisotropy = 1.02, Window Width = 50 ms, Scan Increments = 20 ms and 54 ft/sec, Anisotropy Scan Level = 1.02

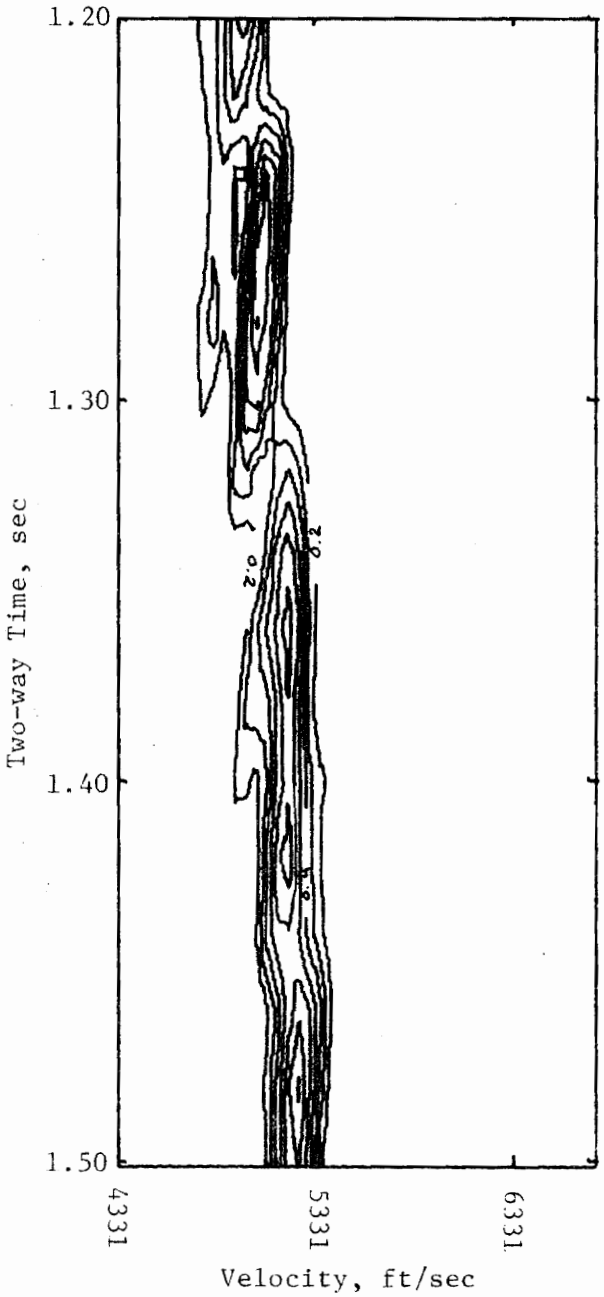

Figure 7.3-8d. Velocity Analysis of SV Component
Data Anisotropy = 1.02, Window Width = 50 ms,
Scan Increments = 20 ms and 54 ft/sec,
Anisotropy Scan Level = 1.03

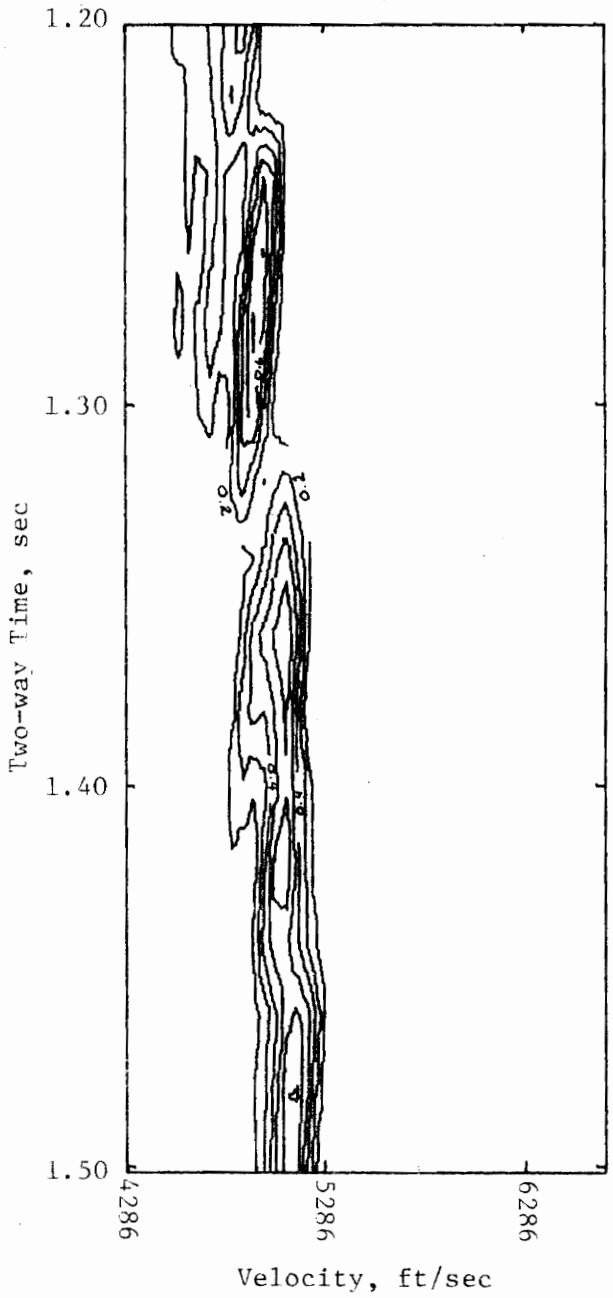

Figure 7.3-8e. Velocity Analysis of SV Component
Data Anisotropy = 1.02, Window Width = 50 ms,
Scan Increments = 20 ms and 53 ft/sec,
Anisotropy Scan Level = 1.04

Table 7.3-3. Integrated Velocity Analysis Results

Velocity Analysis Parameters: See Figures 7.3-7 and 7.3-8.

Integration Range: Semblance Values > 0.4

Data Anisotropy = 1.02

Assumed Anisotropy Sean Value	Normalized Results of Integration P	SV
1.00	96.6	97.0
1.01	96.7	100.0
1.02	99.6	94.9
1.03	97.2	93.7
1.04	100.0	82.9

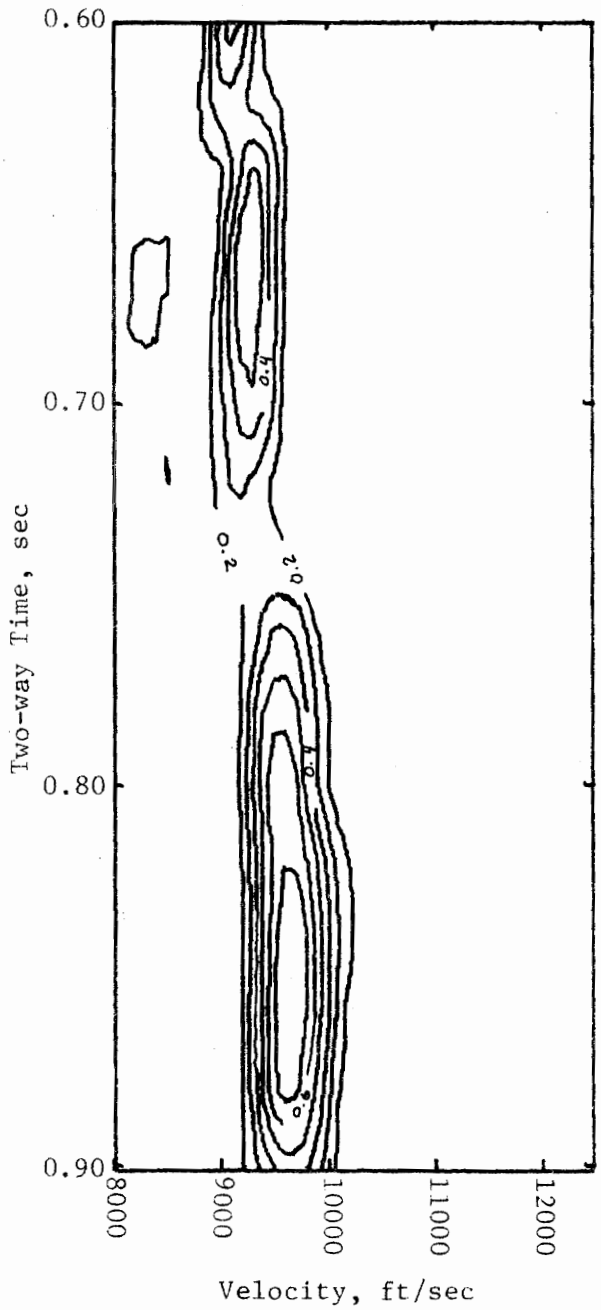

Figure 7.3-9a. Velocity Analysis of P Component Data Anisotropy = 1.08, Window Width = 50 ms, Scan Increments = 20 ms and 100 ft/sec, Anisotropy Scan Level = 1.06

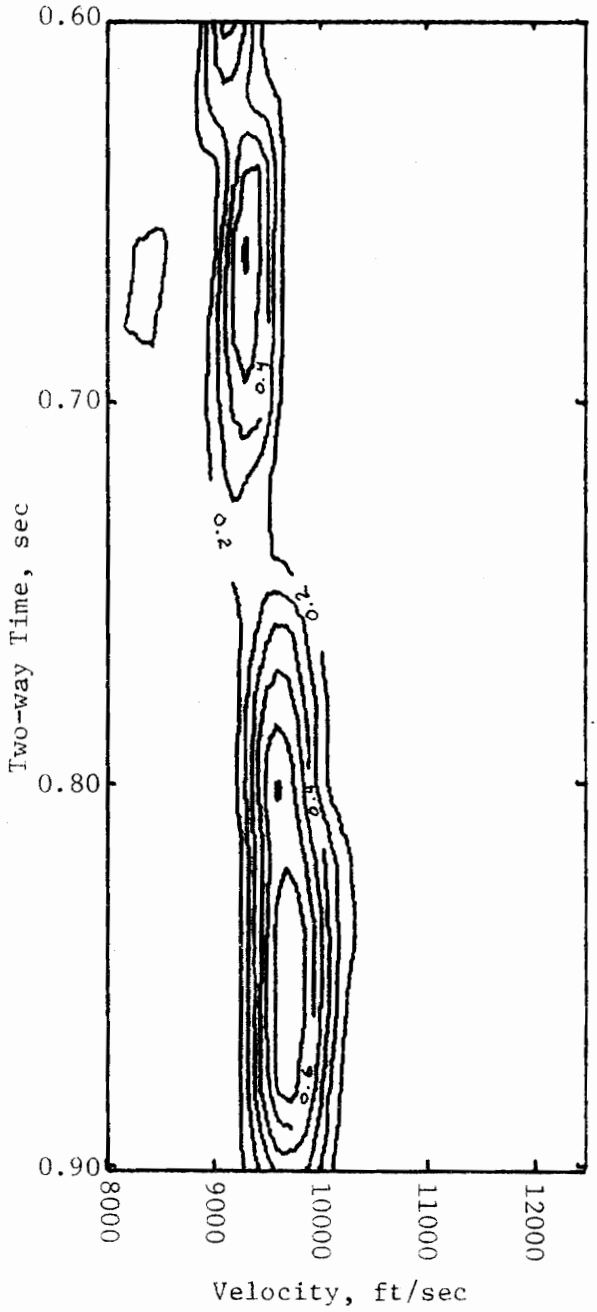

Figure 7.3-9b. Velocity Analysis of P Component Data Anisotropy = 1.08, Window Width = 50 ms, Scan Increments = 20 ms and 100 ft/sec, Anisotropy Scan Level = 1.07

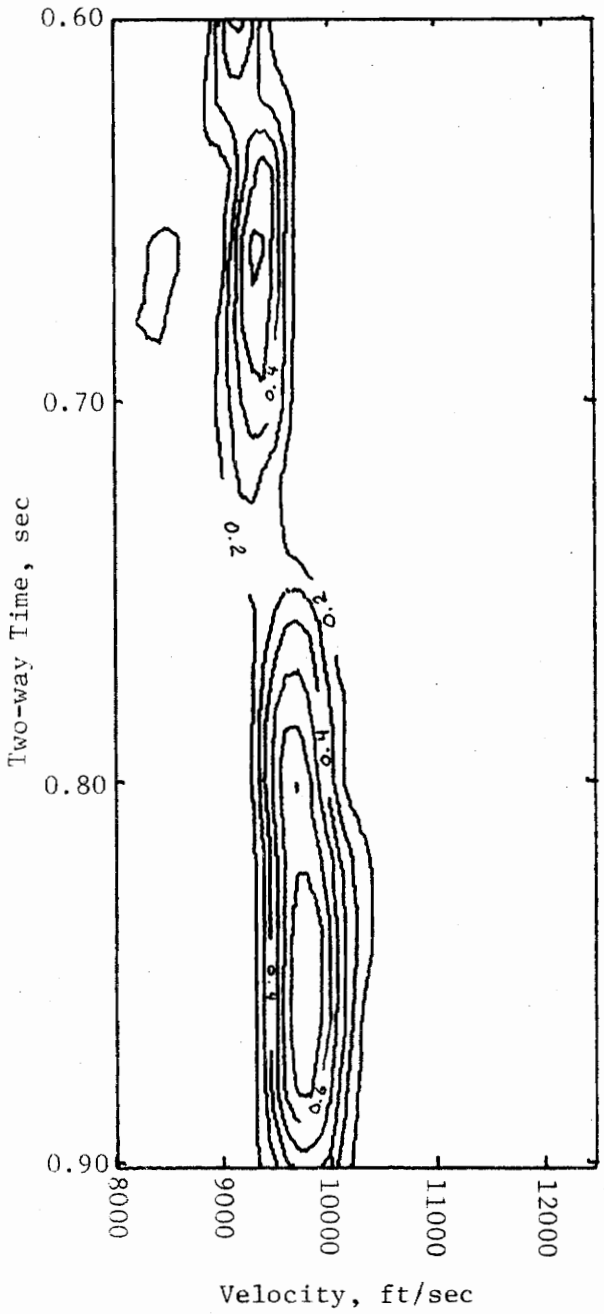

Figure 7.3-9c. Velocity Analysis of P Component Data Anisotropy = 1.08, Window Width = 50 ms, Scan Increments = 20 ms and 100 ft/sec, Anisotropy Scan Level = 1.08

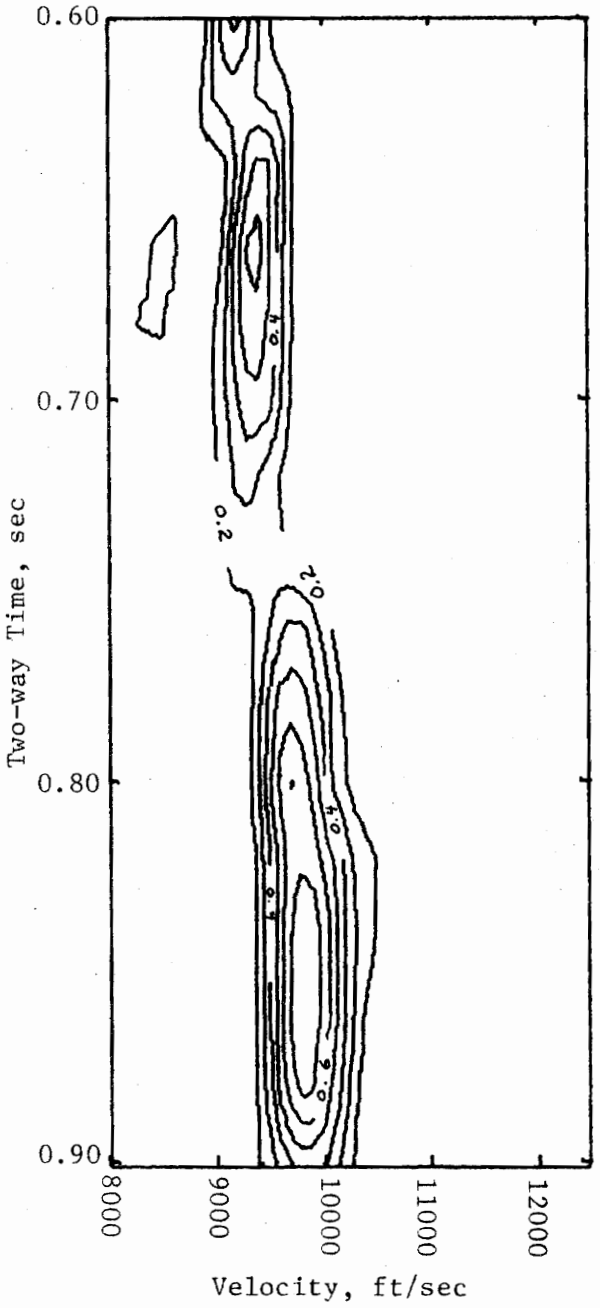

Figure 7.3-9d. Velocity Analysis of P Component Data Anisotropy = 1.08, Window Width = 50 ms, Scan Increments = 20 ms and 100 ft/sec, Anisotropy Scan Level = 1.09

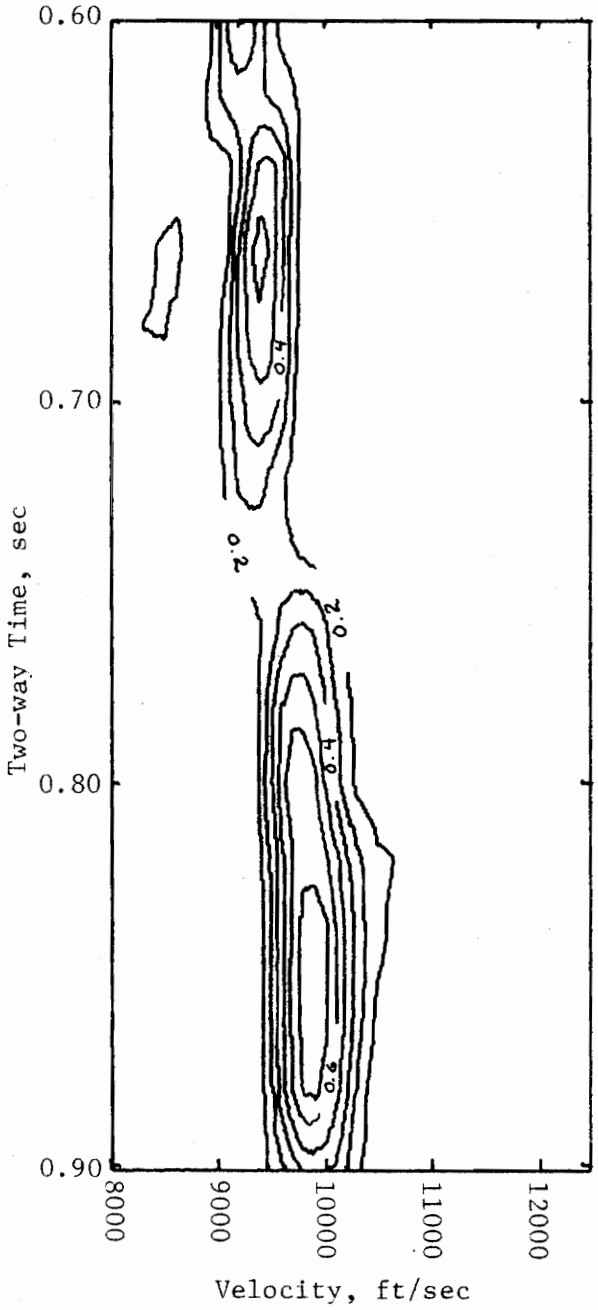

Figure 7.3-9e. Velocity Analysis of P Component Data Anisotropy = 1.08, Window Width = 50 ms, Scan Increments = 20 ms and 100 ft/sec, Anisotropy Scan Level = 1.10

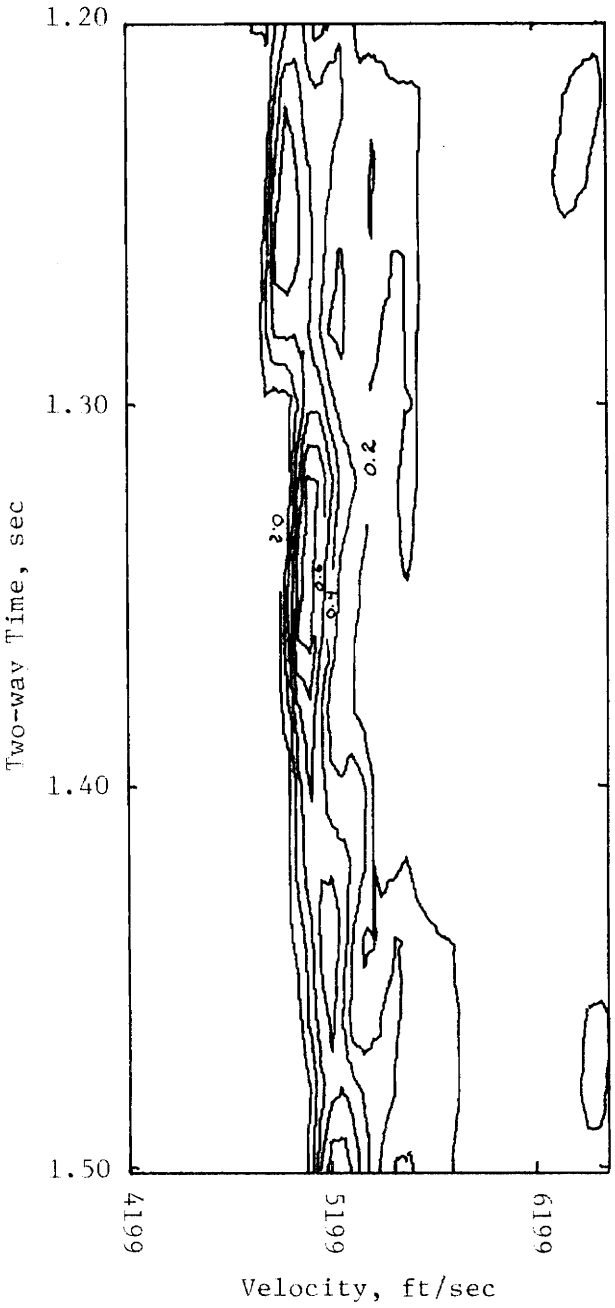

Figure 7.3-10a. Velocity Analysis of SV Component
Data Anisotropy = 1.08, Window Width = 50 ms,
Scan Increments = 20 ms and 52 ft/sec,
Anisotropy Scan Level = 1.06

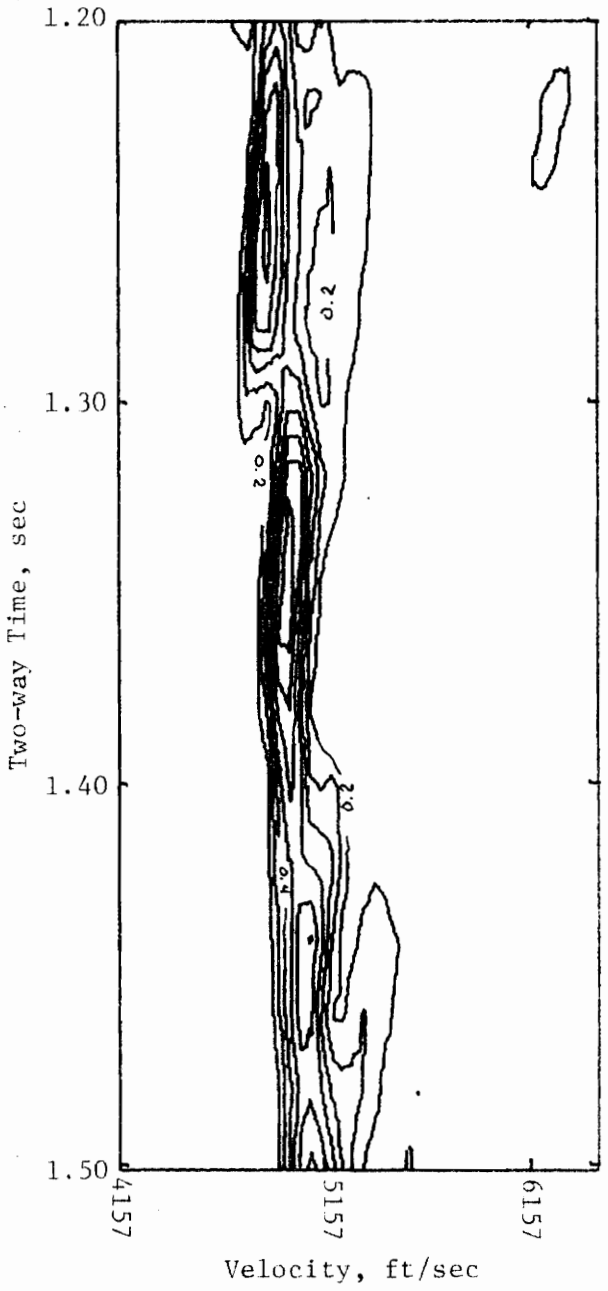

Figure 7.3-10b. Velocity Analysis of SV Component
Data Anisotropy = 1.08, Window Width = 50 ms,
Scan Increments = 20 ms and 51 ft/sec,
Anisotropy Scan Level = 1.07

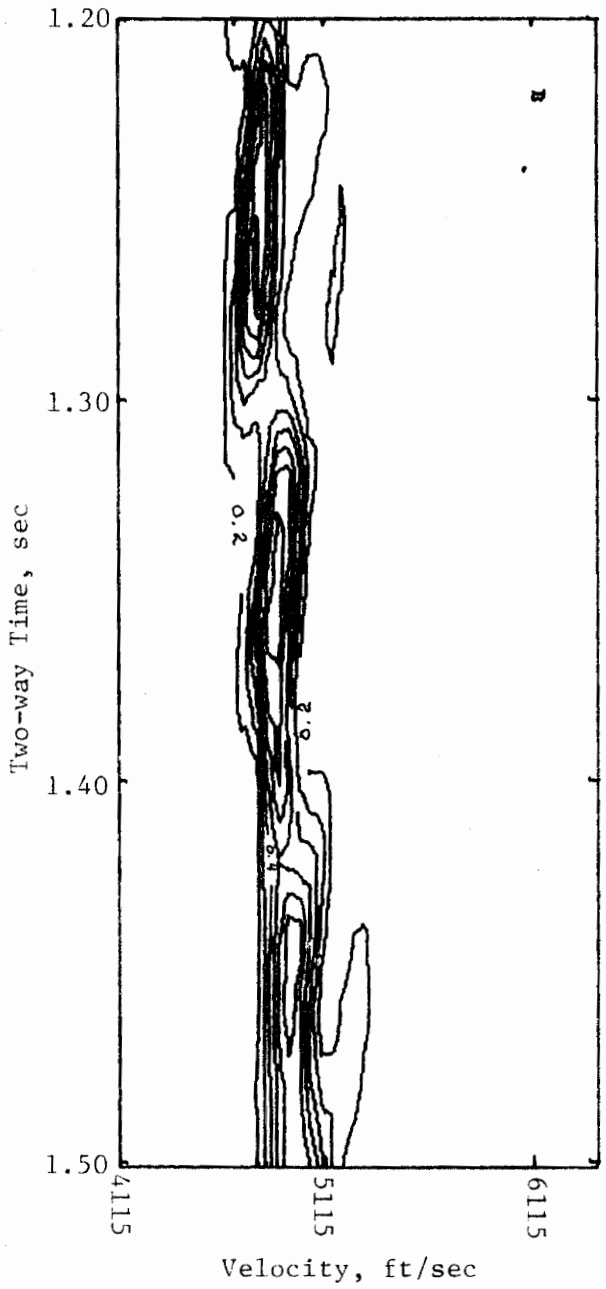

Figure 7.3-10c. Velocity Analysis of SV Component
Data Anisotropy = 1.08, Window Width = 50 ms,
Scan Increments = 20 ms and 51 ft/sec,
Anisotropy Scan Level = 1.08

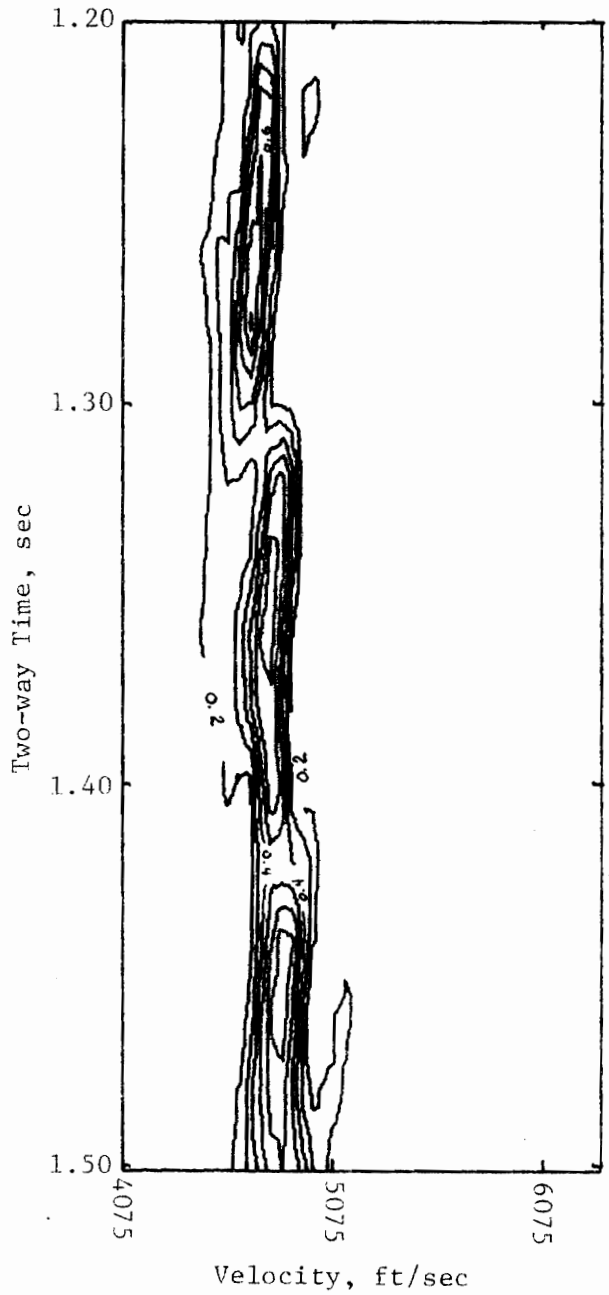

Figure 7.3-10d. Velocity Analysis of SV Component Data Anisotropy = 1.08, Window Width = 50 ms, Scan Increments = 20 ms and 50 ft/sec, Anisotropy Scan Level = 1.09

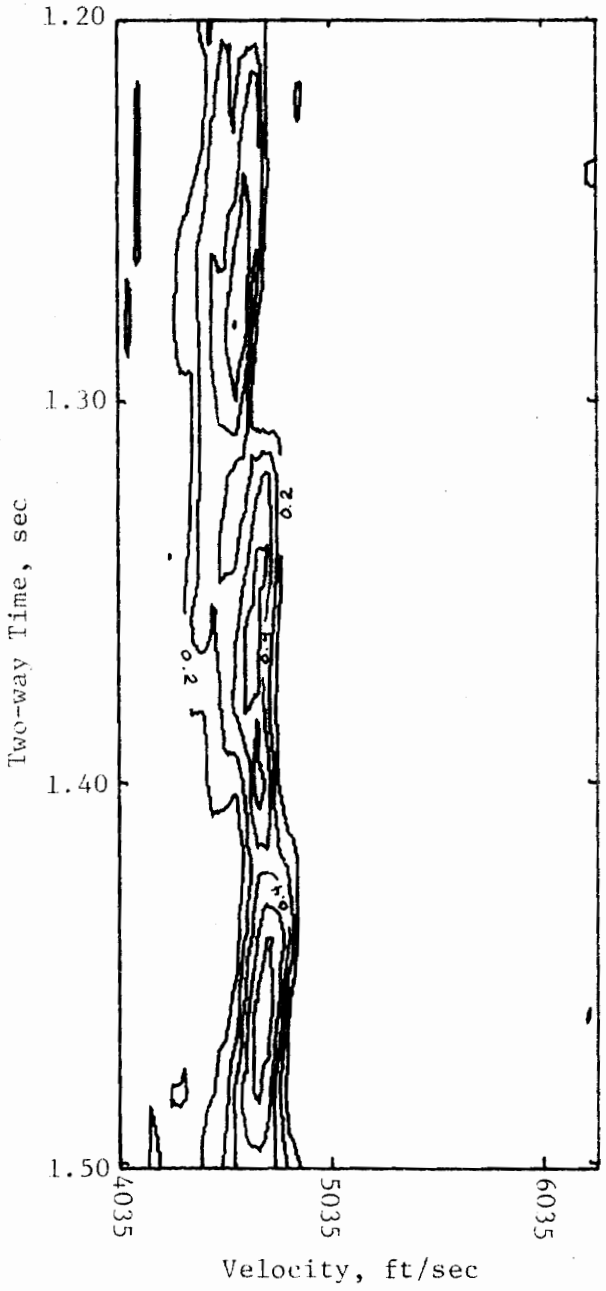

Figure 7.3-10e. Velocity Analysis of SV Component Data Anisotropy = 1.08, Window Width = 50 ms, Scan Increments = 20 ms and 50 ft/sec, Anisotropy Scan Level = 1.10

Table 7.3-4. Integrated Velocity Analysis Results

Velocity Analysis Parameters: See Figures 7.3-9 and 7.3-10.

Integration Range: Semblance Values > 0.4

Data Anisotropy = 1.08

Assumed Anisotropy Scan Value	Normalized Results of Integration	
	P	SV
1.06	92.7	80.9
1.07	96.2	98.7
1.08	96.8	100.0
1.09	95.6	90.4
1.10	100.0	60.9

the degree of anisotropy and this sensitivity increases rapidly with increasing anisotropy. The explanation of the difference in the P and SV results lies in the effects of anisotropy on normal moveout. For P these effects are negligible while they are large for SV.

7.4 Single Anisotropic Layer

This model is a homogeneous half-space in the sense discussed in section 5.3.1. It is a useful model since normal moveout may be studied without effects due to variations in velocity. This model provides a baseline by which to judge the performance of the velocity analysis techniques. Again, as in section 7.3, the horizontal compressional component was chosen as a reference and has the value of 8000 ft/sec. Three sets of synthetic reflection data were generated with anisotropy factors of 1.02, 1.043, and 1.08 respectively.

7.4.1 Effects of Variation of Model Parameters on Velocity Analysis

Spread Dimensions

All reflection data for this model were generated using CDP geometry. The maximum shotpoint-geophone distance used in the generation of the data was 5280 feet. The data are 12-fold with all shotpoint-geophone distances being multiples of 440 feet. This is the same CDP geometry used with the other more complex models.

Variations in Reflection Coefficients

The set of reflection coefficients used in section 7.3 to generate synthetic seismograms was also used for this model. The synthetic seismograms are shown in Figures 7.4-1, 7.4-2, and 7.4-3.

Resolution of Anisotropy

The first set of data analyzed has an anisotropy factor of 1.02. Velocity scans were made utilizing anisotropy factors from 1.00 to 1.04

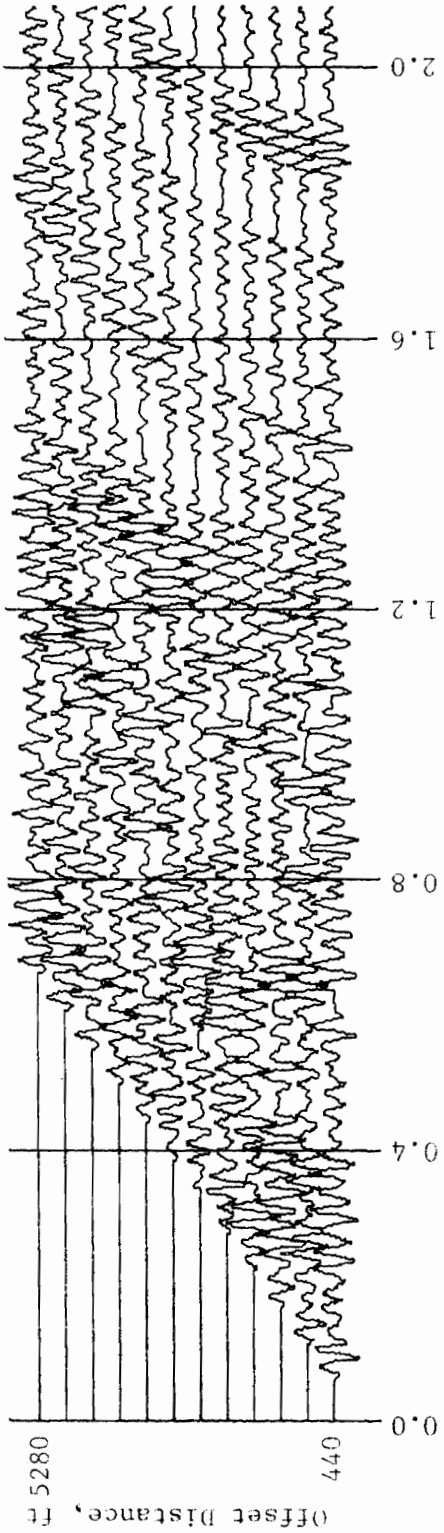

Figure 7.4-1. Single Anisotropic Layer
12-Fold Reflection Seismograms
Data Anisotropy = 1.02

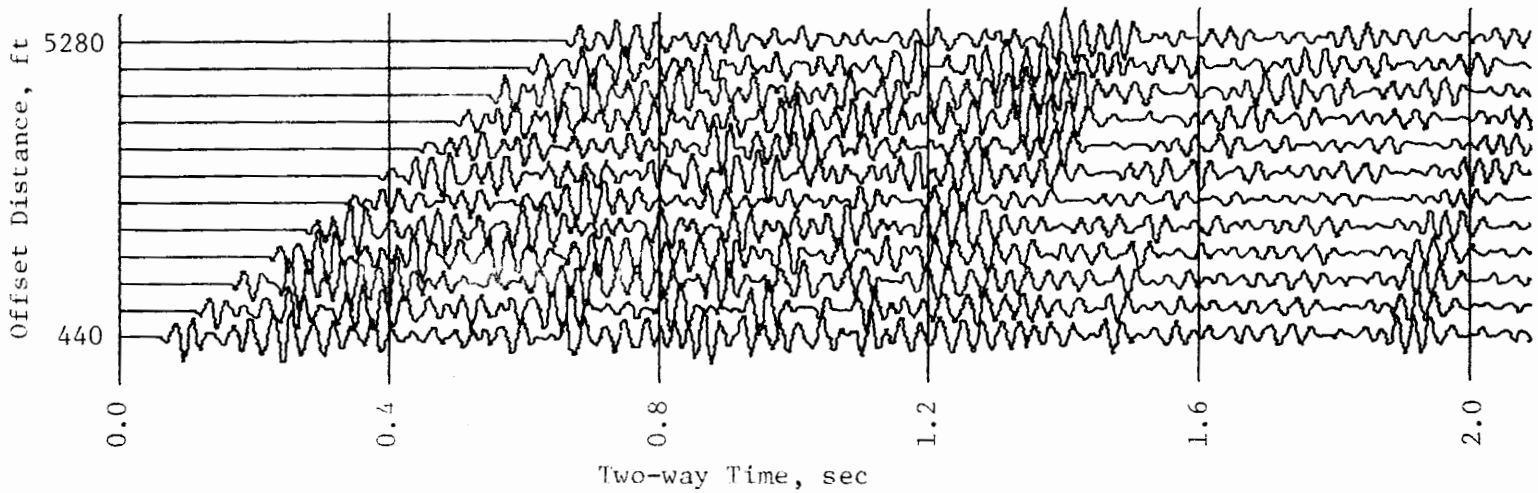

Figure 7.4-2. Single Anisotropic Layer
12-Fold Reflection Seismograms
Data Anisotropy = 1.043

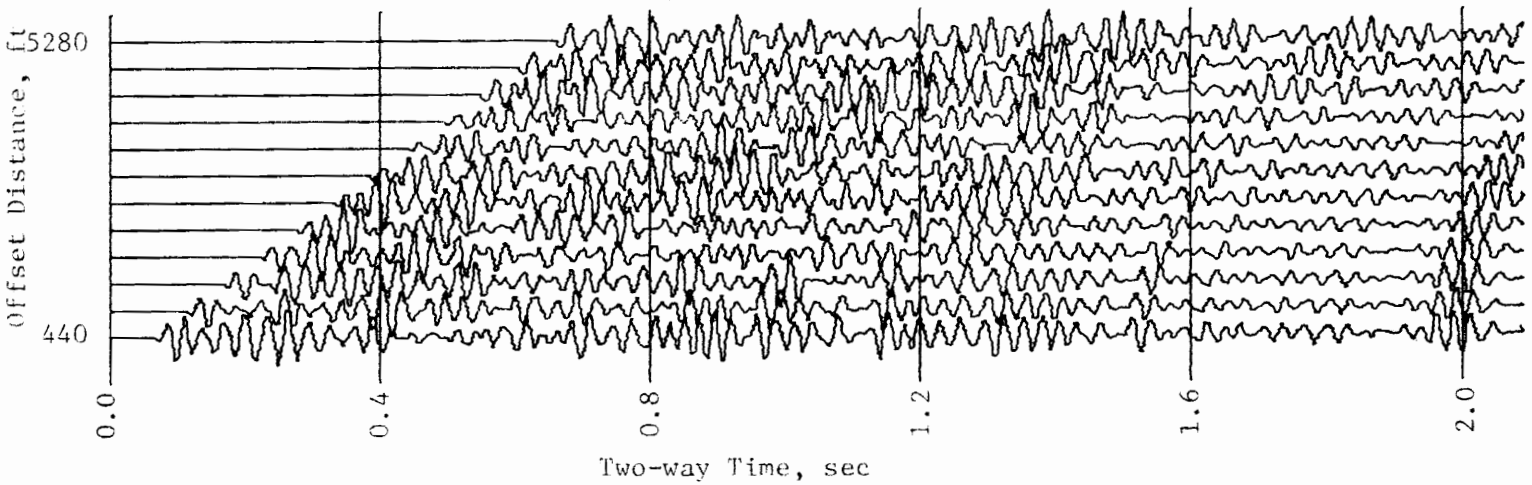

Figure 7.4-3. Single Anisotropic Layer
12-Fold Reflection Seismograms
Data Anisotropy = 1.08

in steps of 0.01. The velocity analyses for the P component of velocity are shown in Figure 7.4-4, and for the SV component in Figure 7.4-5. The volumes under the surfaces defined by the semblance matrices were integrated to determine which anisotropy level best fit the data (See section 7.3). The normalized results of integration are shown for both P and SV in Table 7.4-1. The results of the P analyses is that this component is not useful for the resolution of anisotropy since the integrated matrix values do not possess a sufficient range to allow for the accurate selection of the correct anisotropy factor. The SV results indicate that even for this low level of anisotropy that the resolution is definitely within the range of ± 0.01. Although Table 7.4-1 shows that the anisotropy factor of 1.01 gave better results than the factor of 1.02 by 1 percent, there is no doubt that the choice is only limited to factors 1.01 and 1.02 since the values on either side begin to rapidly decrease in magnitude.

The velocity analyses for the data set having an anisotropy factor of 1.043 are shown in Figures 7.4-6 and 7.4-7 for P and SV respectively. The normalized results of the integration of the semblance matrices are in Table 7.4-2. It will be noted that here the P maximum is the correct one. However, the range of values for P are so close together that this correct P value may be regarded as fortuitous. The correct anisotropy for SV is again the result of integrating the semblance matrices. The nearest value to the maximum is four percent lower and this is regarded as a significant difference.

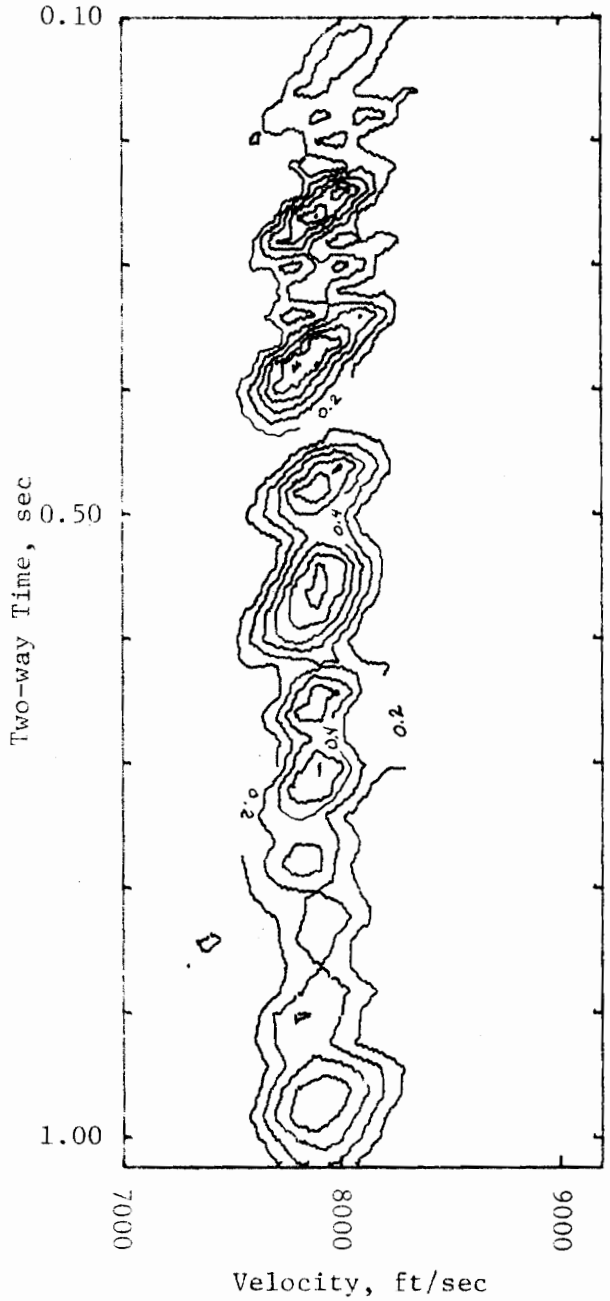

Figure 7.4-4a. Velocity Analysis of P Component Data Anisotropy = 1.02, Window Width = 50 ms, Scan Increments = 20 ms and 100 ft/sec, Anisotropy Scan Level = 1.00

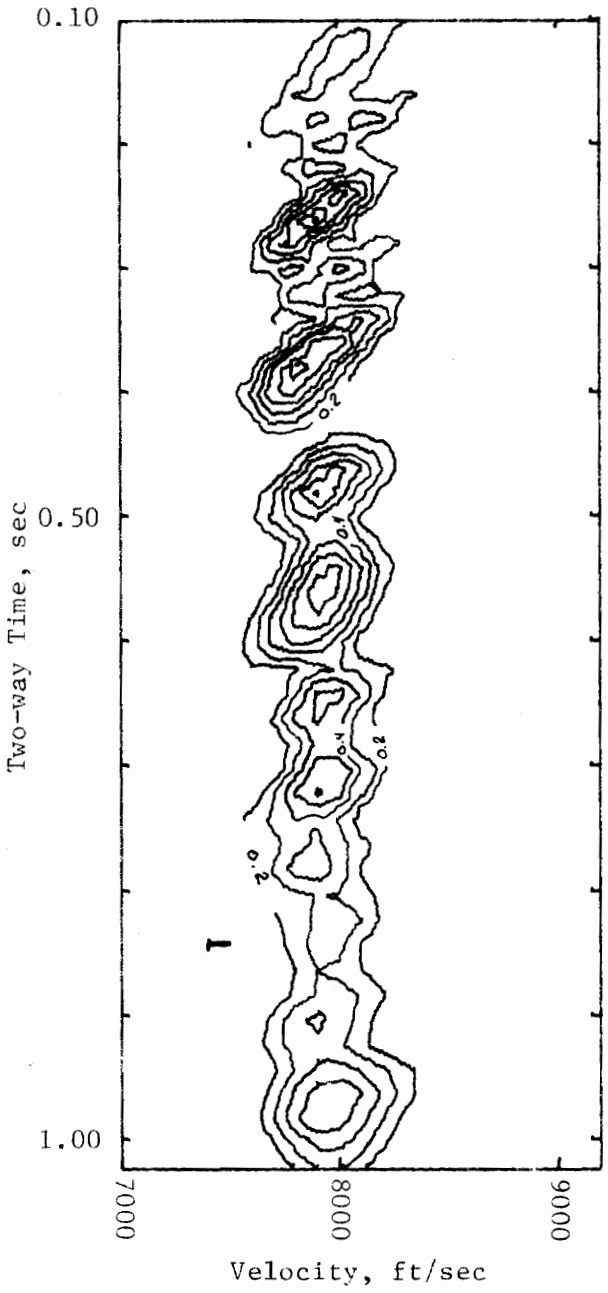

Figure 7.4-4b. Velocity Analysis of P Component Data Anisotropy = 1.02, Window Width = 50 ms, Scan Increments = 20 ms and 100 ft/sec, Anisotropy Scan Level = 1.01

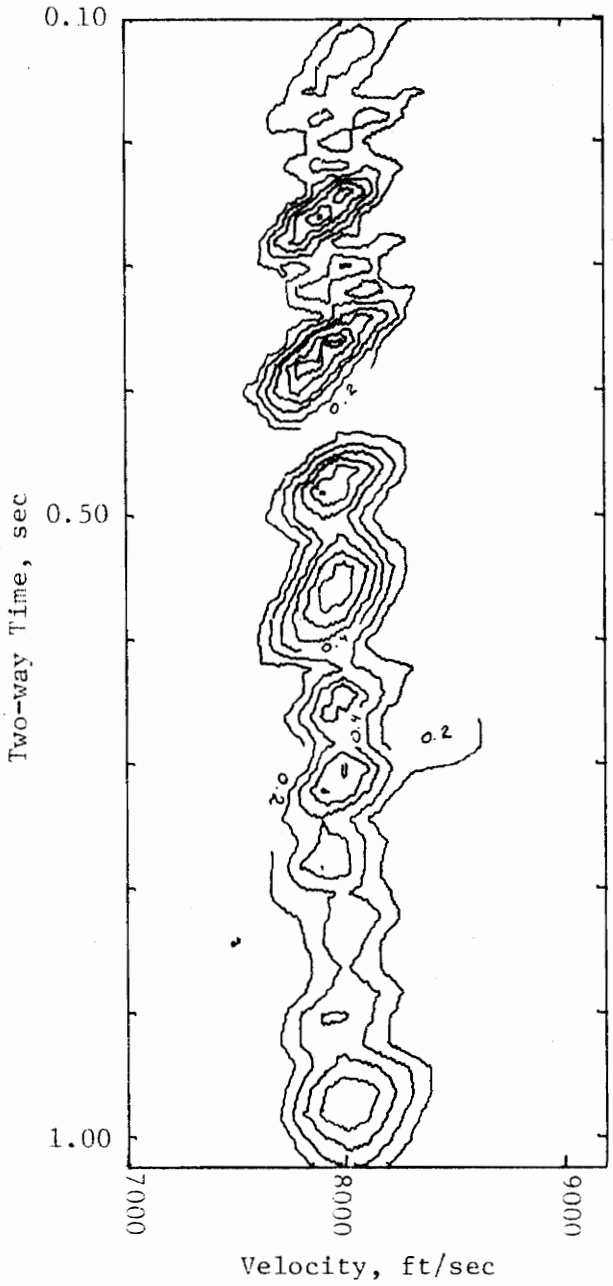

Figure 7.4-4c. Velocity analysis of P Component Data Anisotropy = 1.02, Window Width = 50 ms, Scan Increments = 20 ms and 100 ft/sec, Anisotropy Scan Level = 1.02

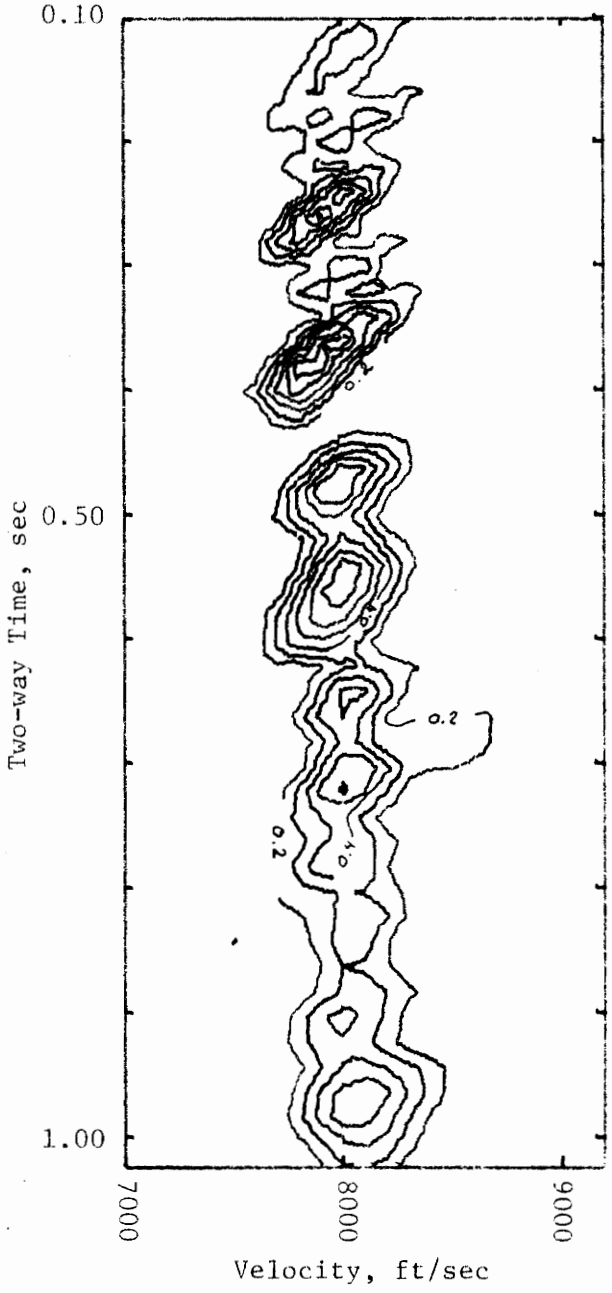

Figure 7.4-4d. Velocity Analysis of P Component Data Anisotropy = 1.02, Window Width = 50 ms, Scan Increments = 20 ms and 100 ft/sec, Anisotropy Scan Level = 1.03

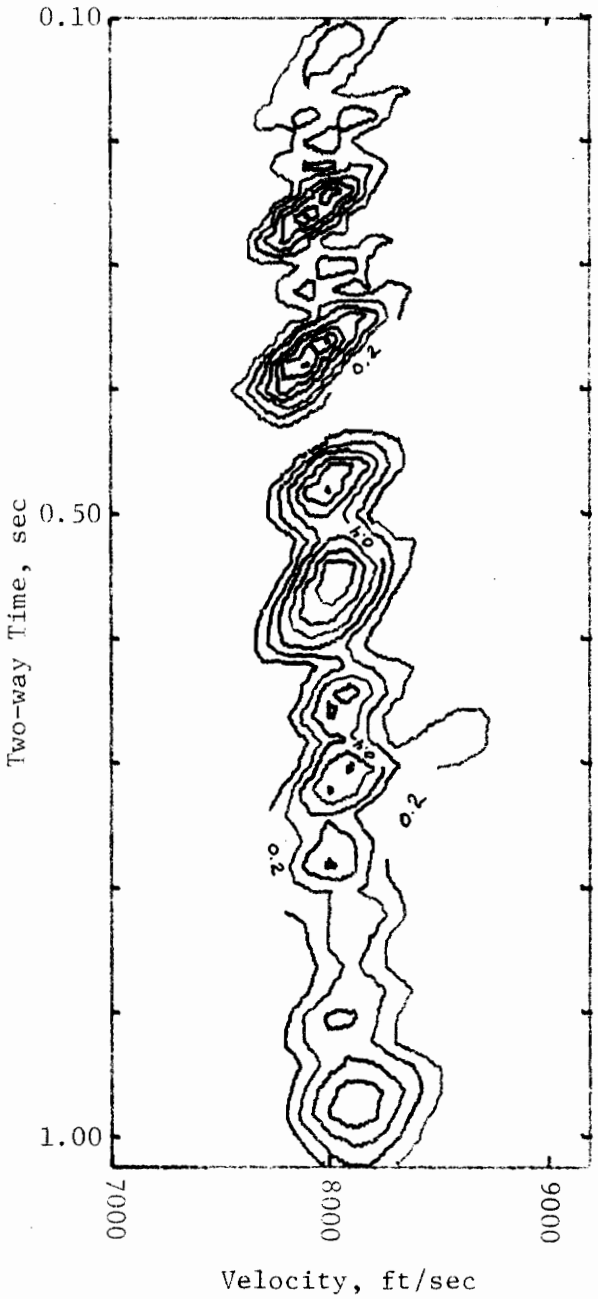

Figure 7.4-4e. Velocity Analysis of P Component Data Anisotropy = 1.02, Window Width = 50 ms, Scan Increments = 20 ms and 100 ft/sec, Anisotropy Scan Level = 1.04

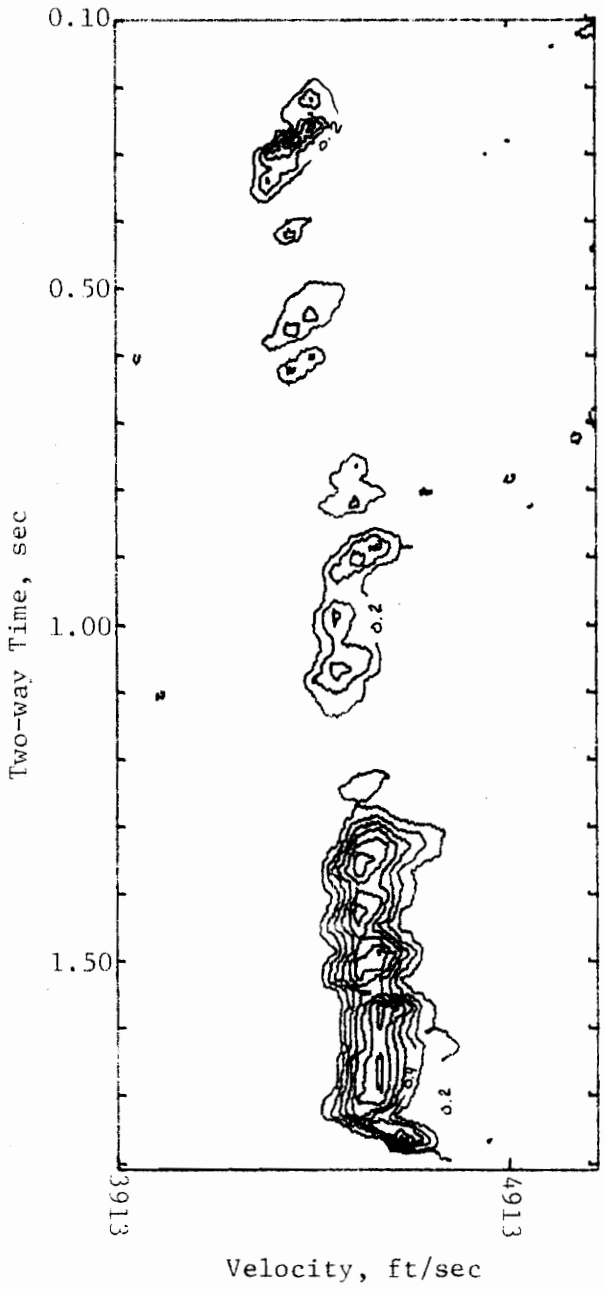

Figure 7.4-5a. Velocity Analysis of SV Component
Data Anisotropy = 1.02, Window Width = 50 ms,
Scan Increments = 20 ms and 55 ft/sec,
Anisotropy Scan Level = 1.00

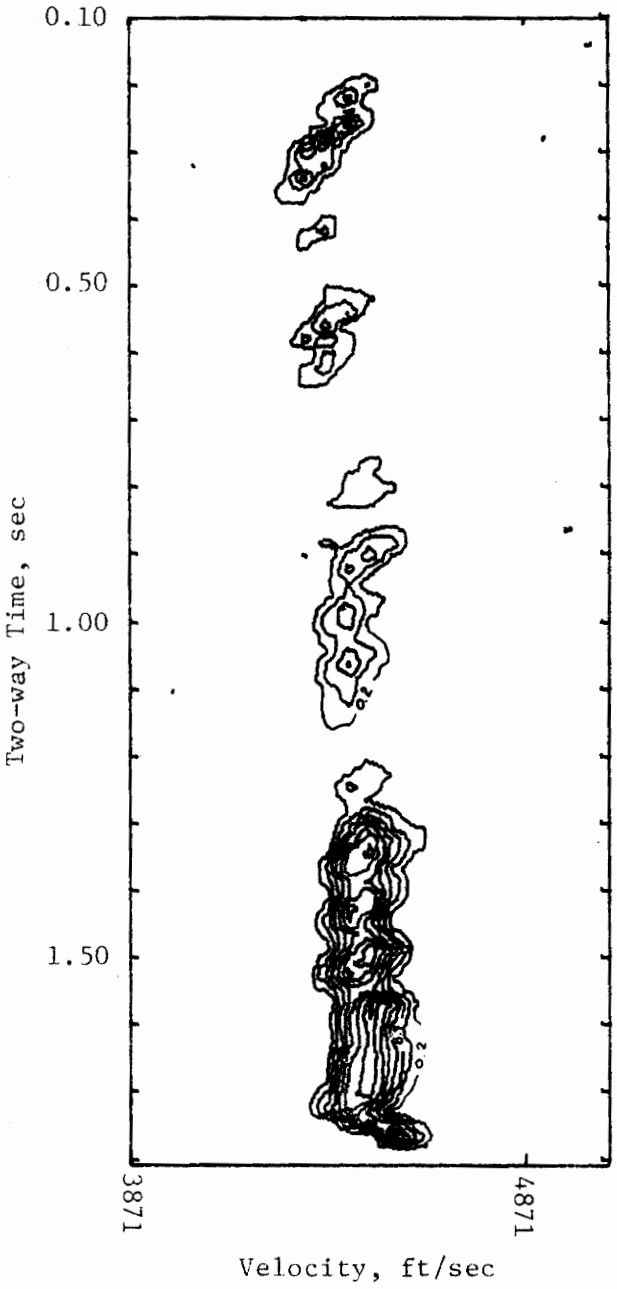

Figure 7.4-5b. Velocity Analysis of SV Component
Data Anisotropy = 1.02, Window Width = 50 ms,
Scan Increments = 20 ms and 55 ft/sec,
Anisotropy Scan Level = 1.01

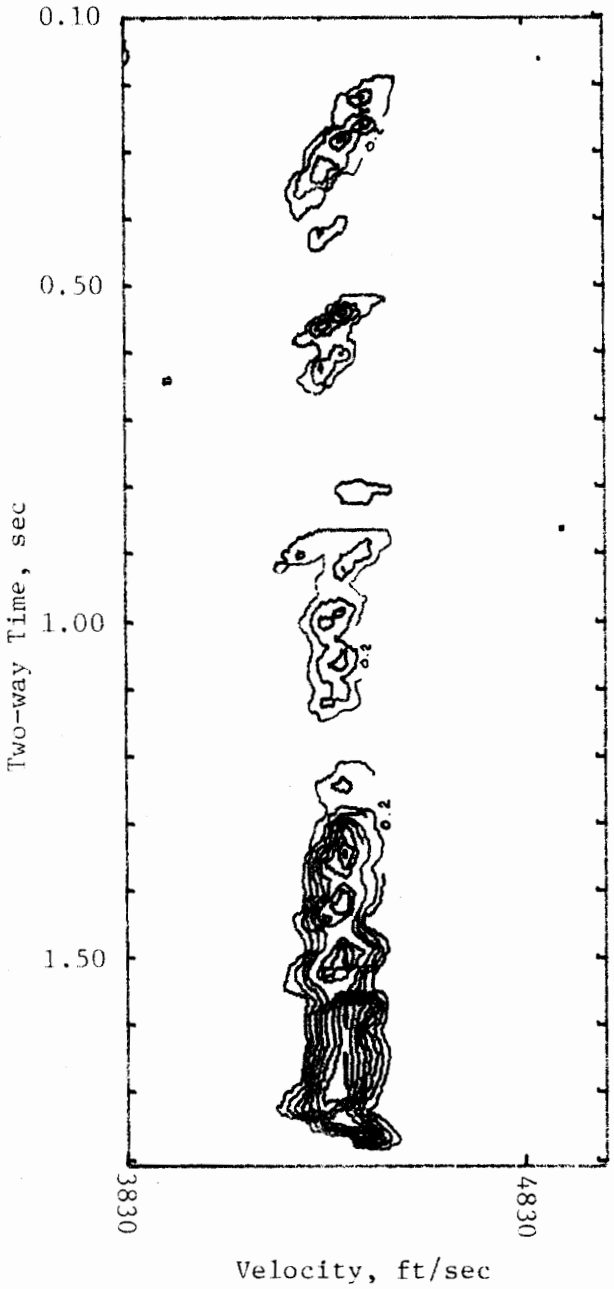

Figure 7.4-5c. Velocity Analysis of SV Component
Data Anisotropy = 1.02, Window Width = 50 ms,
Scan Increments = 20 ms and 54 ft/sec,
Anisotropy Scan Level = 1.02

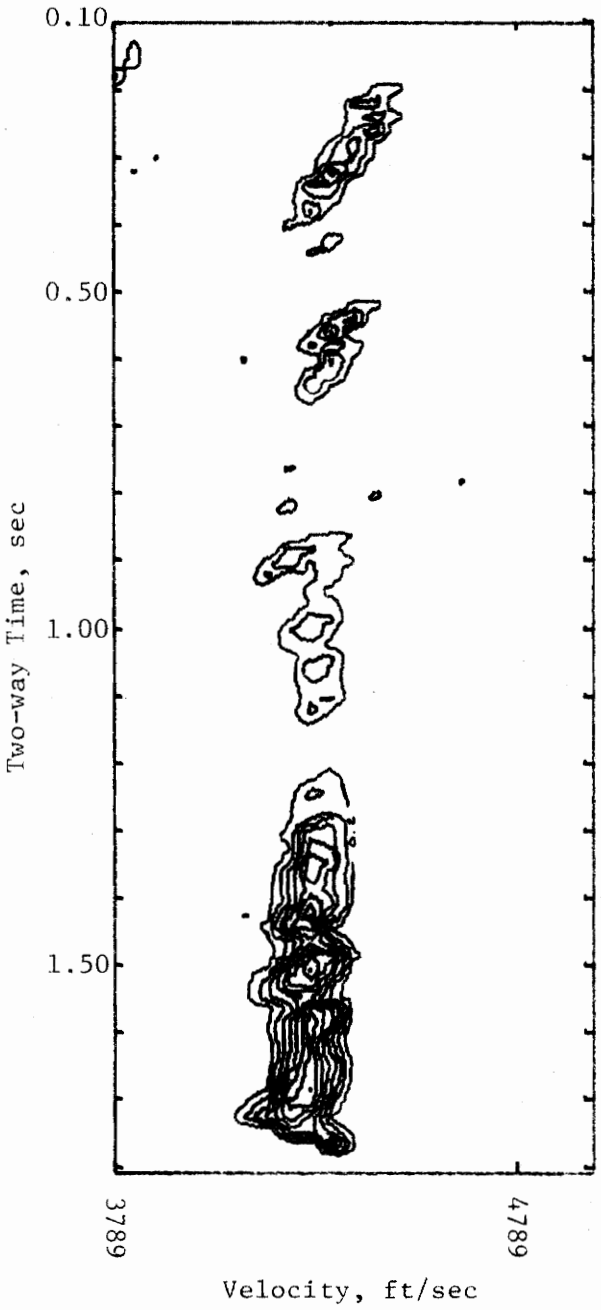

Figure 7.4-5d. Velocity Analysis of SV Component Data Anisotropy = 1.02, Window Width = 50 ms, Scan Increments = 20 ms and 54 ft/sec, Anisotropy Scan Level = 1.03

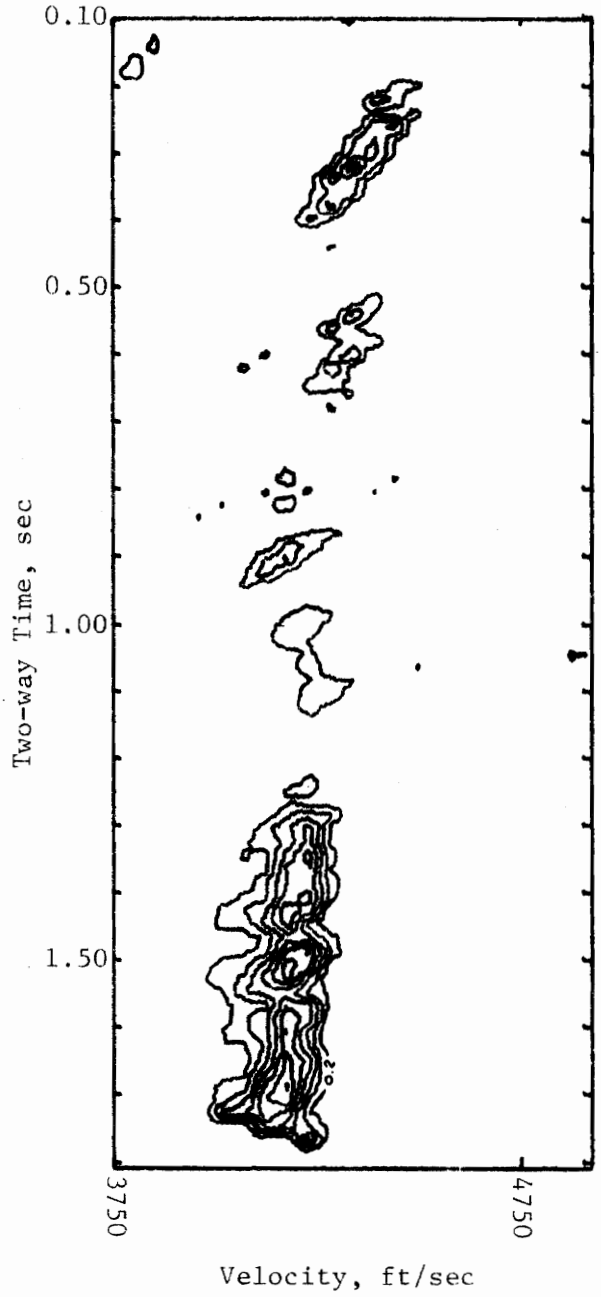

Figure 7.4-5e. Velocity Analysis of SV Component
Data Anisotropy = 1.02, Window Width = 50 ms,
Scan Increments = 20 ms and 53 ft/sec,
Anisotropy Scan Level = 1.04

Table 7.4-1. Integrated Velocity Analysis Results

Velocity Analysis Parameters: See Figures 7.4-4 and 7.4-5.

Integration Range: Semblance Values > 0.4

Data Anisotropy = 1.02

Assumed Anisotropy Scan Value	Normalized Results of Integration	
	P	SV
1.00	95.4	94.6
1.01	98.4	100.0
1.02	99.0	99.0
1.03	99.8	92.1
1.04	100.0	72.1

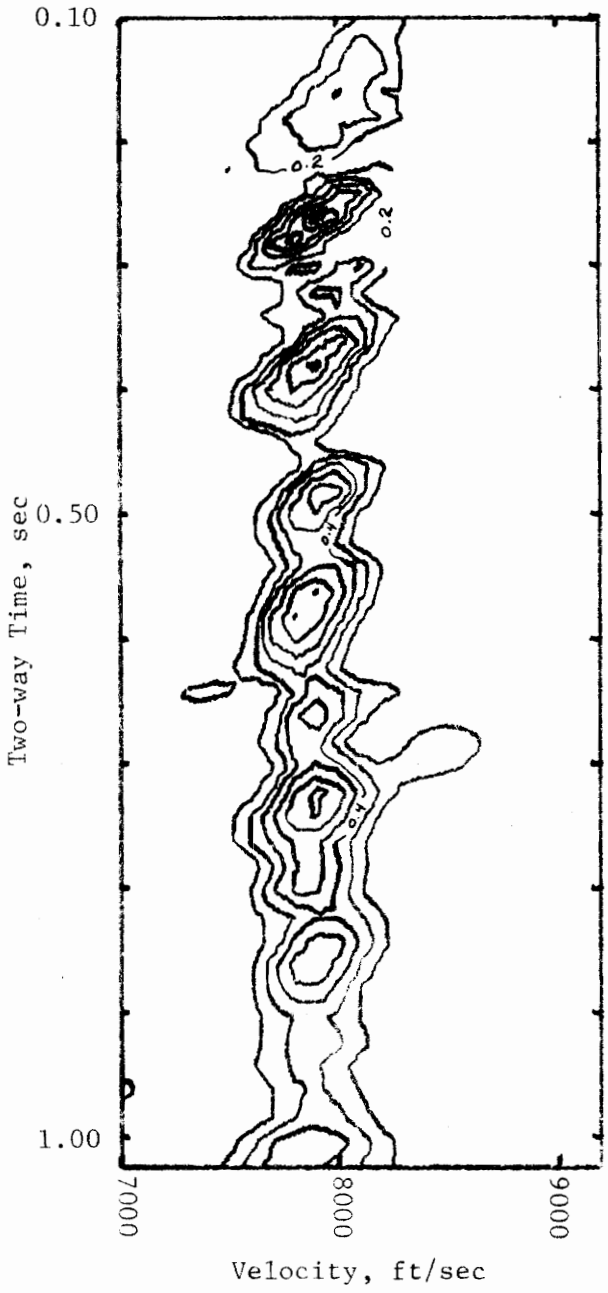

Figure 7.4-6a. Velocity Analysis of P Component Data Anisotropy = 1.043, Window Width = 50 ms, Scan Increments = 20 ms and 100 ft/sec, Anisotropy Scan Level = 1.02

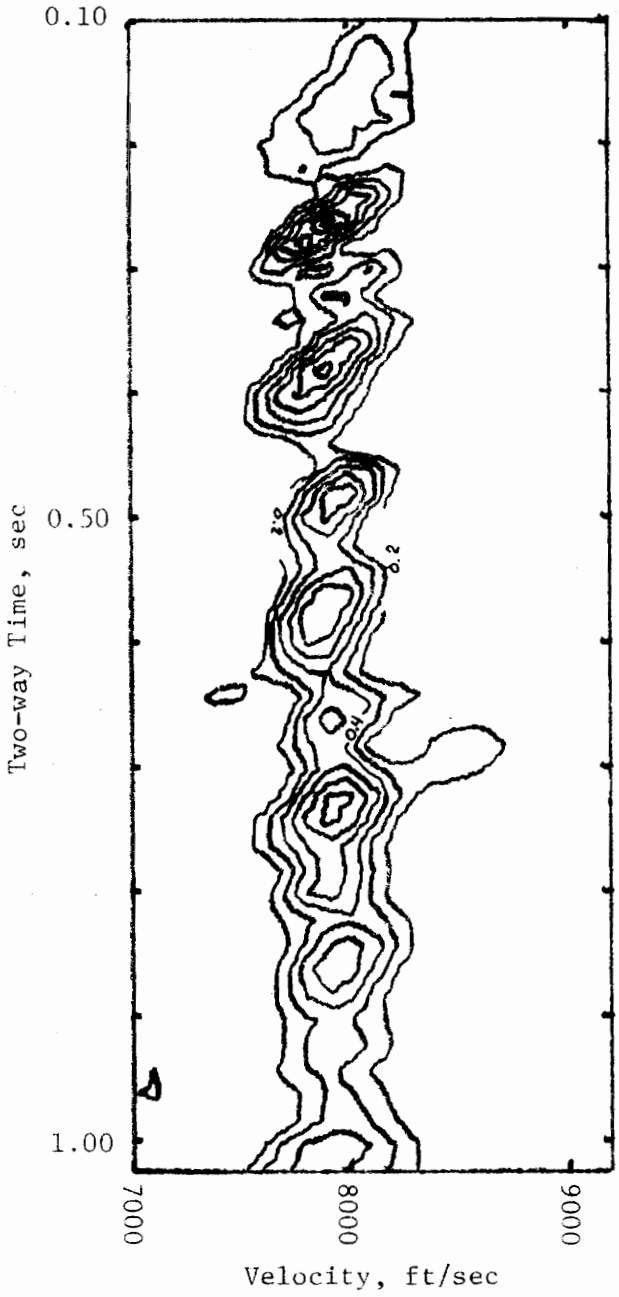

Figure 7.4-6b. Velocity Analysis of P Component Data Anisotropy = 1.043, Window Width = 50 ms, Scan Increments = 20 ms and 100 ft/sec, Anisotropy Scan Level = 1.03

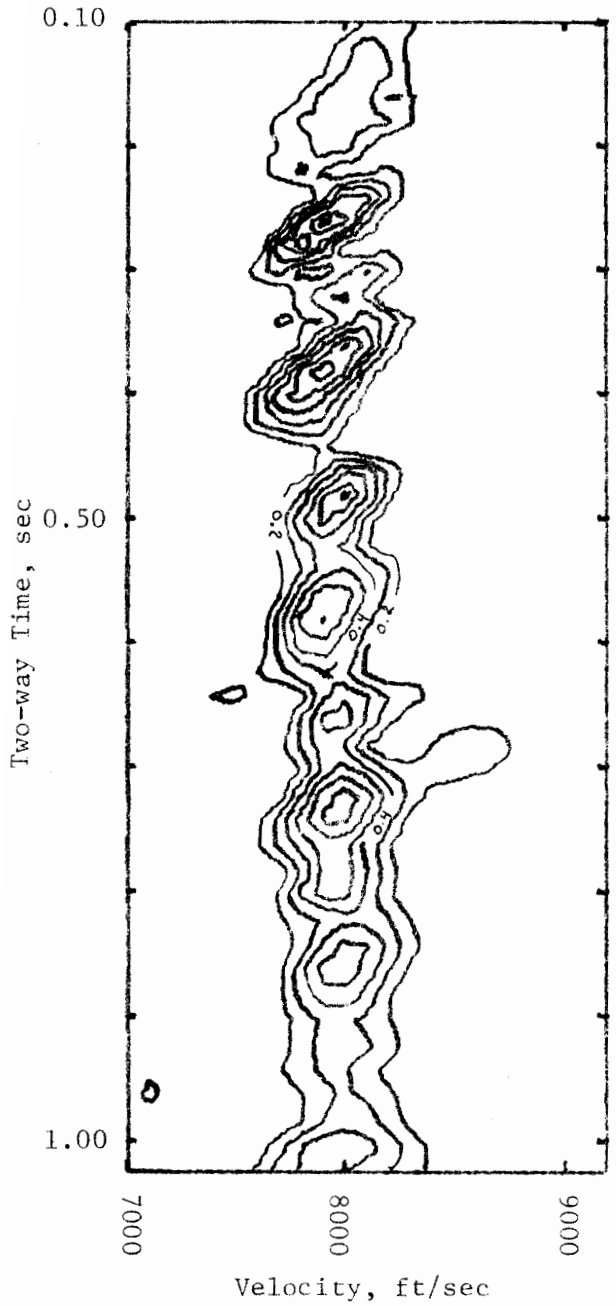

Figure 7.4-6c. Velocity Analysis of P Component Data Anisotropy = 1.043, Window Width = 50 ms, Scan Increments = 20 ms and 100 ft/sec, Anisotropy Scan Level = 1.04

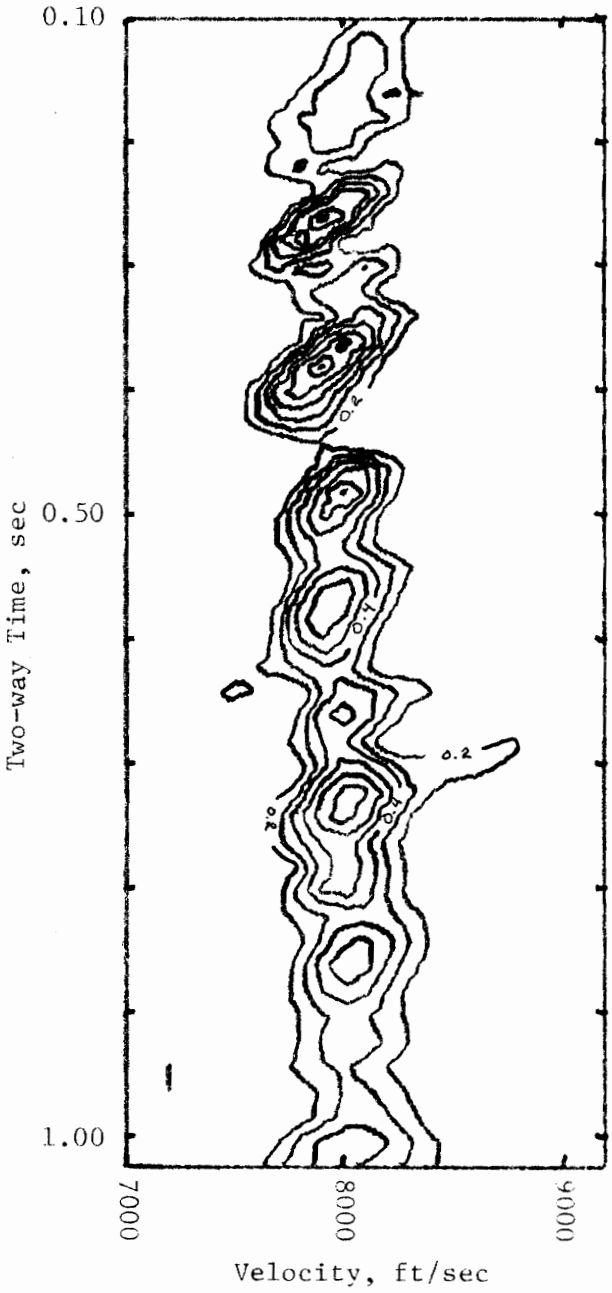

Figure 7.4-6d. Velocity Analysis of P Component Data Anisotropy = 1.043, Window Width = 50 ms, Scan Increments = 20 ms and 100 ft/sec, Anisotropy Scan Level = 1.05

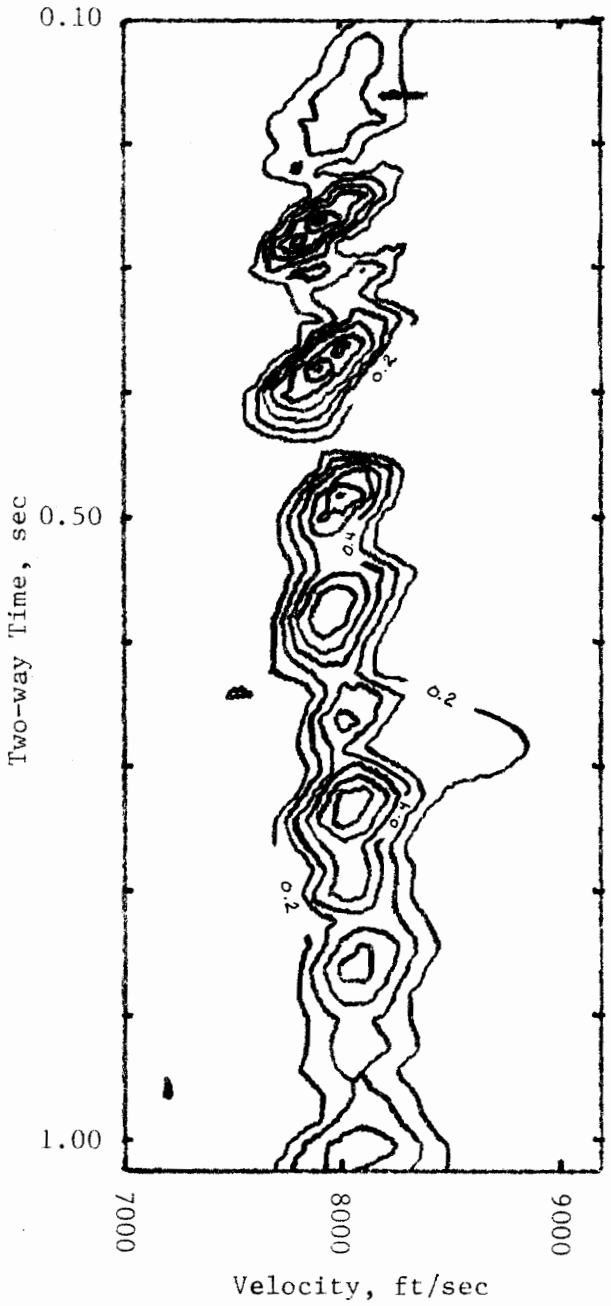

Figure 7.4-6e. Velocity Analysis of P Component
Data Anisotropy = 1.043, Window Width = 50 ms,
Scan Increments = 20 ms and 100 ft/sec,
Anisotropy Scan Level = 1.06

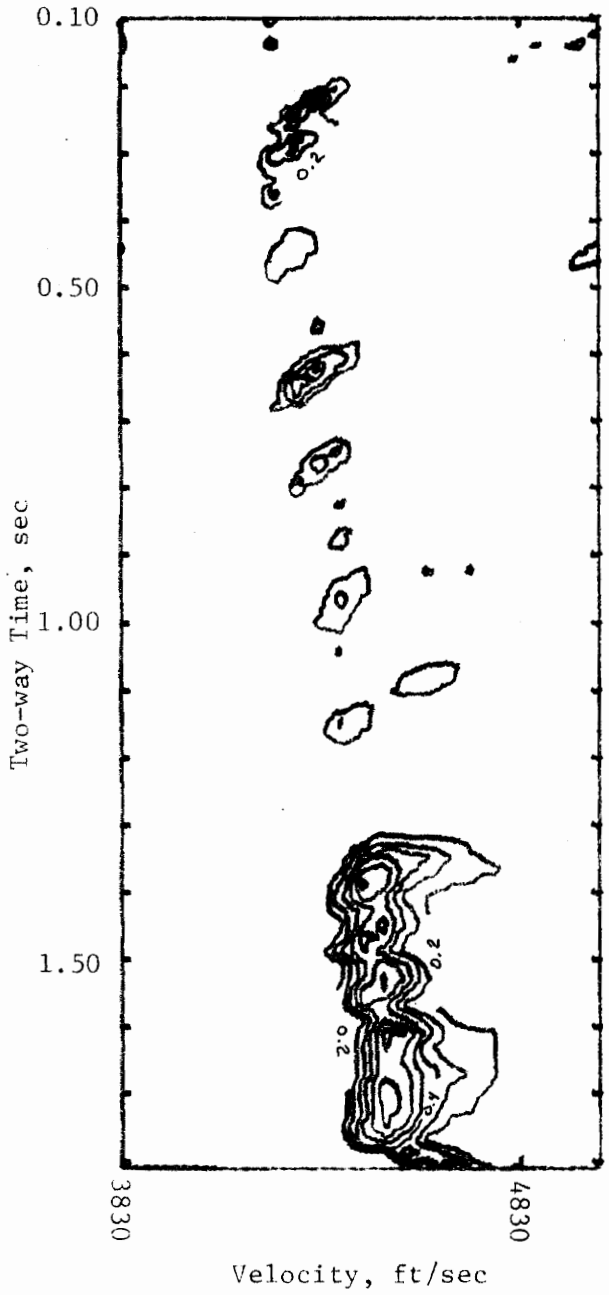

Figure 7.4-7a. Velocity Analysis of SV Component Data Anisotropy = 1.043, Window Width = 50 ms, Scan Increments = 20 ms and 54 ft/sec, Anisotropy Scan Level = 1.02

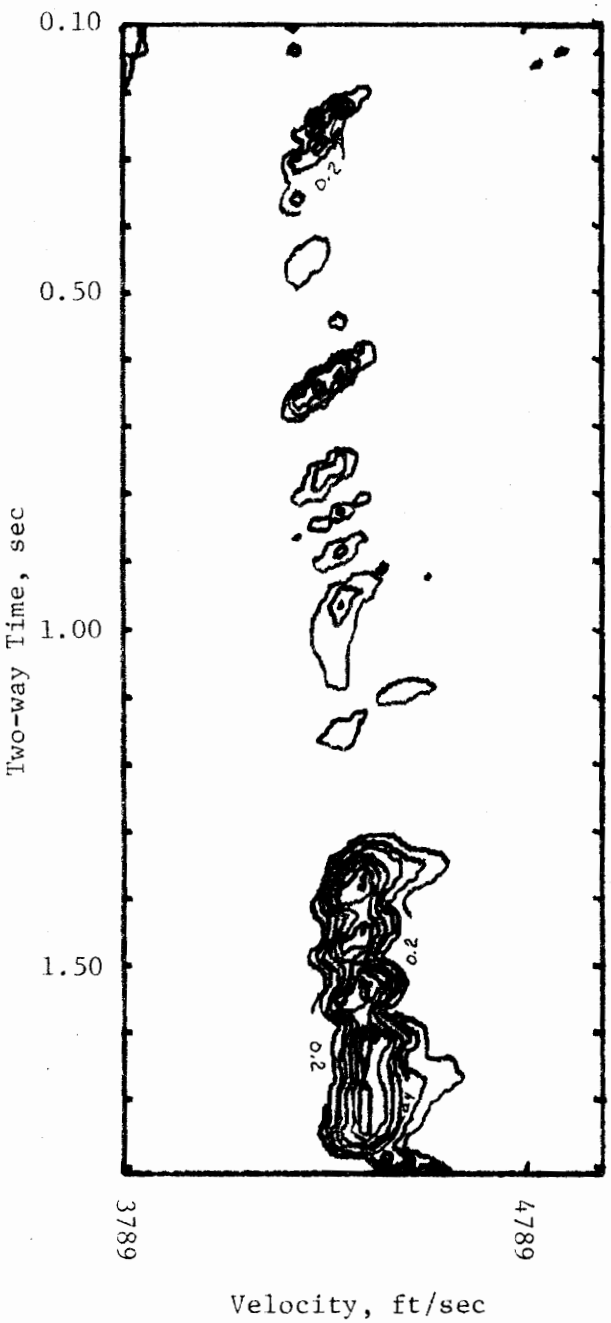

Figure 7.4-7b. Velocity Analysis of SV Component Data Anisotropy = 1.043, Window Width = 50 ms, Scan Increments = 20 ms and 54 ft/sec, Anisotropy Scan Level = 1.03

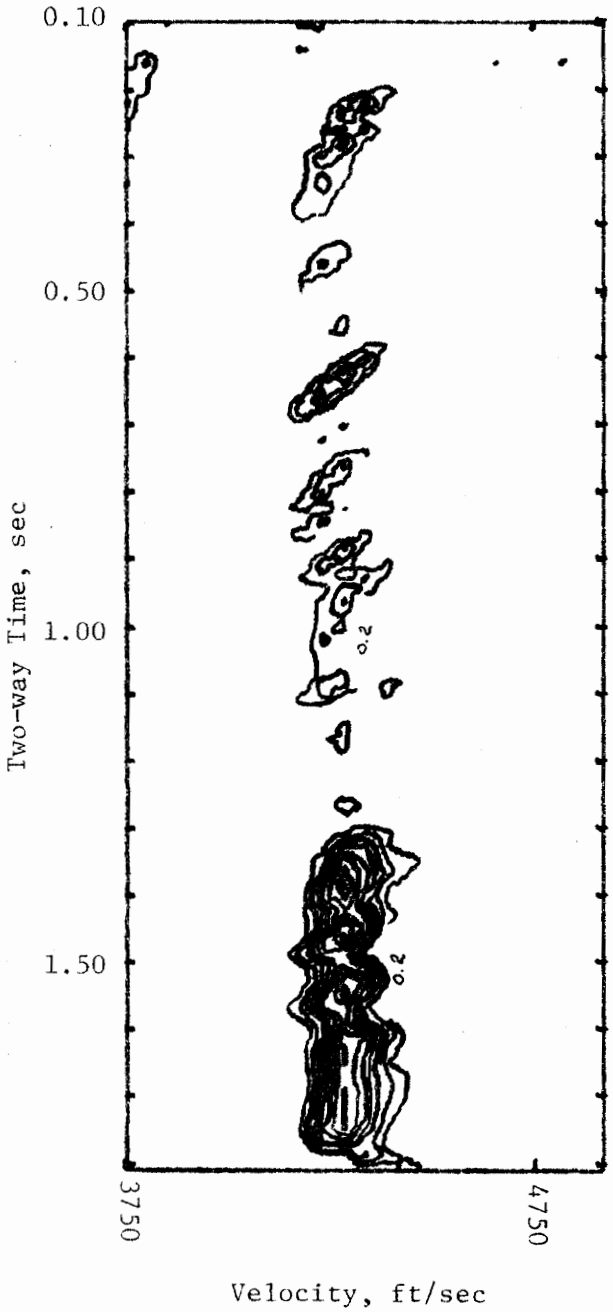

Figure 7.4-7c. Velocity Analysis of SV Component
Data Anisotropy = 1.043, Window Width = 50 ms,
Scan Increments = 20 ms and 53 ft/sec,
Anisotropy Scan Level = 1.04

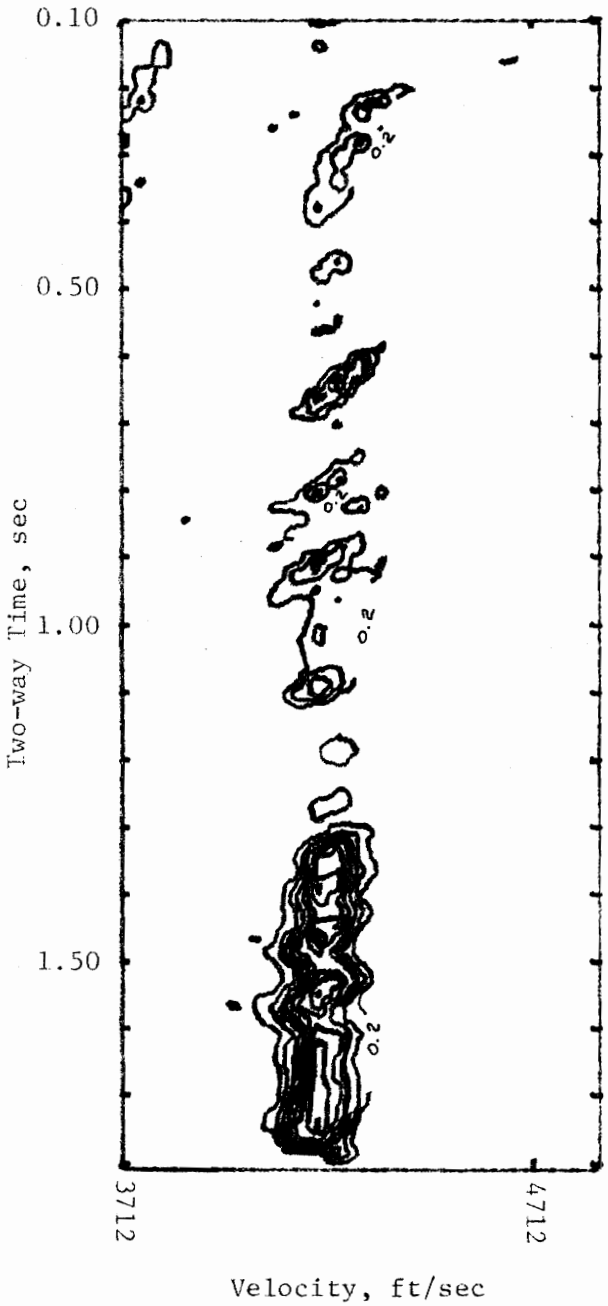

Figure 7.4-7d. Velocity Analysis of SV Component
Data Anisotropy = 1.043, Window Width = 50 ms,
Scan Increments = 20 ms and 53 ft/sec,
Anisotropy Scan Level = 1.05

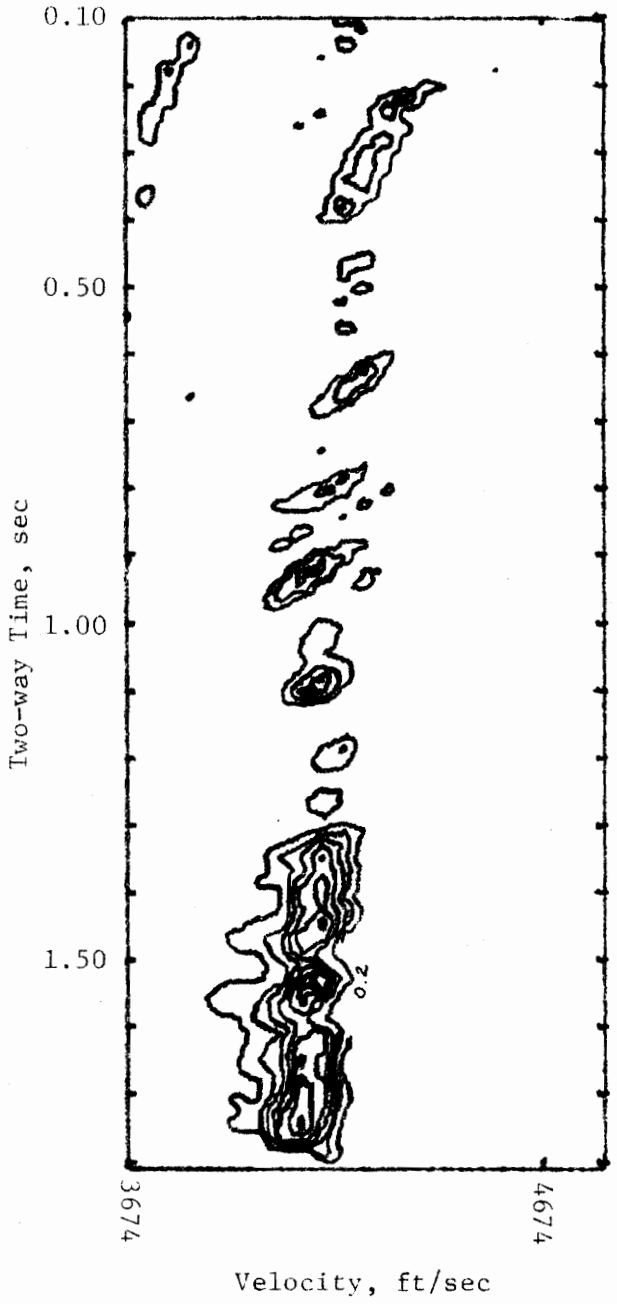

Figure 7.4-7e. Velocity Analysis of SV Component Data Anisotropy = 1.043, Window Width = 50 ms, Scan Increments = 20 ms and 52 ft/sec, Anisotropy Scan Level = 1.06

Table 7.4-2. Integrated Velocity Analysis Results

Velocity Analysis Parameters: See Figures 7.4-6 and 7.4-7.

Integration Range: Semblance Values > 0.4

Data Anisotropy = 1.043

Assumed Anisotropy Scan Value	Normalized Results of Integration P	SV
1.02	96.9	83.9
1.03	97.7	96.1
1.04	100.0	100.0
1.05	98.9	92.1
1.06	99.1	79.2

The results of analysis of the data set with anisotropy factor 1.08 are very similar in general to those of the data set described immediately above. The velocity analyses for P and SV are shown in Figures 7.4-8 and 7.4-9 respectively. The results of integrating the velocity matrices are shown in Table 7.4-3. The results for P are incorrect and it may be noticed that the range of values is small enough that it is not possible to make an unambiguous choice of anisotropy in any event. The SV results show a pronounced maximum which is indicative of only a single correct level of anisotropy. This is the correct value.

The three levels of anisotropy that were analyzed for this velocity model support several conclusions. Anisotropic velocity analysis utilizing the P component is not useful for the recovery of information concerning the value of the anisotropy factor. SV component velocity analysis, on the other hand, is an excellent means for analyzing for anisotropy. The sensitivity of the SV analysis of anisotropy is dependent upon the level of anisotropy encountered. Very simply, it may be stated that, as expected, the greater the anisotropy, the greater is the resolving capability of the method.

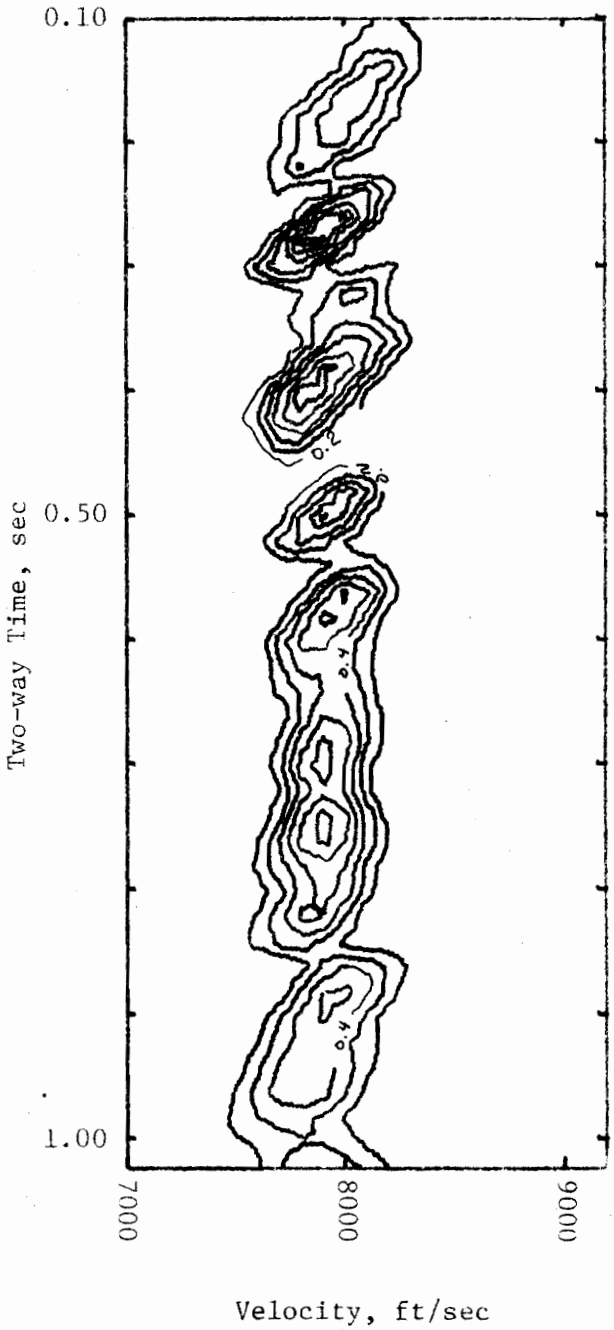

Figure 7.4-8a. Velocity Analysis of P Component Data Anisotropy = 1.08, Window Width = 50 ms, Scan Increments = 20 ms and 100 ft/sec, Anisotropy Scan Level = 1.06

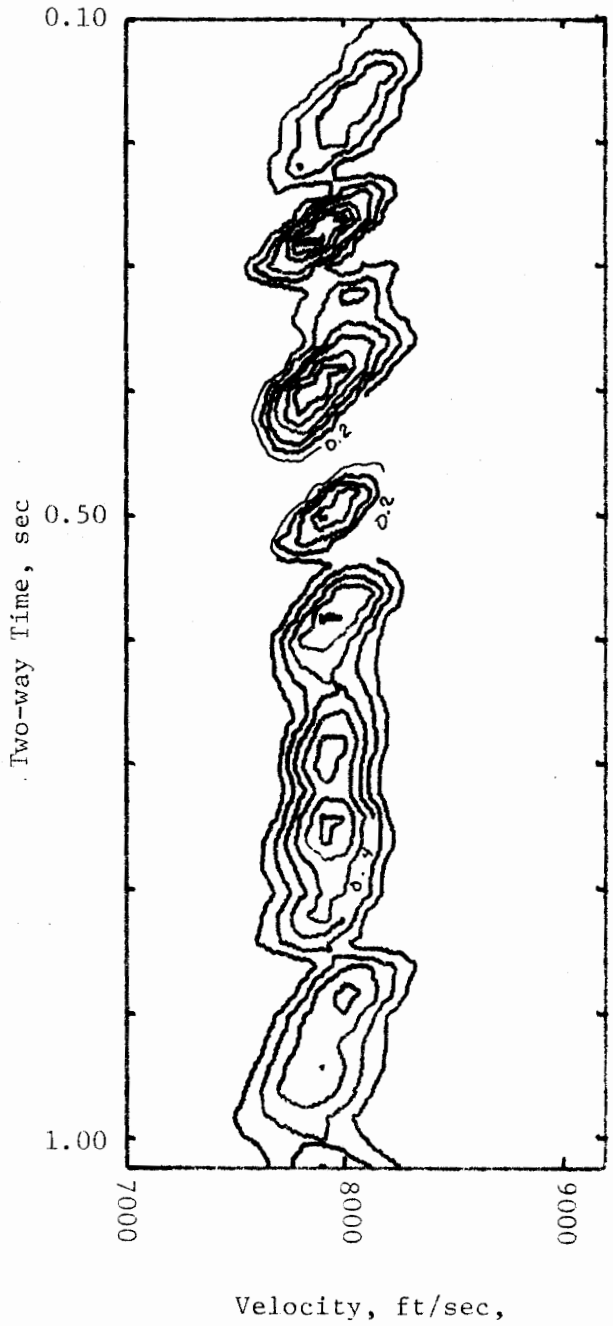

Figure 7.4-8b. Velocity Analysis of P Component Data Anisotropy = 1.08, Window Width = 50 ms, Scan Increments = 20 ms and 100 ft/sec, Anisotropy Scan Level = 1.07

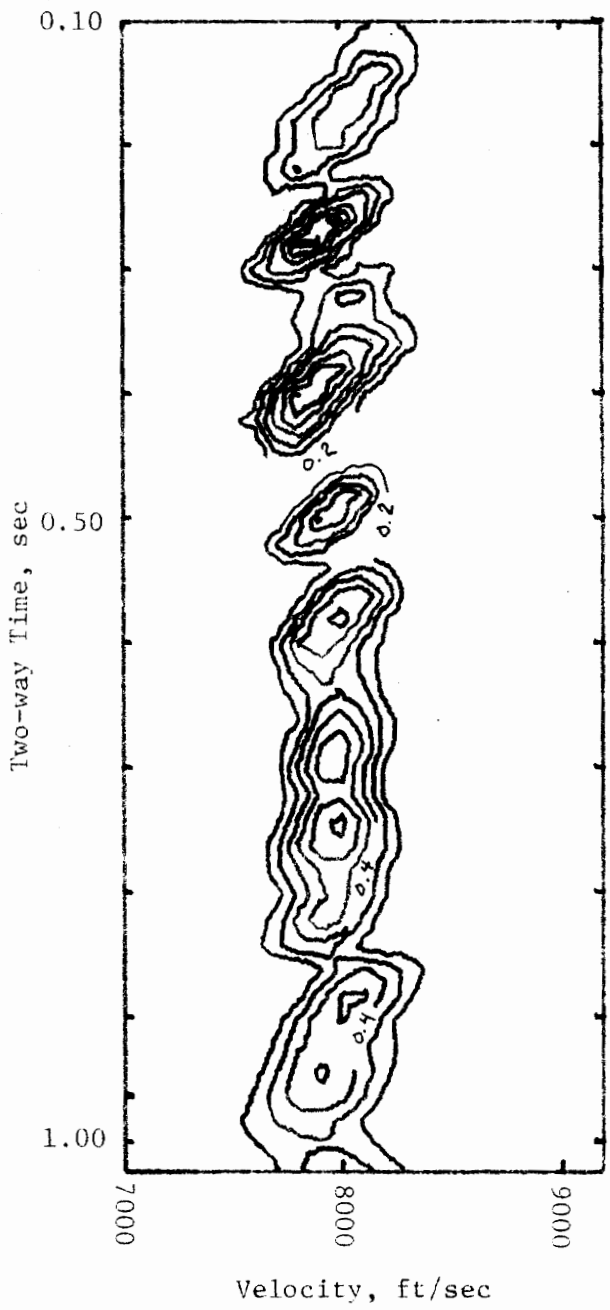

Figure 7.4-8c. Velocity Analysis of P Component Data Anisotropy = 1.08, Window Width = 50 ms, Scan Increments = 20 ms and 100 ft/sec, Anisotropy Scan Level = 1.08

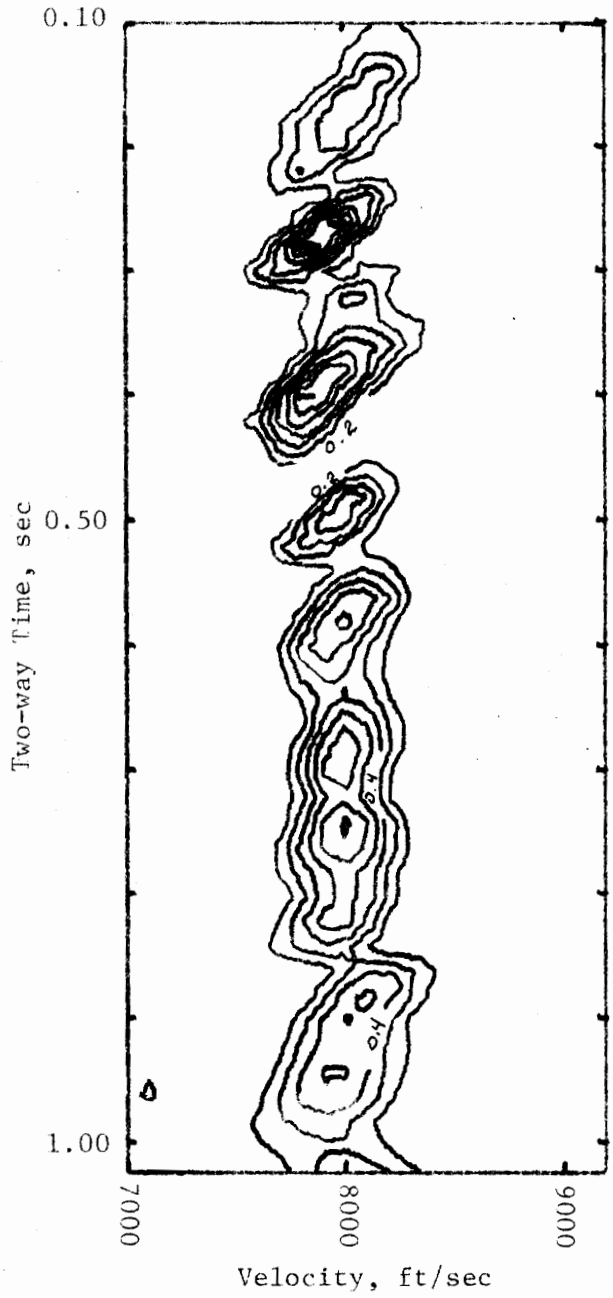

Figure 7.4-8d. Velocity Analysis of P Component Data Anisotropy = 1.08, Window Width = 50 ms, Scan Increments = 20 ms and 100 ft/sec, Anisotropy Scan Level = 1.09

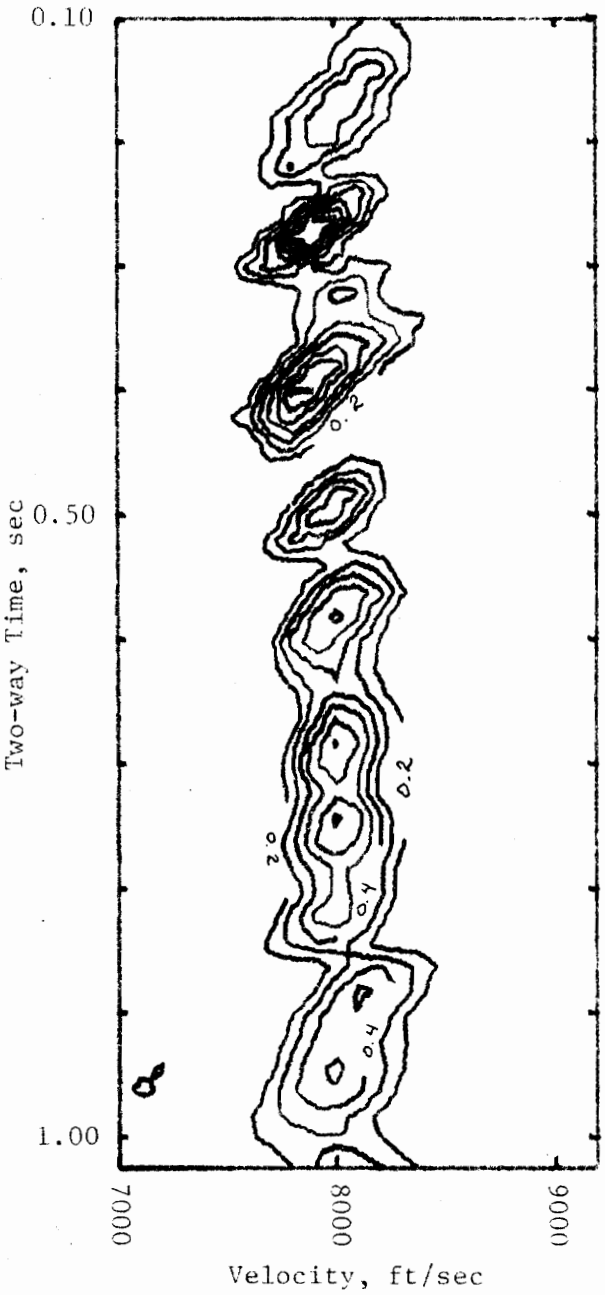

Figure 7.4-8e. Velocity Analysis of P Component Data Anisotropy = 1.08, Window Width = 50 ms, Scan Increments = 20 ms and 100 ft/sec, Anisotropy Scan Level = 1.10

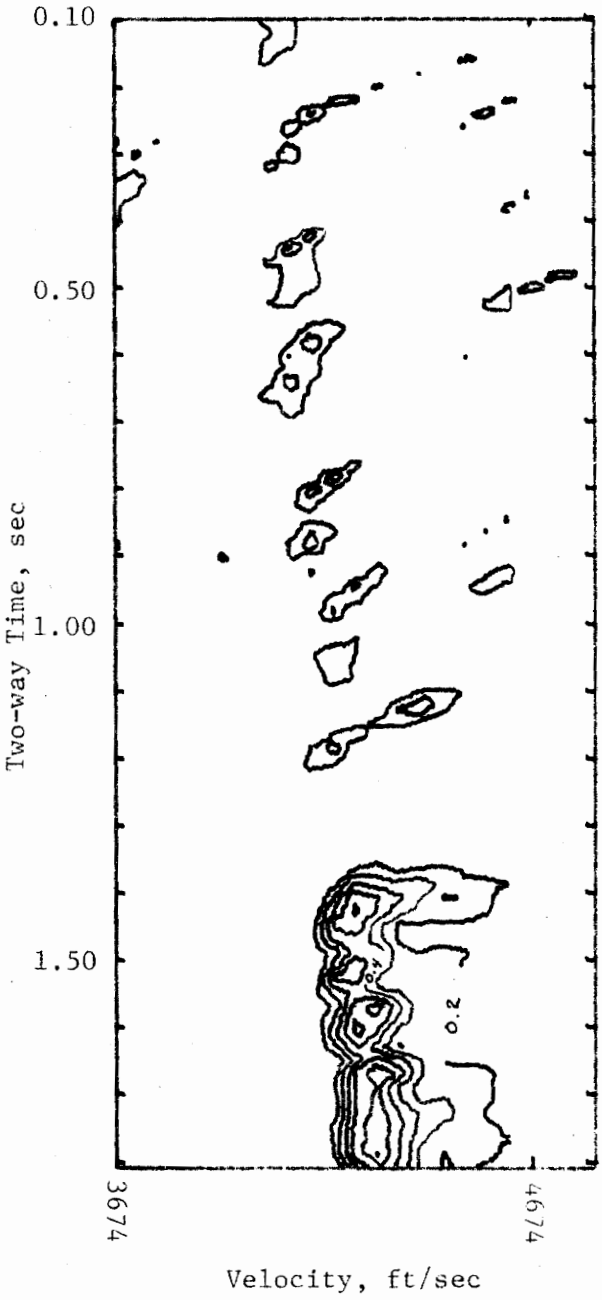

Figure 7.4-9a. Velocity Analysis of SV Component
Data Anisotropy = 1.08, Window Width = 50 ms,
Scan Increments = 20 ms and 52 ft/sec,
Anisotropy Scan Level = 1.06

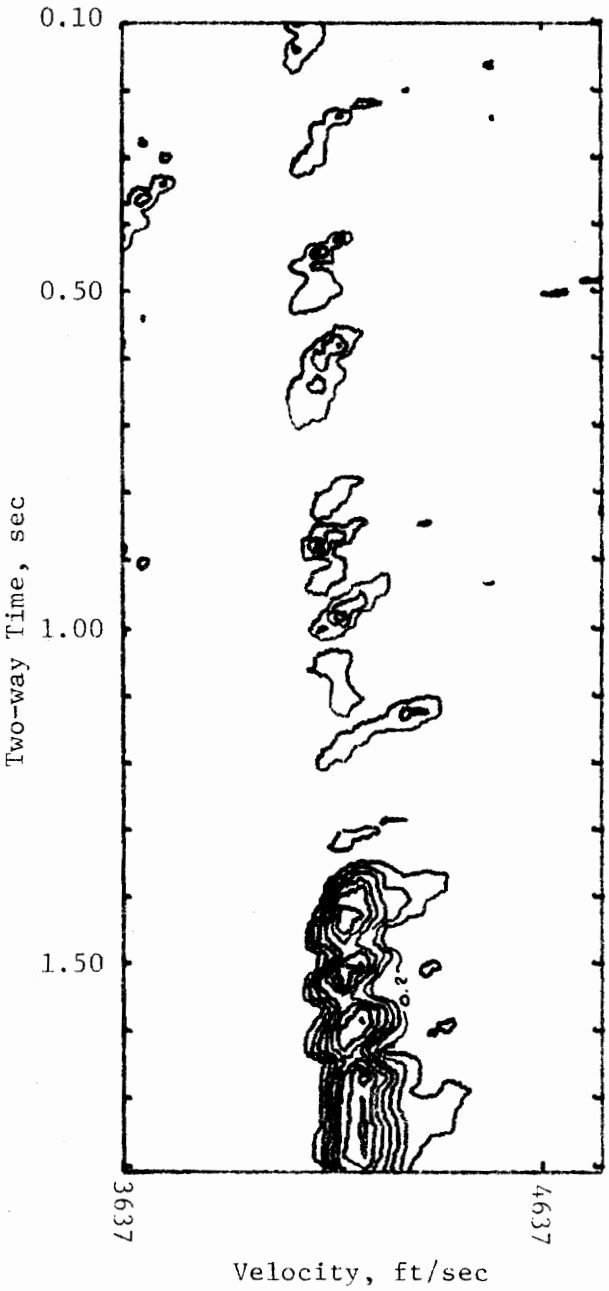

Figure 7.4-9b. Velocity Analysis of SV Component Data Anisotropy = 1.08, Window Width = 50 ms, Scan Increments = 20 ms and 51 ft/sec, Anisotropy Scan Level = 1.07

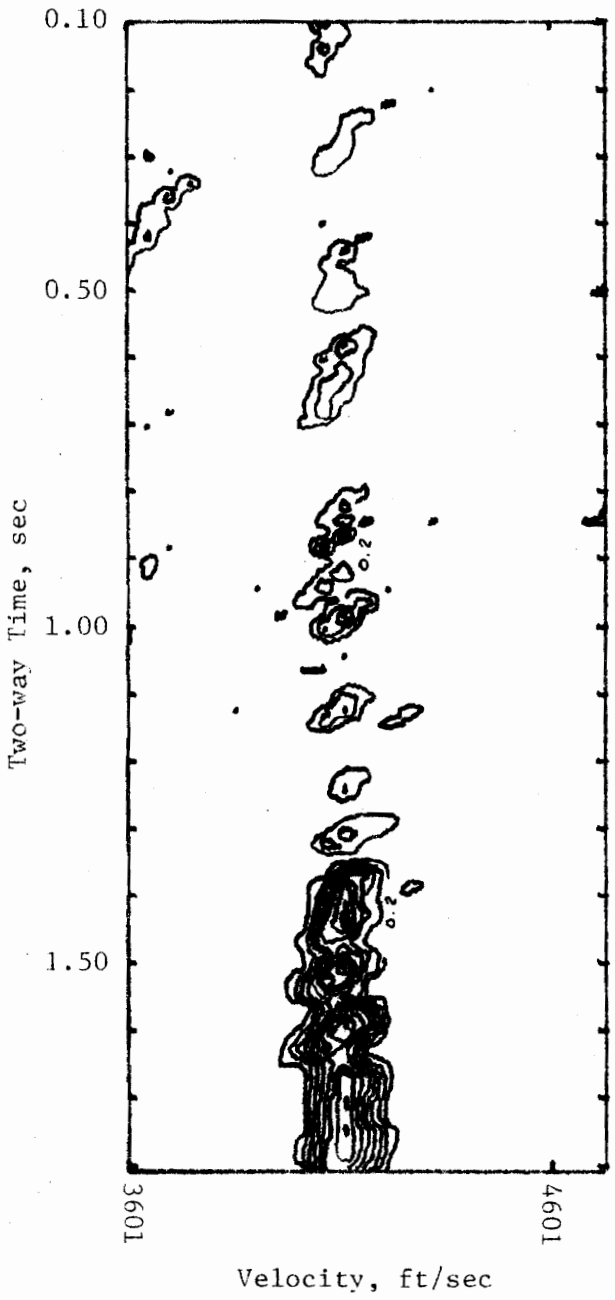

Figure 7.4-9c. Velocity Analysis of SV Component
Data Anisotropy = 1.08, Window Width = 50 ms,
Scan Increments = 20 ms and 51 ft/sec
Anisotropy Scan Level = 1.08

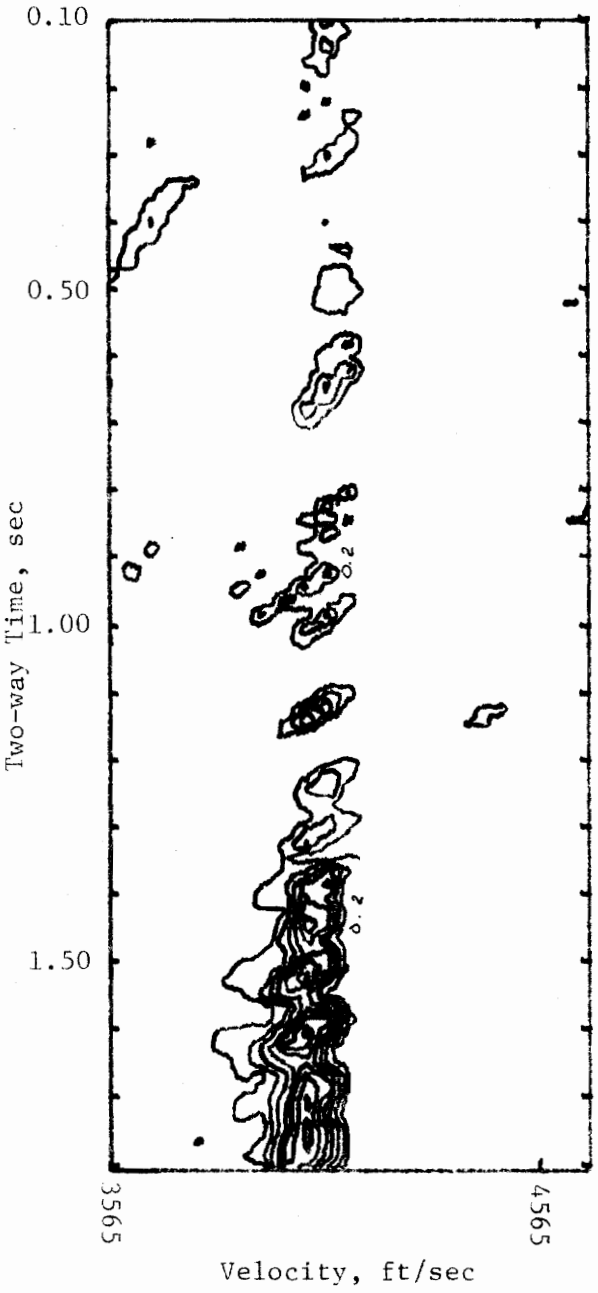

Figure 7.4-9d. Velocity Analysis of SV Component
Data Anisotropy = 1.08, Window Width = 50 ms,
Scan Increments = 20 ms and 50 ft/sec,
Anisotropy Scan Level = 1.09

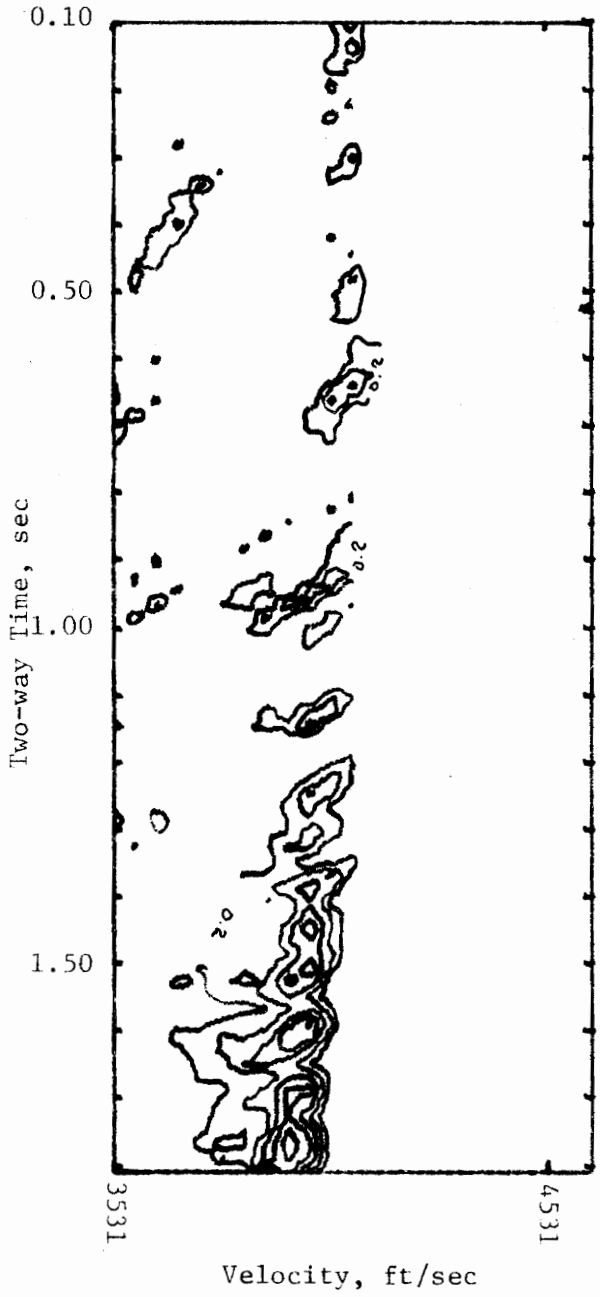

Figure 7.4-9e. Velocity Analysis of SV Component Data Anisotropy = 1.08, Window Width = 50 ms, Scan Increments = 20 ms and 50 ft/sec, Anisotropy Scan Level = 1.10

Table 7.4-3. Integrated Velocity Analysis Results

Velocity Analysis Parameters: See Figures 7.4-8 and 7.4-9.

Integration Range: Semblance Values > 0.4

Data Anisotropy = 1.08

Assumed Anisotropy Scan Value	Normalized Results of Integration	
	P	SV
1.06	96.7	78.7
1.07	98.4	88.4
1.08	98.0	100.0
1.09	98.5	90.4
1.10	100.0	65.9

7.5 Linear Increase of Velocity with Depth

The velocity function for this nodel is described in detail in section 5.3.2. The horizontal compressional velocity component is 8000 ft/sec at the surface and increases at the rate of 1 ft/sec per foot of increase in depth. This velocity function was used to generate three sets of anisotropic data having anisotropy factors of 1.02, 1.043 and 1.08 respectively.

7.5.1 Effects of Variation of Model Parameters on Velocity Analysis

Data Characteristics

All reflection times for this velocity model were generated for a CDP geometry. The maximum shotpoint distance used in the generation of the data was 5280 feet. The data generated are 12-fold with all shotpoint-geophone distances being multiples of 440 feet. Table 7.5-1 shows the first depth from which a reflection is received for each trace. Again, reflections are not received from shallower depths because critical angles are exceeded. The reflection coefficients discussed in section 7.3.1 were used to create the synthetic seismic data shown in Figures 7.5-1, 7.5-2, and 7.5-3.

Resolution of Anisotropy

The initial data analysis was performed on the data set with anisotropy factor 1.02. Velocity scans were made over the range of anisotropy factors extending from 1.00 to 1.04 in steps of 0.01. The results of velocity analysis for P and SV are shown in Figures 7.5-4 and 7.5-5 respectively. The volume under the surfaces defined by the

Table 7.5-1. Depth of First Reflection

Data Anisotropy = 1.02

Trace No. :	1	2	3	4	5	6	7	8	9	10	11	12
P :	100	100	125	200	300	425	600	775	1000	1250	1550	1875
SV :	100	100	125	225	350	500	675	875	1100	1350	1650	1950

Data Anisotropy = 1.043

P :	100	100	100	175	275	400	550	725	925	1175	1450	1775
SV :	100	100	150	250	400	550	725	925	1150	1400	1675	1950

Data Anisotropy = 1.08

P :	100	100	100	175	275	375	500	650	850	1050	1300	1575
SV :	100	100	200	300	450	600	775	975	1200	1450	1700	1975

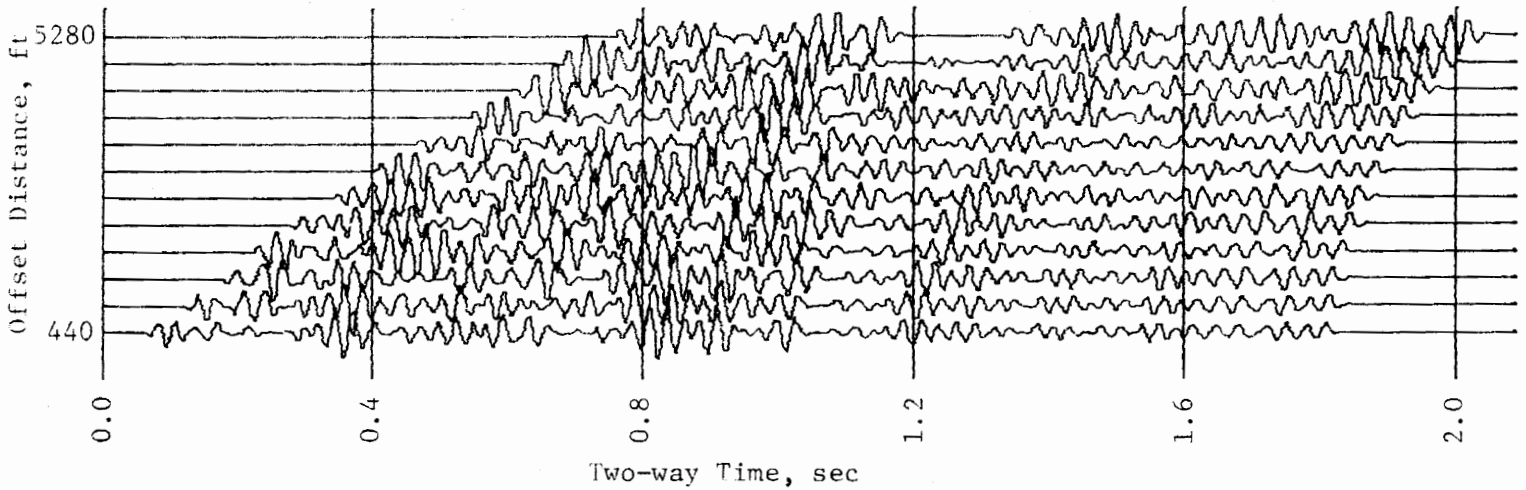

Figure 7.5-1. Linear Increase of Velocity
12-Fold Reflection Seismograms
Data Anisotropy = 1.02

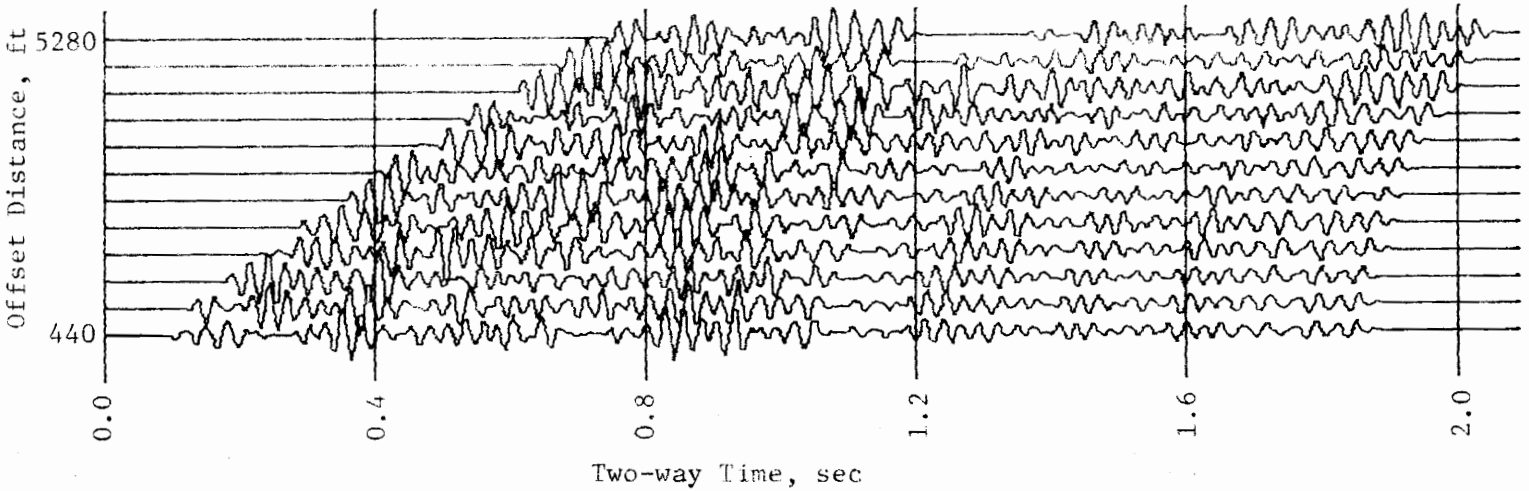

Figure 7.5-2. Linear Increase of Velocity
12-Fold Reflection Seismograms
Data Anisotropy = 1.043

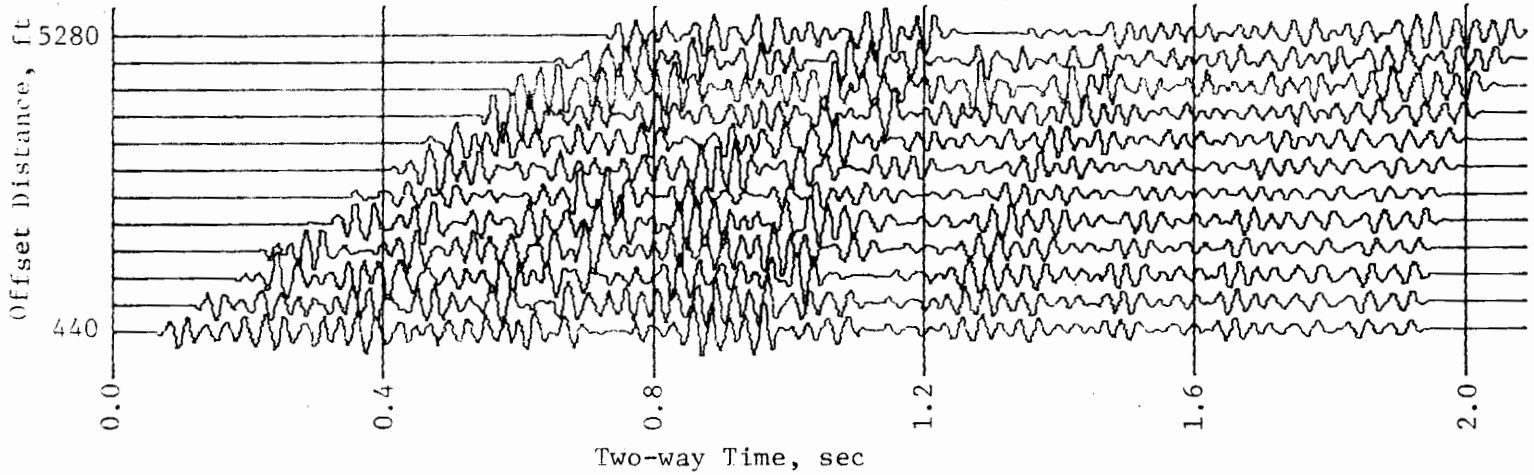

Figure 7.5-3. Linear Increase of Velocity
12-Fold Reflection Seismograms
Data Anisotropy = 1.08

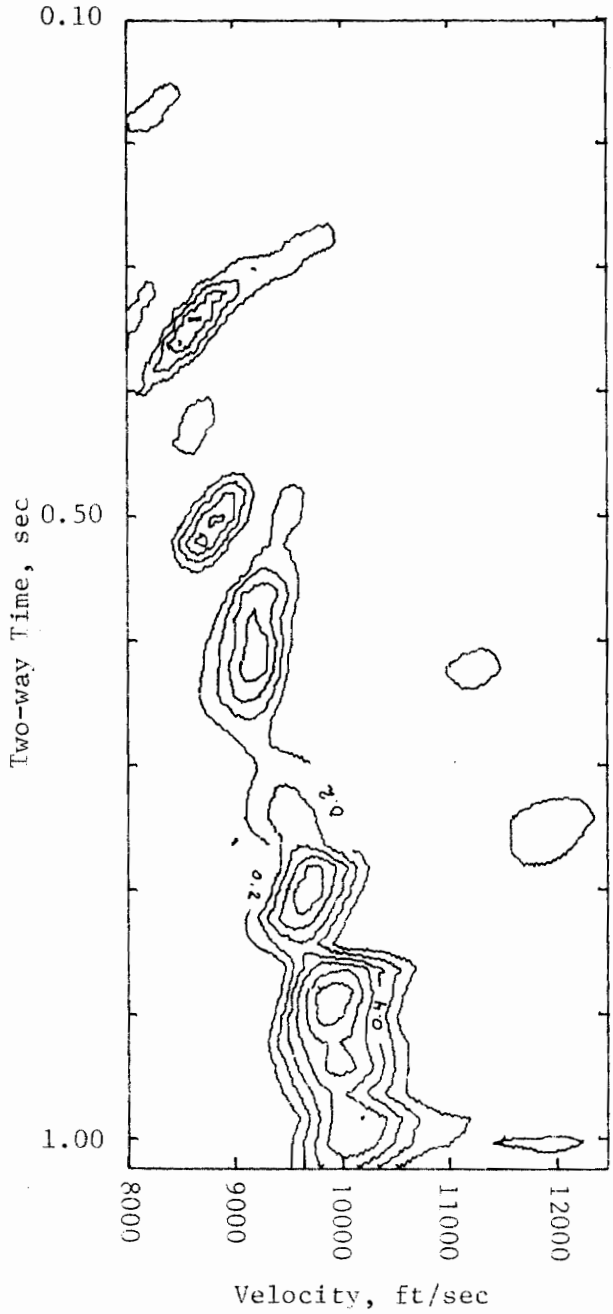

Figure 7.5-4a. Velocity Analysis of P Component Data Anisotropy = 1.02, Window Width = 50 ms, Scan Increments = 20 ms and 100 ft/sec, Anisotropy Scan Level = 1.00

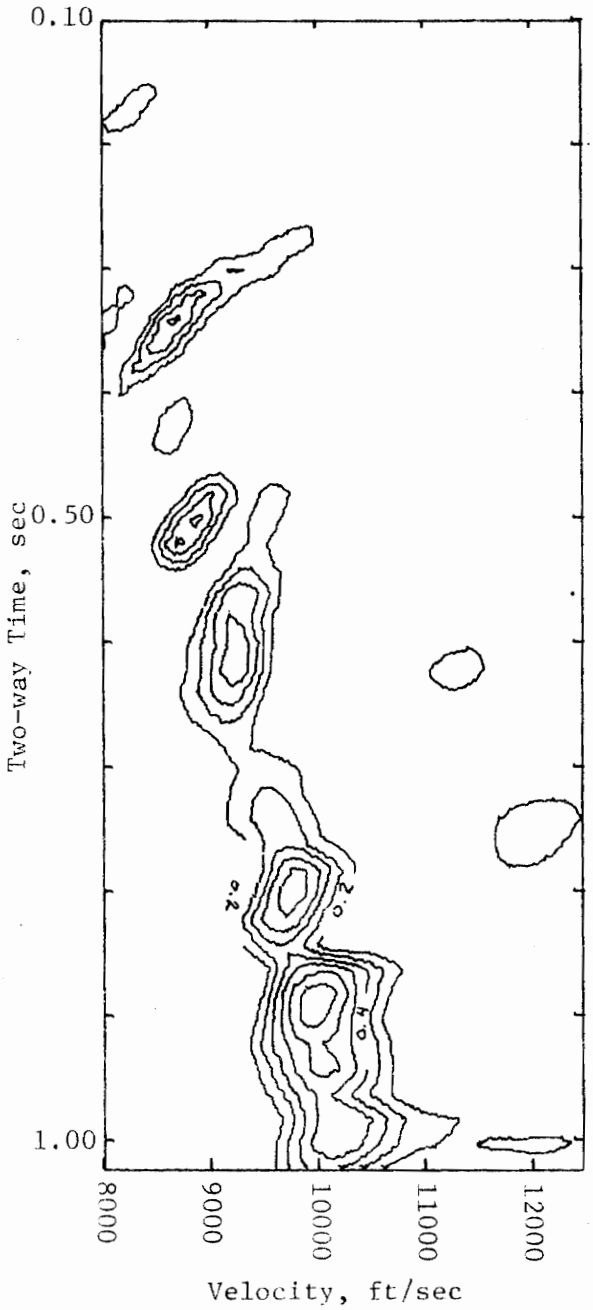

Figure 7.5-4b. Velocity Analysis of P Component
Data Anisotropy = 1.02, Window Width = 50 ms,
Scan Increments = 20 ms and 100 ft/sec,
Anisotropy Scan Level = 1.01

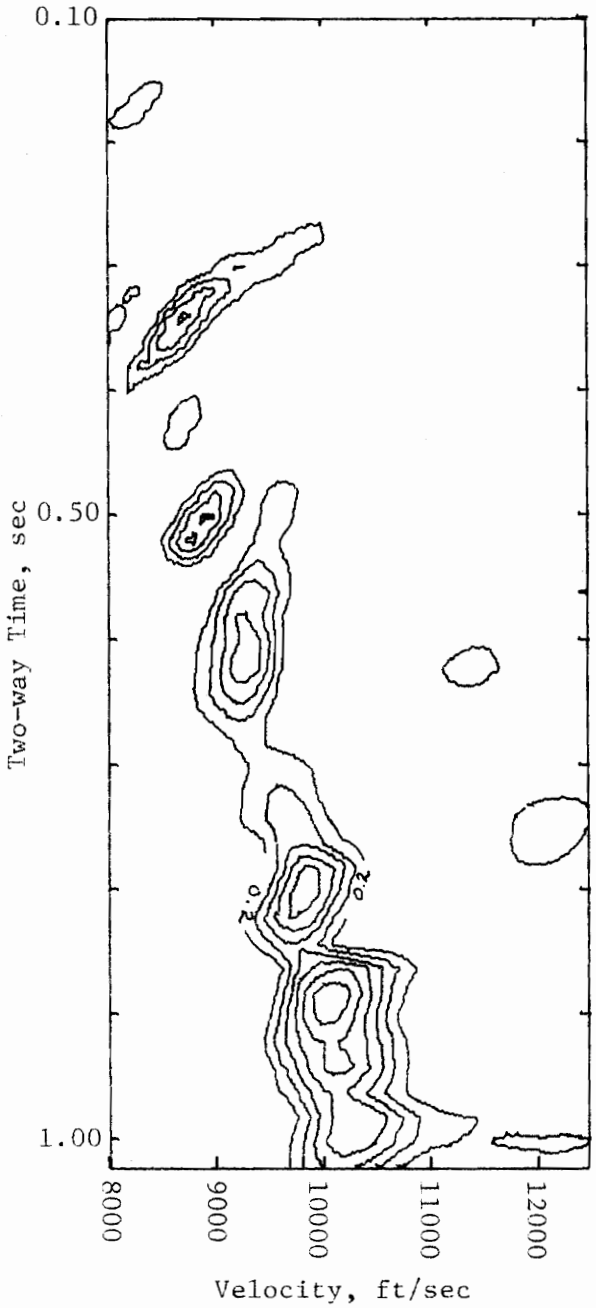

Figure 7.5-4c. Velocity Analysis of P Component Data Anisotropy = 1.02, Window Width = 50 ms, Scan Increments = 20 ms and 100 ft/sec, Anisotropy Scan Level = 1.02

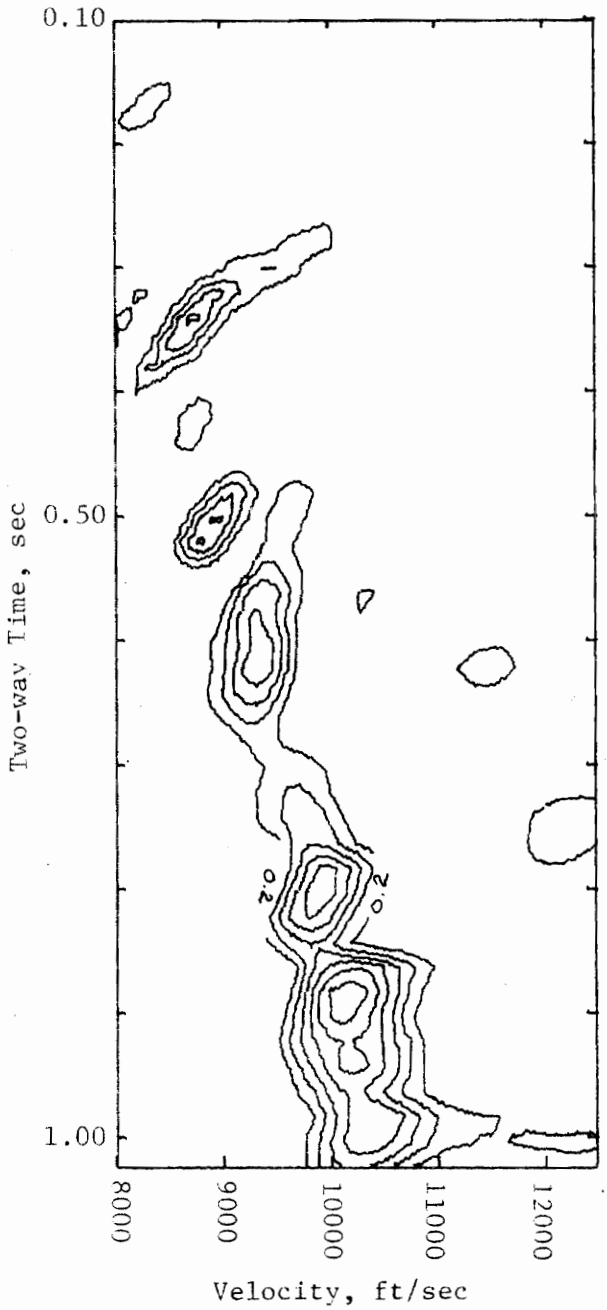

Figure 7.5-4d. Velocity Analysis of P Component
Data Anisotropy = 1.02, Window Width = 50 ms,
Scan Increments = 20 ms and 100 ft/sec,
Anisotropy Scan Level = 1.03

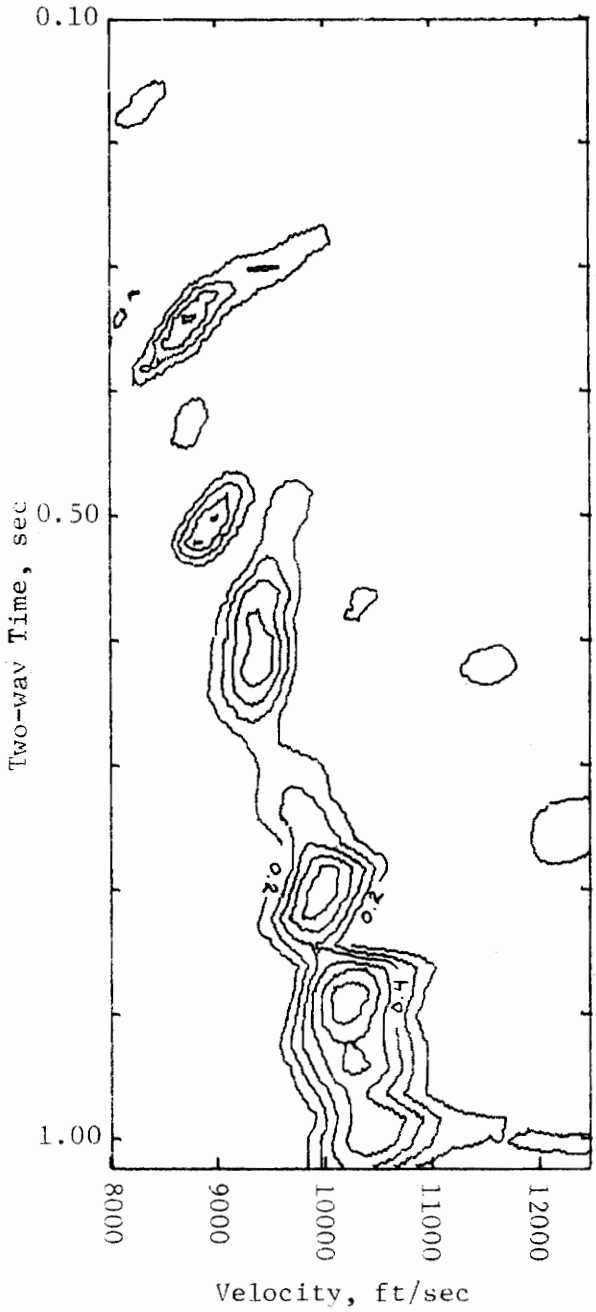

Figure 7.5-4e. Velocity Analysis of P Component Data Anisotropy = 1.02, Window Width = 50 ms, Scan Increments = 20 ms and 100 ft/sec, Anisotropy Scan Level = 1.04

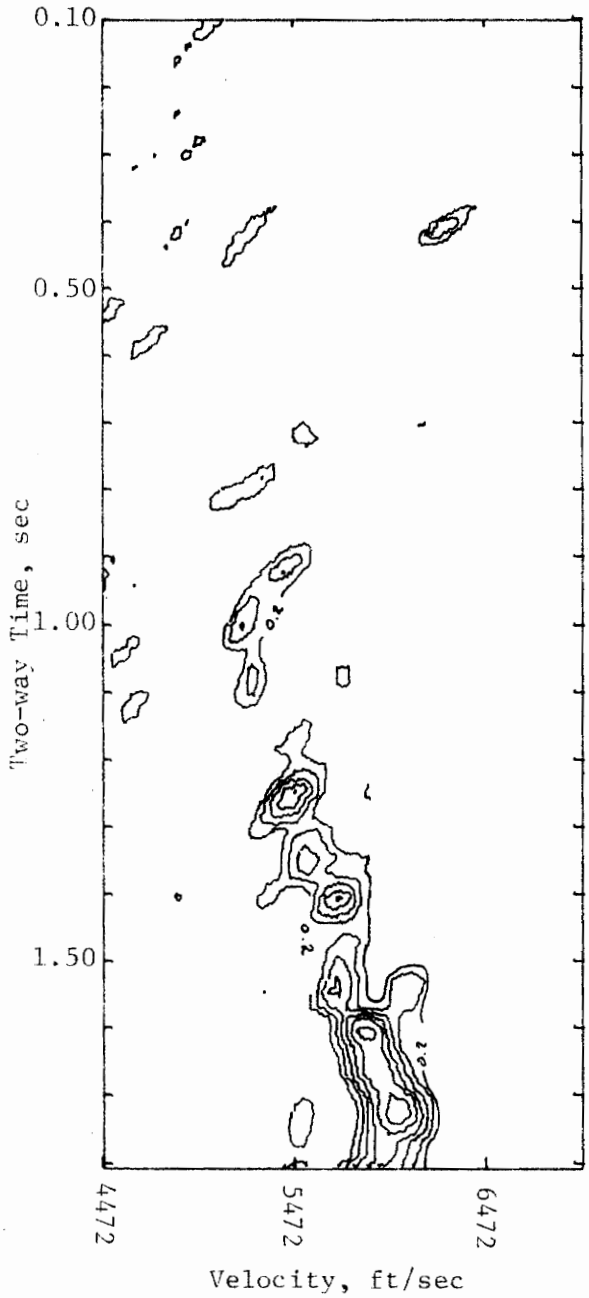

Figure 7.5-5a. Velocity Analysis of SV Component
Data Anisotropy = 1.02, Window Width = 50 ms,
Scan Increments = 20 ms and 55 ft/sec,
Anisotropy Scan Level = 1.00

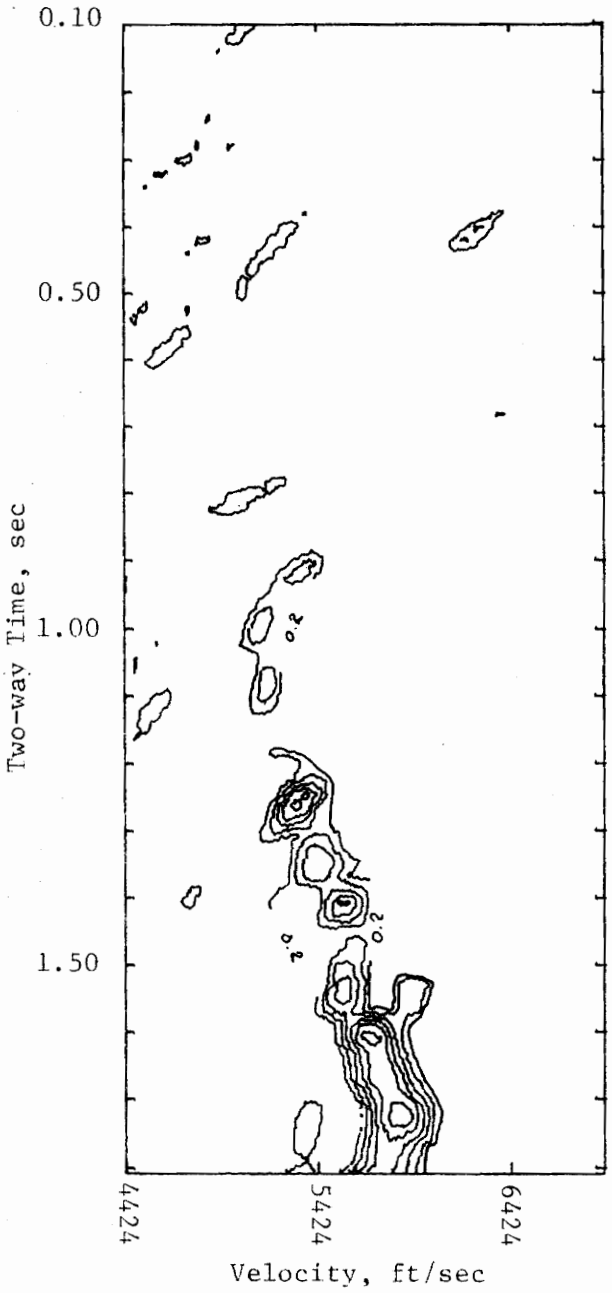

Figure 7.5-5b. Velocity Analysis of SV Component
Data Anisotropy = 1.02, Window Width = 50 ms,
Scan Increments = 20 ms and 55 ft/sec,
Anisotropy Scan Level = 1.01

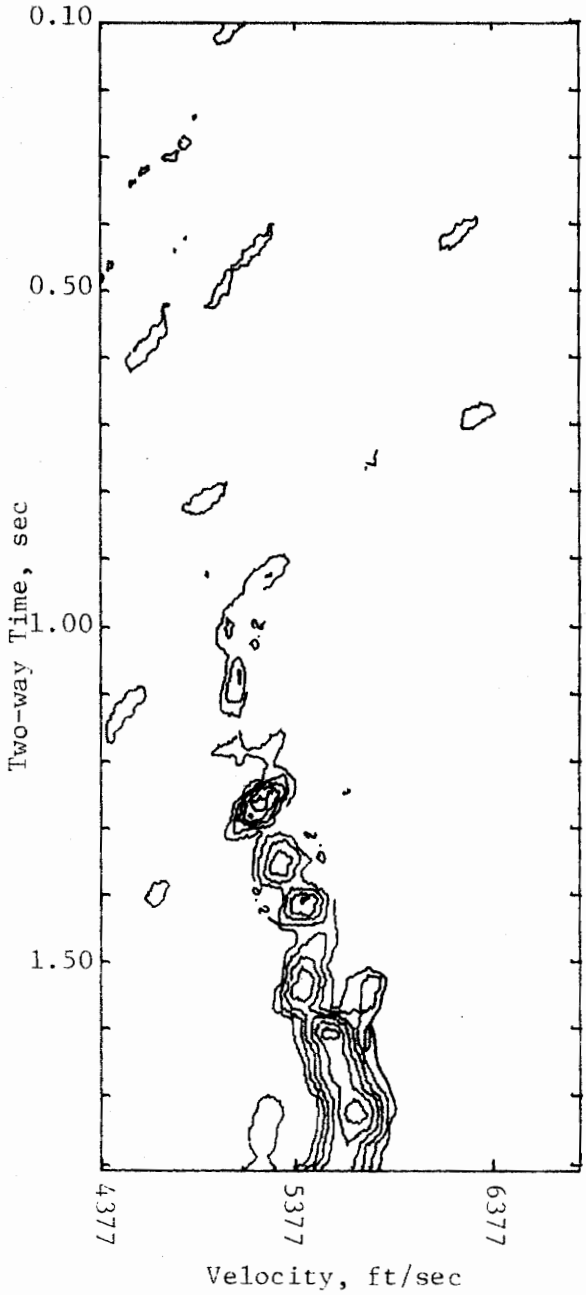

Figure 7.5-5c. Velocity Analysis of SV Component
Data Anisotropy = 1.02, Window Width = 50 ms,
Scan Increments = 20 ms and 54 ft/sec,
Anisotropy Scan Level = 1.02

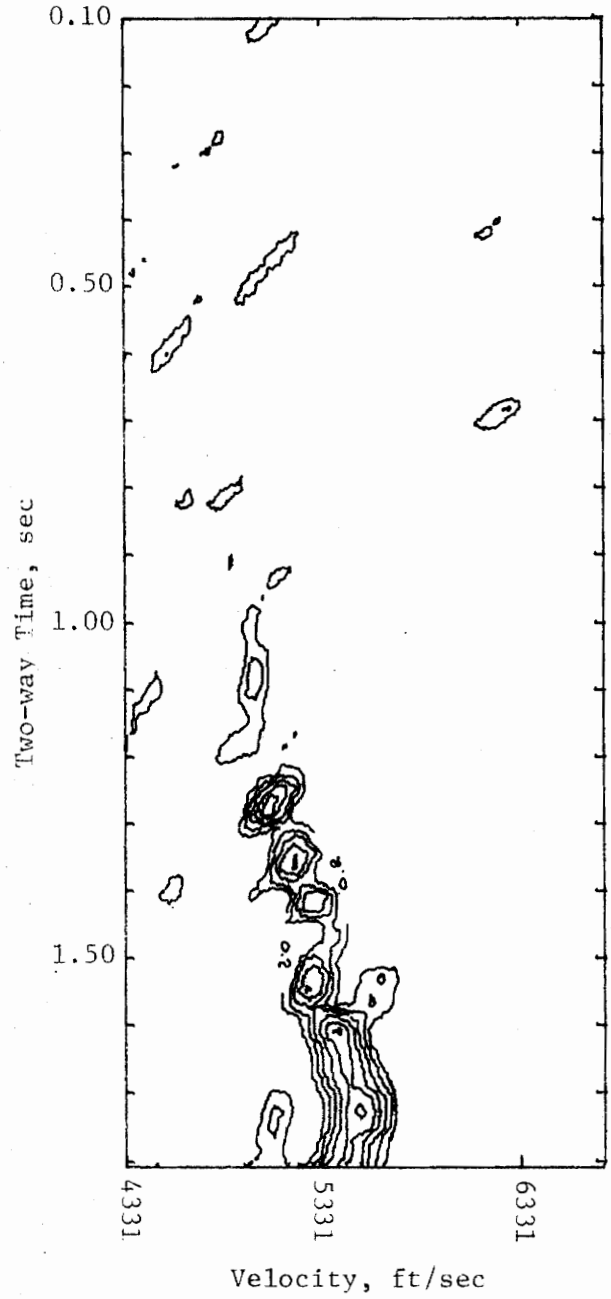

Figure 7.5-5d. Velocity Analysis of SV Component Data Anisotropy = 1.02, Window Width = 50 ms, Scan Increments = 20 ms and 54 ft/sec, Anisotropy Scan Level = 1.03

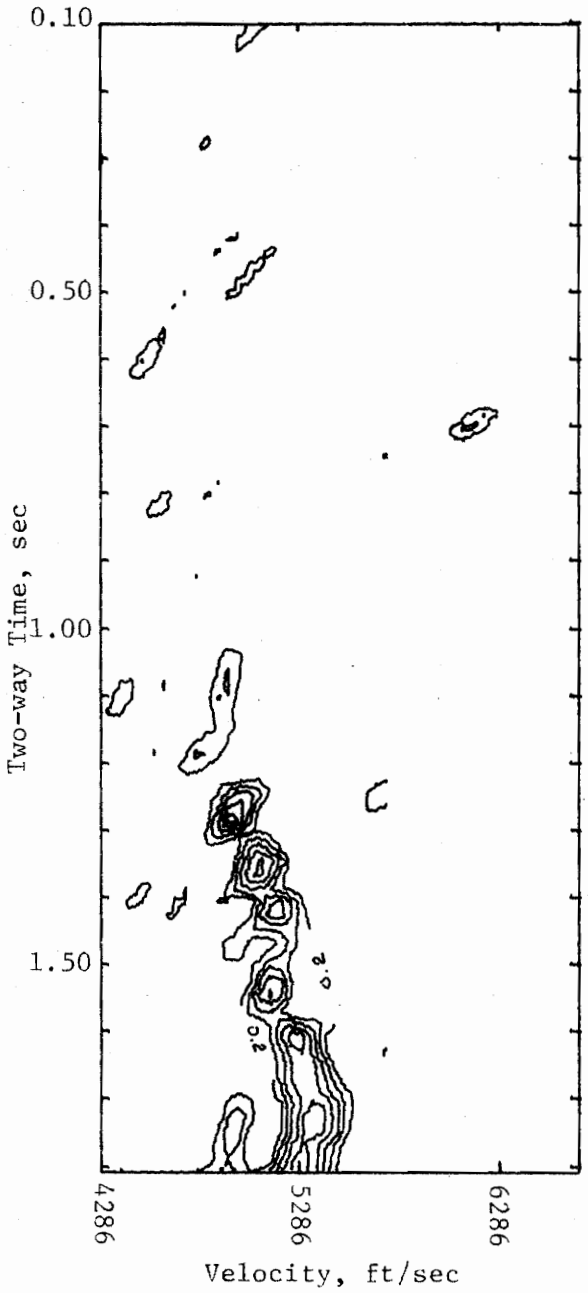

Figure 7.5-5e. Velocity Analysis of SV Component Data Anisotropy = 1.02, Window Width = 50 ms, Scan Increments = 20 ms and 53 ft/sec, Anisotropy Scan Level = 1.04

Table 7.5-2. Integrated Velocity Analysis Results

Velocity Analysis Parameters: See Figures 7.5-4 and 7.5-5.

Integration Range: Semblance Values > 0.4

Data Anisotropy = 1.02

Asumed Anisotropy Scan Value	Normalized Results of Integration	
	P	SV
1.00	94.2	97.2
1.01	95.2	100.0
1.02	98.7	99.4
1.03	98.1	95.9
1.04	100.0	85.0

semblance matrices was integrated (See section 7.3.1) for the purpose of determining which anisotropy level best fit the data. The normalized results of integration are shown for both P and SV in Table 7.5-2. As with the previous cases, the P velocity scans are not useful for the determination of anisotropy. The best choice of anisotropy is indicated to be 1.01. The actual value is 1.02 and the results of integration indicate that, in fact, this value is as good a choice as 1.01. Thus, it is possible to choose the correct anisotropy factor for this particular model to within ± 0.01.

The velocity analyses for the data set having an anisotropy factor of 1.043 are shown in Figures 7.5-6 and 7.5-7 respectively. The anisotropy scan range extended from 1.02 to 1.06 in steps of 0.01. Normalized results of integration are presented in Table 7.5-3. The anisotropic P velocity scans did not result in any useful information concerning the anisotropy factor for this data set. The SV analyses indicated a choice of 1.03 for the anisotropy factor. A value of 1.04 is a better choice. The difference in the integrated matrix values for anisotropy factors 1.03 and 1.04 is so small that either value is an equally good choice. The accuracy for the determination of the anisotropy factor definitely falls within the range of $\pm$ 0.01 of the correct value.

The final set of data for this velocity model has an anisotropy factor of 1.08. Velocity analysis results are shown in Figures 7.5-8 and 7.5-9. The anisotropy scan range was from 1.06 to 1.10 in steps of 0.01. The analysis results for P were not significant for the de-

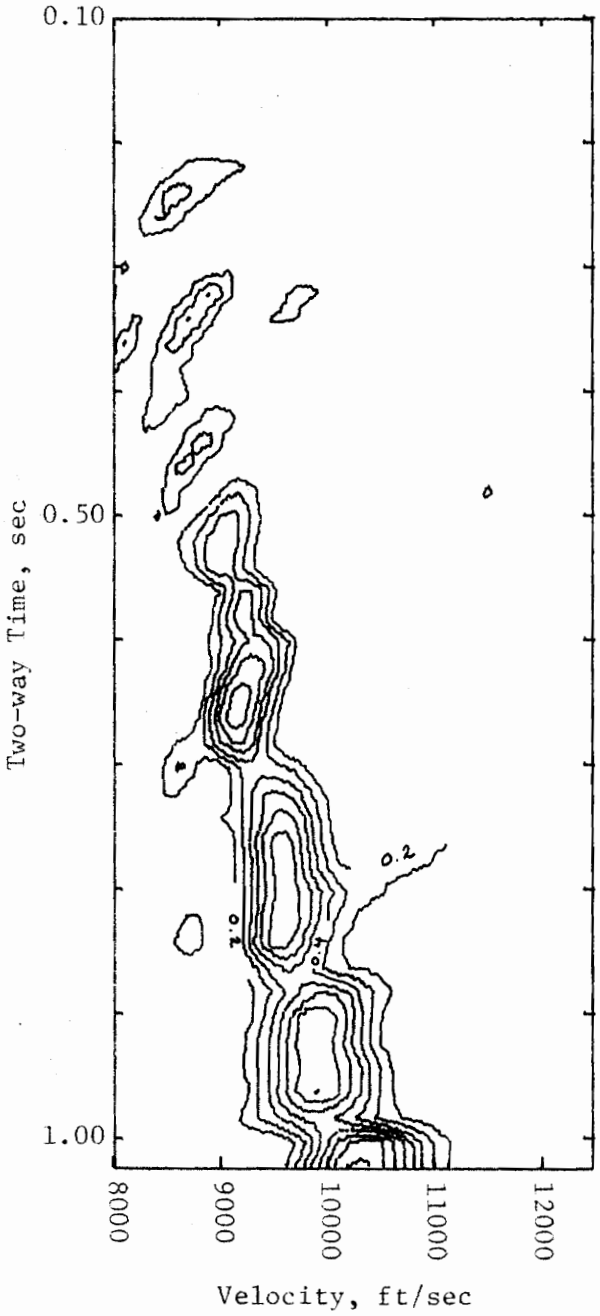

Figure 7.5-6a. Velocity Analysis of P Component Data Anisotropy = 1.043, Window Width = 50 ms, Scan Increments = 20 ms and 100 ft/sec, Anisotropy Scan Level = 1.02

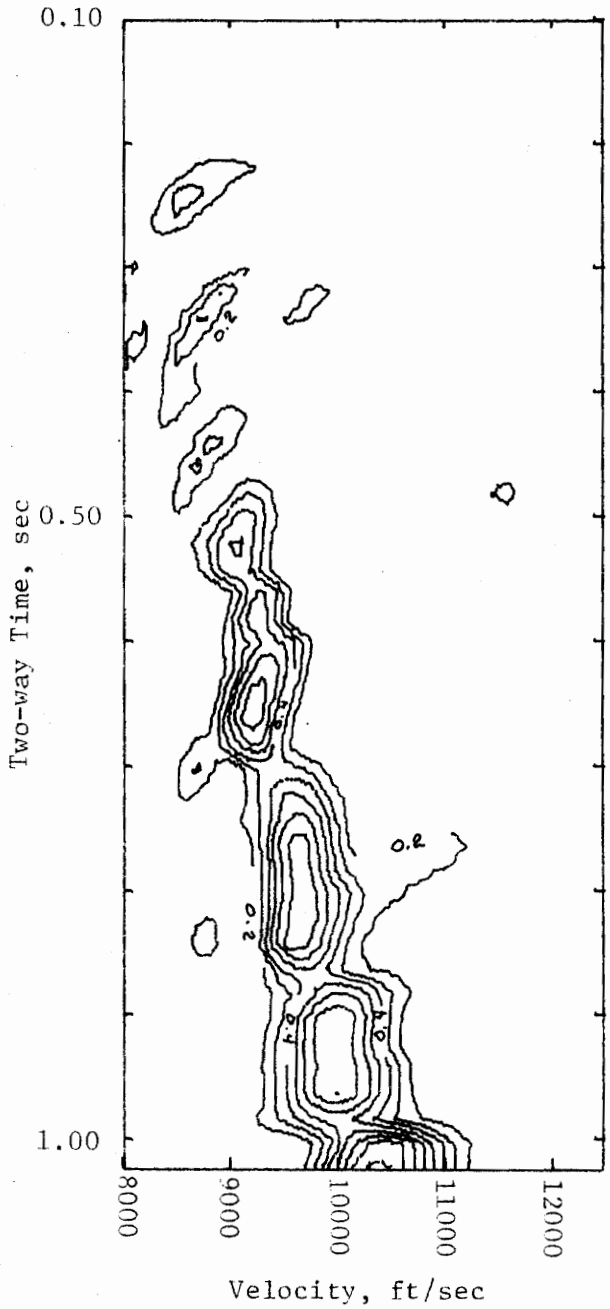

Figure 7.5-6b. Velocity Analysis of P Component Data Anisotropy = 1.043, Window Width = 50 ms, Scan Increments = 20 ms and 100 ft/sec, Anisotropy Scan Level = 1.03

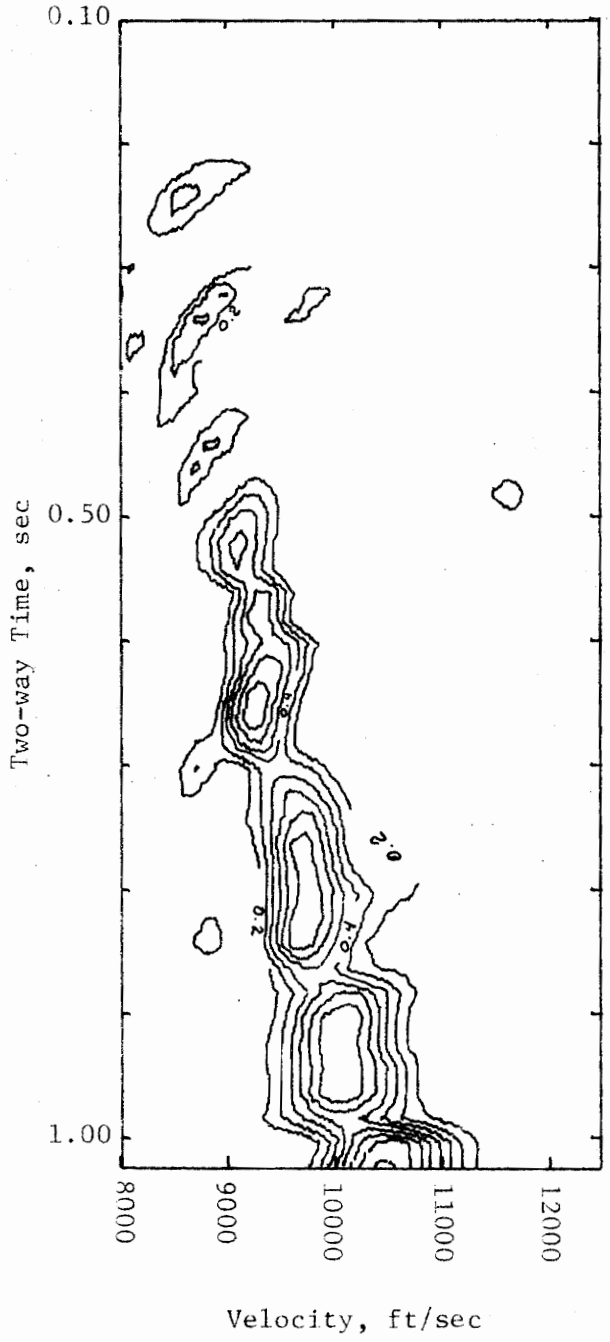

Figure 7.5-6c. Velocity Analysis of P Component Data Anisotropy = 1.043, Window Width = 50 ms, Scan Increments = 20 ms and 100 ft/sec, Anisotropy Scan Level = 1.04

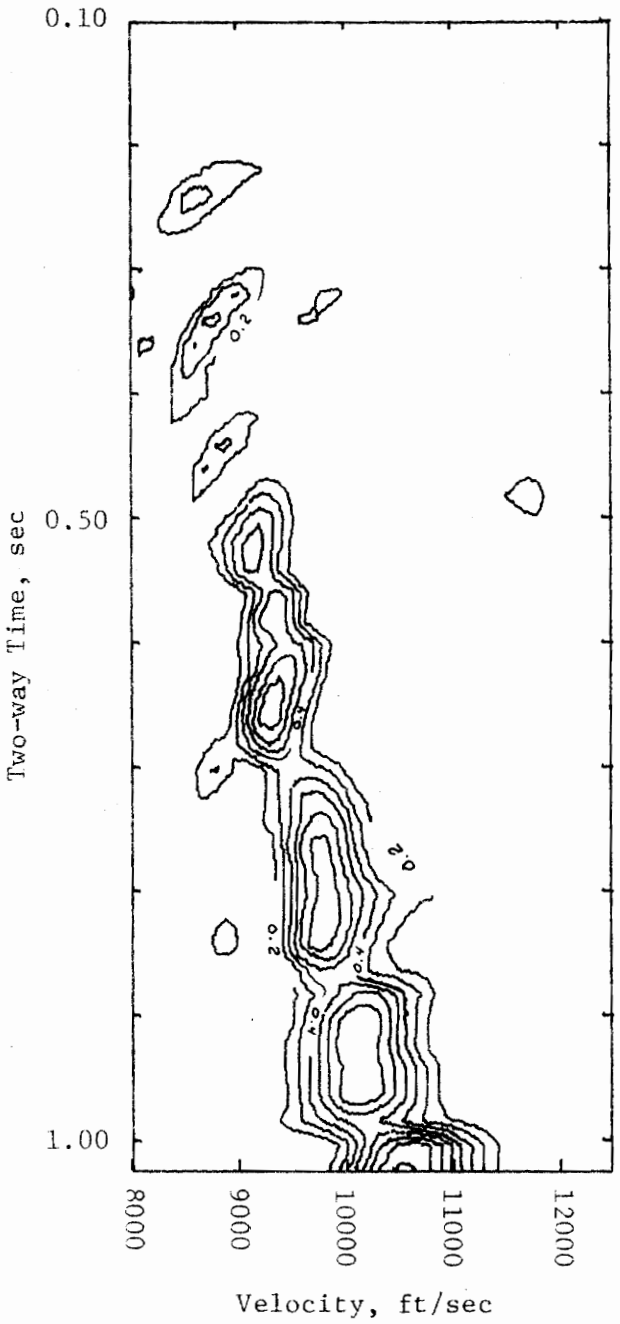

Figure 7.5-6d. Velocity Analysis of P Component Data Anisotropy = 1.043, Window Width = 50 ms, Scan Increments = 20 ms and 100 ft/sec, Anisotropy Scan Level = 1.05

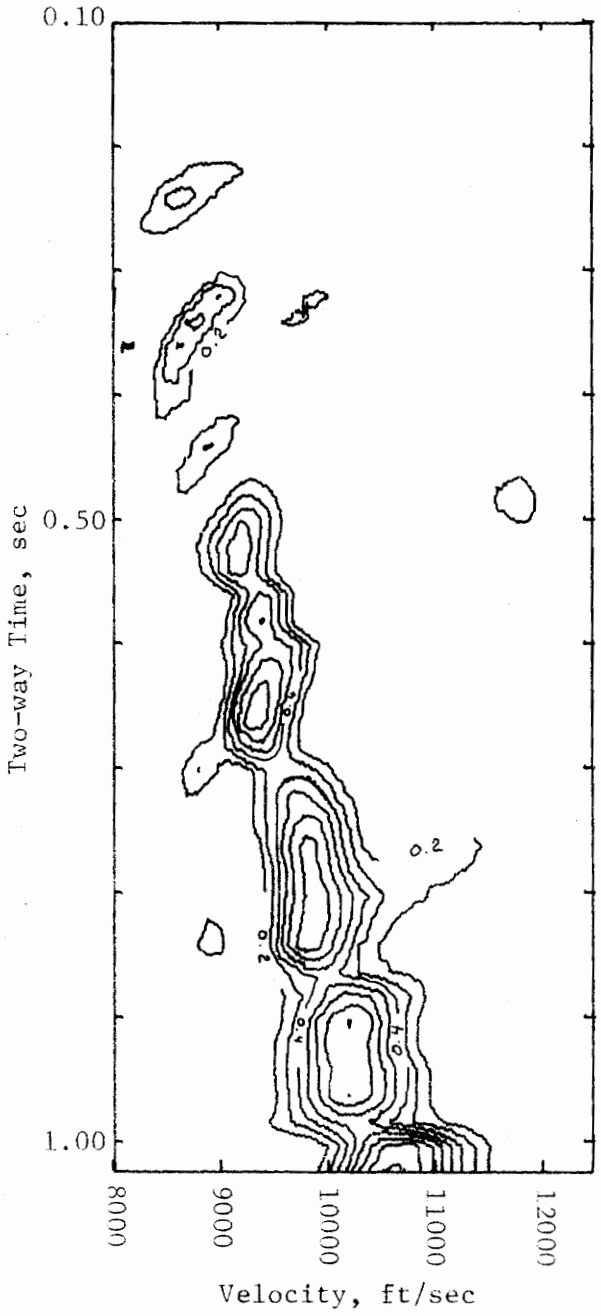

Figure 7.5-6e. Velocity Analysis of P Component Data Anisotropy = 1.043, Window Width = 50 ms, Scan Increments = 20 ms and 100 ft/sec, Anisotropy Scan Level = 1.06

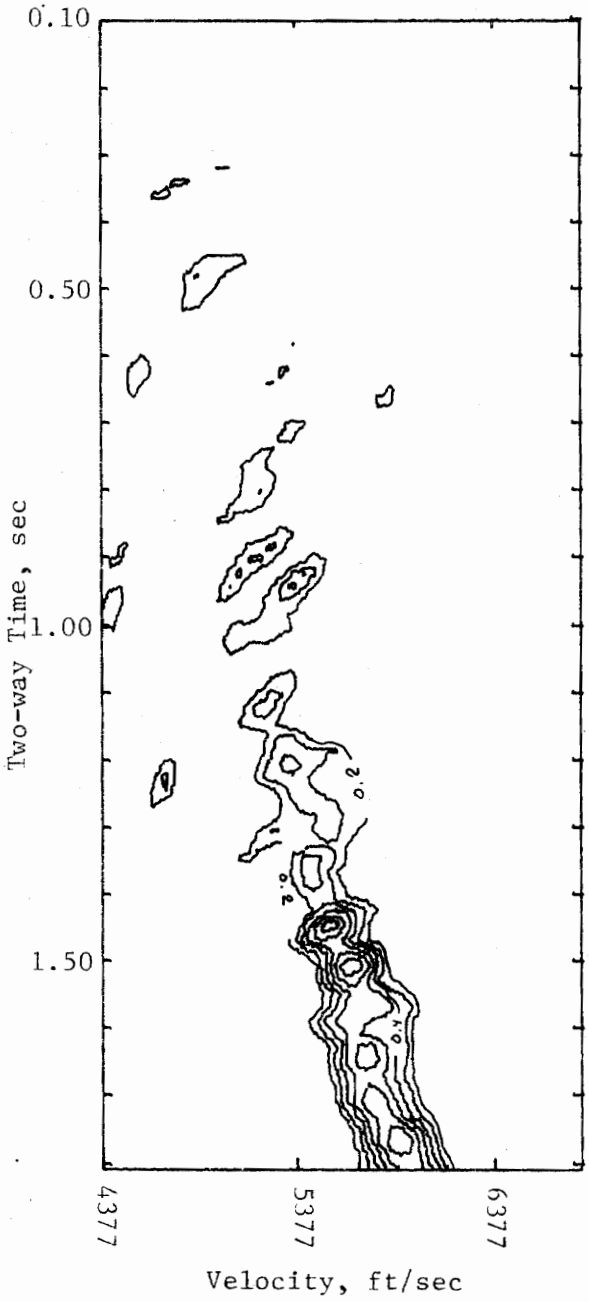

Figure 7.5-7a. Velocity Analysis of SV Component
Data Anisotropy = 1.043, Window Width = 50 ms,
Scan Increments = 20 ms and 54 ft/sec,
Anisotropy Scan Level = 1.02

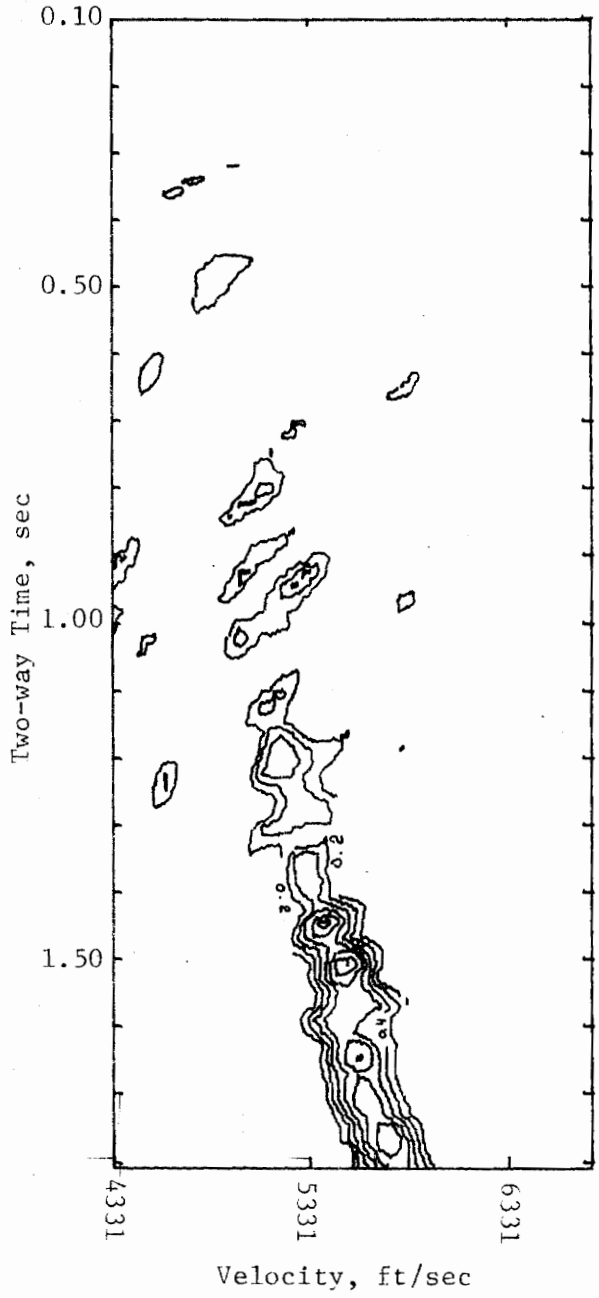

Figure 7.5-7b. Velocity Analysis of SV Component Data Anisotropy = 1.043, Window Width = 50 ms, Scan Increments = 20 ms and 54 ft/sec, Anisotropy Scan Level = 1.03

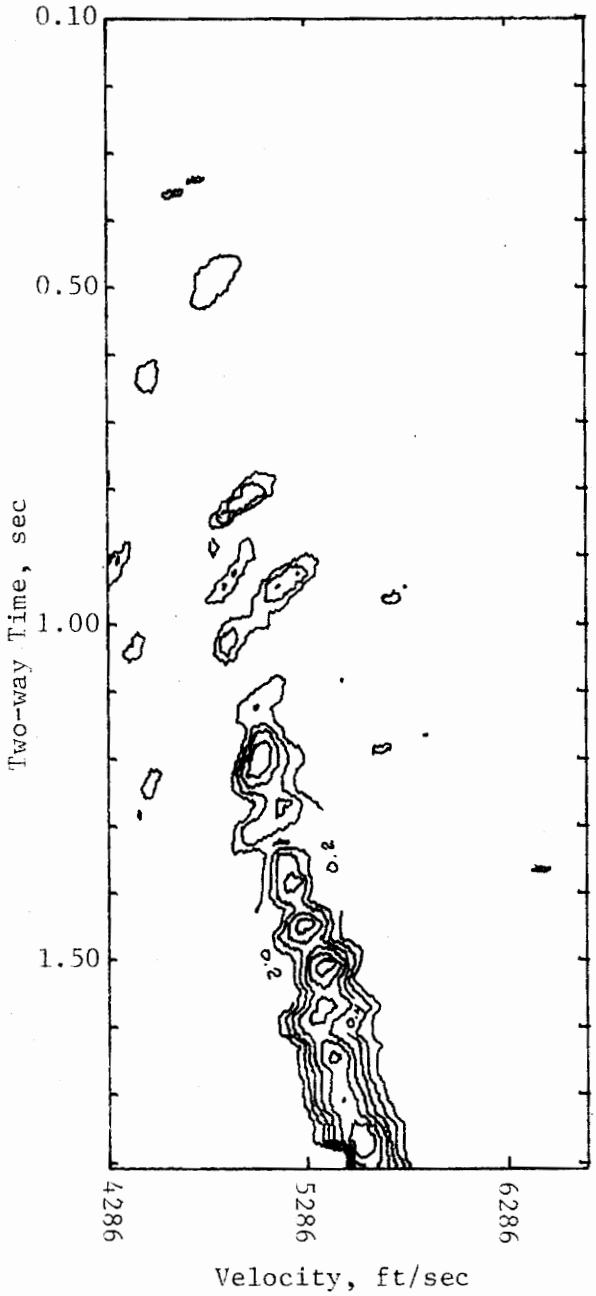

Figure 7.5-7c. Velocity Analysis of SV Component
Data Anisotropy = 1.043, Window Width = 50 ms,
Scan Increments = 20 ms and 53 ft/sec,
Anisotropy Scan Level = 1.04

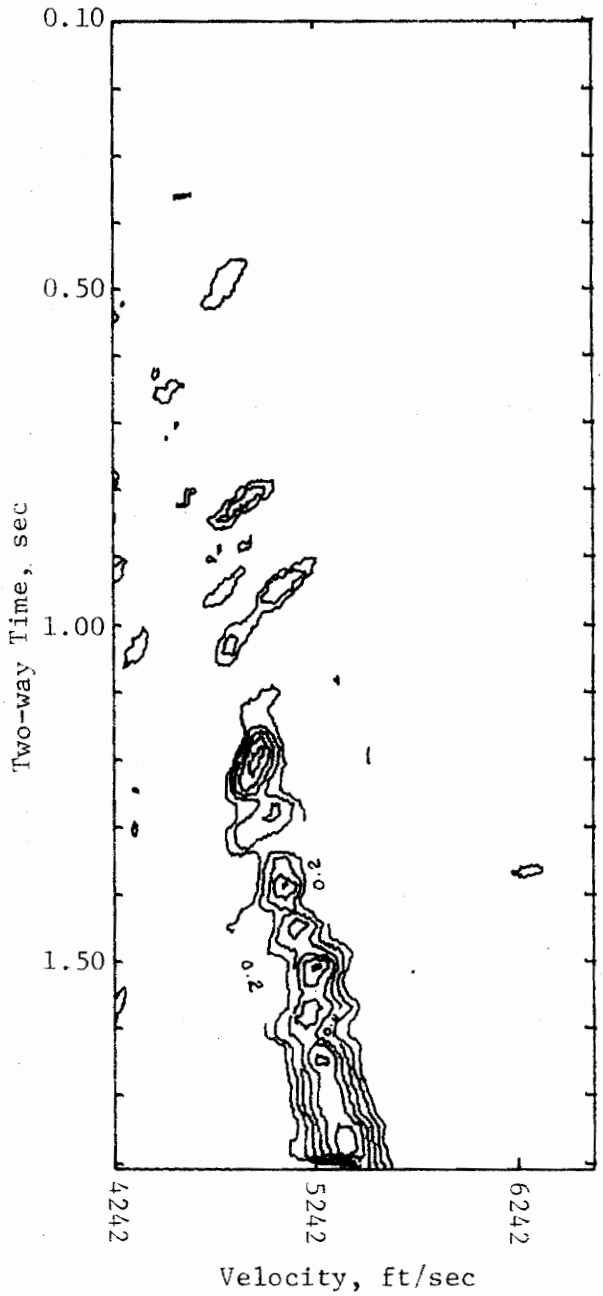

Figure 7.5-7d. Velocity Analysis of SV Component Data Anisotropy = 1.043, Window Width = 50 ms, Scan Increments = 20 ms and 53 ft/sec, Anisotropy Scan Level = 1.05

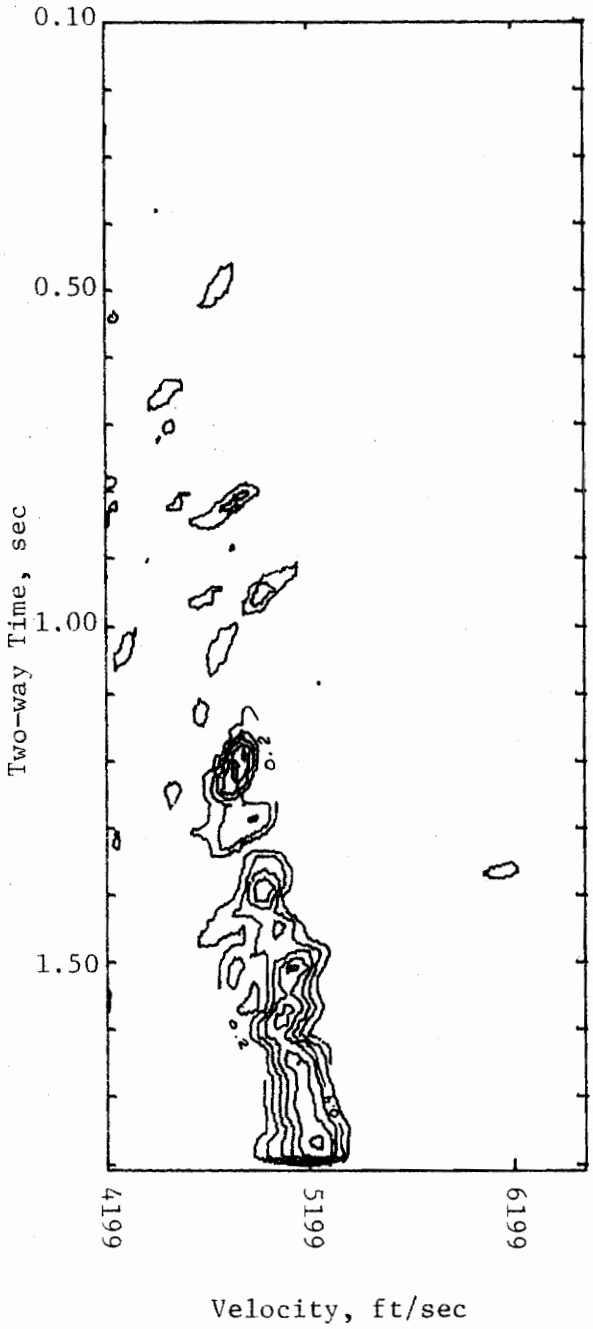

Figure 7.5-7e. Velocity Analysis of SV Component Data Anisotropy = 1.043, Window Width = 50 ms, Scan Increments = 20 ms and 52 ft/sec, Anisotropy Scan Level = 1.06

Table 7.5-3. Integrated Velocity Analysis Results

Velocity Analysis Parameters: See Figures 7.5-6 and 7.5-7.

Integration Range: Semblance Values > 0.4

Data Anisotropy = 1.043

Assumed Anisotropy Scan Value	Normalized Results of Integration	
	P	SV
1.02	93.4	93.5
1.03	95.6	100.0
1.04	95.5	99.3
1.05	99.6	88.9
1.06	100.0	70.3

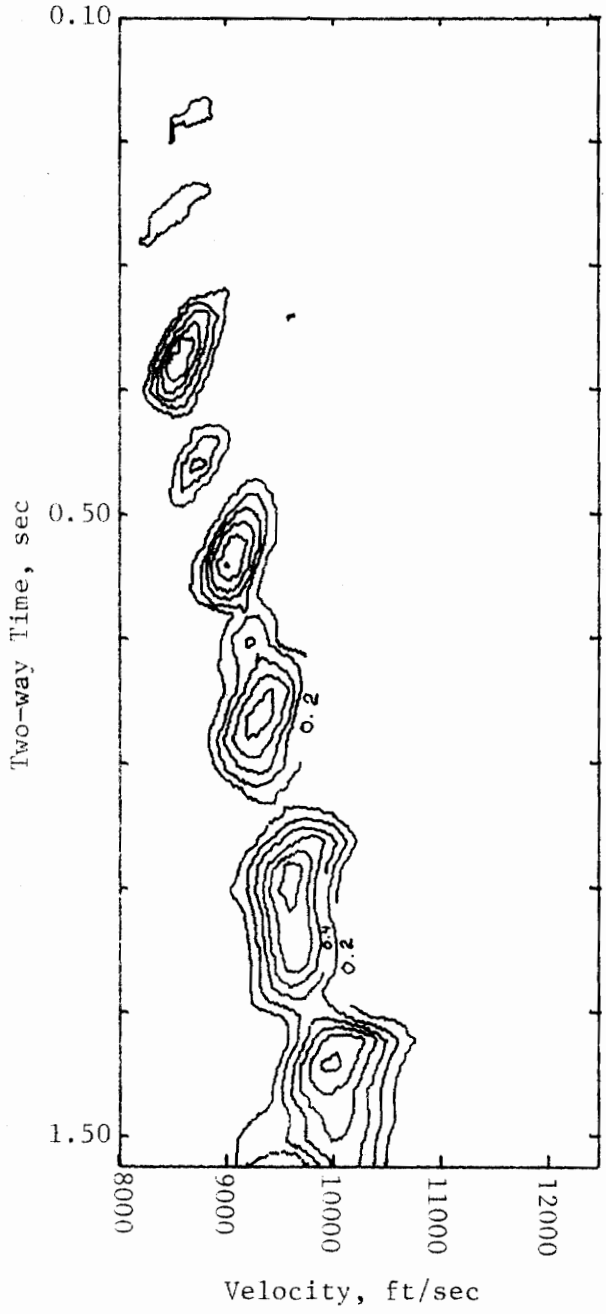

Figure 7.5-8a. Velocity Analysis of P Component Data Anisotropy = 1.08, Window Width = 50 ms, Scan Increments = 20 ms and 100 ft/sec, Anisotropy Scan Level = 1.06

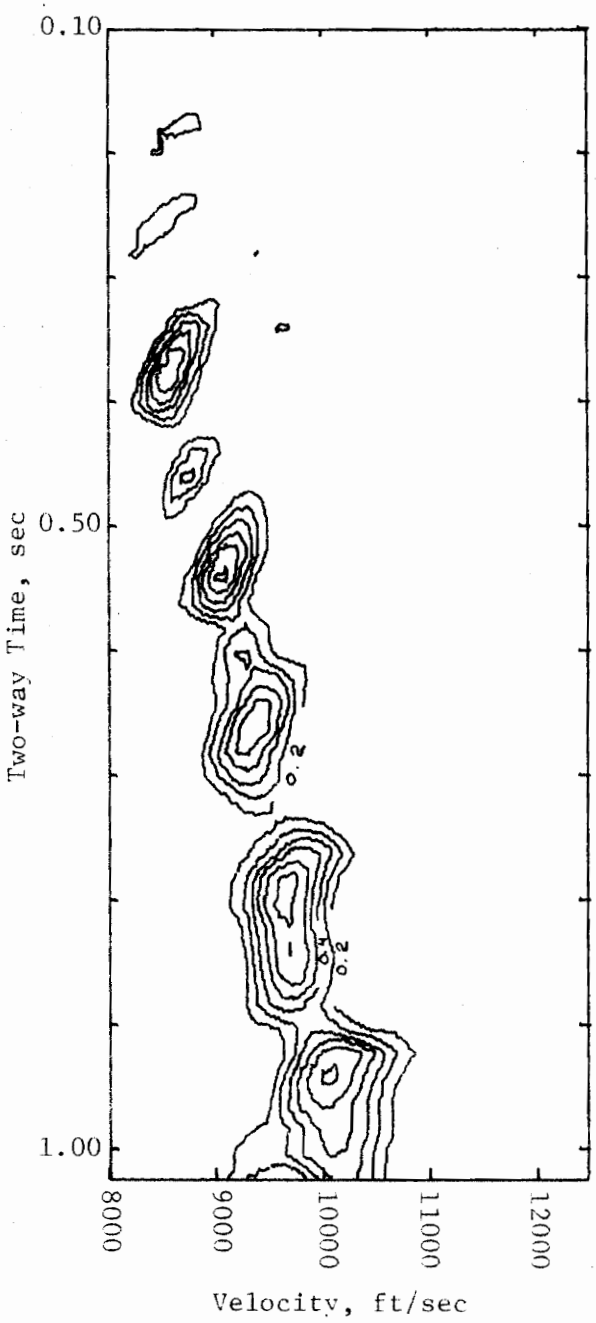

Figure 7.5-8b. Velocity Analysis of P Component Data Anisotropy = 1.08, Window Width = 50 ms, Scan Increments = 20 ms and 100 ft/sec, Anisotropy Scan Level = 1.07

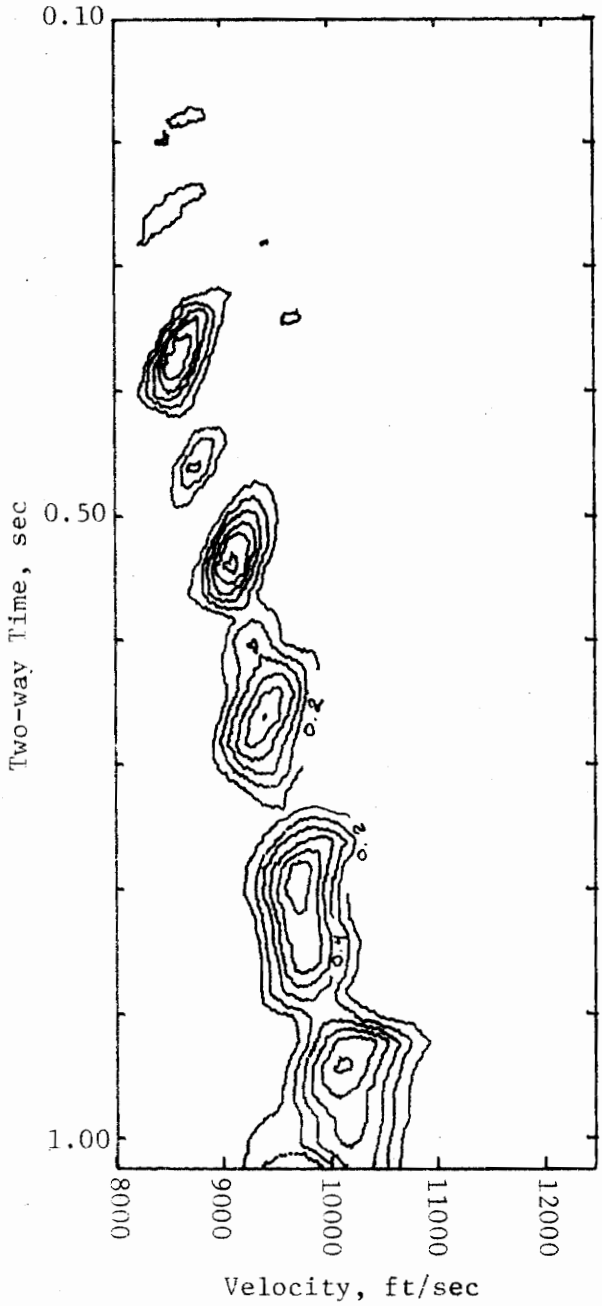

Figure 7.5-8c. Velocity Analysis of P Component Data Anisotropy = 1.08, Window Width = 50 ms, Scan Increments = 20 ms and 100 ft/sec, Anisotropy Scan Level = 1.08

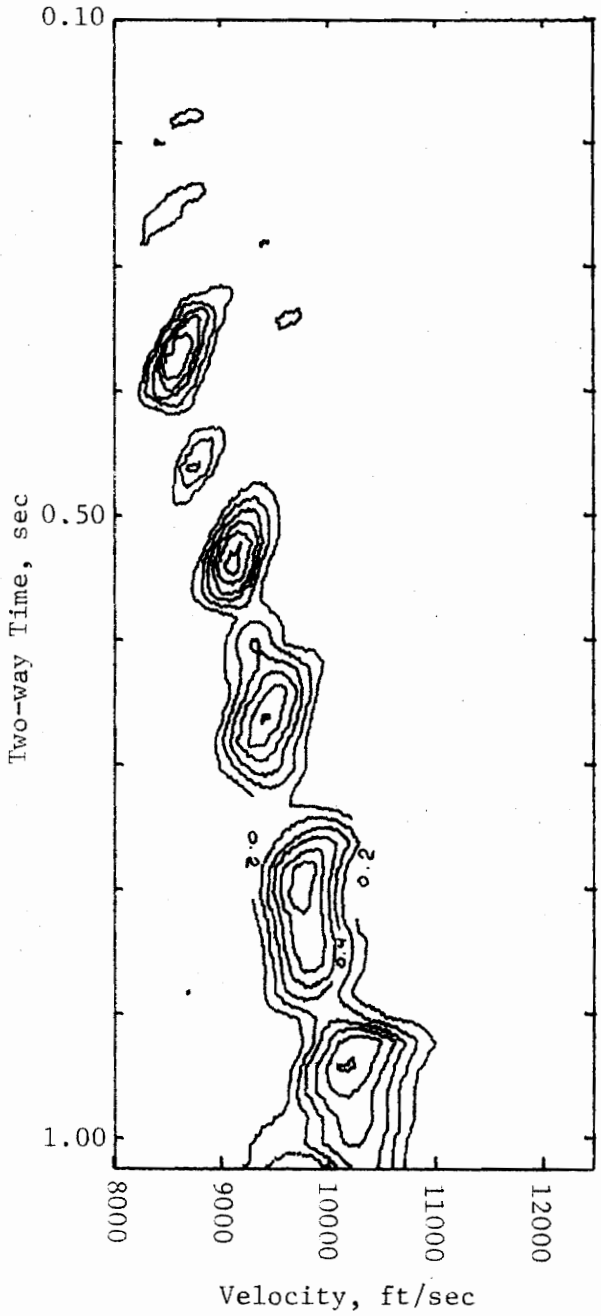

Figure 7.5-8d. Velocity Analysis of P Component Data Anisotropy= 1.08, Window Width = 50 ms, Scan Increments = 20 ms and 100 ft/sec, Anisotropy Scan Level = 1.09

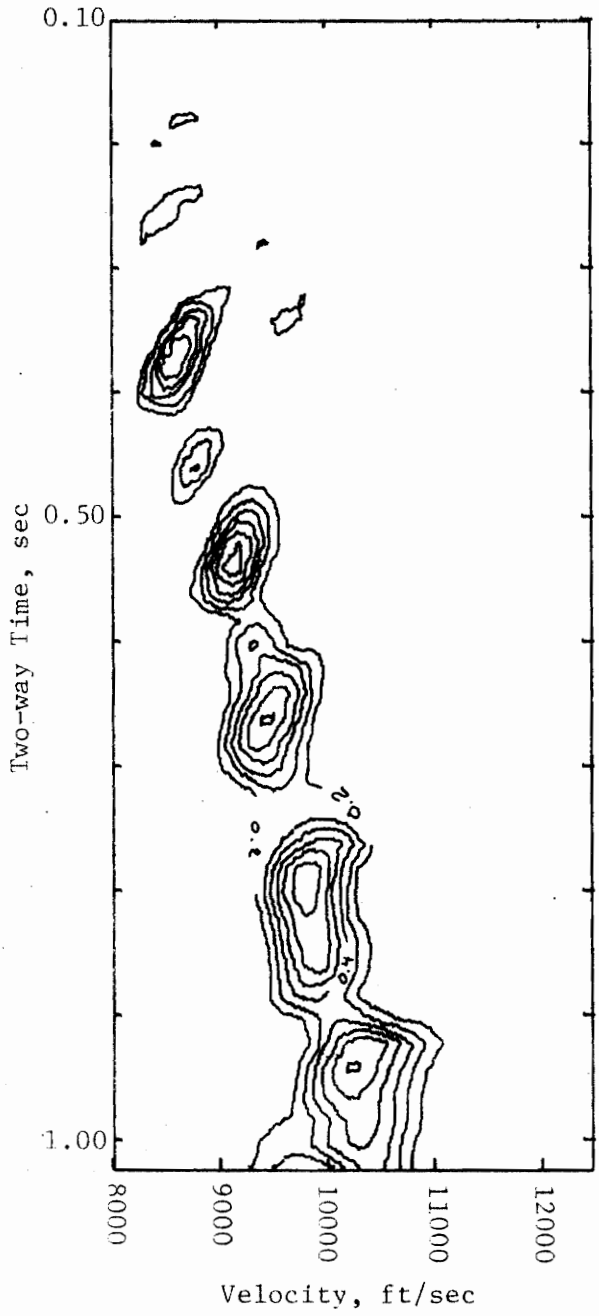

Figure 7.5-8e. Velocity Analysis of P Component Data Anisotropy = 1.08, Window Width = 50 ms, Scan Increments = 20 ms and 100 ft/sec, Anisotropy Scan Level = 1.10

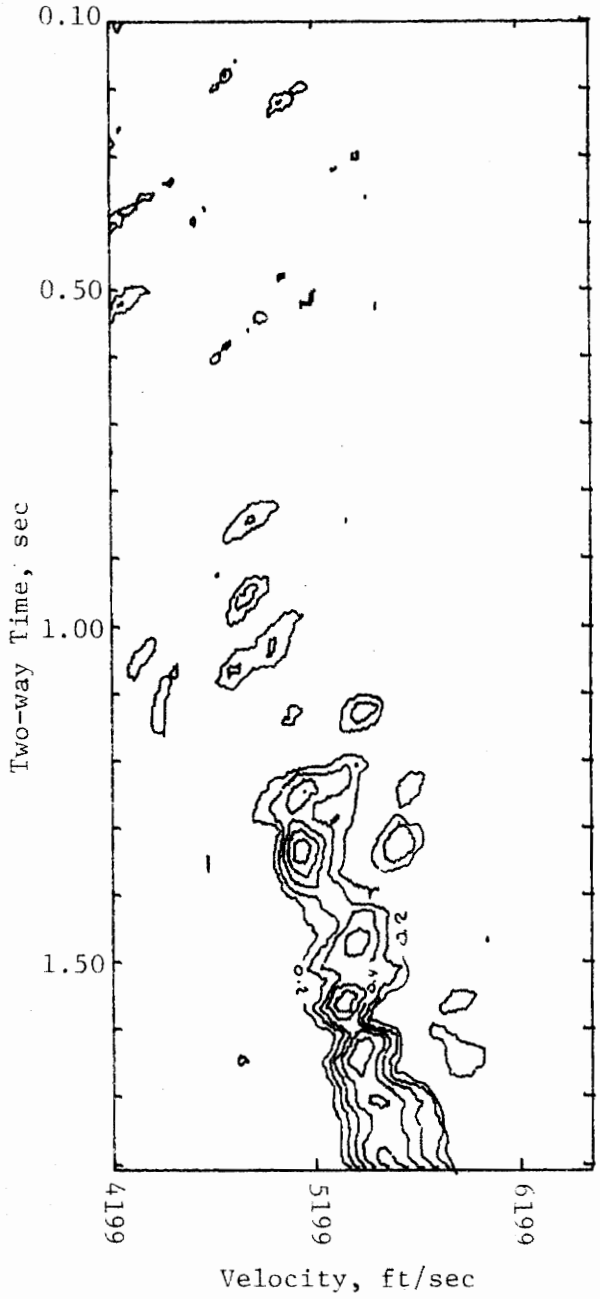

Figure 7.5-9a. Velocity Analysis of SV Component
Data Anisotropy = 1.08, Window Width = 50 ms,
Scan Increments = 20 ms and 52 ft/sec,
Anisotropy Scan Level = 1.06

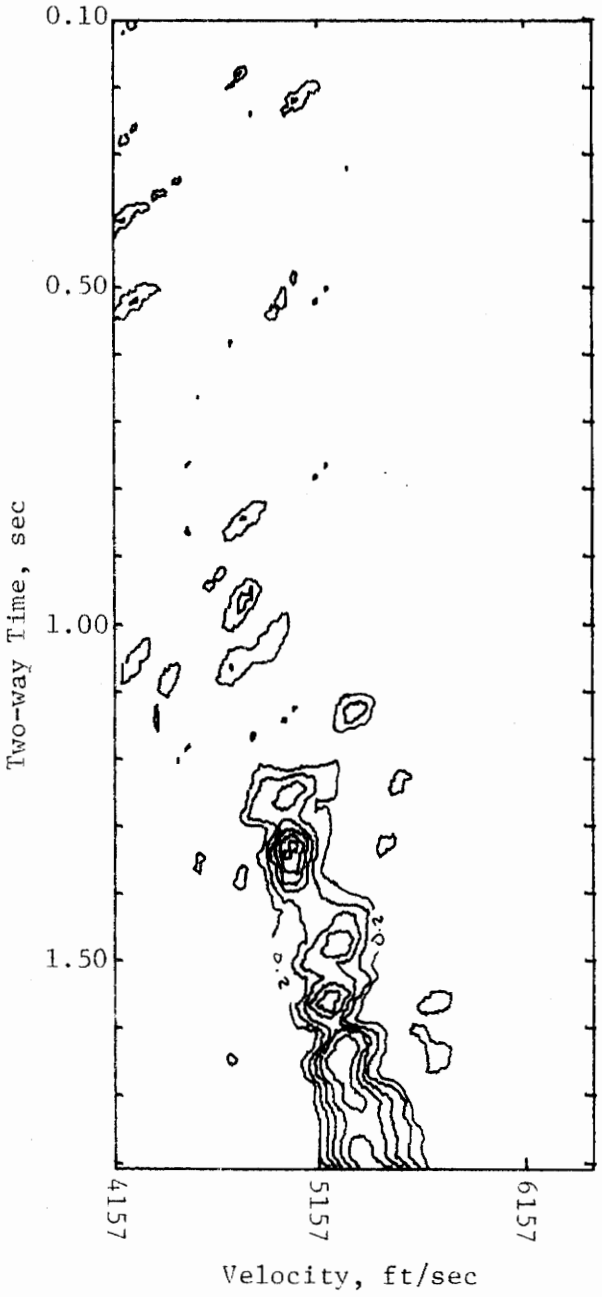

Figure 7.5-9b. Velocity Analysis of SV Component
Data Anisotropy = 1.08, Window Width = 50 ms,
Scan Increments = 20 ms and 51 ft/sec,
Anisotropy Scan Level = 1.07

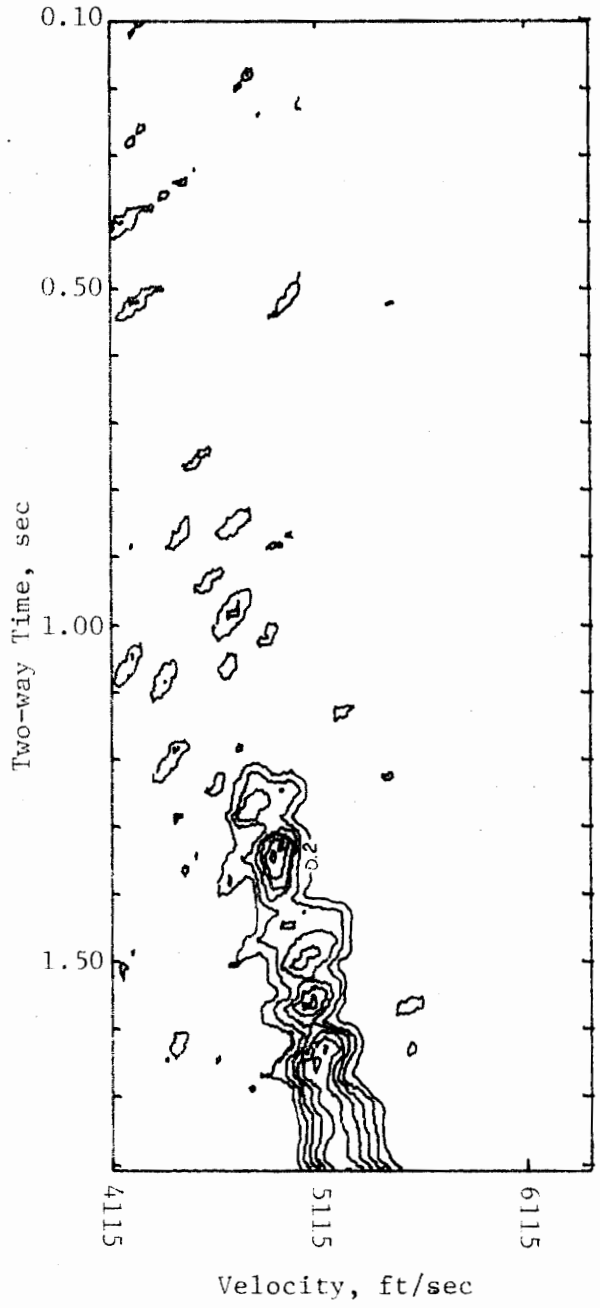

Figure 7.5-9c. Velocity Analysis of SV Component
Data Anisotropy = 1.08, Window Width = 50 ms,
Scan Increments = 20 ms and 51 ft/sec,
Anisotropy Scan Level = 1.08

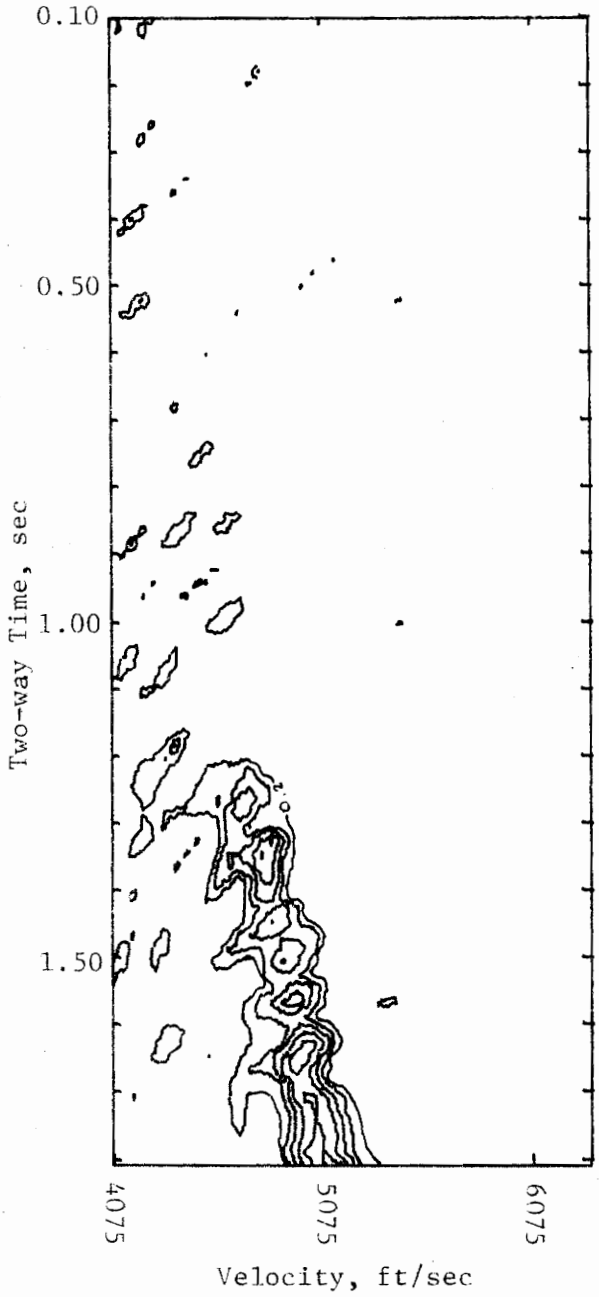

Figure 7.5-9d. Velocity Analysis of SV Component
Data Anisotropy = 1.08, Window Width = 50 ms,
Scan Increments = 20 ms and 50 ft/sec,
Anisotropy Scan Level = 1.09

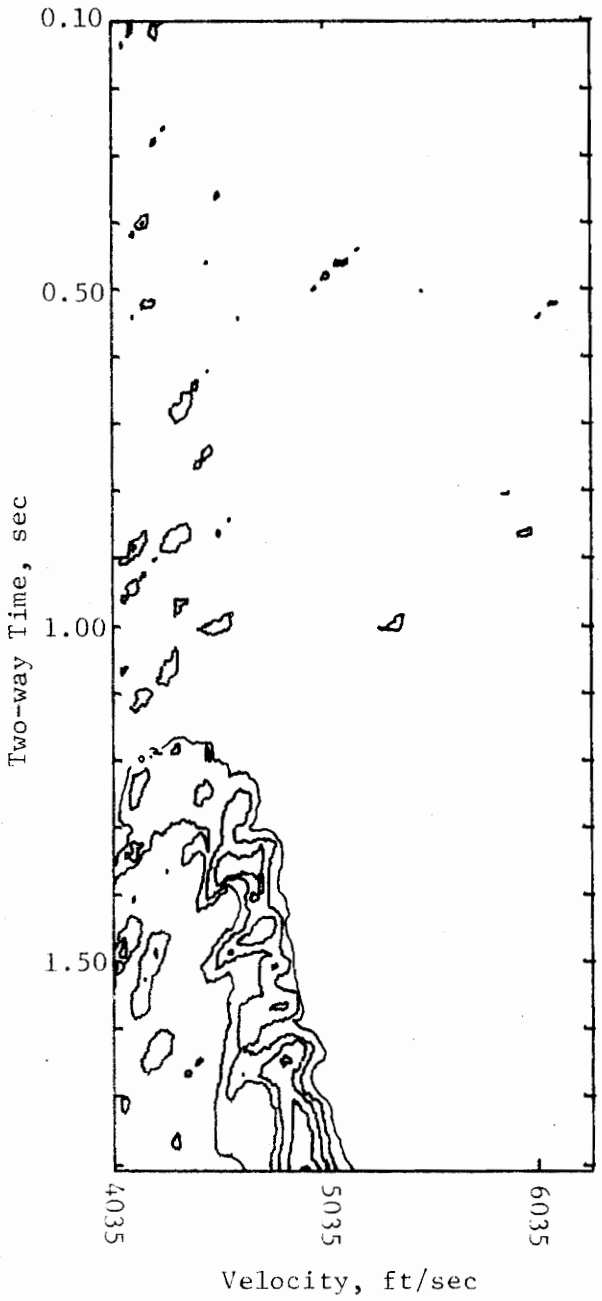

Figure 7.5-9e. Velocity Analysis of SV Component
Data Anisotropy = 1.08, Window Width = 50 ms,
Scan Increments = 20 ms and 50 ft/sec,
Anisotropy Scan Level = 1.10

Table 7.5-4. Integrated Velocity Analysis Results

Velocity Analysis Parameters: See Figures 7.5-8 and 7.5-9.

Integration Range: Semblance Values > 0.4

Data Anisotropy = 1.08

Assumed Anisotropy Scan Value	Normalized Results of Integration P	SV
1.06	92.3	96.8
1.07	95.0	100.0
1.08	95.6	92.0
1.09	97.6	75.0
1.10	100.0	46.8

tection of anisotropy. The results of semblance matrix integration are shown in Table 7.5-4. The SV results indicate a choice of 1.07 for the anisotropy factor. This value is low by the amount of 0.01.

This model again supports the earlier conclusion that velocity scans over the P velocity component are not suitable for the detection of anisotropy. The SV velocity scans in each of the three cases studied indicated an anisotropy factor that was 0.01 lower than the correct value. In the first two cases, the actual anisotropy factor was an equally good choice as the value indicated by integration of the semblance matrices.

7.6 Buried Anisotropic Interval

The velocity function associated with this model is described in section 5.3.4. The horizontal compressional component of velocity varies in the manner described in section 7.3. From the surface to a depth of 3000 feet the section is isotropic. From 3000 to 4000 feet in depth, the section is anisotropic with an anisotropy factor of 1.10. The top of the anisotropic interval occurs at two-way reflection times of 0.640 and 1.150 sec for the P and SV velocity components respectively. Below 4000 feet, the section is once again isotropic.

7.6.1 Effects of Variation of Model Parameters on Velocity Analysis

Data Characteristics

The maximum shotpoint-geophone distance is 5280 feet as in the previous models. A CDP geometry was utilized and 12-fold data were generated. The same set of reflection coefficients as discussed in section 7.3 were used in the generation of the data shown in Figure 7.6-1.

Analysis Results

Table 7.6-1 shows the first depth from which reflection is received for each trace. Reflections are not received from shallower depths because critical angles are exceeded. The velocity analyses for both P and SV are shown in Figures 7.6-2 and 7.6-3 respectively. As in previous models, the P velocity analyses were insensitive to the presence of aniostropy. The isotropic portion of the SV record prior to 1.15 sec may be correctly resolved as being isotropic by the inte-

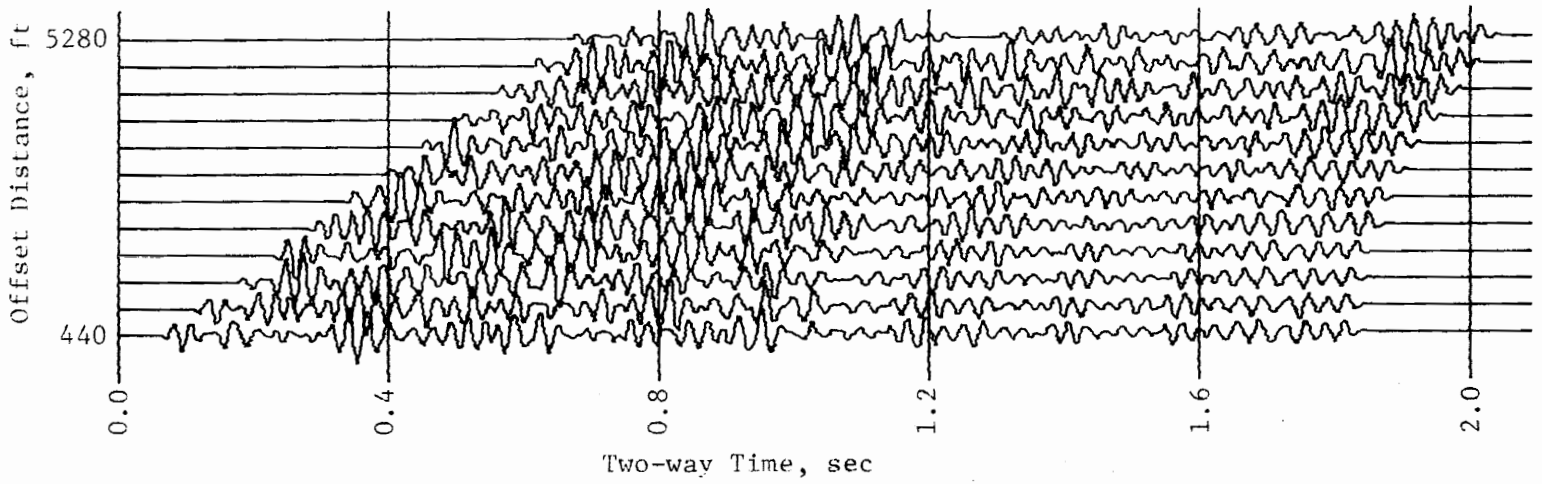

Figure 7.6-1. Buried Anisotropic Interval
12-Fold Reflection Seismograms
Data Anisotropy = 1.00: <3000 & >4000 ft
and 1.10 from 3000-4000 ft

Table 7.6-1. Depth of First Reflection

Trace No. :	1	2	3	4	5	6	7	8	9	10	11	12
P :	100	100	100	150	275	450	575	775	975	1275	1575	1950
SV :	100	100	100	150	275	450	575	775	975	1275	1575	1950

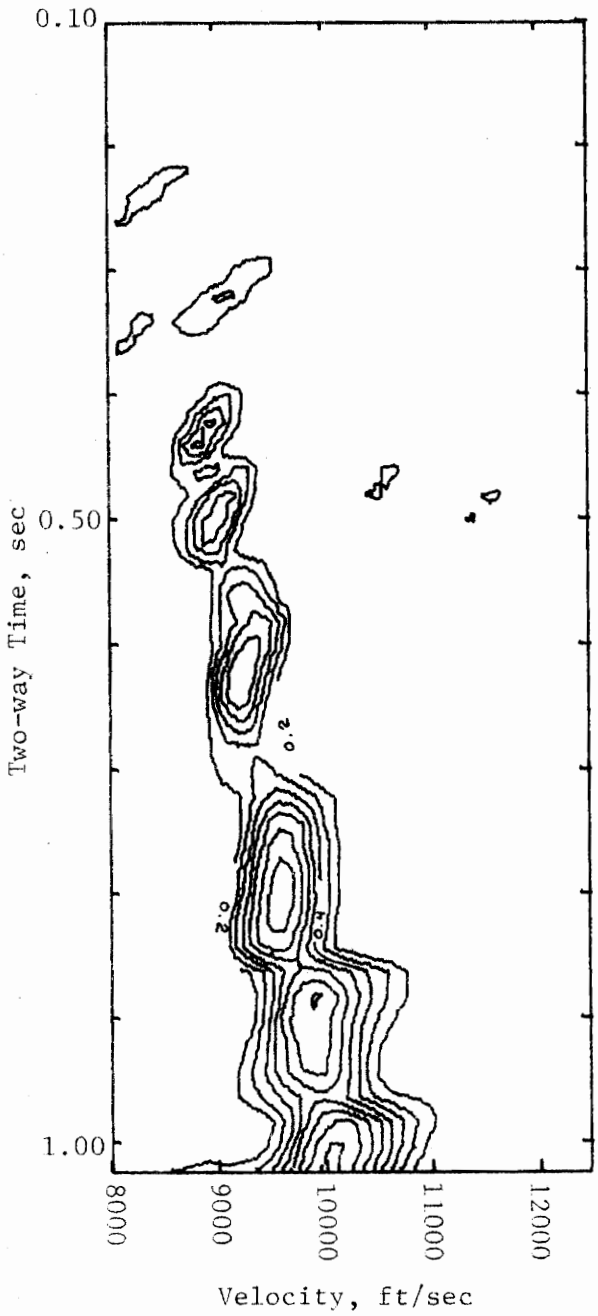

Figure 7.6-2a. Velocity Analysis of P Component
Data Anisotropy = 1.00: <3000 & >4000 ft and 1.10
from 3000-4000 ft, Window Width = 50 ms,
Scan Increments = 20 ms and 100 ft/sec,
Anisotropy Scan Level = 1.00

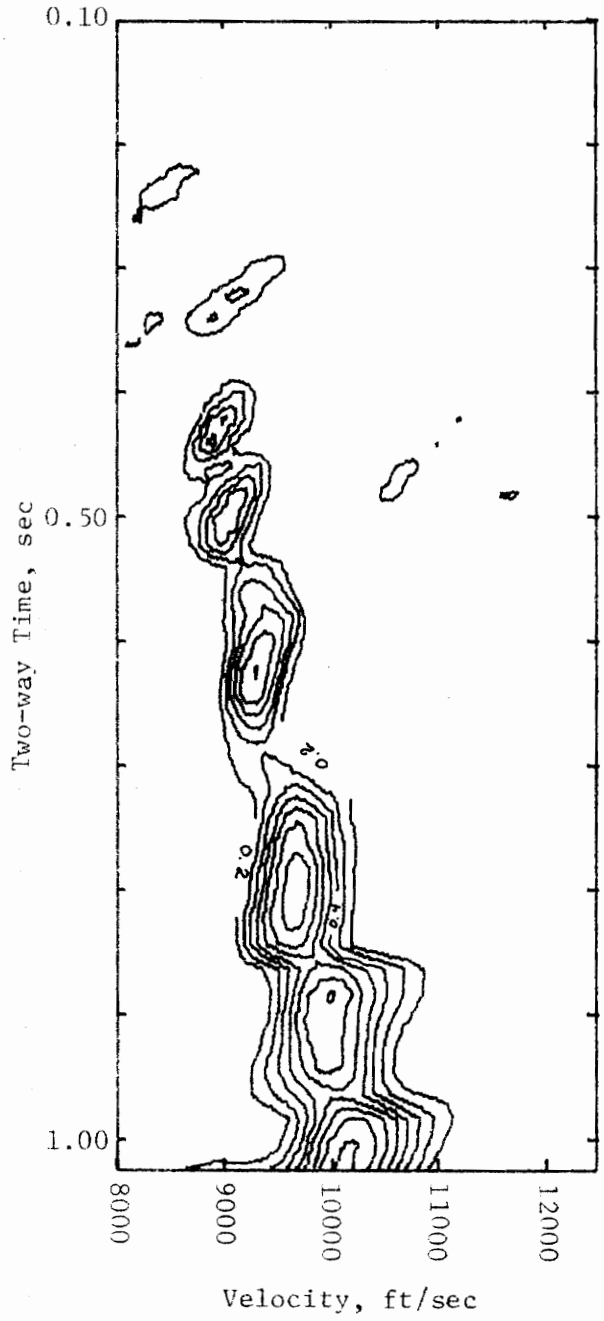

Figure 7.6-2b. Velocity Analysis of P Component
Data Anisotropy = 1.00: <3000 & >4000 ft and 1.10 from 3000-4000 ft, Window Width = 50 ms, Scan Increments = 20 ms and 100 ft/sec, Anisotropy Scan Level = 1.01

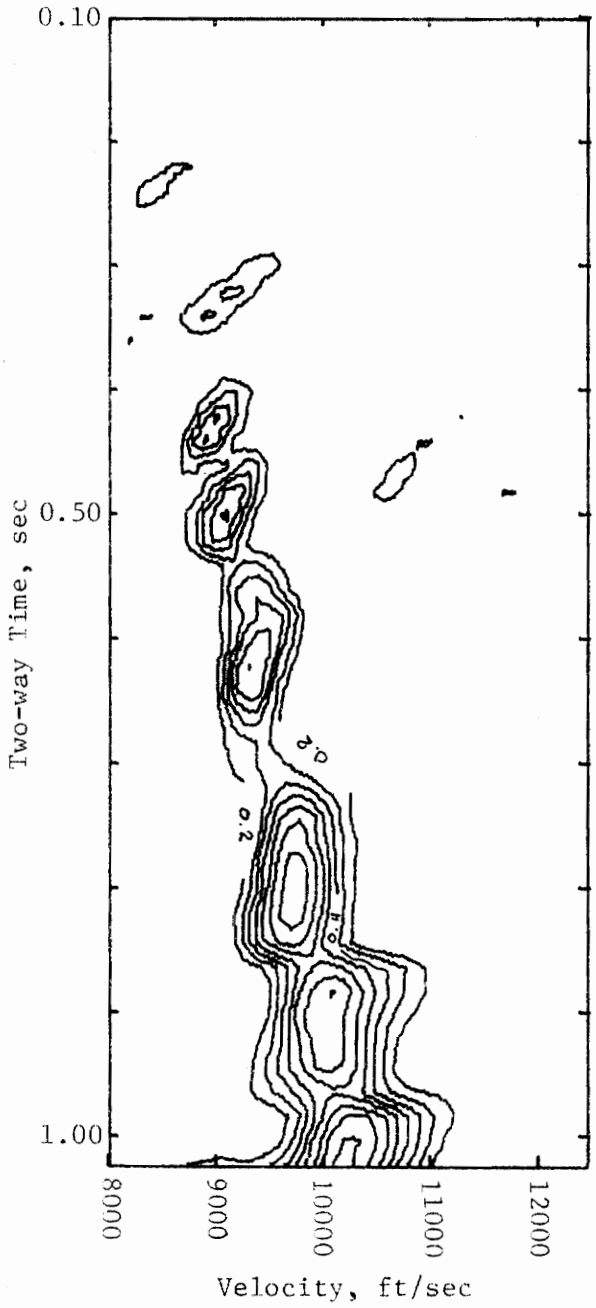

Figure 7.6-2c. Velocity Analysis of P Component
Data Anisotropy = 1.00: <3000 & >4000 ft and 1.10
from 3000 to 4000 ft, Window Width = 50 ms,
Scan Increments = 20 ms and 100 ft/sec,
Anisotropy Scan Level = 1.02

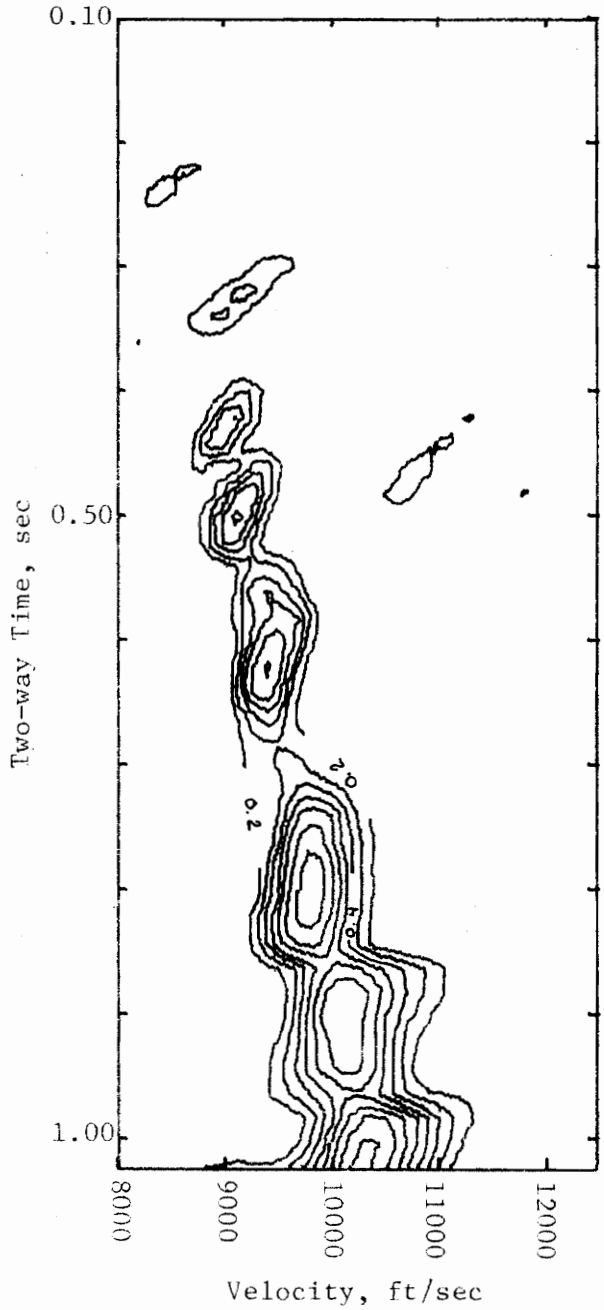

Figure 7.6-2d. Velocity Analysis of P Component
Data Anisotropy = 1.00: <3000 & >4000 ft and 1.10
from 3000-4000 ft, Window Width = 50 ms,
Scan Increments = 20 ms and 100 ft/sec,
Anisotropy Scan Level = 1.03

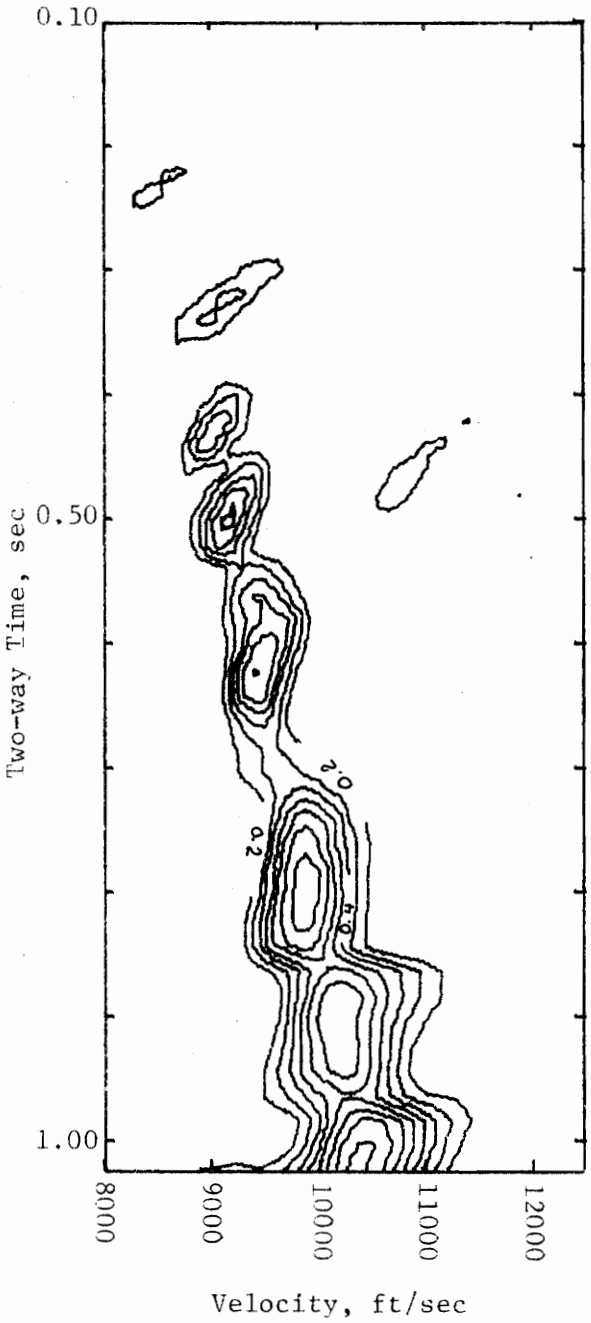

Figure 7.6-2e. Velocity Analysis of P Component
Data Anisotropy = 1.00: <3000 & >4000 ft and 1.10
from 3000-4000 ft, Window Width = 50 ms,
Scan Increments = 20 ms and 100 ft/sec,
Anisotropy Scan Level = 1.04

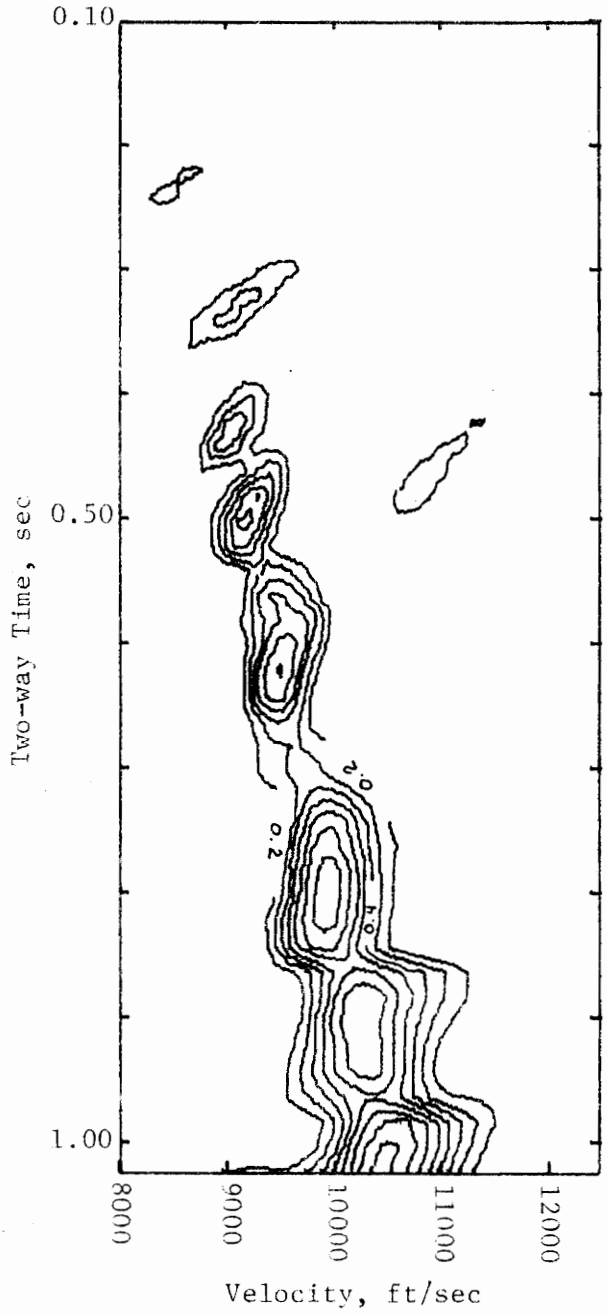

Figure 7.6-2f. Velocity Analysis of P Component
Data Anisotropy = 1.00: <3000 & >4000 ft and 1.10
from 3000-4000 ft, Window Width = 50 ms,
Scan Increments = 20 ms and 100 ft/sec,
Anisotropy Scan Level = 1.05

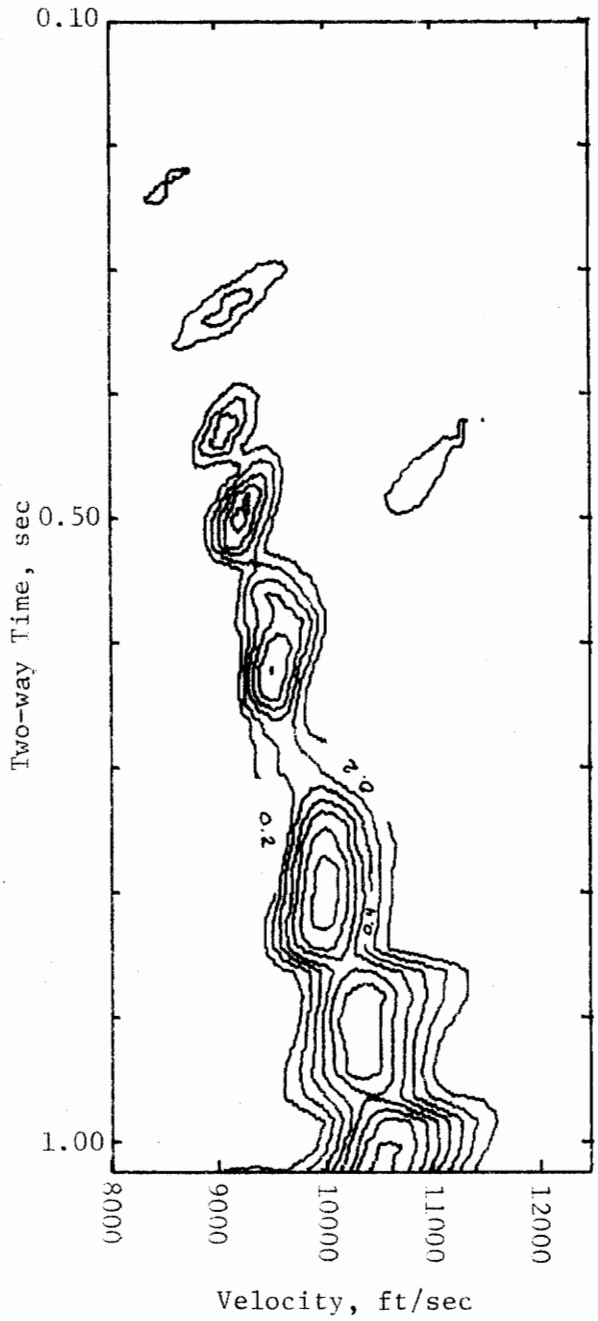

Figure 7.6-2g. Velocity Analysis of P Component Data Anisotropy = 1.00: <3000 & >4000 ft and 1.10 from 3000-4000 ft, Window Width = 50 ms, Scan Increments = 20 ms and 100 ft/sec, Anisotropy Scan Level = 1.06

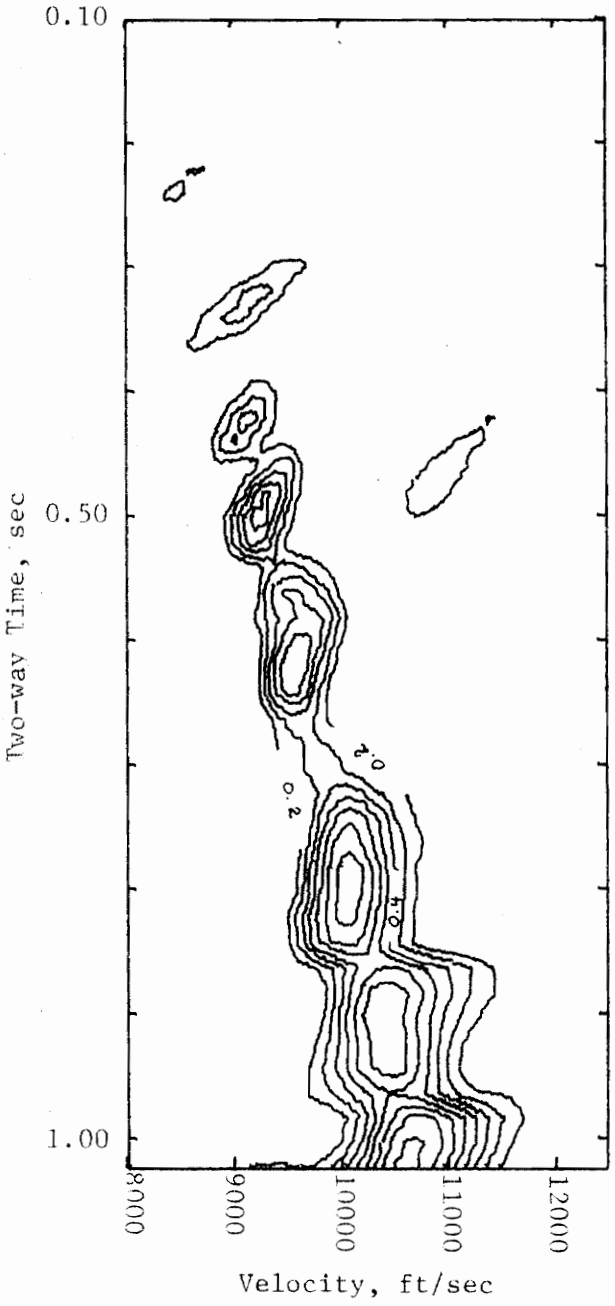

Figure 7.6-2h. Velocity Analysis of P Component
Data Anisotropy = 1.00: <3000 & >4000 ft and 1.10
from 3000-4000 ft, Window Width = 50 ms,
Scan Increments = 20 ms and 100 ft/sec,
Anisotropy Scan Level = 1.07

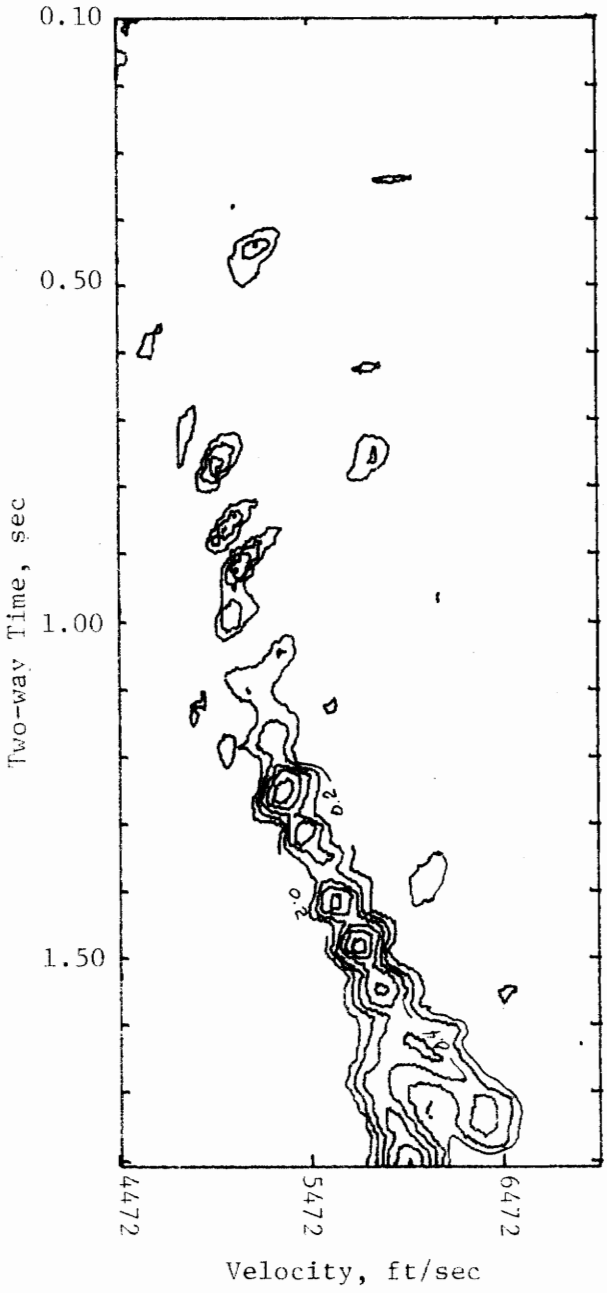

Figure 7.6-3a. Velocity Analysis of SV Component
Data Anisotropy = 1.00: <3000 & >4000 ft and 1.10
from 3000-4000 ft, Window Width = 50 ms,
Scan Increments = 20 ms and 55 ft/sec,
Anisotropy Scan Level = 1.00

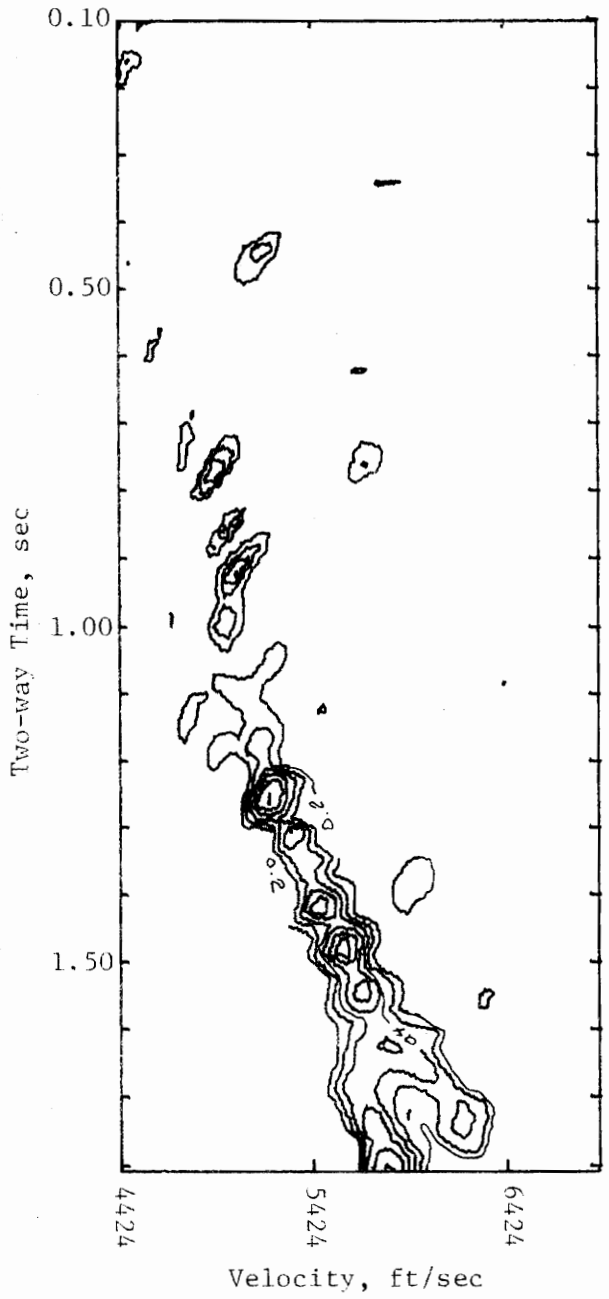

Figure 7.6-3b. Velocity Analysis of SV Component Data Anisotropy = 1.00: <3000 & >4000 ft and 1.10 from 3000-4000 ft, Window Width = 50 ms, Scan Increments = 20 ms and 55 ft/sec, Anisotropy Scan Level = 1.01

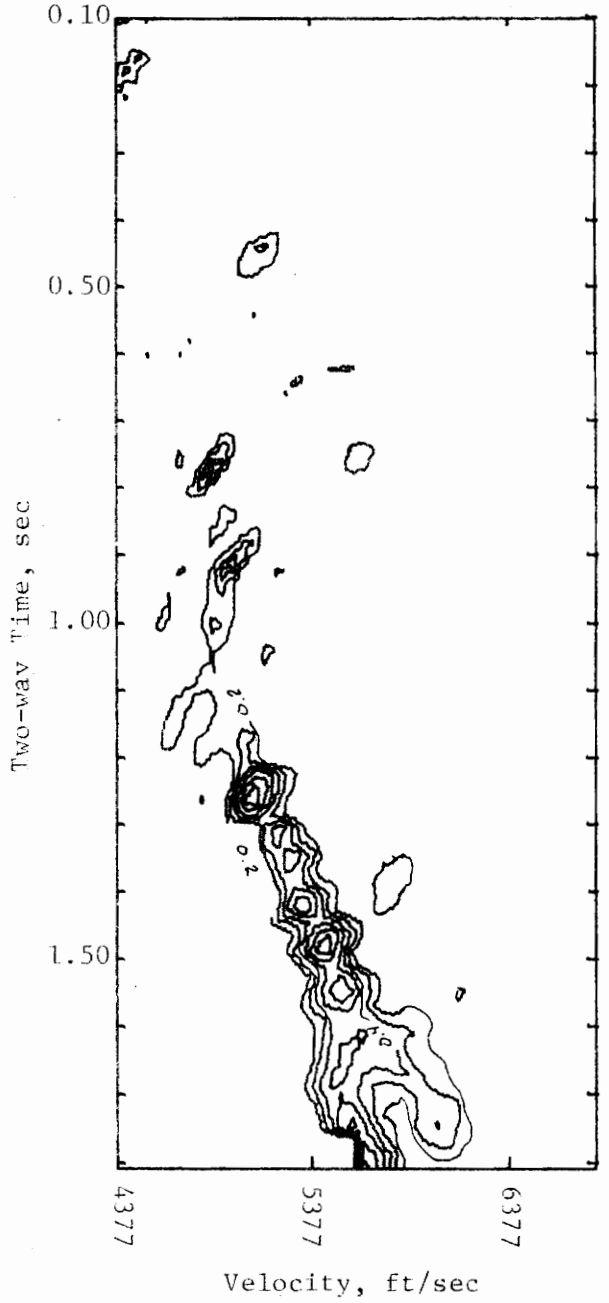

Figure 7.6-3c. Velocity Analysis of SV Component Data Anisotropy = 1.00: <3000 & >4000 ft and 1.10 from 3000-4000 ft, Window Width = 50 ms, Scan Increments = 20 ms and 54 ft/sec, Anisotropy Scan Level = 1.02

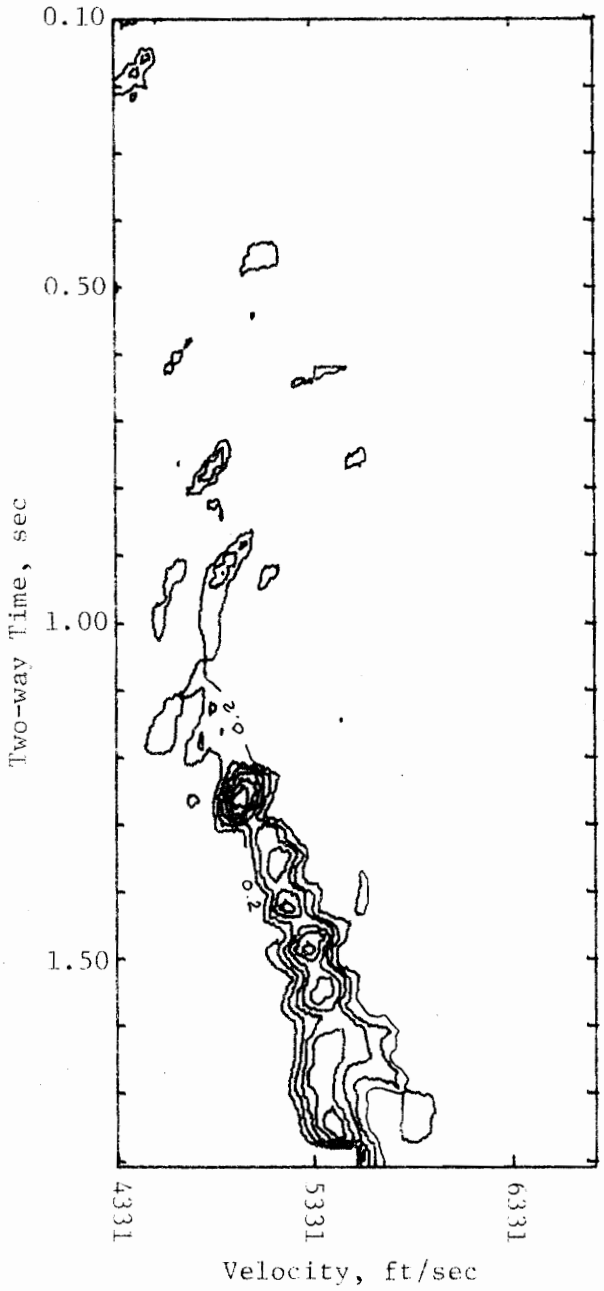

Figure 7.6-3d. Velocity Analysis of SV Component Data Anisotropy = 1.00: <3000 & >4000 ft and 1.10 from 3000-4000 ft, Window Width = 50 ms, Scan Increments = 20 ms and 54 ft/sec, Anisotropy Scan Level = 1.03

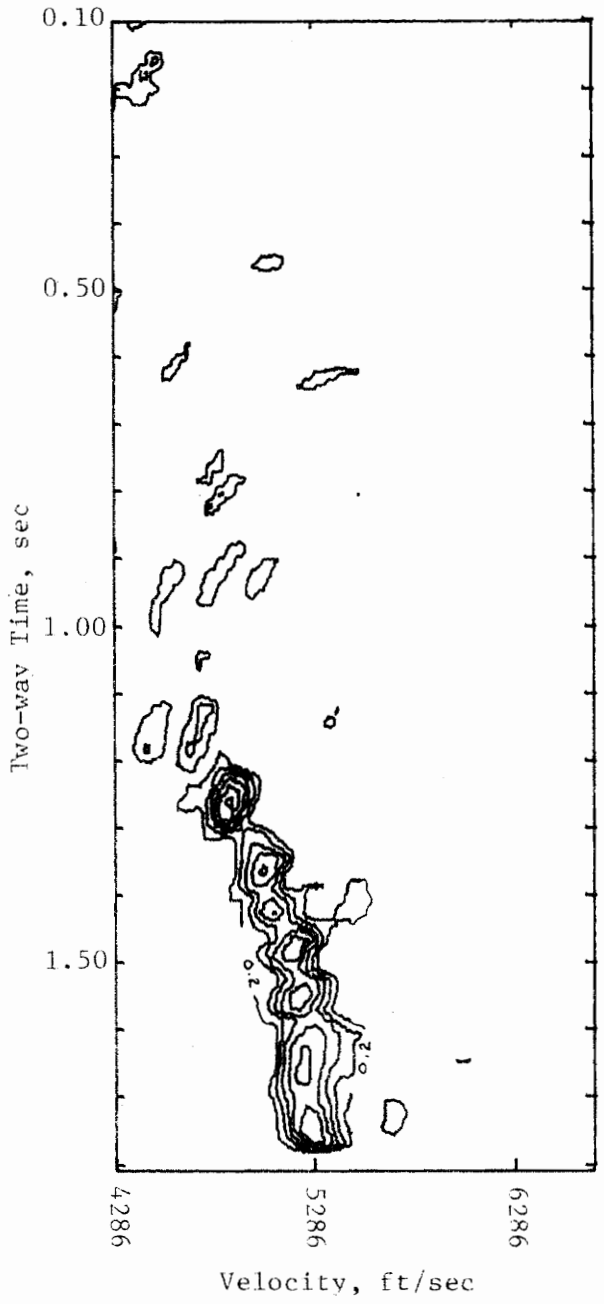

Figure 7.6-3e. Velocity Analysis of SV Component
Data Anisotropy = 1.00: <3000 & >4000 ft and 1.10
from 3000-4000 ft, Window Width = 50 ms,
Scan Increments = 20 ms and 53 ft/sec,
Anisotropy Scan Level = 1.04

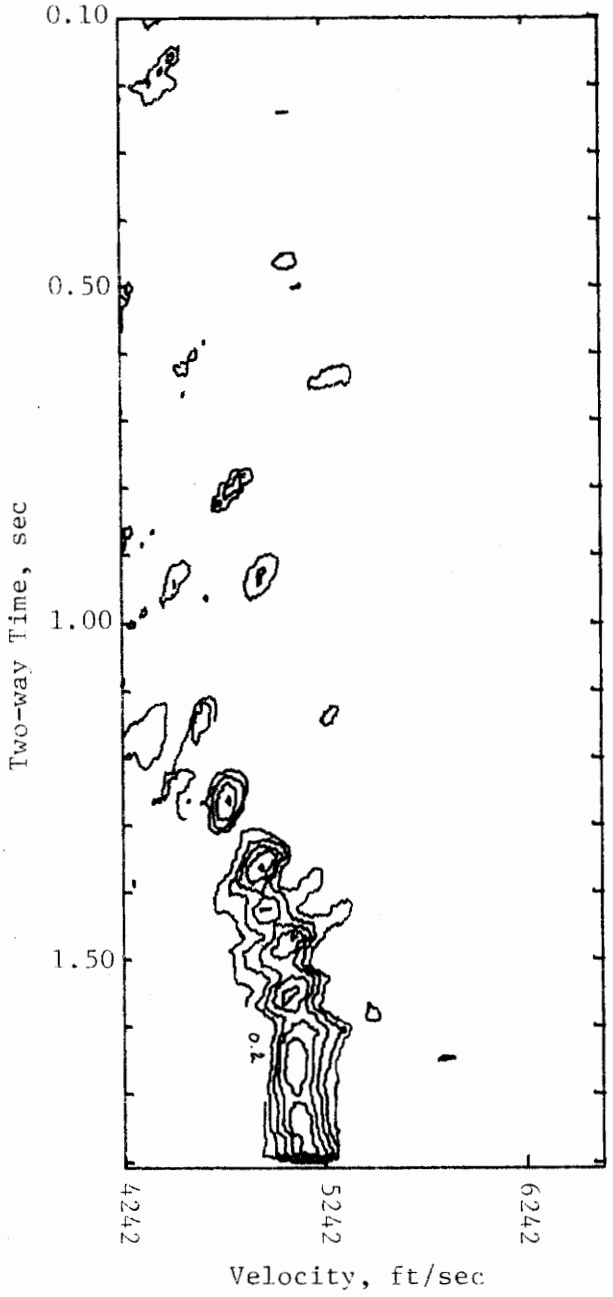

Figure 7.6-3f. Velocity Analysis of SV Component Data Anisotropy = 1.00: <3000 & >4000 ft and 1.10 from 3000-4000 ft, Window Width = 50 ms, Scan Increments = 20 ms and 53 ft/sec, Anisotropy Scan Level = 1.05

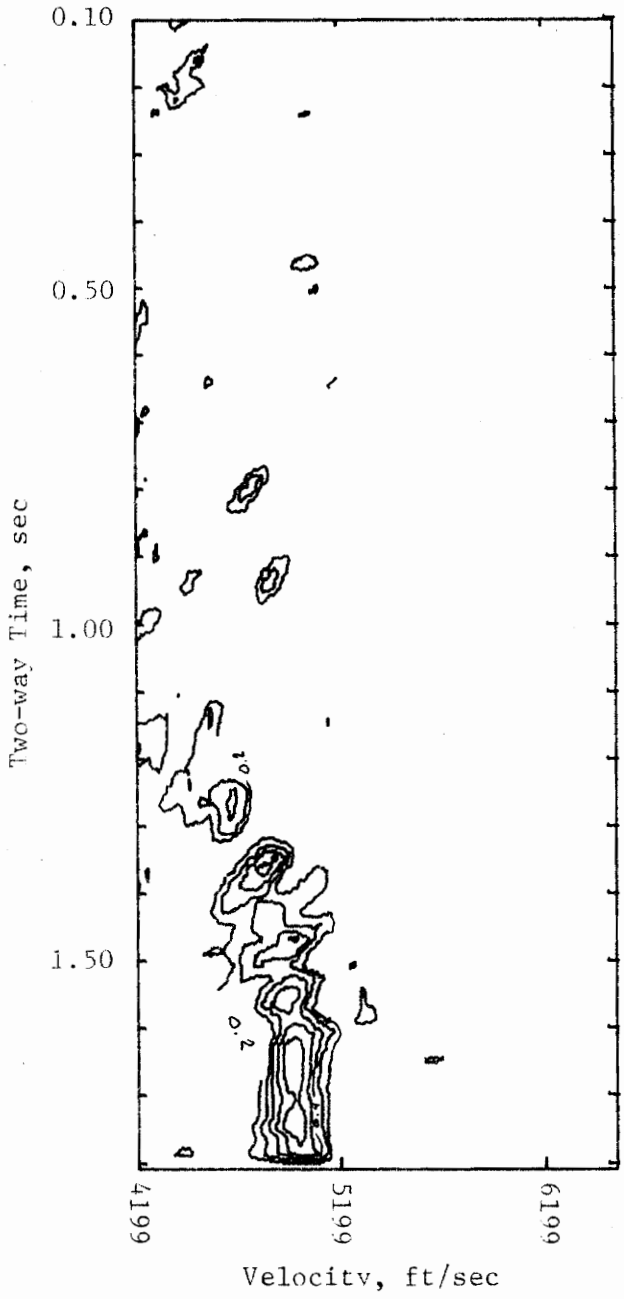

Figure 7.6-3g. Velocity Analysis of SV Component
Data Anisotropy = 1.00: <3000 & >4000 ft and 1.10
from 3000-4000 ft, Window Width = 50 ms,
Scan Increments = 20 ms and 52 ft/sec,
Anisotropy Scan Level = 1.06

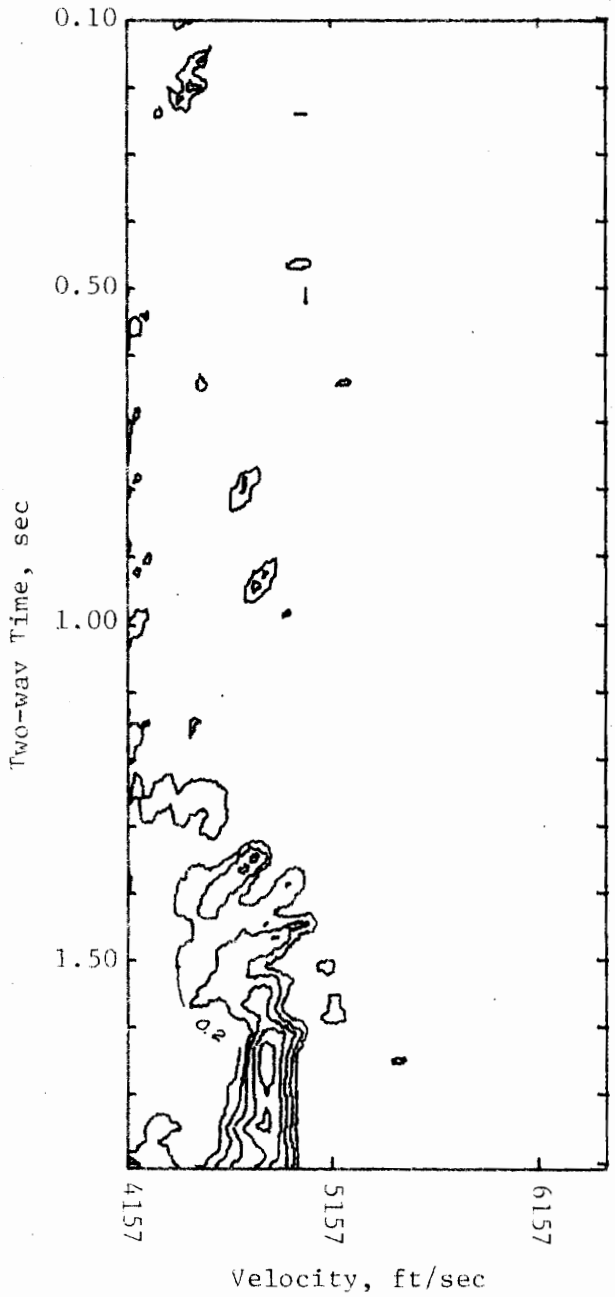

Figure 7.6-3h. Velocity Analysis of SV Component Data Anisotropy = 1.00: <3000 & >4000 ft and 1.10 from 3000-4000 ft, Window Width = 50 ms, Scan Increments = 20 ms and 51 ft/sec, Anisotropy Scan Level = 1.07

gration technique discussed earlier. However, for reflection times (SV) in excess of 1.15 sec, it is possible to detect the presence of anisotropy, but the correct magnitude of the anisotropy is not determinable with the anisotropic scan techniques developed in section 7.2 since the assumption of constant anisotropy is no longer true. For reference purposes, average anisotropy values were calculated for normal incidence reflections for the range of SV reflection times that spanned the anisotropic interval and for 0.250 sec beyond. These are simple arithmetic averages. The integration technique discussed in section 7.3 was modified for use in this situation in two ways. First, the integration was performed only over the semblance values for a particular scan time. Second, the integration was expanded to include the semblance values one scan interval in time above and below the time of interest. The hope was that one of these methods would yield the variation of the average anisotropy value. In fact, neither of these methods was adequate. However, the second method yielded somewhat less erratic, but still incorrect values of anisotropy. When these integrations failed, the semblance peaks were compared and the anisotropy factor was chosen on the basis of the highest semblance value. This proved to be more erratic than either integration method. Table 7.6-2 contains the results of the above analyses. Although it did not prove possible to perform a quantitative determination of the variation of anisotropy, considerable useful information was obtained. The first of the integration methods, while erratic, is useful for putting upper bounds to the anisotropy. At this point, the most reliable technique

Table 7.6-2. Anisotropic Interval

Results of Anisotropy Determination Tests

Two-way Time	Average Anisotropy Zero Offset	Anisotropy Semblance	Anisotropy Single Line Integration	Anisotropy Three Line Integration	Semblance A < 1.04
1.16	1.000	1.00	1.00	1.00	1.00
1.20	1.004	1.00	1.00	1.00	1.00
1.24	1.007	1.02	1.00	1.00	1.02
1.28	1.011	1.04	1.03	1.00	1.03
1.32	1.013	1.01	1.01	1.01	1.01
1.36	1.016	1.04	1.04	1.04	1.03
1.40	1.019	1.01	1.01	1.01	1.01
1.44	1.021	1.01	1.03	1.03	1.01
1.48	1.024	1.01	1.03	1.03	1.01
1.52	1.024	1.02	1.02	1.00	1.02
1.56	1.023	1.04	1.01	1.00	1.03
1.60	1.022	1.06	1.04	1.00	1.02
1.64	1.022	1.05	1.00	1.00	1.03
1.68	1.021	1.05	1.00	1.01	1.03
1.72	1.020	1.06	1.02	1.01	1.03
1.76	1.020	1.04	1.00	1.00	1.03

for determining the average anisotropy variation is strictly qualitative. It is believed that an experienced observer could determine the anisotropy variation to a quite satisfactory degree. This may be illustrated by comparison of the various portions of Figure 7.6-3. The portion prior to 1.15 sec is isotropic. Although the integration method of section 7.3 is adequate to determine the anisotropy factor (A = 1.00) for this part of the record, the same result may be ascertained by visual comparison of Figure 7.6-3a with 7.6-3b,c,...,h. The semblance values decrease rapidly for all scan values greater than 1.00. When the anisotropic portion of the analysis (times greater than 1.15 sec) is compared, it becomes obvious by the general character of the semblance variations that the anisotropy variation must be confined to values less than 1.04. In part, this limit to less than 1.04 is due to the magnitudes of semblance values and part is comparing the forms of the general envelope of the analyses. For scan values less than 1.04, the envelopes are all essentially the same. From 1.04 on, this envelope becomes distorted until the extremes shown in Figures 7.6-3g and 7.6-3h are reached. When anisotropy scan vlaues are limited to the range 1.00 to 1.03, the average anisotropy values specified by the semblance peaks come close to the correct values for the most part. These values are in the last column of Table 7.6-2. A simple smoothing of these values would appear to yield quite satisfactory results. The fundamental problem with the analysis of a section with varying anisotropy is that the velocity in a transversely isotropic medium is a

function of orientation with respect to the unique direction in the section. When a section is composed of intervals of differing anisotropy, then the variation of velocity with orientation for the entire section will not be properly measured by a velocity scan which is the arithmetic average of the anisotropy for the section. This may be understood by examining the mathematical form of the velocity (SV) in a transversely isotropic medium as given in equation 7.2-2. When reflections from known depths are analyzed, it is possible to assign average velocities for each reflection path. When we average two or more velocities, where some or all of them are anisotropic with differing degrees of anisotropy, the resultant average velocity is still a function of the direction of propagation, but the mathematical description of transverse isotropy is no longer valid. The velocity scan process in calculating velocities, in effect, averages the elastic constants rather than the interval velocities. The two averaging processes are not equivalent. This becomes obvious when equation 7.2-2 is examined. The mathematical form of this equation is such that averaging elastic constants is not the same as averaging interval velocities, each of which individually conforms to this mathematical description. It does not appear that this problem is amenable to solution since it would be necessary to know the thicknesses of each interval and the anisotropy factor for each as well in order to average velocities. This is impractical as it presupposes knowledge of just the information being sought. The end result for this case is that it is possible to deter-

mine if anisotropy is present, but is not a simple matter to determine just how much anisotropy is present.

7.7 Dipping Interfaces

Models with dipping interfaces are studied to demonstrate the effects of dip on a velocity analysis when the assumption of flat layering is violated. The mathematical description of the velocity functions used in the study of the effects of dip are described in section 5.3.5. The reflector geometry for the two models studied is shown in Figure 5.3-4. Dip varies continuously with depth for the polar velocity model but varies only at discrete intervals for the constant velocity dipping layer model (See section 5.3.5). The forms of velocity variation represented by these models may be considered as idealized forms of several structures of geological interest such as deltaic deposits, offshore marine shelf deposits, and the limbs of anticlines or synclines. In particular, the geometry approximates some areas of offshore Texas very well.

While the velocities for the polar velocity model are isotropic at any particular point, horizontal as well as vertical velocity gradients do exist. The purpose of this model is to demonstrate the effects of this particular kind of directional dependence of velocity, as opposed to anisotropy, on a velocity analysis. The constant velocity dipping layer model acts as a reference since this model does not possess horizontal velocity gradients. For compatibility with earlier models studied, the compressional velocity at the surface is 8000 ft/sec for each of these models. For the polar velocity model, the velocity along the reflector dipping 15 degrees, for example, increases

by 613 ft/sec over a distance of 5280 ft along the reflector. The corresponding velocity variation along the 25 degree dip reflector is 1702 ft/sec.

7.7.1 Effects of Variation of Model Parameters on Velocity Analysis

Data Characteristics

Standard CDP data were generated for these models. All shotpoint-geophone distances are multiples of 440 feet. The maximum distance is 5280 feet. The same reflection coefficients used with the other models were used here. The seismic traces for the polar velocity model and for the constant velocity dipping layer model are shown in Figures 7.7-1 and 7.7-2 respectively. Typical reflection paths are shown for each of these models in Figures 7.7-3 and 7.7-4. Reflections from interfaces with dips greater than 25 degrees do not return to the surface for the majority of traces. Only isotropic data were generated for these models.

Analysis Results

Velocity scans for both P and SV velocity components were performed on each set of data. Analysis results are shown in Figure 7.7-5 for the polar velocity model and in Figure 7.7-6 for the constant velocity dipping layer model. The velocity values corresponding to the semblance peaks for each separate velocity analysis were compared with the velocities calculated for reflections with zero offset from the shot location (normal incidence reflections). The effects of

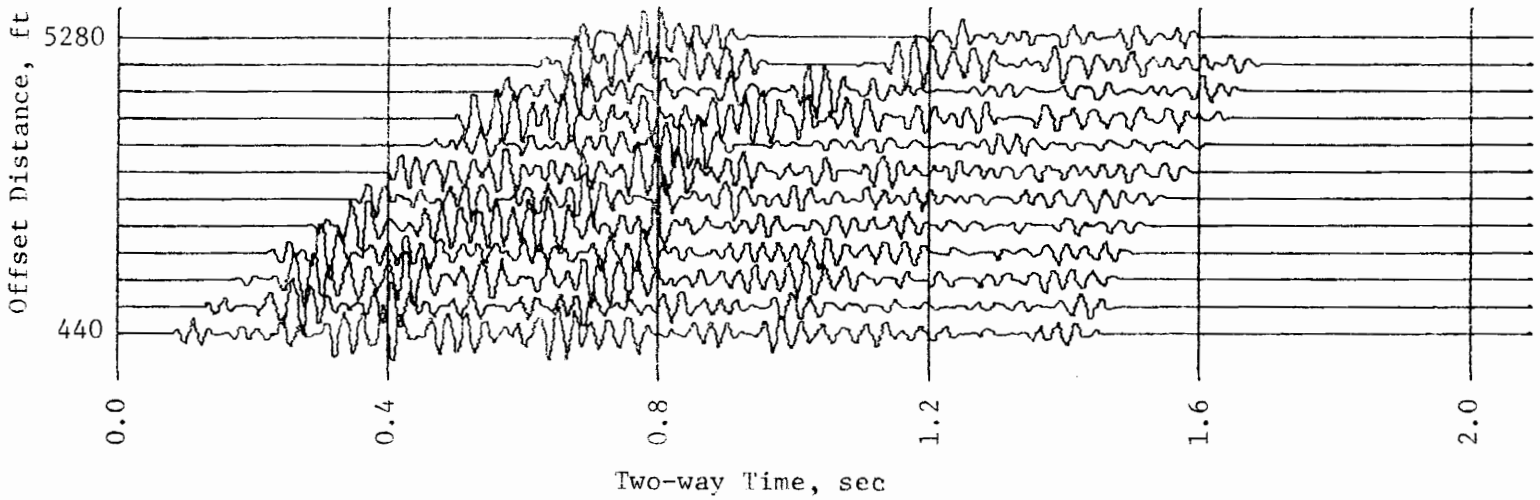

Figure 7.7-1. Dipping Interfaces
12-Fold Reflection Seismograms
Polar Velocity Model

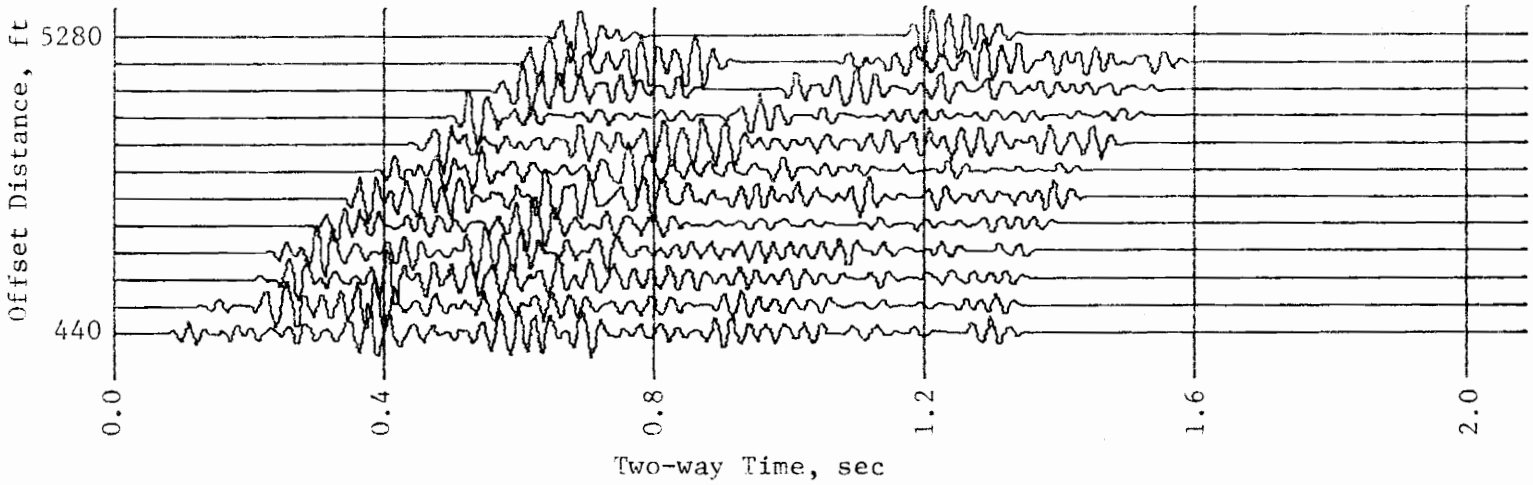

Figure 7.7-2. Dipping Interfaces
12-Fold Reflection Seismograms
Constant Velocity Layers

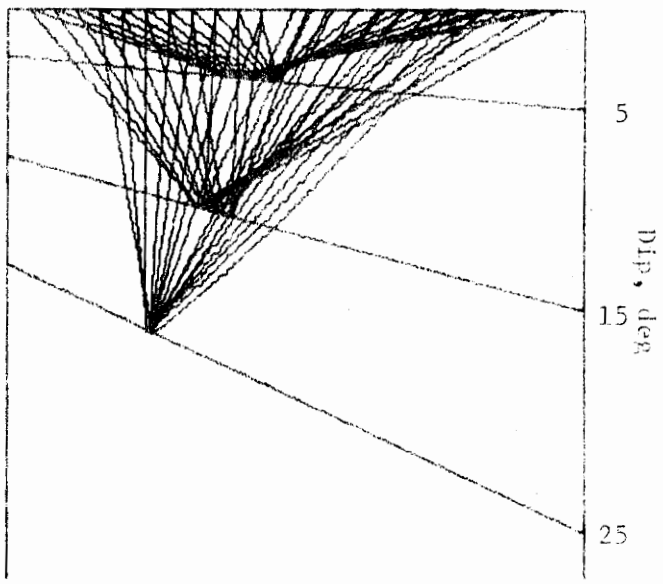

Figure 7.7-3. Polar Velocity Model
Typical Reflection Paths

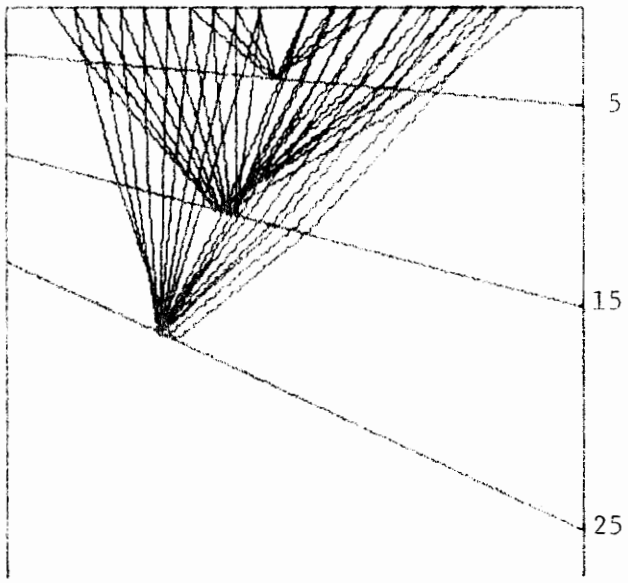

Figure 7.7-4. Constant Velocity Layers
Typical Reflection Paths

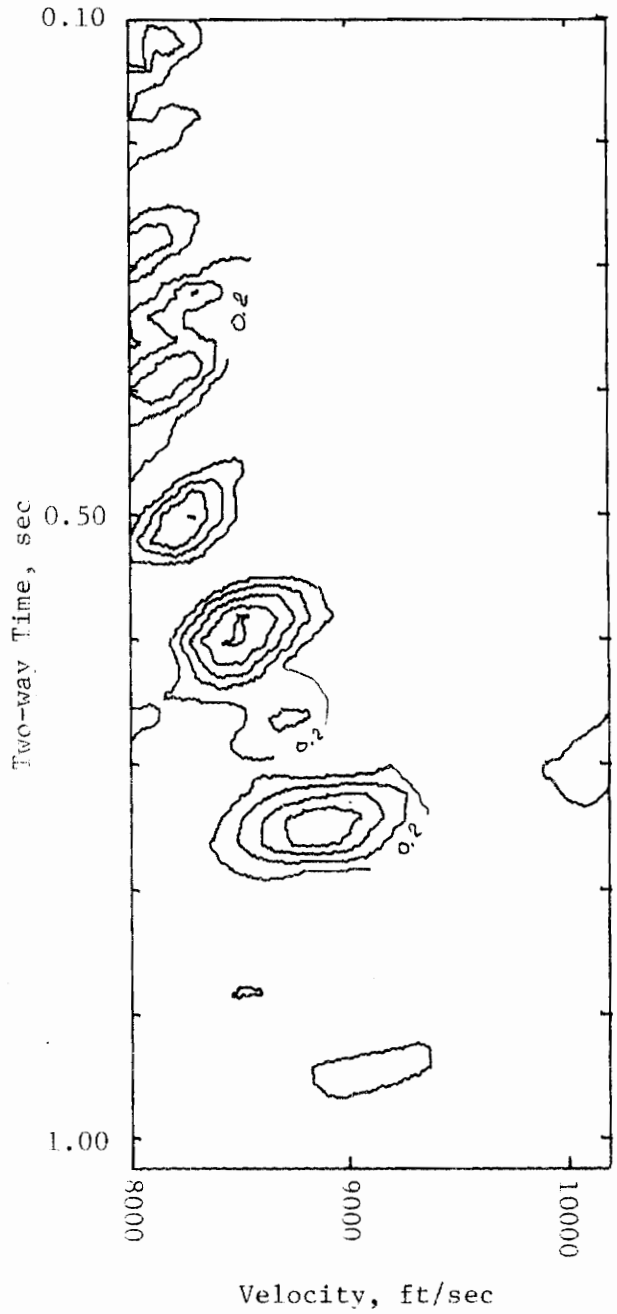

Figure 7.7-5a. Velocity Analysis of P Component
Polar Velocity Model
Data Anisotropy = 1.00, Window Width = 50 ms,
Scan Increments = 20 ms and 100 ft/sec,
Anisotropy Scan Level = 1.00

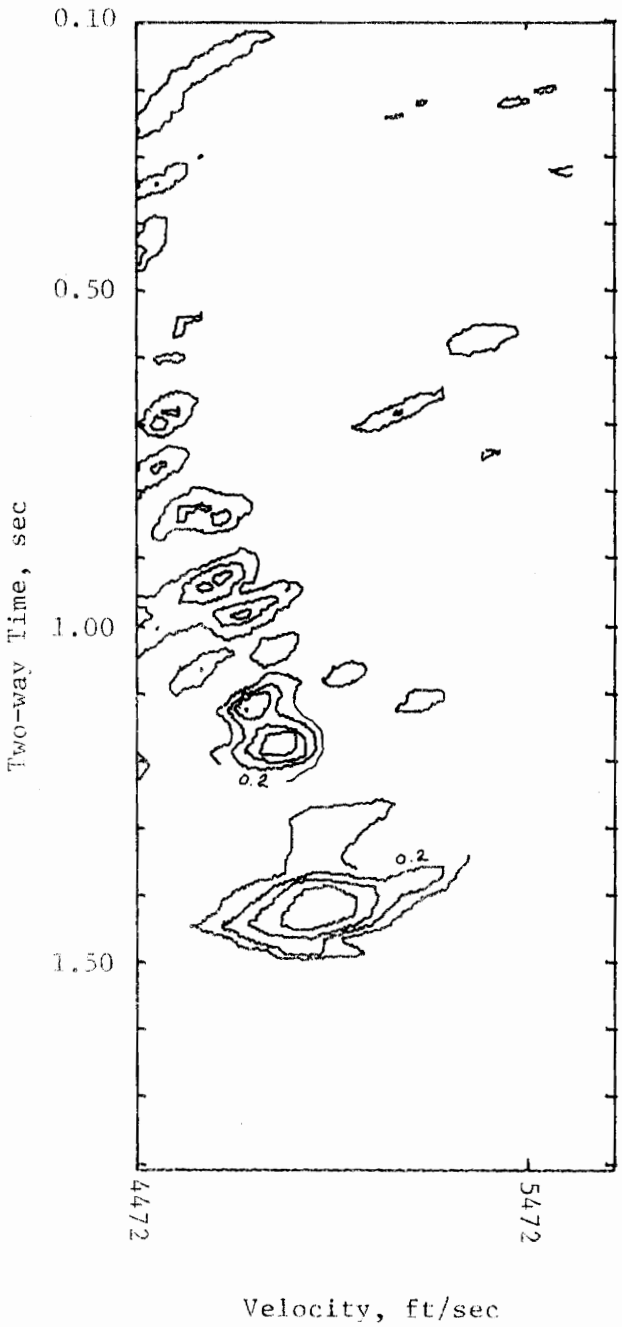

Figure 7.7-5b. Velocity Analysis of SV Component
Polar Velocity Model
Data Anisotropy = 1.00, Window Width = 50 ms,
Scan Increments = 20 ms and 55 ft/sec,
Anisotropy Scan Level = 1.00

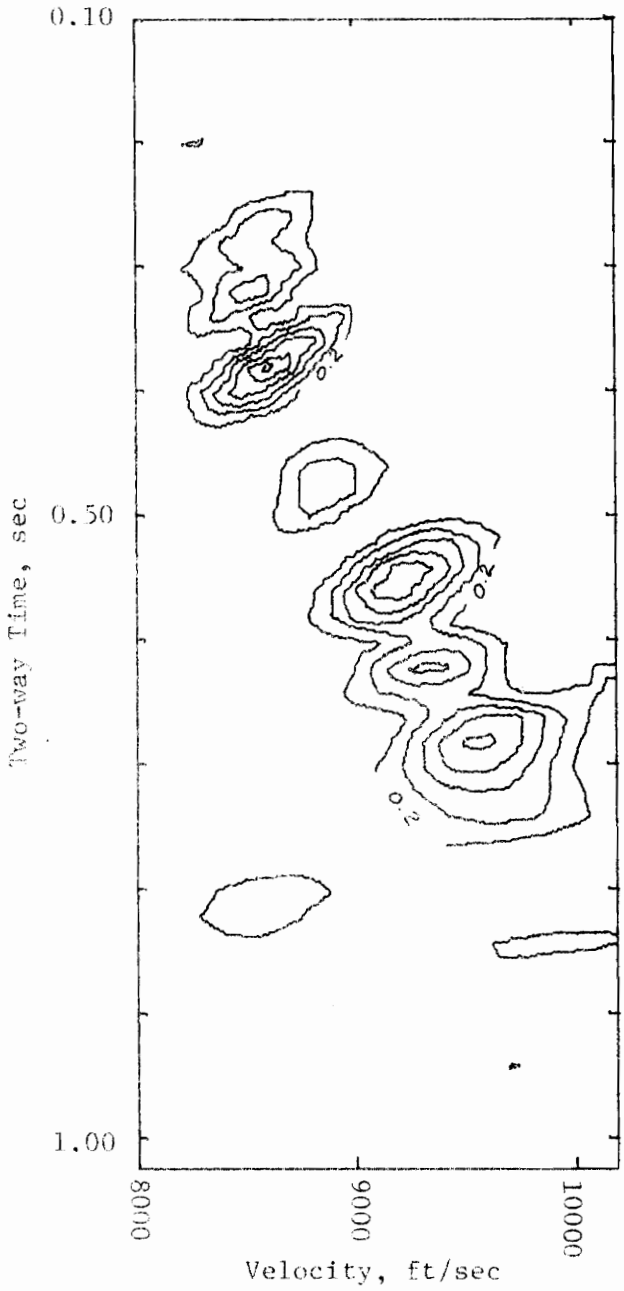

Figure 7.7-6a. Velocity Analysis of P Component
Constant Velocity Dipping Layers
Data Anisotropy = 1.00, Window Width = 50 ms,
Scan Increments = 20 ms and 100 ft/sec,
Anisotropy Scan Level = 1.00

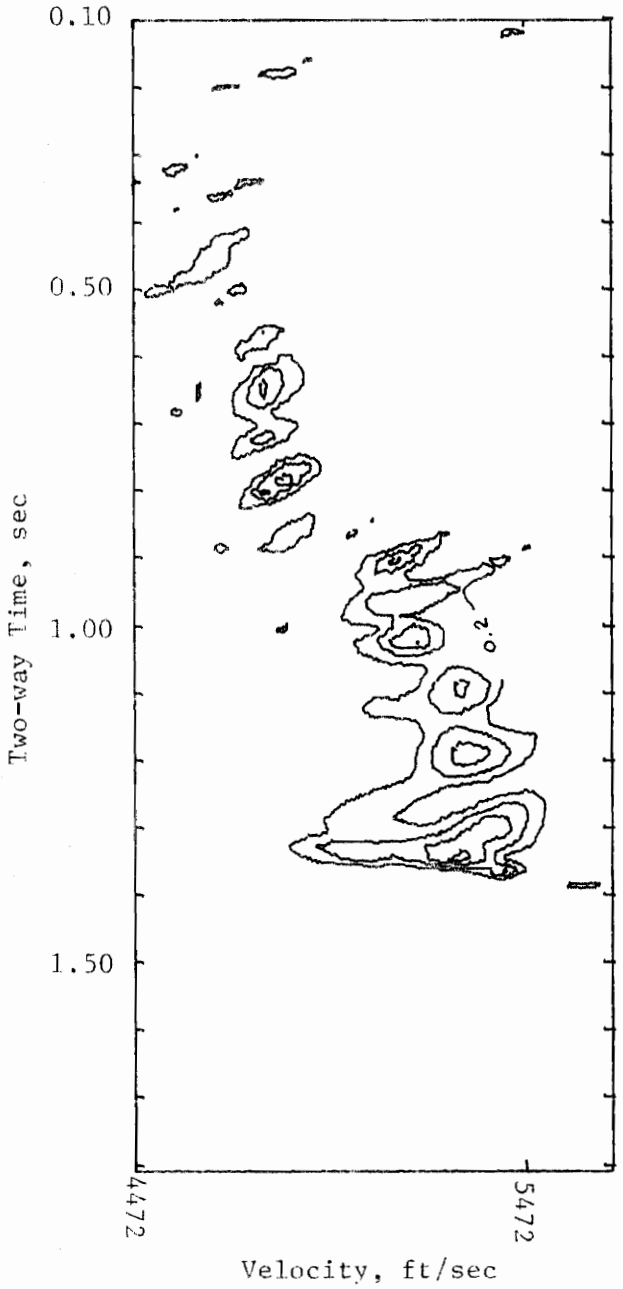

Figure 7.7-6b. Velocity Analysis of SV Component
Constant Velocity Dipping Layers
Data Anisotropy = 1.00, Window Width = 50 ms,
Scan Increments = 20 ms and 55 ft/sec,
Anisotropy Scan Level = 1.00

dip were identical for each model and for both P and SV. For all dips less than approximately 12 degrees, the results of the velocity analysis were correct to within less than one velocity scan interval. The velocity scan interval for the P component was 100 ft/sec and the corresponding interval for SV was 55 ft/sec. For dips greater than about 15 degrees, the rms velocities determined from the velocity analyses are in error by at least two velocity scan intervals. The apparent rms velocities determined by the velocity analyses were always greater than the actual velocities in the presence of dip. Finally, an unexpected and significant result of the analysis was that the horizontal velocity gradients of the polar velocity model did not affect the results of the velocity analysis for dips less than 12 degrees. This conclusion is supported by the fact that the correct rms velocities were recovered over the same range of dips. The most likely explanation for the horizontal velocity gradient of the polar velocity model not having any noticeable effect on the velocity analysis is that the CDP geometry employed has the effect, for a linear horizontal velocity gradient, of averaging the horizontal velocity over the reflection path. This average velocity corresponds to the velocity existing at the common-depth-plane. Since all traces share the same common-depth-plane, there is only one horizontal velocity associated with a given depth for any one plane. In this case, the horizontal velocity gradient would only become apparent when the data from a sequence of common-depth-planes were analyzed and compared.

7.8 Effects of Random Noise on Velocity Analysis

The velocity analyses performed on preceding models have all been on noise-free data. As could be expected, the presence of noise should act to degrade velocity analyses. A test was conducted to determine how much effect random noise has on velocity analysis. The conditions were quite limited in scope, but are believed to be far more severe than those normally encountered in the field. The data used were 12-fold CDP data of the kind discussed in previous sections. All shot-point-geophone distances were multiples of 440 feet with the maximum distance being 5280 feet. Different random noise was added to each trace. The amount of noise added to each trace was such that the rms amplitude of the noise was equal to the rms amplitude of the trace. The noise-free data are shown in Figure 7.8-1 and the noisy data in Figure 7.8-2. Velocity analyses were performed for both P and SV seismic components for each data set and thr results are shown in Figures 7.8-3 and 7.8-4. It is immediately obvious that this amount of noise severely degrades the results of velocity analysis. However, these analyses are not degraded to the point of being useless. The correct rms velocity functions are still determined, although there are fewer well defined semblance peaks. This test demonstrates the effects of large amounts of noise on velocity analysis. Lesser amounts of noise will of course cause less degradation to velocity analyses.

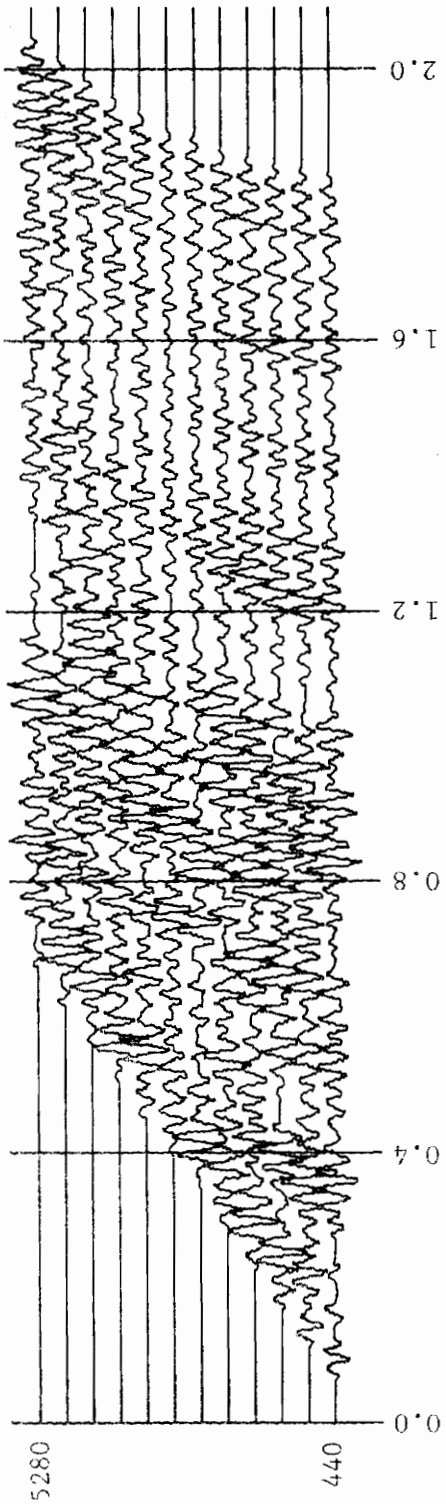

Figure 7.8-1. Noise-Free Traces
12-Fold Reflection Seismograms

Figure 7.8-2. High Noise Level Traces
12-Fold Reflection Seismograms

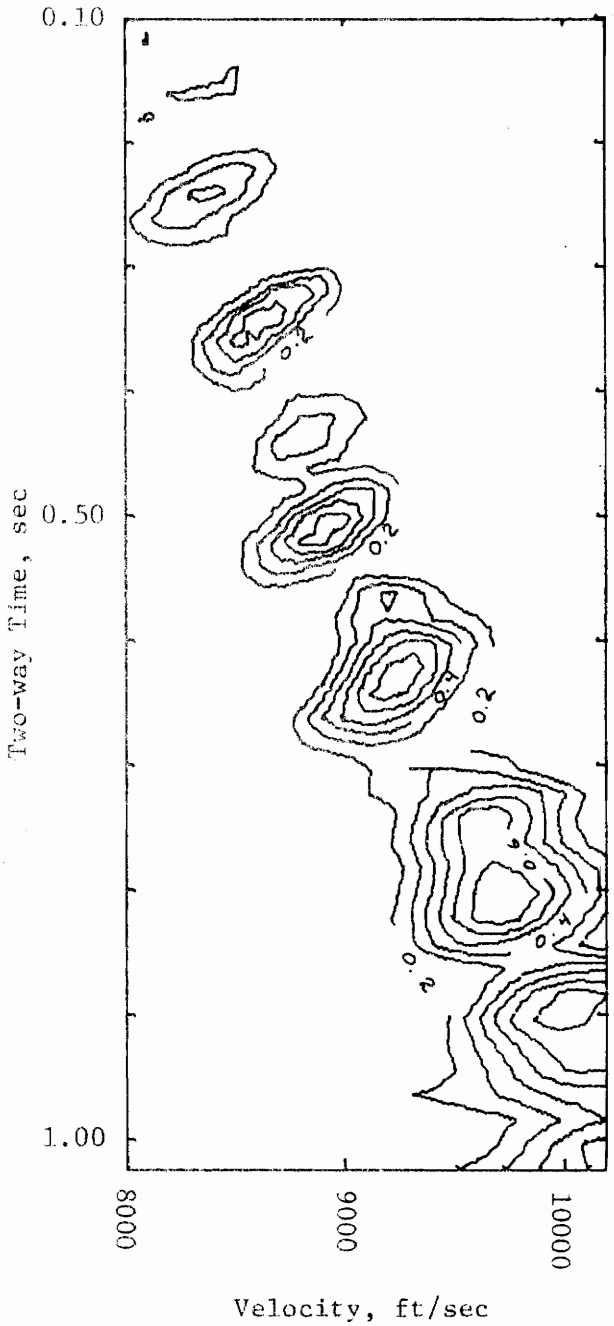

Figure 7.8-3a. Velocity Analysis of P Component
Scan Increments = 20 ms and 100 ft/sec,
Window Width = 50 ms

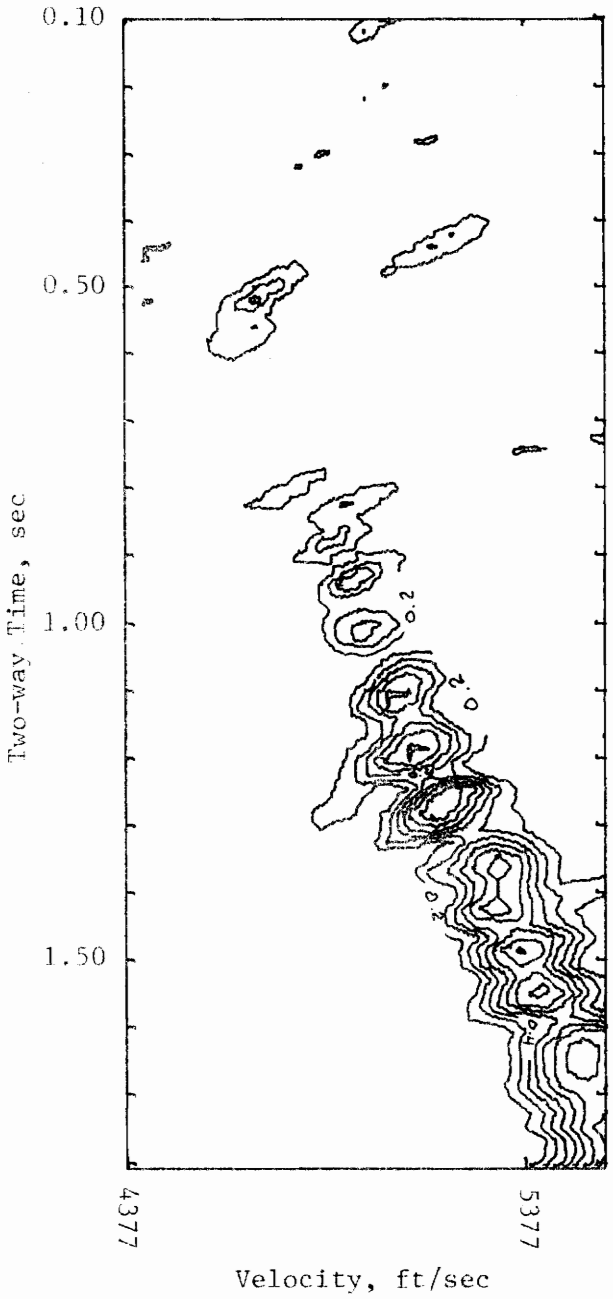

Figure 7.8-3b. Velocity Analysis of SV Component
Scan Increments = 20 ms and 54 ft/sec,
Window Width = 50 ms

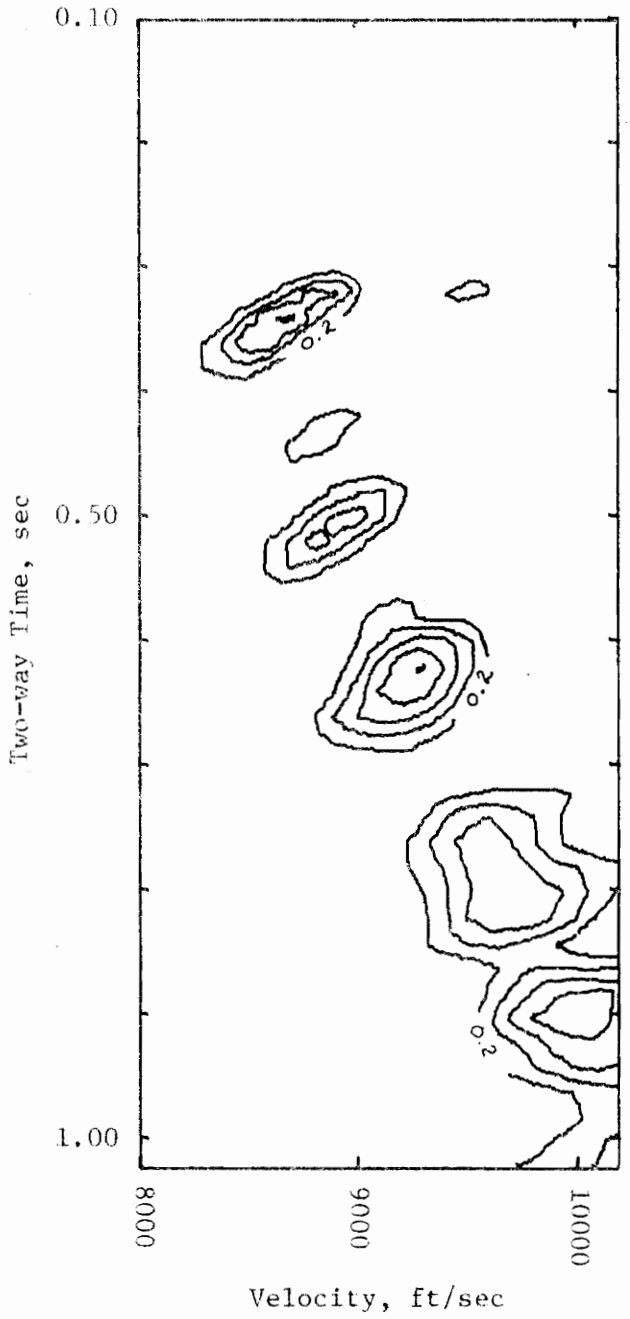

Figure 7.8-4a. Velocity Analysis of P Component
Scan Increments = 20 ms and 100 ft/sec,
Window Width = 50 ms

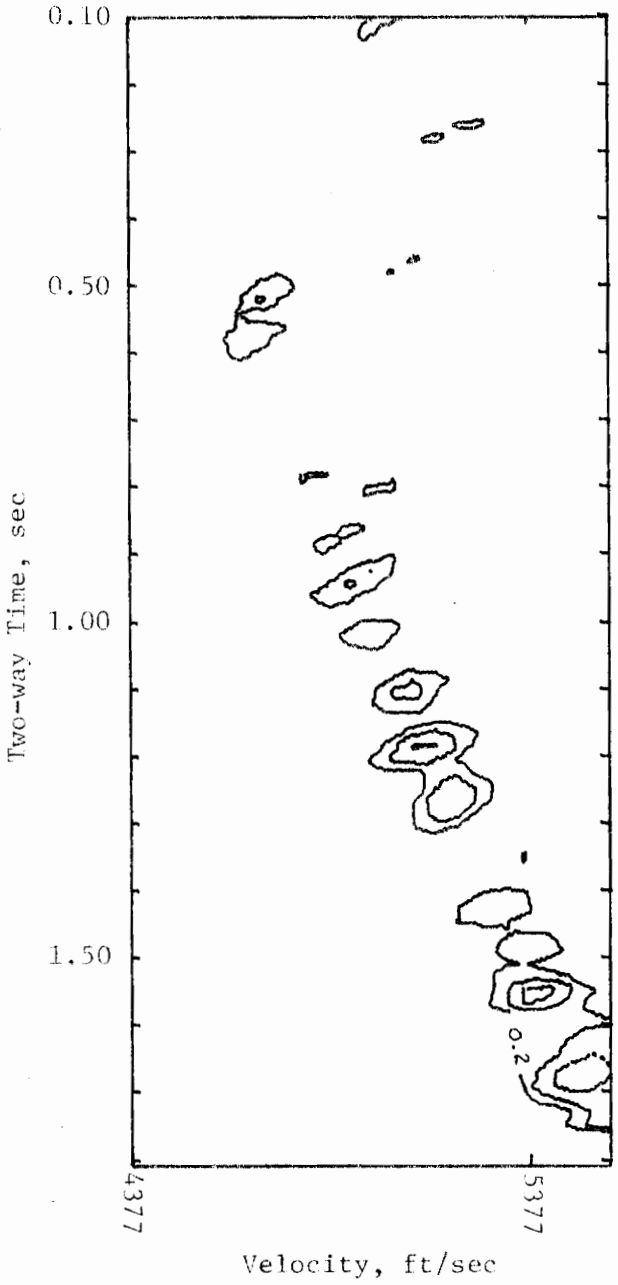

Figure 7.8-4b. Velocity Analysis of SV Component
Scan Increments = 20 ms and 54 ft/sec,
Window Width = 50 ms

8. Sensitivity of Velocity Scans for Anisotropy

The sensitivity of velocity analysis techniques for determining anisotropy will be discussed for two general cases. The first is that the entire stratigraphic section is uniformly anisotropic. The second considers the possibility that anisotropy may vary within the section. It is necessary to divide this discussion into two parts since the conclusions reached for the simpler position of uniform anisotropy will imply the potential resolving power for the more complex case of variable anisotropy.

Uniform Anisotropy

The problem of resolving anisotropy in a uniformly anisotropic section by the use of surface seismic data has been discussed in sections 7.3, 7.4, and 7.5. It is believed that these models are sufficiently general that the conclusions drawn may be extended beyond just the particular models studied. The velocity variation conforms to the range of velocities commonly observed in the field. The forms of velocity variation vs. depth used in these models may be said to characterize common types of velocity variations observed in field data.

The general results of this study are that in a uniformly anisotropic section the anisotropy factor may be readily determined. The accuracy with which the anisotropy may be determined depends upon the value of the anisotropy factor. For anisotropy factors within the range of about 1.00 to 1.02, the correct value may be determined to within about $\pm$ 0.01. For factors in the range of 1.03 to 1.05, the

accuracy is about $\pm$ 0.005. For values in excess of 1.05, there is virtually no uncertainty in the determination of anisotropy to the accuracy necessary for use in reflection seismic exploration.

Another important result of this study is the effect of the choice of seismic wave component on the analysis for anisotropy. It has been traditional in reflection seismic exploration to work with P wave data and to ignore shear wave components. However, one of the first conclusions of the anisotropy study was that P wave data are insensitive to anisotropy. The explanation for this is that the difference in normal moveout for different amounts of anisotropy is so small that it may be considered to be negligible. The SV wave component, on the other hand, is a sensitive tool for the detection of velocity anisotropy because SV normal moveout differs significantly for small differences in anisotropy. The discussion above concerning the accuracy with which the anisotropy factor could be determined is with reference to SV velocity analyses as the primary tool of anisotropy determination.

Varying Anisotropy

After studying the possibilities of resolving anisotropy in a uniformly anisotropic media, the next step is to study the problem of anisotropy resolution in sections where the anisotropy may vary. The model chosen for this test was discussed in section 7.6. This model is more realistic than a model with a uniform level of anisotropy throughout. The P wave component exhibited the same lack of sensitivity to anisotropy as in the uniformly anisotropic study. The SV component

remained quite sensitive to the presence of anisotropy. However, the results for SV were not the same as for the uniform anisotropy case. although it was possible to detect the presence of anisotropy, it was not possible to correctly determine the amount of anisotropy actually present by strictly quantitative methods. A visual examination of the various anisotropy scans appears to yield satisfactory results for the model studied. If an arithmetic average of the anisotropy in the section is performed, the velocity analysis results for that level of anisotropy are correct and do yield the correct rms velocities. Table 7.6-2 contains the results of the analyses performed together with the average anisotropy. The problem lies in the determination of which anisotropic velocity scan is the correct one. As discussed in section 7.6, this can be traced back to the type of velocity averaging that occurs physically and the manner in which velocities are calculated in the velocity scanning process. The velocity scan moveout calculations implicitly assume a condition of uniform anisotropy. When energy is reflected in such a composite medium, the averaging process yields velocities with a different directional variation than a simple averaging of the anisotropy factor would indicate. Presently, there does not appear to be any way to avoid this problem. Although the anisotropy factor resulting from the analysis of such a composite section is itself incorrect, it does place an upper limit on the actual anisotropy factor since the calculated factor is higher than the true value.

A short demonstration of the sensitivity of the velocity analysis

process in the presence of noise was given in section 7.8. This test consisted of adding random noise to a set of 12-fold traces such that the rms level of the noise added to each trace was equal to the rms level of the noise-free trace. This is regarded as a rather severe test that would far exceed the amount of random noise normally observed in the field. The results of this test were that it was still possible to correctly determine the P and SV velocities for the noisy data.

9. Recommendations for Field Tests

Field tests of the anisotropic velocity scan techniques developed herein should be performed to verify the conclusions reached through digital modelling of idealized anisotropic structures. Such a program should include a variety of locations and should progress from the stage of carefully controlled field conditions to the more general kind of field conditions normally encountered by a field party.

The first consideration of such a program must center about the location where tests are to be conducted. The location should, first of all, be on land rather than offshore for several reasons. The most important single reason centers about the role that shear waves play in an anisotropic velocity analysis. Shear waves do not propagate through water and therefore a marine location does not have any value. Tests should be conducted either in areas that have been previously determined to contain anisotropic formations or in areas where formations similar to those reported elsewhere as anisotropic exist. This latter situation is not as desirable of course since the question arises as to how much anisotropy really exists at such a location. In any event, the amount of anisotropy existing at a given location must be independently verified. Some of the techniques discussed in chapter 2 could be used for the purpose of verification. The well-geophone technique is recommended for this purpose since it allows for direct measurement within the actual formations under consideration. A continuous velocity log should be obtained over the length of the bore-hole in order

to provide a precise knowledge of the vertical distribution of velocity. The bore-hole should be logged for the shear velocity (SV) distribution as well as for the compressional (P) velocity. The geologic section should be composed ideally of non-dipping strata possessing uniform physical properties over a wide geographical area. This is to minimize any disturbing effects that might tend to lower confidence in the validity of the results. Upon completion of this initial phase of testing, conditions may be gradually relaxed to the point of normal field operations.

The manner in which data are recorded for anisotropy experiments is important. The principal point to be made is that both P and SV should ideally be recorded separately. In practice, this implies that individual horizontal and vertical geophones recorded on separate channels must be used in the field. While both shear and compressional waves possess both horizontal and vertical components, it is usually safe to assume for reflection seismology that compressionaal wave motion will be primarily vertical and shear wave motion will be primarily vertical and shear wave motion will be primarily horizontal. Total motion geophones would be far simpler to use in the field, but the resulting superposition of P and SV has the effect of degrading the results of subsequent velocity analyses. For a compressional velocity analysis, the SV information acts like noise to degrade the results of the analysis. The same situation, of course, holds for an SV analysis where P information is also present. This is illustrated by two an-

alyses of the data shown in Figure 9-1. The seismic traces shown here contain both P and SV. The seismic wavelet used for SV is twice the length of the P wavelet and the frequency content is such that the spectral peaks are at frequencies one half the values for the P wavelet. A velocity analysis over the seismic P component without any SV present on the traces is shown in Figure 9-2. This analysis will serve as a reference so that comparison may be made with later analyses performed on data for which both P and SV are present. A velocity analysis of the data in Figure 9-1 is shown in Figure 9-3. The location of the semblance peaks is identical in both Figures 9-2 and 9-3. However, the magnitudes of these peaks differ considerably when these figures are compared. The effect on the semblance peak at 0.65 sec, for example, is typical of the entire analysis. In the analysis of P without SV present, the peak value is greater than 0.8. When SV is present, the peak value decreases to just over 0.5. Similar degradation of semblance values occurs for the remainder of the analysis. One additional comparison of P plus SV will be made. Figure 9-4 shows the seismic traces to be analyzed. Both P and SV are present and the wavelet discussed in section 5.4 was used for both velocity components. The analysis of this data is shown in Figure 9-5. When Figures 9-2 and 9-5 are compared, it is immediately obvious that the semblance values are far less severely degraded when P and SV have identical spectral characteristics. One important possibility suggested by this lesser degrading of the velocity analysis when P and SV have the identical

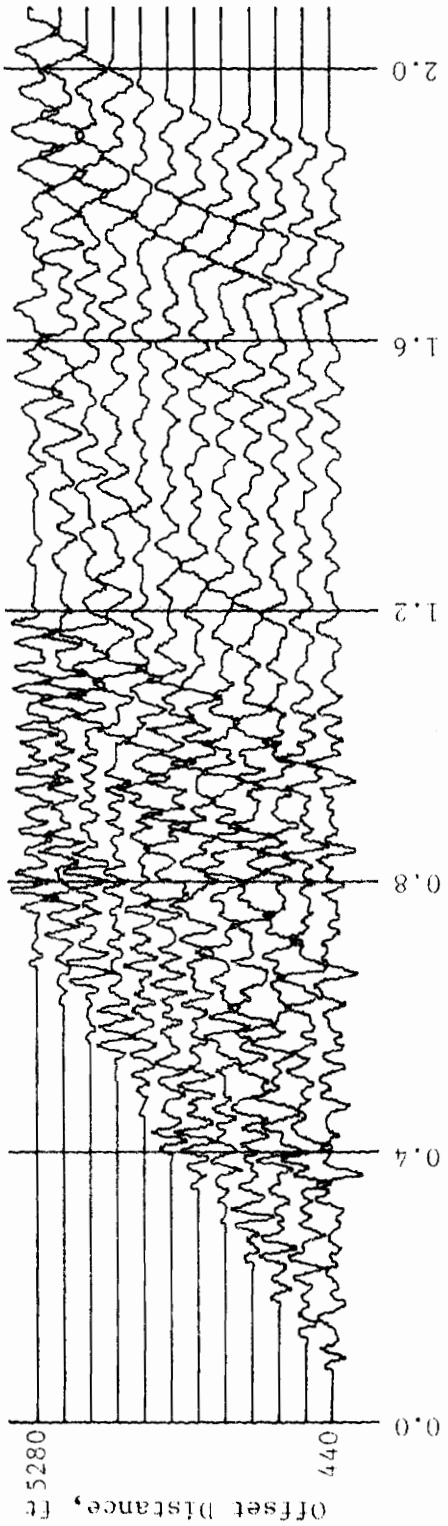

Figure 9-1. Field Test Program
12-Fold Reflection Seismograms
Different P & SV Wavelets

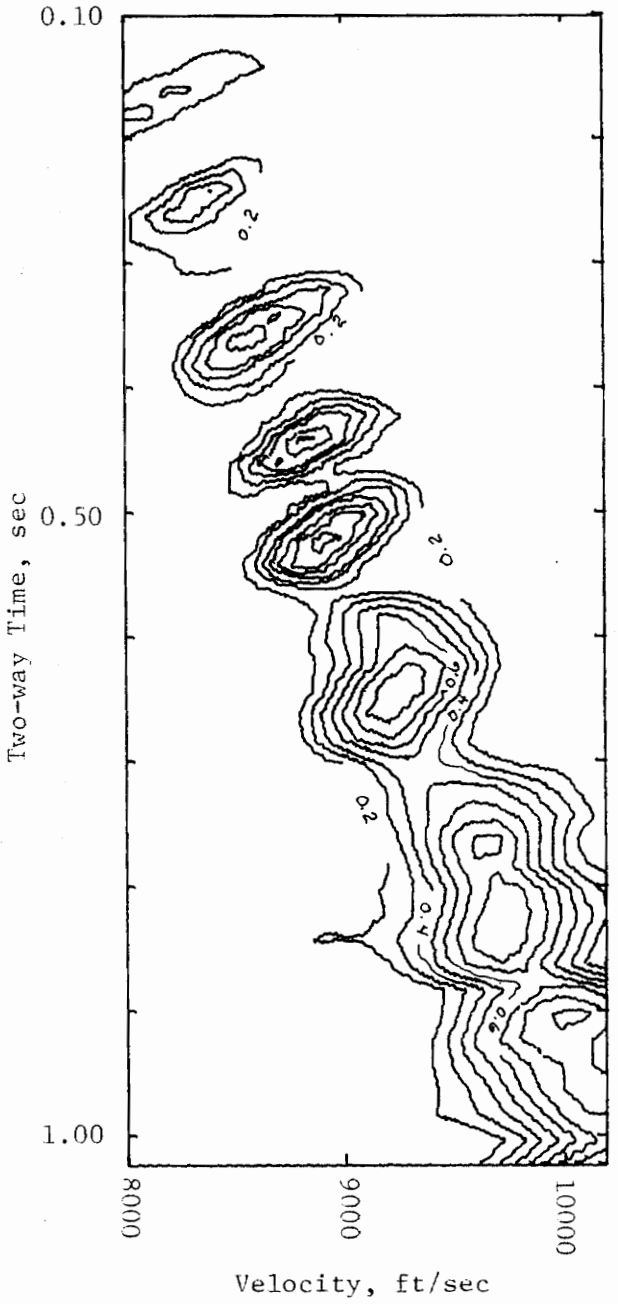

Figure 9-2. Velocity Analysis of P Component
Data Anisotropy = 1.043, Window Width = 50 ms,
Scan Increments = 20 ms and 100 ft/sec,
Anisotropy Scan Level = 1.04
P Component Only Present

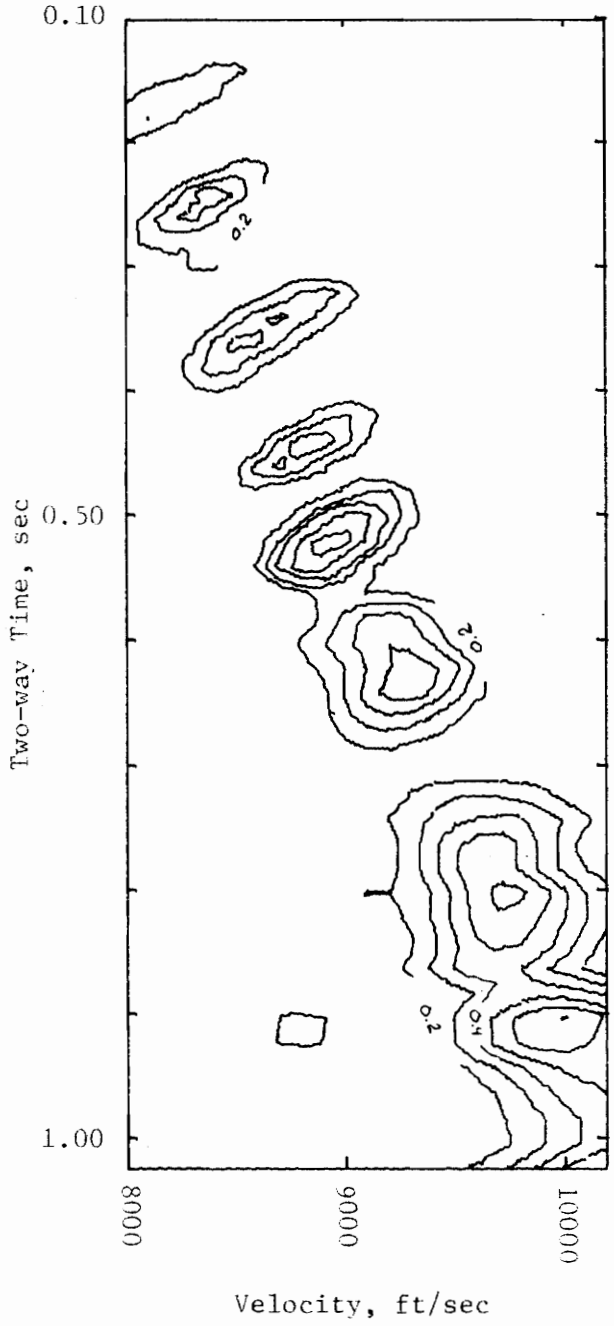

Figure 9-3. Velocity Analysis of P Component
Data Anisotropy = 1.043, Window Width = 50 ms,
Scan Increments = 20 ms and 100 ft/sec,
Anisotropy Scan Level = 1.04
P & SV Present, Different Wavelets

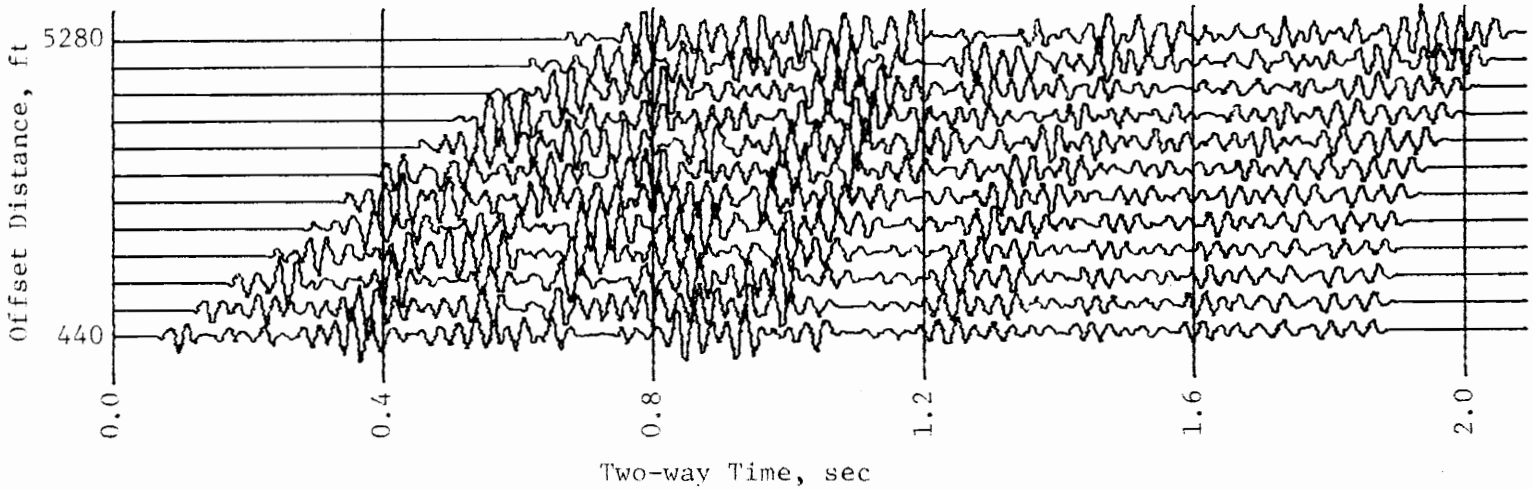

Figure 9-4. Field Test Program
12-Fold Reflection Seismograms
Identical P & SV Wavelets

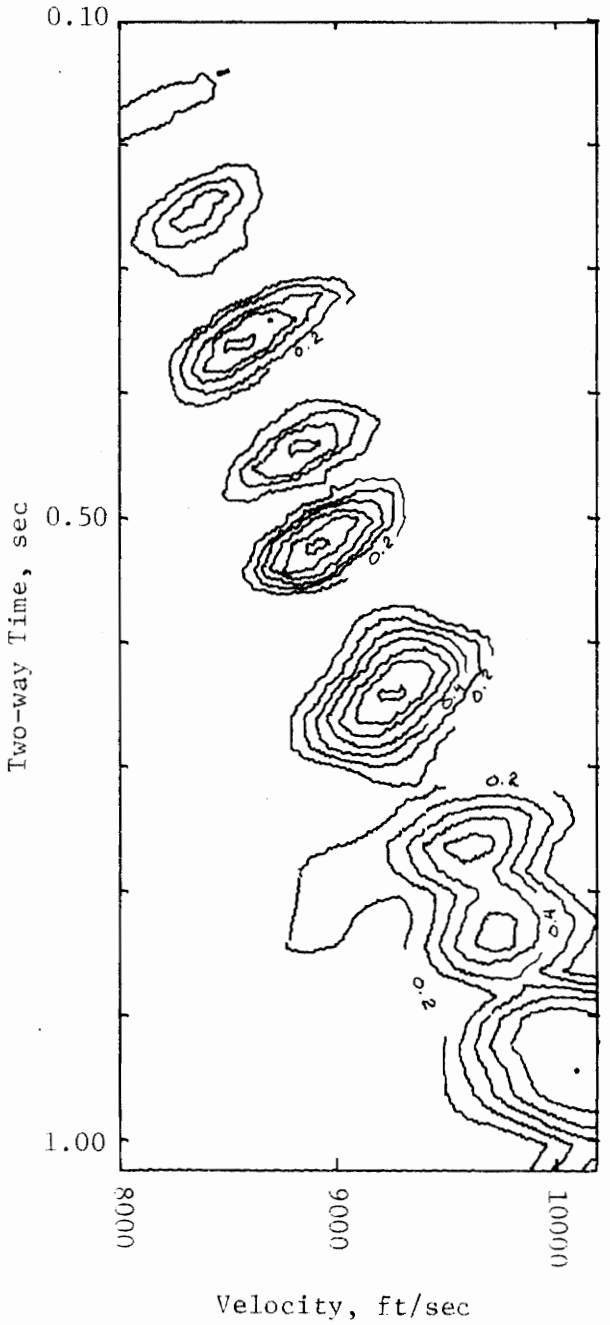

Figure 9-5. Velocity Analysis of P Component
Data Anisotropy = 1.043, Window Width = 50 ms,
Scan Increments = 20 ms and 100 ft/sec,
Anisotropy Scan Level = 1.04
P & SV Present, Identical Wavelets

spectral characteristics, is the design of field methods where P and SV will in practice have the same spectral content. This is not as feasible with explosive sources because of the greater attenuation of high frequency shear energy, but is quite possible when a source of the Vibroseis type is used for generating SV, since the possible spectrum of the signal is variable over a wide range. This would be of economic significance because of the simplification of data processing by eliminating half of the geophones needed to record each component separately. Whenever P and SV do not have the same spectrum, the amount that the velocity analyses are degraded would argue against recording both signals on the same channel and the earlier comments regarding separate recording of P and SV would apply. The synthetic data of this study are noise-free so that field data contaminated by other forms of noise should be even more suscepible to velocity analsis degradation when P and SV are recorded together. Therefore, the considerations regarding the mixing or non-mixing of the P and SV signals becomes of some importance for the field-testing program.

In summary, recommendations are made for field testing techniques for the determination of subsurface velocity in an anisotropic medium by the use of surface seismic reflection data. Testing should be conducted on land rather than in a marine environment and should be located in an area of known anisotropy. Continuous velocity log data are necessary for control purposes. The ideal test location would be in an area of non-dipping strata which is uniform in its properties over an

extensive geographical area. The location where Jolly (1956) performed his experiments would be such an ideal test site. Finally, shear and compressional data could be recorded separately on horizontal and vertical geophones to avoid each acting as noise in the analysis of the other or on a single channel in the case where each component possesses nearly identical spectra.

10. Summary and Conclusions

The fundamental purpose of this study was to evaluate the feasibility of determining the subsurface velocity in anisotropic media by using surface seismic reflection techniques. A practical reason for undertaking such a study is that many investigators have looked for the occurrence of velocity anisotropy in the field and in all instances it has been found to varying degrees. All available evidence points to the fact that velocity anisotropy is widespread and thus worthy of detailed consideration. Vander Stoep (1966) in particular showed that for the long shotpoint-geophone offsets in common use today even small amounts of anisotropy cause significant deviations in traveltime from the usual hyperbolic traveltime relation. The traveltime deviations due to the effects of anisotropy are especially important when we consider that it is the outer traces, where these effects are greatest, that yield the most information concerning velocity at intermediate and deeper depths.

It is of interest that of the two simplest anisotropic models, elliptical anisotropy, which is intuitively the more "natural" approach, is not physically possible from theory and from a practical point of view it also has the least utility. Transverse isotropy is a more sophisticated model which requires a knowledge of the shear as well as the compressional characteristics of the transmitting medium. Elliptical anisotropy has been used for many years in anisotropy studies because it arises mathematically from a simple extension of the old and

familiar hyperbolic traveltime equation. The transverse isotropy model, on the other hand, does not follow from the isotropic model, but comes instead from a re-examination of the effects of transverse isotropy on the elastic constants of the transmitting medium. The reason for the simplicity of the elliptical model is that it implicitly assumes that the characteristics of the medium are adequately described by the compressional velocities normal and parallel to the bedding. Theoretically, the velocity characteristics (compressional or shear) for any anisotropic medium depend on combinations of elastic coefficients that are far more complex than in the isotropic case.

An important objective of this work was to determine if it would be possible to detect the presence of anisotropic strata by the analysis of surface data alone. When the model of elliptical anisotropy is used, it can be shown (Dix, 1955) that it is impossible to detect the presence of anisotropy using only surface data. Using this model, it is always necessary to have some form of vertical (well) control if anisotropy is to be detected. Even where well control is available, anisotropy cannot be detected at depths below the deepest extent of the well. On the other hand, the theory of transverse isotropy predicts that the parameters of an anisotropic medium should be recoverable from surface data alone without the necessity of well control.

A constant value of Poisson's ratio of 0.283 was used for all of the synthetic modelling in this study. This value is the same as that used by Postma (1955) in his Case I. Birch (1966) has tabulated values

of Poisson's ratio for sedimentary rocks. The majority of rocks listed fell within the range of 0.25 to 0.35. Limestones and sandstones in particular had ranges of 0.25 to 0.34 and 0.17 to 0.29 respectively. The use of a constant value of Poisson's ratio is not necessarily detrimental since the seismic energy propagating through a section at any instant sees an averaged value over a distance of one wavelength and existing variations tend, in effect, to be smoothed. For a Poisson's ratio of 0.30, the ratio of the shear to the compressional velocity is 0.535. This velocity ratio is 0.580 and 0.480 for Poisson's ratios of 0.25 and 0.35 respectively. The overall range of variation of the shear-compressional velocity ratio is about 20 percent for Poisson's ratio in the range from 0.25 to 0.35.

A seismic ray tracing technique was developed for the generation of two-way reflection times for use in digital modelling. The technique was developed for the two dimensional transversely isotropic case, but could easily be extended to handle the general three dimensional case. This method allows for continuous as well as discrete velocity variation models. In addition, the technique used allows complete flexibility in the variation of both vertical and lateral velocity distributions. The practical effect of this is to allow for the modelling of extremely complex geological situations.

The velocity scan (velocity analysis) process was mathematically developed in detail, first for the isotropic case, and then for the case of transversely isotropic media. The velocity analysis techniques

were used to analyze a variety of synthetic data for the purpose of determining the possibilities of resolving the amount of anisotropy, and thus the correct vertical velocity distribution, in the various models. For models that were uniformly anisotropic, it was possible to identify correctly the degree of anisotropy and to recover the correct velocity distribution for these models. A velocity analysis was judged to be successful if it could recover the correct rms velocities to within one velocity scan interval (100 ft/sec for P). The criteria for judgment was the comparison of rms velocities for a so-called zero offset trace with the values defined by the semblance peaks on the velocity analysis. The zero offset data were calculated for each model at the same time that arrival times were calculated for the other traces. The major peaks on the velocity analyses were compared to the appropriate zero offset rms velocities and were found to agree within one velocity scan interval. An unexpected outcome of this study was that P wave velocity analysis is insensitive to anisotropy and is in fact useless for the purpose of determination of anisotropy. SV velocity analysis, on the other hand, is extremely sensitive to anisotropy.

When studies were made of varying anisotropy in a model, the results were not as conclusive as for the case of uniform anisotropy. The same results hold for P as in the uniform case, but this is not true for SV. For the situation of variable anisotropy, it was possible, using SV, to detect the presence of anisotropy quite readily. However, unlike the uniform case, it was impossible to specify the

actual anisotropy factor. The apparent anisotropy factors resulting from such an analysis are always greater than the actual anisotropy factors which does set limiting values to the amount of anisotropy that can be present. Although it is not possible to determine the exact degree of anisotropy present, it is important to recognize the presence of anisotropic strata. The importance of this capability lies in the fact that this technique may provide a means of stratigraphic correlation from location to location for strata that do not possess other distinguishing characteristics.

The study of the effects of dip on velocity analysis produced two results. The first was that dips up to about 12 degrees do not significantly degrade the results of velocity analysis. Secondly, horizontal velocity gradients do not noticeably affect the velocity analysis.

The theory derived in section 7.2 describing reflection times indicated that a velocity analysis of either P or SV for a transversely isotropic medium should yield the identical horizontal and vertical velocity components for both P and SV. This is, of course, not true for the isotropic case since P and SV each consist of only a single velocity component. However, the velocity analyses of the models discussed in chapter 7 demonstrated that it is not possible to make practical use of the redundancy of information contained in the P and SV wave components since only the SV component is sensitive to velocity anisotropy.

It is recommended that land data be recorded in such a manner as

to include SV as well as P energy. Presently, geophones are used which are sensitive only to the vertical component of motion. The effect of this is to discriminate against horizontal shear energy since the plane of vibration would be essentially at right angles to the direction of sensitivity of the geophones. Either a second set of geophones should be used to record SV, or geophones sensitive to any motion in a vertical plane may be used for recording P and SV on the same channel. However, P and SV should only be recorded on the same channel if they possess nearly identical spectral characteristics. Otherwise, each component should be recorded on separate channels to prevent either component from significantly degrading the velocity analysis of the other component. Either total motion geophones or horizontal geophones with their direction of horizontal sensitivity radially aligned with the source to maximize the discrimination against the SH wave component should be employed. Since, in the anisotropic case, SV and SH possess differing normal moveout characteristics, the presence of SH with SV would seriously degrade SV velocity analyses for the same reasons that the presence of P energy would cause velocity analysis degradation.

This study has been carried to the point that field testing of the proposed analysis methods should be undertaken for the purpose of verifying the results of digital modelling. Once field tests have been performed, there should exist sufficient information to define the directions in which further research is needed.

References Cited

Agard, J. and G. Grau, 1961, Etude statistique de sismogrammes: Geophys. Prosp., v. 9, p. 503-525.

Anderson, D. L., 1961, Elastic wave propagation in layered anisotropic media: Jour. Geophys. Res., v. 66, p. 2953-2963.

Anderson, D. L., 1962, Love wave propagation in heterogeneous anisotropic media: Geophysics, v. 27, p. 445-454.

Bennett, H. F., 1968, An investigation into velocity anisotropy through measurements of ultrasonic wave velocities in snow and ice cores from Greenland and Antarctica: Ph.D. dissertation, University of Wisconsin.

Birch, Francis, 1966, Compressibility; Elastic constants: Handbook of Physical Constants, Geo. Soc. Am., p. 97-174.

Cherry, J. T. and K. H. Waters, 1968, Shear wave recording using continuous signal methods Part I-Early development: Geophysics, v. 33, p. 229-239.

Cholet, J. and H. Richard, 1954, A test on elastic anisotropy measurements at Berriane: Geophys. Prosp., v. 2, p. 232-246.

Dix, C. H., 1955, Seismic velocities from surface measurements: Geophysics, v. 20, p. 68-86.

Dobrin, M. B., 1960, Introduction to geophysical prospecting: McGraw-Hill Book Company, p. 120-121.

Dunoyer de Segonzac, Ph. and J. Laherrere, 1959, Application of the continuous velocity log to anisotropy measurements in Northern Sahara: Geophys. Prosp., v. 7, p. 202-217.

Erickson, E. L., D. E. Miller, and K. H. Waters, 1968, Shear wave recording using continuous signal methods Part II-Later experimentation: Geophysics, v. 33, p. 240-254.

Goldstein, H., 1950, Classical Mechanics: Addison-Wesley Publishing Co., p. 30-36.

Hagedoorn, J. G., 1954, A practical example of an anisotropic velocity layer: Geophys. Prosp., v. 2, p. 52-60.

Haskell, N. A., 1953, dispersion of surface waves on multilayered media: Bull. Seism. Soc. Am., v. 43, p. 17-34.

Helbig, K., 1966, Refraction seismics with an anisotropic overburden: A graphical method of interpretation: Geophys. Prosp., v. 12, p. 383-396.

Hodgkinson, J., 1970, The in situ determination of velocity anisotropy in sedimentary rocks by the analysis of normal moveout data: M. S. Thesis, University of Calgary.

Jolly, R. N., 1956, Investigation of shear waves: Geophysics, v. 21, p. 905-938.

Kleyn, A. H., 1956, On seismic wave propagation in anisotropic media with applications in the Betun area, South Sumatra: Geophys. Prosp., v. 4, p. 56-69.

Love, A. E. H., 1944, A treatise on the mathematical theory of elasticity: Dover Publications, p. 159-161.

McCollum, B. and F. A. Snell, 1932, Asymmetry of sound velocity in stratified formations: Early Geophysical Papers, SEG, p. 216-227.

Postma, G. W., 1955, Wave propagation in a stratified medium: Geophysics, v. 20, p. 780-806.

Richards, T. C., 1960, Wide angle reflections and their application to finding limestone structures in the foothills of western Canada: Geophysics, v. 25, p. 385-407.

Taner, M. T. and F. Koehler, 1969, Velocity spectra-digital computer derivation and application of velocity functions: Geophysics, v. 34, p. 859-881.

Uhrig, L. F. and F. A. Van Melle, 1955, Velocity anisotropy in stratified media: Geophysics, v. 20, p. 774-779.

Vander Stoep, D. M., 1966, Velocity anisotropy measurements in wells: Geophysics, v. 31, p. 900-916.

Warnaca, C. E. and C. M. Ferree, 1967, How "random" is a geologic section: Presented at the 37th annual meeting, Society of Exploration Geophysicists.

Weatherby, B. B., W. T. Born, and R. L. Harding, 1934, Granite and limestone velocity determination in Arbuckle mountains, Oklahoma: Bull. A.A.P.G., v. 18, p. 106-118.

White, J. E. and R. L. Sengbush, 1953, Velocity measurements in near-surface formations: Geophysics, v. 17, p. 54-70.

Appendix

Digital Modelling Programs

Subroutine DREFL is the primary computer program used for the calculation of the reflection times for the models described in chapters 5 and 7. DREFL calls subroutines P123, SYGN, and VEL which function as parts of the modelling program. Subroutine VINIT, with multiple entry VEL, is included as an example of a model program used in conjunction with DREFL. VINIT in the version included here was used to generate the arrival times for the models discussed in section 7.3.

DREFL uses an iterative process to determine which ray yields the desired shot-geophone distance. The process utilizes an initial angle (read in) measured from the vertical and then divides the difference between this angle and 90 degrees by 10 to be used as an angular increment. This increment is then used to increment or decrement the initial angle until successive rays have bracketed the desired distance. Once this happens, the angular increment is halved each successive iteration until the previously selected precision is reached. The number of steps in the numerical integration is controlled by the size of the depth increment, dz, which is also read into the program.

The description of the velocity field is contained in a separate program called by the integration program (subroutine VEL). This arrangement allows greater flexibility in the use of the program. That is, many velocity models may be used without requiring modification to the integration program. The two programs work as one with the integration program supplying the model program with a set of x,z coordin-

ates. In return, the model program returns the velocity, the dip of the bedding, the depth to the reflector for the current x-value, and a test parameter which indicates whether or not the reflection depth has been reached. The actual computing process proceeds as indicated schematically below:

Computation Scheme

1.	Start:	$x = 0,\ z = 0,\ t = 0$
2.	Read:	$dz,\ \theta$
3.	Calculate:	$dx,\ dt$
4.	New Parameters:	$x \rightarrow x+dx,\ z \rightarrow z+dz,\ t \rightarrow t+dt$
5.	Apply Snell's Law:	$\theta \rightarrow \theta+d\theta$
	Loop back to 3. until--6.	
6.	Reflection Point:	$dz \rightarrow -dz,\ \theta \rightarrow \theta'$
7.	Stop:	$x = \text{Distance},\ z = 0,\ t = T$

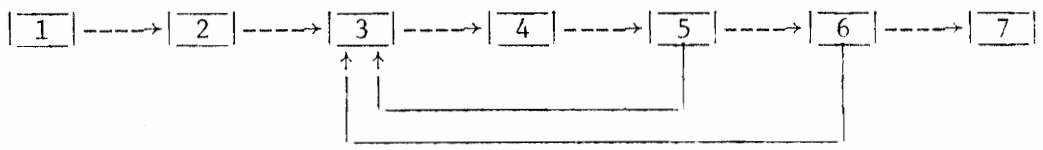

The principal assumption made is, that for proper choice of dz, the variation of velocity between successive points is small enough for the media to be treated as if it were homogeneous about the point x,z. For any given model, it is quite simple to determine the correct magnitude limit for dz. The integration program has an option to print x,z,V for each point along the path. The maximum error introduced by

poor choice of dz will occur at the reflection-point. When the proper range for dz is found, the reflection-point rapidly converges to one position and does not vary to any significant degree thereafter for smaller values of dz. The choice of dz is important in a practical sense as the time required for computation is directly proportional to the magnitude of dz. For example, the computations for a dz of 100 feet will proceed 100 times faster than those for a dz of 1 foot. The value of dz used for modelling was 25 ft in each case. This value yielded satisfactory results in the sense discussed above.

```
      SUBROUTINE DREFL(THETAI,DZ,L,PREC,IPLT,SCALE,XREF,XX,TT,IERR,IP)
C
C     THIS VERSION FOR TRANSVERSE ISOTROPY
C
C     THETAI = INITIAL ANGLE IN RADIANS
C     DZ = DEPTH INCREMENT
C     L = INTERFACE WHERE REFLECTION OCCURS
C     PREC = ALLOWABLE ERROR IN CALCULATED DISTANCE; PREC = |XREF-XX|
C     IPLT = 0 NO PLOT, STILL NEED DUMMY PLOT SUBROUTINE
C          = 1 PLOTS RAY PATH FOR REFLECTION
C     SCALE = LENGTH (IN.) TO WHICH XREF SCALED FOR PLOTTING
C     XREF = SHOT-GEOPHONE DISTANCE
C     XX = PROGRAM APPROXIMATION TO XREF
C     T = TWO-WAY TRAVEL TIME
C     IERR = 0 OUTPUT GOOD
C          = 1 |XREF-XX| > PREC
C     IP = 1, CALCULATE P
C        = 0, CALCULATE SV
C        =-1, CALCULATE SH
C
C     NOTE:
C     VEL: CHECKS DEPTH AS BEFORE; DOES NOT CALCULATE VELOCITY
C     DIRECTLY, BUT JUST ELASTIC PARAMETERS FOR USE IN P123.
C     P123: CALCULATES RAY PARAMETERS, NEW ANGLE, AND VELOCITY
C
C     W = DIP OF BEDDING AT POINT X,Z
C
C
      COMMON /DR/X,Z,D,W,ICHK,LL,KP,W2
      COMMON /PP/V1X,V1Z,V2X,V2Z
      COMMON D3,DTHETA,SREFL,STOTAL,TREFL,VINTH,VINTV
      PREC=ABS(PREC)
```

```
      PREC=25.
      PREC=50.
C                                                                     FERX*5.0=FERX
      PI2=6.283185/4.
      PI=6.283185/2.
      PI2I=1.0/PI2
      KPLT=0
      IF(IERR.EQ.2)KPLT=1
      IERR=0
      LL=L
      KP=IP
      KNTC=0
C
      IF(KPLT.EQ.1)PRINT 900,LL,THETAI
  900 FORMAT(' LAYER#, THETAI =',I5,F15.6)
C
      IFIRST =0
      INUM=0
C                                          .01/))IATEHT(SBA-597075.1(=ATEHTD
C                                            .01/))IATEHT(SBA-5075.1(=ATEHTD
C                                             .2/))IATEHT(SBA-5075.1(=ATEHTD
C                                            .05/))IATEHT(SBA-5075.1(=ATEHTD
      DTHETA=ABS(DTHETA)
      SCAL=1.0
      IF(IPLT.EQ.1)SCAL=SCALE/ABS(XREF)
  100 THETA=THETAI
      TTHETA=THETAI
      IF(ABS(THETA).GE.PI2)GO TO 7
      SGN=1.0
      ISIGN=1
      ICHK=0
      KNT=0
```

```
      X=0.0
      Z=0.0
      T=0.0
      S=0.
      ANGLE=THETA+W
   39 IF(ANGLE)40,41,41
   40 MARK=4+IFIX(ANGLE/PI2)
      GO TO 42
   41 MARK=ANGLE/PI2+1.
   42 CONTINUE
      TLD=ANGLE
      CALL VEL
      CALL P123(ANGLE,IP,0,P,V,&8)
      DX=DZ*TAN(THETA)
C     DT=SQRT(DX*DX+DZ*DZ)/V
      DS=SQRT(DX**2+DZ**2)
      DT=DS/V
      S=S+DS
C
      IF(KPLT.EQ.1)PRINT 905,DENOM,V,P,DX,DZ
  905 FORMAT(' DENOM,V,P,DX,DZ=',5E15.6 )
C
    1 X=X+DX
      Z=Z+DZ*SGN
      T=T+DT
      IF(ABS(THETA).GT.PI2)GO TO 8
C
      IF(KPLT.EQ.1)PRINT 901,X,Z,T,V,ANGLE,THETA
  901 FORMAT(' X,Z,T,V,ANGLE,THETA ',6E15.6)
C
      KNT=KNT+ISIGN
      IF(KNT.EQ.0)GO TO 2
```

```
      CALL ANG
      ANGLE=THETA+W2                                                    C
      CALL P123(ANGLE,IP,0,P,V,&8)
      CALL VEL
      CALL P123(ANGLE,IP,1,P,V,&8)
      IF(ICHK)20,20,10
   10 SGN=-1.0
      ISIGN=-1
      ICHK=0
      SGNT=SYGN(THETA)
      DDZ=ABS(Z-D)
      ALPHA=PI2+W*SGNT
      DDL=DDZ*SIN(ALPHA)/SIN(PI2-(THETA+W)*SGNT)
      DELZ=DDL*COS(THETA)*1.001
      DELX=DDL*SIN(THETA)*1.001
      Z=Z-DELZ
      X=X-DELX
      T=T-DT*DELZ/DZ
      S=S-DS*DELZ/DZ
      SREFL=S
      TREFL=T
C                                                  4 OT OG)1-.QE.NGISI(FI
      D3=Z                                                              C
      CALL VEL
      VINTH=SQRT(V1X+V2X)
      SGNV=1.
      IF(IP.EQ.0)SGNV=-1.
      VINTV=SQRT(V1Z+SGNV*V2Z)
      ICHK=0
      CALL P123(ANGLE,IP,1,P,V,&8)
      ANGLE=PI-ANGLE
      P=-P
```

```
      CALL P123(ANGLE,IP,1,P,V,&8)
      IF(ANGLE)70,71,71
   70 MARK=4+IFIX(ANGLE/PI2)
      GO TO 72
   71 MARK=ANGLE/PI2+1.
   72 CONTINUE
      THETA=ANGLE-W
      IF(THETA)163,165,165
  163 IF(THETA*PI2I+1.0)164,167,167
  164 THETA=-(PI+THETA)
      GO TO 167
  165 IF(THETA*PI2I-1.0)167,167,166
  166 THETA=PI-THETA
  167 TLD=ANGLE
C
      IF(KPLT.EQ.1)PRINT 902,X,Z,T,V,ANGLE,THETA
  902 FORMAT(' REFL PT.: X,Z,T,V,ANGLE,THETA ',6E15.6)
C
      SGWT=SYGN(TLD)
      IF(IPLT.EQ.1)CALL PLOT(Z*SCAL,X*SCAL,2)
      GO TO 30
   20 IF(IPLT.EQ.1)CALL PLOT(Z*SCAL,X*SCAL,2)
      IF(THETA.GE.PI2.AND.ISIGN.EQ.1)GO TO 3
      THETA=ANGLE-W
      IF(THETA) 63, 65, 65
   63 IF(THETA*PI2I+1.0) 64, 67, 67
   64 THETA=-(PI+THETA)
      GO TO  67
   65 IF(THETA*PI2I-1.0) 67, 67, 66
   66 THETA=PI-THETA
   67 TLD=ANGLE
   30 DX=DZ*TAN(THETA)
```

```
C       DT=SQRT(DX*DX+DZ*DZ)/V
        DS=SQRT(DX**2+DZ**2)
        DT=DS/V
        S=S+DS
        GO TO 1
      2 CONTINUE
        IF(Z.EQ.0.)GO TO 49
        DF=Z/DZ
        Z=0.0
        X=X+DF*DX
        T=T+DF*DT
        S=S+DF*DS
     49 IF(IPLT.EQ.1)CALL PLOT(0.,X*SCAL,2)
        IF(IPLT.EQ.1)CALL PLOT(0.,0.,3)
        IF(IPLT.EQ.1)GO TO 7
        GO TO 4
      3 THETAI=THETAI-DTHETA/2.
C
        IF(KPLT.EQ.1)PRINT 912,X,Z,T,V,ANGLE,THETA
    912 FORMAT(' CRITICAL ANGLE: X,Z,T,V,ANGLE,THETA ',6E15.6)
C
        KNTC=KNTC+1
        IF(KNTC.GT.10)GO TO 8
        GO TO 100
      8 IERR=1
        STOTAL=S
        TT=-100.
        THETAI=TTHETA
C                                                          FERX*.2=FERX
        RETURN
      4 IF(ABS(XREF-X).LE.PREC)GO TO 7
C
```

```
      IF(KPLT.EQ.1)PRINT 911,XREF,X,IFIRST,INUM,THETAI,DTHETA
  911 FORMAT(' XREF,X,  IFIRST,INUM,THETAI,DTHETA=',2E15.6,2I5,2E15.6)
C
      IF(XREF-X) 5,6,6
    5 IF(IFIRST.GT.0)DTHETA=DTHETA/2.
      THETAI=THETAI-DTHETA
      INUM=INUM+1
      IF(INUM.EQ.20)GO TO 7
      GO TO 100
    6 IF(INUM.GT.0)DTHETA=DTHETA/2.
      THETAI=THETAI+DTHETA
      IFIRST=IFIRST+1
      IF(IFIRST.EQ.20)GO TO 7
      GO TO 100
    7 THETAI=TTHETA
      KNTC=0
      TT=T
      XX=X
      STOTAL=S
      IF(ABS(XREF-X).GT.PREC)IERR=1
C                                                          XX*.2=XX
C                                                          TT*.2=TT
C                                                       FERX*.2=FERX
      RETURN
      END
```

```
      FUNCTION SYGN(X)
      IF(X)1,2,2
    1 SYGN=-1.0
      RETURN
    2 SYGN=1.0
      RETURN
      END
```

```
      SUBROUTINE P123(ANGLE,IP,INIT,P,V,*)
      COMMON/PP/A,B,C,D,E,AA,BB
      CALL ERRSET(207,300,-1,1,1,209)
      CALL ERRSET(259,300,-1,1,1,259)
      DANG=0.04
      INEG=0
      IPOS=0
      IF(ANGLE.GT.6.283185)RETURN 1
   10 T=TAN(ANGLE)
      T2=T*T
      T21=T2+1.0
      TWOT=2.*T
      IF(IP)300,100,100
  100 AT=A*T
      ATB=A*T2+B
      CDE=1./SQRT((C*T2-D)**2+E*T2)
      CTE=C*T*(C*T2-D)+0.5*E*T
      IF(IP)300,200,101
  101 VP=1./SQRT(ATB+1./CDE)
      VP3=VP*VP*VP
      P1=TWOT*VP-T21*(AT+CTE*CDE)*VP3
      IF(INIT)102,102,103
  102 P=P1
      GO TO 1000
  103 IF(ABS(P-P1).LT.1.0E-09)GO TO 1000
      SP1=SYGN(P-P1)
  104 IF(SP1)105,106,106
  105 INEG=INEG+1
      IF(IPOS.GT.0)DANG=0.5*DANG
      ANGLE=ANGLE-DANG
      IF(INEG.GT.20)RETURN 1
      GO TO 10
```

```
  106 IPOS=IPOS+1
      IF(INEG.GT.0)DANG=0.5*DANG
      ANGLE=ANGLE+DANG
      IF(IPOS.GT.20)RETURN 1
      GO TO 10
  200 VM=1./SQRT(ATB-1./CDE)
      VM3=VM*VM*VM
      P2=TWOT*VM -T21*(AT-CTE*CDE)*VM3
      IF(INIT)201,201,202
  201 P=P2
      GO TO 1000
  202 IF(ABS(P-P2).LT.1.0E-09)GO TO 1000
      SP1=SYGN(P-P2)
      GO TO 104
  300 VAB=1./(AA*T2+BB)
      VAB2=SQRT(VAB)
      P3=T*(AA*(T2-1.0)+2.*BB)*VAB*VAB2
      IF(INIT)301,301,302
  301 P=P3
      GO TO 1000
  302 IF(ABS(P-P3).LT.1.0E-09)GO TO 1000
      SP1=SYGN(P-P3)
      GO TO 104
 1000 CN=ABS(COS(ANGLE))
      IF(IP)3000,2000,1001
 1001 V=CN/VP
      RETURN
 2000 V=CN/VM
      RETURN
 3000 V=CN/VAB2
      RETURN
      END
```

```
      SUBROUTINE VINIT
      COMMON /DR/X,Z,DD,W,ICHK,L,IP
      COMMON/PP/A,B,C,D,E,AA,BB
C     MODEL 8002.2--AC = 1.043
C     DATA C11,C33,C13,C44,C66/76.182,70.,26.333,21.724,24.095/
      DATA C11,C33,C13,C44,C66/76.182,70.,26.333,21.724,24.095/                C
C     MODEL 8003--AC = 1.02
C     DATA C11,C33,C13,C44,C66/1.,0.9611,0.3609,0.2993,1./
      DATA C11,C33,C13,C44,C66/1.,0.9611,0.3609,0.2993,1./                     C
C     MODEL 8004--AC = 1.08
C     DATA C11,C33,C13,C44,C66/1.,0.8573,0.3235,0.2647,1./
      DATA C11,C33,C13,C44,C66/1.,0.8573,0.3235,0.2647,1./                     C
      W=0.
      RA=(C11+C44)/(2.*C11)
      RB=(C33+C44)/(2.*C11)
      RC=(C11-C44)/(2.*C11)
      RD=(C33-C44)/(2.*C11)
      RE=(C13+C44)/C11
      RAA=C66/C11
      RBB=C44/C11
      RETURN
      ENTRY VEL
C     STEPWISE INCREASE VELOCITY FUNCTION
C     V=(8000.+100.*AINT(Z/100.01))**2
C     LINEAR INCREASE VELOCITY FUNCTION
      V=(8000.+Z)**2
      A=V*RA
      B=V*RB
      C=V*RC
      D=V*RD
      E=(V*RE)**2
      AA=V*RAA
```

```
      BB=V*RBB
      IF(Z.LT.DD)RETURN
      ICHK=1
      RETURN
      END
```

Velocity Analysis

Subroutine TIVA was designed to perform isotropic or anisotropic velocity analyses for both P and SV components simultaneously. TIVA calls subroutine VEL which is used for the calculation of seismic velocity components.

Semblance calculations are performed for data sampled along trajectories defined by a range of reflection times and velocities. This program is the digital embodiment of the mathematics presented in sections 6.2 and 7.2. Figure 6.1-1 is an example for isotropic data of the operation of this program. In the figure cited, one reflection time and three velocities are utilized. In practice, as many reflection times and velocities may be used as desired.

```
      SUBROUTINE TIVA(TR,LT,NT,W,GD,AOUT,OUT,DV,V1,NV,AC,LG,NTIMES,
     1 TO,TI,DT)
C
C
C     TRANSEVERSE ISOTROPIC VELOCITY ANALYSIS UTILIZING P & SV
C
C     TR = SEISMIC TRACES
C     LT = LENGTH OF TRACES
C     NT = NUMBER OF TRACES
C     W = WORK SPACE (LG X NT X 2)
C     GD = SP-GEOPHONE DISTANCES
C     AOUT = OUTPUT ARRAY CONTAINING SCAN VELOCITIES FOR V1X, V1Z,
C        V2X: NV X 3
C     OUT = VELOCITY MATRICES FOR P & SV: NV X NTIMES X 2
C     DV = VELOCITY INTERVAL FOR V1X
C     V1 = INITIAL VELOCITY FOR V1X
C     NV = NUMBER VELOCITIES TO SCAN OVER (I.E., SCAN RANGE)
C     LG = GATE LENGTH IN MS
C     NTIMES = NUMBER TWO-WAY TIMES THAT SCANS DESIRED FOR
C     TO = INITIAL SCAN TIME
C     TI = INTERVAL BETWEEN SCANS
C     DT = TRACE DIGITIZING INTERVAL
C
      DIMENSION W(LG,NT,2),GD(NT),OUT(NV,NTIMES,2),AOUT(NV,3),
     1 TR(LT,NT),V(100,4),GD2(24)
      COMMON /IID/NAME
      WRITE(8,25)NAME,AC
   25 FORMAT('1 ID = ',A4,'    AC = ',F6.2/)
      DO 14  I=1,NT
   14 GD2(I)=GD(I)**2
      DO 1  I=1,NV
    1 V(I,1)=(V1+FLOAT(I-1)*DV)**2
```

```
      DO 30  J=1,NTIMES
      DO 30  I=1,NV
      OUT(I,J,1)=0.0
   30 OUT(I,J,2)=0.0
      DTI=1./DT
      FLG=LG/2
      NDT=DT/0.001+0.01
      LGG=LG/(2*NDT)*2+1
      TIMEL=TO
      TF=0.001*FLG
      AM1=1./FLOAT(NT)
      DO 2  I=1,NV
      CALL VEL(AC,V(I,1),V(I,2),V(I,3),V(I,4))
      AOUT(I,1)=SQRT(V(I,1))
      AOUT(I,2)=SQRT(V(I,2))
      AOUT(I,3)=SQRT(V(I,3))
    2 CONTINUE
      DO 13  III=1,NTIMES
      DO 11  II=1,NV
      TT=TIMEL
      T=TT*TT
      DO 4  J=1,NT
      T1=2.*(GD2(J)+T*V(II,2))**2/(GD2(J)*(V(II,1)+V(II,3))+T*V(II,2)*
     1 (V(II,2)+V(II,3))+SQRT((GD2(J)*(V(II,1)-V(II,3))-T*V(II,2)*
     2 (V(II,2)-V(II,3)))**2+4.*T*GD2(J)*V(II,2)*(V(II,4)+V(II,3))**2))
      T1=SQRT(T1)
      T2=2.*(GD2(J)+T*V(II,3))**2/(GD2(J)*(V(II,1)+V(II,3))+T*V(II,3)*
     1 (V(II,2)+V(II,3))-SQRT((GD2(J)*(V(II,1)-V(II,3))-T*V(II,3)*
     2 (V(II,2)-V(II,3)))**2+4.*T*GD2(J)*V(II,3)*(V(II,4)+V(II,3))**2))
      T2=SQRT(T2)
      IT1=IFIX(T1*DTI)+1
      IT2=IT1+1
```

```
      IT3=IFIX(T2*DTI)+1
      IT4=IT3+1
      IF(IT4.GT.LT)RETURN
      TIME1=FLOAT(IT1)*DT-DT
      F1=(T1-TIME1)*DTI
      TIME2=FLOAT(IT3)*DT-DT
      F2=(T2-TIME2)*DTI
      DO 3  I=1,LGG
      W(I,J,1)=F1*(TR(IT2,J)-TR(IT1,J))+TR(IT1,J)
      W(I,J,2)=F2*(TR(IT4,J)-TR(IT3,J))+TR(IT3,J)
      IT1=IT1+1
      IT2=IT2+1
      IT3=IT3+1
      IT4=IT4+1
    3 CONTINUE
    4 CONTINUE
      DO 10  IPSV=1,2
      UP=0.0
      DOWN=0.0
      DO 6  I=1,LGG
      S=0.
      DO 5  J=1,NT
      S=S+W(I,J,IPSV)
    5 CONTINUE
      UP=UP+S*S
    6 CONTINUE
      DO 7  J=1,NT
      DO 7  I=1,LGG
    7 DOWN=DOWN+W(I,J,IPSV)**2
      IF(DOWN)8,8,9
    8 OUT(II,III,IPSV)=0.0
      GO TO 10
```

```
 9 OUT(II,III,IPSV)=AM1*UP/DOWN
10 CONTINUE
11 CONTINUE
   WRITE(8,12)III,TIMEL,(OUT(I,III,1),I=1,NV)
   WRITE(8,12)III,TIMEL,(OUT(I,III,2),I=1,NV)
12 FORMAT(1X,I5,F10.5/(5X,18F7.4))
   TIMEL=TIMEL+TI
13 CONTINUE
   RETURN
   END
```

```
      SUBROUTINE VEL(A,V1X,V1Z,V2X,V13)
      AA=A*A
      AK=AA-1.0
      IF(A.NE.1.0)GO TO 1
      D=0.0
      GO TO 2
    1 D=0.5*(1.9475/AK-2.0-SQRT((1.9475/AK-2.0)**2-4.0))
    2 C11=1600.*(1.+D)**2+3116.*D
      C13=(1.+D)*(600.+640.*D)
      C44=150.*(1.+D)/(6.+25.*D)
      DD=(1.+D)*(20.+80.*D)
      V1Z=V1X/AA
      V2X=V1X*C44*DD/C11
      V13=V1X*C13/C11
      RETURN
      END
```

VITA

Name	Donald Alan Vossler
Birthdate	March 16, 1940
Degrees	B. S., Physics, 1962 St. Mary's College of California M. S., Geophysics, 1967 Oregon State University
Honors	NSF Trainee, 1969-1970 Virginia Polytechnic Institute and State University
Professional Organizations	American Geophysical Union Society of Exploration Geophysicists

ANISOTROPIC MEDIA AND THE DETERMINATION OF SUBSURFACE VELOCITY BY THE USE OF SURFACE SEISMIC REFLECTION DATA

by

Donald Alan Vossler

(ABSTRACT)

Velocity anisotropy is present at a point in a medium if the seismic velocity in one direction in general differs from that in another direction. The problems associated with the determination of subsurface velocity in anisotropic media by the use of surface seismic reflection data are analyzed. Previous studies of anisotropy in exploration seismology required bore-hole data as well as surface data to detect the presence of velocity anisotropy.

Three special types of wave propagation are of interest in reflection seismology, in addition to the general case. The theory of isotropic media is commonly utilized in exploration seismology. Elliptical anisotropy has been the method for handling anisotropic media in the past. The theory of transversely isotropic media is studied in detail since this is a reasonable anisotropy model for exploration use. Layered periodic isotropic structures are considered because of the relationships between the elastic coefficients that yield transverse isotropy in the limiting case for which the isotropic layers are thin in comparison to the wavelength of a propagating disturbance.

Synthetic common-depth-point reflection seismic traces were generated for a uniformly anisotropic halfspace, a model with seismic velocity increasing linearly with depth, velocity increasing stepwise with depth, a buried anisotropic interval in an otherwise isotropic section, and models characterized by the dip varying continuously with depth. Correlation methods (velocity analysis) are developed for the determination of rms velocity vs. two-way reflection time for both isotropic and anisotropic (transversely isotropic) media. These methods are applied to the models discussed above for varying amounts of anisotropy for each model. When the surfaces defined by the velocity analysis correlation matrices are integrated to determine the volume under the surface, it is possible to determine within about one percent the degree of anisotropy in a uniformly anisotropic medium. In a medium of varying anisotropy, it does not appear possible to obtain the same degree of accuracy as for the uniform case. Two isotropic dipping layer models were studied to determine the effects of dip on velocity analysis. The effects of dip are such that the analysis methods yield erroneous results for dips in excess of about 10-12 degrees for the models studied. Random noise degrades the velocity analysis (i.e., the magnitudes of the correlation peaks), but does not affect the accuracy or the results. Lateral velocity gradients appear to have no discernible effects on a velocity analysis for the models studied.

Results of this study indicate that the compressional wave data normally used in reflection seismic work may not be useful for the

detection of velocity anisotropy. Shear wave (SV) data, on the other hand, are ideally suited to this purpose. However, the necessity of shear wave data for the detection of anisotropy may limit these methods strictly to land use. This study indicates that the probability of detecting anisotropy by using surface methods is sufficiently high to warrant field testing.